Bioactive Natural Products From Nature

By

Harry Charilaos Brastianos

B.Sc., The University of British Columbia, 2001

A THESIS SUBMITTED IN PARTIAL FULFILMENT OF

THE REQUIREMENTS FOR THE DEGREE OF

DOCTOR OF PHILOSOPHY

in

THE FACULTY OF GRADUATE STUDIES

(Chemistry)

THE UNIVERSITY OF BRITISH COLUMBIA

October 2007

Abstract

Bioassay guided fractionation of a crude extract of the marine sponge *Neopetrosia exigua* resulted in the first reported isolation of exiguamines A (**2.58**) and B (**2.59**). These pyrroloquinone alkaloids have an unprecedented hexacyclic skeleton that has not been previously encountered in natural products. Biological studies have identified exiguamine A (**2.58**) as a potent *in vitro* inhibitor of the enzyme indoleamine-2,3-dioxygenase (IDO). IDO is an enzyme expressed by tumor cells to evade the immune system. Inhibitors against this enzyme may allow the immune system to attack cancer cells, making this enzyme a potential drug target for anti-cancer agents.

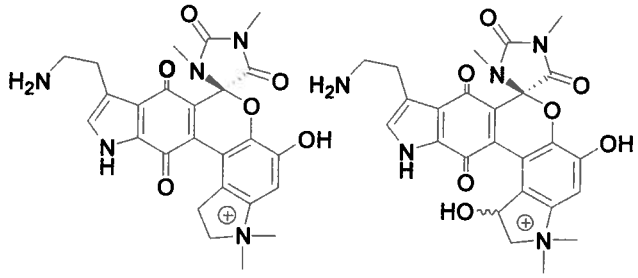

2.58 **2.59**

Investigation of the crude extract of a *Bacillus* sp. collected in Dominica led to the isolation of the known diketopiperazine cyclo(S-Val-S-Phe) (**3.9**). *In vitro* biological studies revealed that cyclo(S-Val-S-Phe) (**3.9**) is able to promote neurite outgrowth, even in the presence of physiological inhibitors. *In vivo* studies have shown that cyclo(S-Val-S-Phe) (**3.9**) is able promote sprouting in serotonergic and adrenergic axons. Synthesis of the other three diastereomers led to the discovery that cyclo(R-Val-R-Phe) (**3.22**) is also an *in vitro* activator of axonal outgrowth.

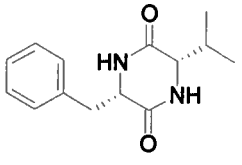

3.9

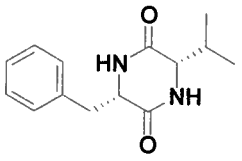

3.22

Inhibitors of the G_2 checkpoint are able to increase the cytotoxicity of DNA damaging chemotherapeutics. Bioassay guided fractionation of an extract of the South American plant *Duguetia odorata* led to the isolation of the G_2 checkpoint abrogator, oliveroline (**4.32**). This investigation also led to the isolation of the previously unreported alkaloid *N*-methylguatterine (**4.33**), and the known alkaloids dehydrodiscretine (**4.34**) and pseudopalmatine (**4.35**).

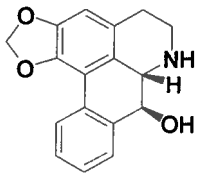

4.32

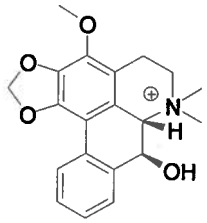

4.33

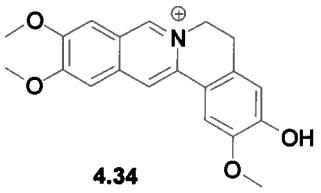

4.34

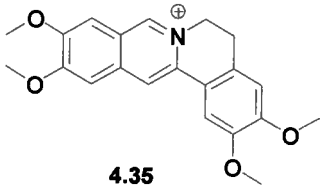

4.35

Chemical investigation of the marine sponge *Myrmekioderma granulatum* led to the isolation of the new compounds abolenone (**5.24**) and myrmekioside C (**5.26**), as well as the known compounds curcudiol (**5.23**), curcuphenol (**5.25**), abolene (**5.22**) and sesquiterpenoid (**5.21**). Biological studies of these compounds revealed that curcudiol is a ligand of the sex hormone-binding globulin (SHBG). This protein is involved in transporting and regulating the

concentration of steroids such as testosterone and estradiol. Many pathological conditions have a lower plasma concentration of these steroids. Ligands to SHBG can release steroids into the blood, so this protein is a potential drug target to treat conditions where a hormone insufficiency is present.

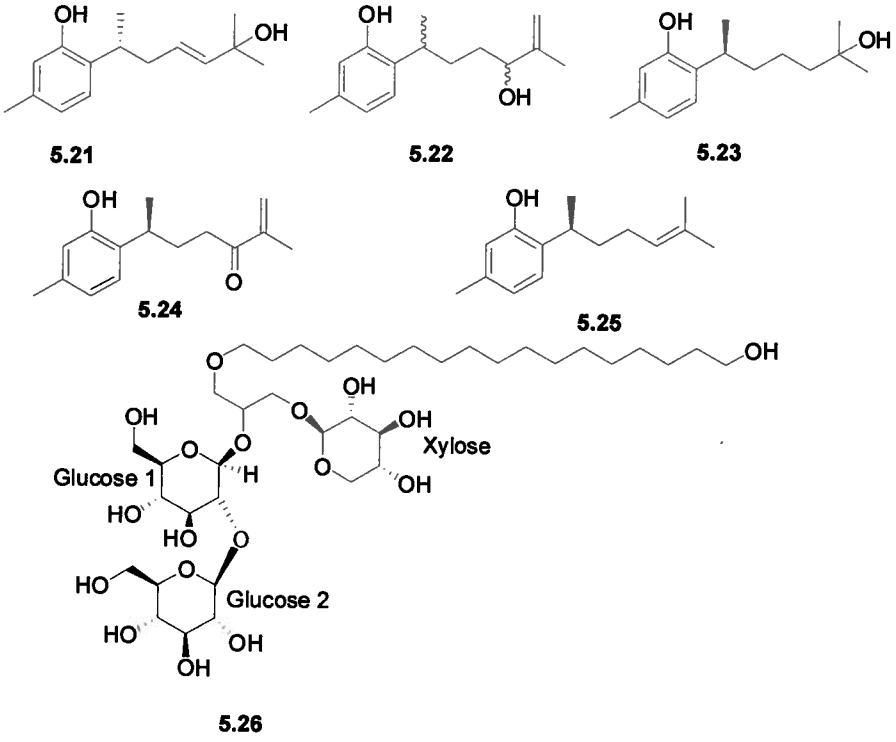

Table of Contents

List of Tables

List of Figures

List of Schemes

List of Abbreviations

^{o}	-degrees
^{o}C	-degrees Celsius
1D	-one dimensional
2D	-two dimensional
(-)	-negative optical rotation
(+)	-positive optical rotation
^{1}H	-proton
^{1}H, ^{15}N LR-HMQC	-(^{1}H, ^{15}N) long range heteronuclear multiple quantum coherence
^{13}C	-carbon-13
3OHKG	-3-hydroxykynurenine glucoside
3OHKyn	-3-hydroxykynurenine
α	-1, 2 relative position or below the plane of the ring
ABP	-androgen binding protein
$[\alpha]_D^{25}$	-specific rotation at wavelength of sodium D line at 25° C
ACN	-acetonitrile
Ara-C	-cytosine arabinoside
ArH	-aromatic proton(s)
ATM	-ataxia telangiectasia mutated kinase
ATR	-ataxia telangiectasia mutated-related kinase
β	-1, 3 relative position or above the plane of the ring
BC	-before Christ

BLAST	-Basic Local Alignment Search Tool
BnBr	-benzyl bromide
bs	-broad singlet
Bu	-butyl
c	-concentration
C	-carbon(s)
CAN	-ceric ammonium nitrate
C_6D_6	-deuterated benzene
calc'd	-calculated
CD	-circular dichroism
$CDCl_3$	-deuterated chloroform
cdc2	-cyclin-dependent kinase 1
cdc25c	-cell division cycle 25C kinase
CH	-methine
CH_2	-methylene
CH_3	-methyl
CH_2Cl_2	-methylene chloride
$CHCl_3$	-chloroform
CH_3NO_2	-nitromethane
Chk1	-CHK1 checkpoint homolog
Chk2	-CHK2 checkpoint homolog
cm	-centimeter(s)
CNS	-central nervous system

coll no	-collection number
COSY	(^{1}H, ^{1}H) homonuclear correlation spectroscopy
CSPG	-chondroitin-sulfate proteoglycans
C-X	-carbon number X
Cys	-cysteine
d	-doublet
δ_C	-carbon chemical shift (in parts per million from tetramethyl silane)
dd	-doublet of doublets
$\Delta\varepsilon$	-extinction coefficient difference
δ_H	-proton chemical shift (in parts per million from tetramethyl silane)
DEPT	-distortionless enhancement by polarization transfer spectroscopy
di	-two
DMF	-*N,N*-dimethylformamide
DMSO	-dimethyl sulfoxide
DMSO-d_6	-deuterated dimethyl sulfoxide
δ_N	-nitrogen chemical shift (in parts per million from nitrous methane)
DNA	-deoxyribonucleic acid
DOPA	-3,4-dihydroxy-phenylalanine
Dr.	-doctor
ε	-extinction coefficient

EC_{50}	-concentration required for obtaining 50% of a maximum effect in vivo
ELISA	-enzyme linked immunosorbant assay
EPOCH II	-etoposide, prednisone, vincristine, cyclophosphamide, doxorubicin
ESI	-electrospray ionization
EtOAc	-ethyl acetate
EtOH	-ethanol
FDA	-U.S. Food and Drug Administration
g	-grams
G_1	-growth phase one of the cell cycle
G_2	-growth phase two of the cell cycle
Glu1	-glucose one
Glu1-C-X	-glucose one, carbon number X
Glu1-H-X	-glucose one hydrogen number X
Glu2	-glucose two
Glu2-C-X	-glucose two, carbon number X
Glu2-H-X	-glucose two, hydrogen number X
Gly	-glycerol
Gly-C-X	-glycerol carbon number X
Gly-H-X	-glycerol hydrogen number X
GTPase	-guanosine triphosphatase
Gy	-gray
h	-hour(s)

H	-hydrogen(s)
HCl	-hydrochloric acid
HCT-116	-human colon carcinoma cell line
[^{3}H]-DHT	-tritium labeled dihydrotestoterone
His	-histidine
H_2O	-water
HL-60	-human leukemia cell line
HMBC	-(^{1}H, ^{13}C) heteronuclear multiple bond coherence
HMQC	-(^{1}H, ^{13}C) heteronuclear multiple quantum coherence
HPLC	-high performance liquid chromatography
H-Ras	-V-Ha-Ras Harvey Rat Sarcoma Viral Oncogene Homolog
HRESIMS	-high resolution electrospray ionization mass spectrometry
HRESIMS-TOF	-high resolution electrospray ionization mass spectrometry time of flight
H_2SO_4	-sulphuric acid
H-X	-hydrogen number X
Hz	-hertz
IC_{50}	-the half maximal inhibitory concentration
IDO	-indoleamine-2,3-dioxygenase
J	-coupling constant in hertz
K_i	-dissociation constant for inhibitor binding
Kyn	-kynurenine
L	-liter(s) or levorotatory

LC	-liquid chromatography
LC_{50}	-the dose required to kill half the population
LCT	-liquid chromatrograph-time of flight
LHMDS	-lithium hexamethyl disilazide
LRESIMS	- low resolution electrospray ionization mass spectrometry
λ_{max}	-wavelength at maximum intensity in nanometers
m	-multiplet or meter
M	-mitosis
$[M]^+$	-molecular ion
m^3	-meter cubed
MAG	-myelin-associated glycoprotein
$[M+H]^+$	-molecule plus hydrogen ion
$[M+Na]^+$	-molecule plus sodium ion
MCF-7	-human breast adenocarcinoma cell line
Me	-methyl
Me-X	-methyl number X
MeOD	-deuterated methanol
MeOH	-methanol
mg	milligram(s)
µg	-microgram(s)
$MgSO_4$	-magnesium sulphate
MHz	-megahertz
MIC	-minimum inhibitory concentration

min	-minute(s)
mL	-milliliter(s)
μM	-micromolar
μm	-micrometer(s)
mm	-millimeter(s)
mmol	-millimole(s)
MS	-mass spectrometry
mp53	-mutated cellular tumor antigen p53
M-Phase	-mitotic phase
m/z	-mass to charge ratio
^{15}N	-nitrogen-15
NaCl	-sodium chloride
NAD^+	-nicotinamide adenine dinucleotide
$NADP^+$	-nicotinamide adenine dinucleotide phosphate
NaH	-sodium hydride
NAPS	-Nucleic Acids and Protein Services, U.B.C.
n-BuLi	-*n*-butyl lithium
n-BuOH	-1-butanol
ng	-nanogram(s)
NgR	-Nogo receptor
NH_4Cl	-ammonium chloride
NCI	-National Cancer Institute
nm	-nanometer(s)

nM	-nanomolar
NMR	-nuclear magnetic resonance
N-X	-nitrogen number X
ODS	-octadecyl silane
OH	-hydroxide
OMe	-methoxy
OMgp	-oligodendrocyte-myelin glycoprotein
p	-para
P	-phosphorylated
p53	-cellular tumor antigen p53
PCR	-polymerase chain reaction
*p*MeOBnCl	- paramethoxybenzyl chloride
PLL	-poly-L-lysine
ppm	-parts per million
Pro	-proline
R	-rectus (configuration)
ref no	-reference number
RhoA	-ras homolog gene family, member A
RNA	-ribonucleic acid
RNase	-ribonuclease
rRNA	-ribosomal ribonucleic acid
ROCK	- RhoA associated coiled-coil-containing protein kinase
s	-singlet

S	-synthesis phase of cell cycle or sinister (configuration) or south
SAB	-standardized azide buffer
SCI	-spinal cord injuries
SCUBA	-self-contained underwater breathing apparatus
sec	-seconds
Sept	-September
Ser	-serine
SHBG	-sex hormone-binding globulin
sp.	-species
sp^2	-sp^2 hybrid orbital
sp^3	-sp^3 hybrid orbital
S-phase	-synthesis phase
t	-triplet
t	-tertiary
TCA	-trichloroacetic acid
TDO	-trypotophan-2,3-dioxygenase
tert	-tertiary
THF	-tetrahydrofuran
Thr	-threonine
TFA	-trifluoroacetic acid
TG-3	-thyroglobulin antibody three
TLC	-thin layer chromatography
TM	-trademark

TRH	-thyrotopin-releasing hormone
Tyr	-tyrosine
Val	-valine
XH	-X number of hydrogens
Xyl	-xylose
Xyl-C-X	-xylose carbon number X
Xyl-H-X	-xylose hydrogen number X
U.B.C.	-University of British Columbia
U.S.	-United States
UV	-ultraviolet
wt	-weight

Acknowledgements

First and foremost, I would like to express my gratitude to my supervisor, Dr. Raymond Andersen for the opportunity to be a graduate student in his laboratory. His mentorship throughout the years have given me the skills to succeed in any scientific endeavor.

I am indebted to Dr. David Williams. He has been helpful throughout my graduate student career, and has always been willing to answer my countless questions. The Andersen lab is a wonderful environment to work in, and all the members have helped make my time in this lab unforgettable. Special thanks go to Rob Keyzers, and Gavin Carr for their assistance in my thesis research. Dr. Eduardo Vottero, Dr. Chris Sturgeon, Jennifer Wong, and Maghid Fallahi have conducted the biological aspects of the research. Mike LeBlanc collected the sponge samples, as well as consistently providing assistance with the equipment in the lab.

Finally, I will always leave the best for last. My parents, John and Maria Brastianos, and my sister Dr. Priscilla Brastianos have supported me tremendously throughout my life. Without their many sacrifices, I would not be the person I am today.

Chapter 1: Introduction to the Field of Natural Products

1.1. Historical Overview of Natural Products as Therapeutic Drugs

For thousands of years, humanity has used the extracts of organisms to cure ailments. These drugs were usually preparations of herbs, shrubs, or other plants. An example of a plant that was used extensively in ancient times was the bark of the willow tree. Willow tree was first used by the Assyrians (4000 BC) and Babylonians (600 BC) as an anti-inflammatory and analgesic agent. The Greek physician Hippocrates in 400 BC recognized its pain-relieving properties and used it to treat the pain of child bearing in women.[1]

For over two thousand years this bark was used as a cure for pain before chemical studies were undertaken to discover the source of the biological activity. In 1829, the French pharmacist Henri Leroux isolated the pure crystalline bioactive material known as salicin (**1.1**, Figure 1.1.1). Synthetic modifications of salicin led to aspirin (**1.2**, Figure 1.1.1), which is among the highest selling drugs of all time. The development of aspirin is an early landmark in natural product chemistry. Salicin represents one of the earliest bioactive compounds ever purified, and aspirin is the first synthetic drug based on a natural product lead.[1]

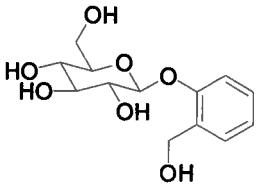

1.1

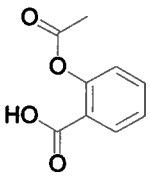

1.2

Figure 1.1.1. Structures of salicin (**1.1**) and aspirin (**1.2**).

The use of secondary metabolites from organisms as a resource for the treatment of diseases has had a tremendous impact in medicine. From 1981-2002, 28% of all drugs that entered the market were either natural products or natural-product derived compounds.[2] Furthermore, an additional 24% of the drugs introduced were synthetic derivatives of natural product lead compounds. More than half (52%) the small molecule therapeutics were developed from natural products.[2] The impact of natural products is even more pronounced in the fields of oncology and infectious diseases where 60 and 75 percent, respectively, of drugs entering the market in that 21-year period were from a natural product origin.[2] Clearly, secondary metabolites from nature will continue to play a prominent role in the development of novel pharmaceuticals.

1.2. Bioactive Metabolites from Terrestrial Plants

Terrestrial plant secondary metabolites have been the main source of therapeutics since ancient times, and currently it has been estimated that approximately 80% of the world's population uses plant-based medicines.[3] Current estimations indicate that there are approximately 350,000 different species of plants growing on earth. Out of the 350,000 plants, one-third of these plants have not been discovered.[4] Out of the remaining two-thirds, only a small

fraction (15%) of these species have been studied for biologically active secondary metabolites, so there remains potential to find novel bioactive compounds.[5]

The natural products of plants have played a key role in the treatment of cancer. A significant discovery in cancer therapy was the isolation of paclitaxel (taxol™, **1.3**, Figure 1.2.1) as the cytotoxic component from the Pacific yew tree, *Taxus brevifolia*.[6] Elucidation of its biological activity showed that it induces mitotic arrest by promoting the polymerization of tubulin.[7] Paclitaxel has become one of the most important drugs for the treatment of ovarian and breast cancers.[8,9] Vinblastine (**1.4**, Figure 1.2.2) and vincristine (**1.5**, Figure 1.2.2) are two other plant natural products currently used clinically that interact with tubulin. These alkaloids isolated from the periwinkle known as *Catharanthus roseus* are mainly used to treat leukemias and lymphomas.[10] Other plant entities in clinical use include derivatives of the antineoplastic agent camptothecin (**1.6**, Figure 1.2.2). Camptothecin was originally isolated from the extracts of the Chinese ornamental tree, *Camptotheca acuminatea*. Since camptothecin was too toxic to be used in the clinic, its analogues topotecan (**1.7**) and irinotecan (**1.8**) were developed and are currently used to treat various cancers. Camptothecin is cytotoxic due to its interactions with DNA-topoisomerase I, which ultimately leads to the inhibition of DNA synthesis and cell death.[11]

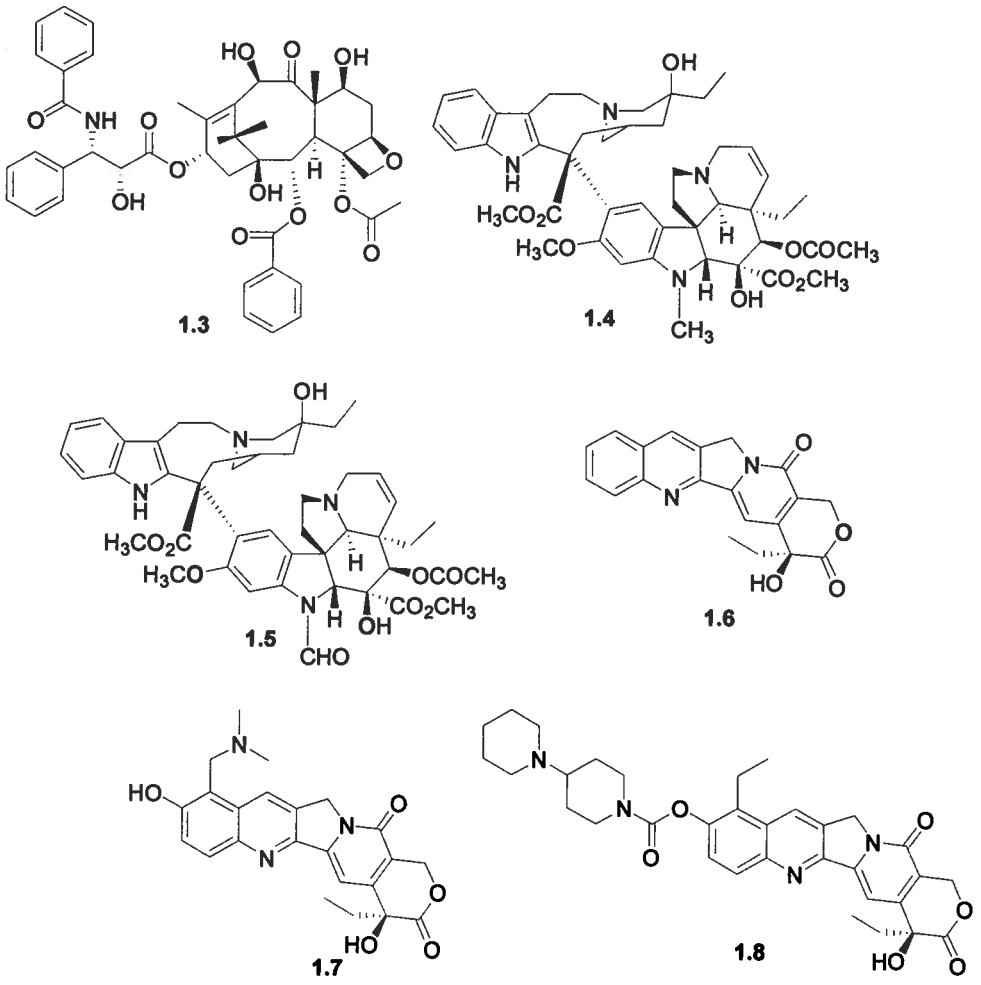

Figure 1.2.1. Plant derived anti-cancer compounds.

Numerous plant derived natural products have been approved for clinical use in the last seven years. Galantamine hydrobromide (**1.9**) is an alkaloid that is used to treat Alzheimer's disease by slowing the process of neural degeneration. This compound was isolated from the plant *Galanthus nivalis,* which is found in Turkey and Bulgaria.[12] Another neuroactive alkaloid that has been approved in the clinic is apomorphine hydrochloride (**1.10**), which is used for Parkinson's disease.[13] It is clear that based on the number of compounds recently being approved for medicinal use, plant-derived secondary metabolites remain a promising field for drug discovery.

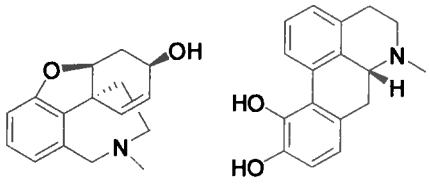

1.9 1.10

Figure 1.2.2. Examples of plant derived natural products recently approved for medicinal use.

1.3 Overview of Natural Products from Microorganisms

Current estimations indicate that only 5% of fungal and 1% of bacterial species have ever been cultured in the laboratory, and even smaller numbers have been examined for secondary metabolites. Despite the low number of species studied, over 22,000 bioactive compounds have been isolated from microorganisms. This illustrates the impressive chemical diversity of secondary metabolites produced by microorganisms. As culturing conditions for microorganisms improve, the potential to study an even greater number of microorganisms and isolate additional novel biologically active compounds increases tremendously.[14]

The explosion of the use of microorganisms as a source of medicinally relevant compounds started in the 1930's and 1940's with the discovery of penicillin (**1.11**). After that discovery, drug companies realized that culturing microorganisms provided access to a wide chemical diversity of bioactive secondary metabolites and an almost limitless supply of a drug. Therefore, drug companies started isolating large collections of cultivatable microorganisms which led to the discovery of antibiotics such as streptomycin (**1.12**) and chlorotetracycline (**1.13**) during the 1950's.[15] Microorganisms have not only

been studied for potential antibiotics, but also for compounds that affect cell metabolism and signaling pathways. Other drugs produced by microorganisms that are used clinically include the immunosuppressive drug FK-506 (**1.14**), which is produced by *Streptomyces tsukubaensis*,[16] the cholesterol-lowering agent lovastatin (**1.15**), isolated from *Aspergillus terreus*,[17] and the antidiabetic drug acarbose (**1.16**), from the *Actinoplanes* sp.[18]

In the past year, there have been several interesting bioactive secondary metabolites that were isolated from microorganisms. The compound garnering perhaps the most attention was the novel antibiotic platensimycin (**1.17**).[19] Platensimycin was isolated from the extracts of *Streptomyces platensis*, a soil bacterium collected in South Africa. This compound contains a unique tetracycle and an uncommon 3-amino-2,4-dihydroxybenzoic acid head group. Biologically, platensimycin selectively inhibits lipid biosynthesis in both *Staphylococus aureas* and *Staphylococus pneumoniae* and does not affect other metabolic processes. *In vitro* studies reveal that platensimycin has potent activity against Gram-positive bacteria including ones resistant to antibiotics. Studies in mice infected with *S. aureas* show that platensimycin has promising *in vivo* activity as well.[19] In an era of increasing antibiotic resistance, the discovery of novel antibiotics can have a substantial effect on the course of human disease.

Other promising novel antibacterial compounds isolated in the past year include marinomycins A-D. These polyketide-derived secondary metabolites were isolated from a previously unclassified species of marine actinomycete. Fenical and co-workers suggested the name of *Marinispora* for the bacterial

genus.[20] Marinomycin A (**1.18**) was found to be the most potent antibacterial agent of all the marinomycins with an *in vitro* minimum inhibitory concentration (MIC) of 130 nM against menthicillin-resistant *S. aureus* and vancomycin-resistant *Streptococcus faecium*. The marinomycins were found to be inactive as anti-fungal agents, with only marinomycin A showing weak activity against *Candida albicans*. The marinomycins also demonstrated potent and selective anti-tumor activity. When the marinomycins were tested in the NCI's panel of 60 cancer lines, marinomycin A, B and C were very active against six out of the eight melanoma cell lines. More importantly though, the marinomycins showed only very weak activity against the leukemia cell lines which suggests selective cytotoxicity.[20]

Rhizoxin (**1.19**) is one of the most potent anti-mitotic agents known and it was found to be very active against human and murine tumor cells *in vitro*. Due to its promising biological activity, rhizoxin has undergone clinical trials as a compound to treat cancer.[21] Unfortunately, due to low *in vivo* activity, rhizoxin was removed from clinical trials. This compound was first isolated from the pathogenic plant fungus *Rhizopus microsporus,* which causes rice seedling blight. In 2000, Andersen and co-workers discovered several analogues of rhizoxin from a bacterium in the genus *Pseudomona*. This was the first time rhizoxin derivatives were isolated from bacteria and not from a fungus.[22] Other studies have shown that rhizoxin is biosynthesized by the bacterium *Burkholderia rhizoxina,* which are endosymbiotic bacteria that reside in the fungus. Very recently, the symbiotic bacteria were cultivated and numerous rhizoxin

derivatives were isolated from the bacteria. Three derivatives, rhizoxin M1 (**1.20**), M2 (**1.21**), and Z2 (**1.22**) were 1000-10000 times more active than rhizoxin at inhibiting the proliferation of K-562 leukemia cells and were found to be among the most potent anti-mitotic agents ever found. Perhaps these derivatives will yield more promising *in vivo* activity than rhizoxin.[21]

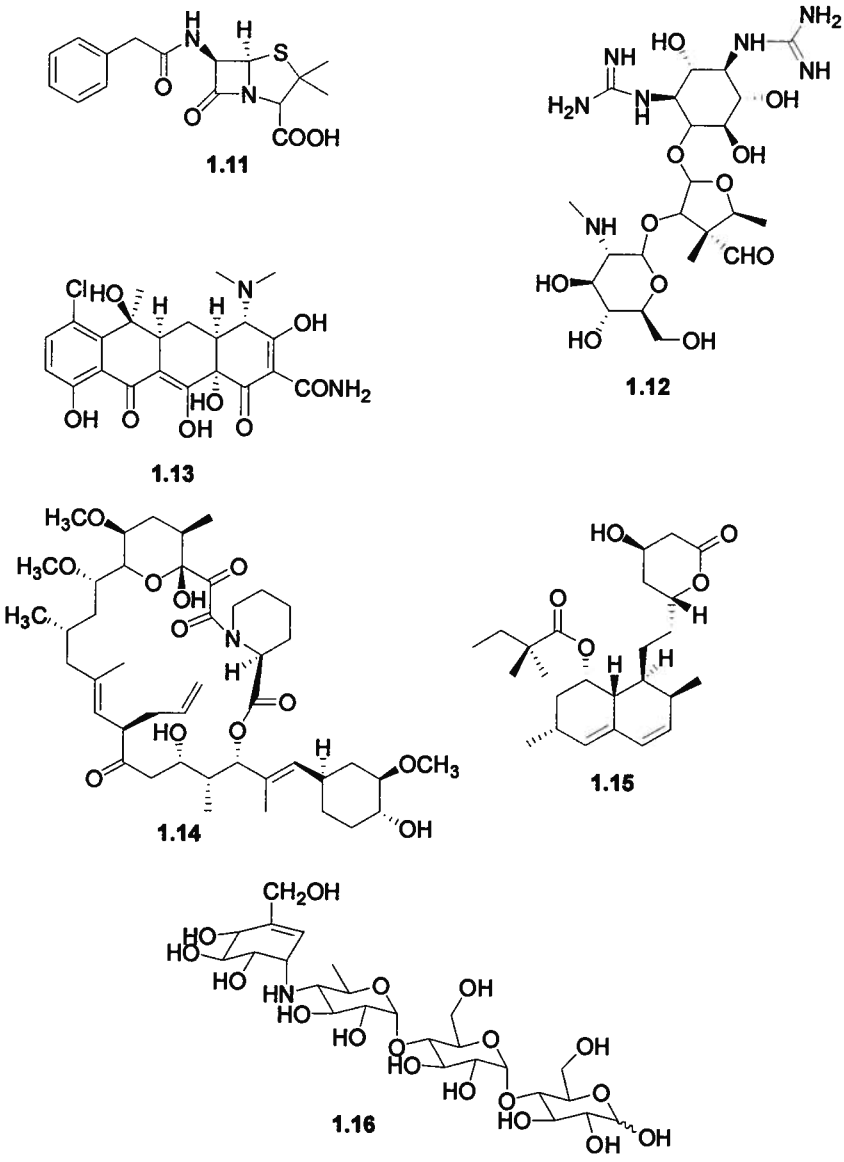

Figure 1.3.1. Significant natural products isolated from microorganisms.

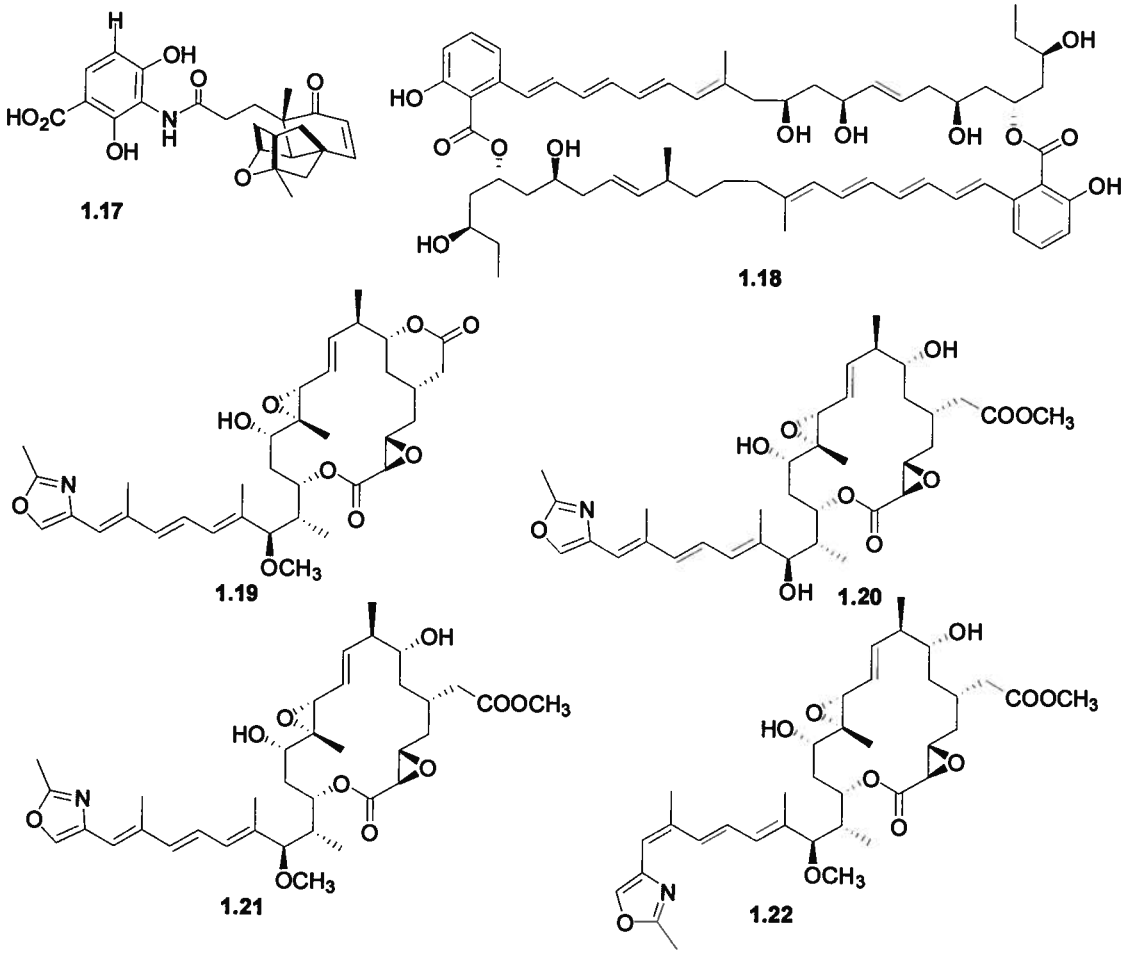

Figure 1.3.2. Significant natural products isolated from microorganisms in 2006.

1.4 Overview of Marine Natural Products from Invertebrates

Oceans cover approximately two-thirds of the world's surface and contain over 100,000 species of marine invertebrates; however, only a small fraction of these species have been examined for the presence of biologically active compounds. Many of the invertebrates that live in the ocean including porifera, echinodermata, bryozoa and coelentara have soft bodies and are sessile, yet they are able to thrive in the ocean. These organisms contain secondary metabolites which protect them from predators, deter competitors, and assist

them in catching prey.[23] Chemists have exploited these compounds produced by marine invertebrates to yield very promising medicinally active drugs.

The field of marine natural products is relatively young, being only studied extensively in the last thirty five years. Despite its youth, several compounds of marine origin that have been approved to be used clinically, as well as numerous marine invertebrate-derived drug candidates that are in clinical trials. Among the earliest bioactive compounds from marine invertebrates were the nucleosides spongouridine (**1.26**) and spongothymidine (**1.27**) from the Caribbean sponge *Cryptotheca crypta*.[24] Synthetic modifications of the two nucleosides led to the discovery of cytosine arabinoside (Ara-C; **1.28**), the first drug introduced in the clinic that was based on a marine natural product lead. Cytosine arabinoside was approved by the FDA in 1969 as an anti-cancer agent, and is currently used to treat leukemia and lymphomas.[24]

A promising drug from the sea to enter clinical trials is the isoquinoline alkaloid ecteinascidin 743 (**1.29**), which was isolated from the marine tunicate *Ecteinascidia turbianta*. This alkaloid is currently in phase III clinical trials for numerous cancers including ovarian and soft tissue sarcoma.[25,26] Another anti-tumor drug in phase II clinical trials is alpidine (**1.30**), which was first isolated from the Mediterranean ascidian, *Aplidium albicans*. The mechanism of its anti-cancer action is that it arrests cells at the G_1 or G_2 phases of the cell cycle, and is an inhibitor of angiogenesis. It is presently in phase II clinical trials for various cancers including melanoma, pancreatic, and non-Hodgkin lymphoma.[27]

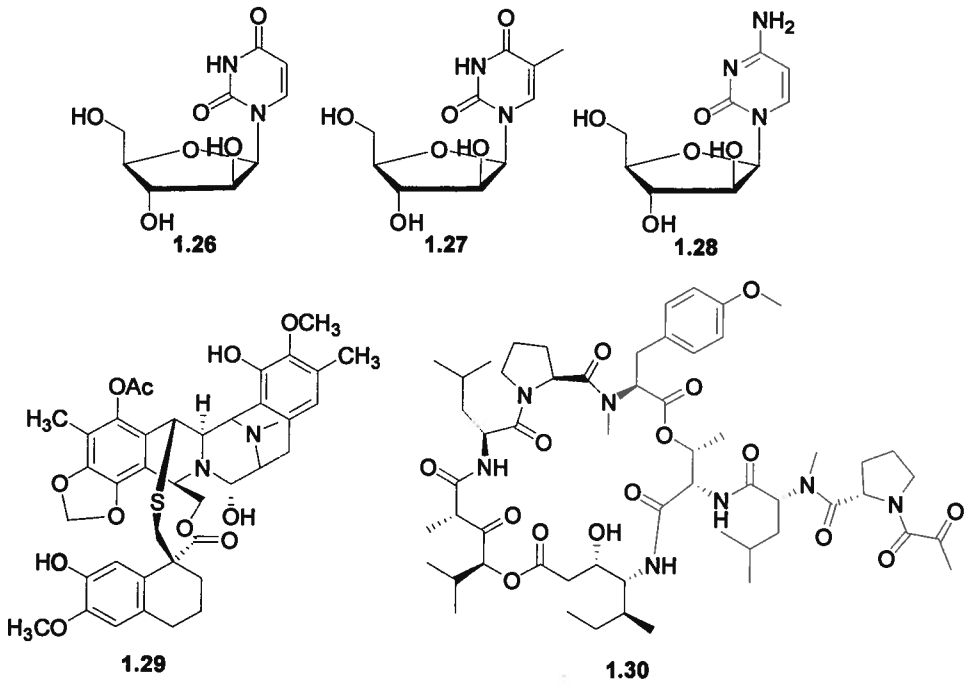

Figure 1.4.1. Significant marine natural products.

In the past year, there have been several novel bioactive compounds isolated from marine invertebrates. One anti-cancer agent recently discovered was the polyketide palmerolide A (**1.31**) which was isolated from the Antarctic tunicate *Synoicum adareanum*. This macrolide targets melanoma (LC_{50}= 18 nM) with three orders of magnitude greater sensitivity relative to other cell lines that were tested.[28,29] Specificity for certain cell lines is beneficial therapeutically when used in humans, because of fewer side effects.

Cortistatins A-D were isolated from a MeOH extract of *Corticium simplex,* which was collected in Indonesia. The cortistatins contain an isoquinoline moiety and a bicyclic octene which are both rare structural elements in steroids. All four cortistatins were able to selectively inhibit the proliferation of human umbilical vein endothelial tumor cells. Cortistatin A (**1.32**) was also found to be a potent *in*

vivo inhibitor of angiogenesis.[30] Other anti-cancer agents isolated from sponges were azumamides A-E. These cyclic peptides were isolated from the Japanese sponge *Mycale izuensis* and were active inhibitors of histone deacetylases. Furthermore, azumamide A (**1.33**) was also found to inhibit angiogenesis.[31]

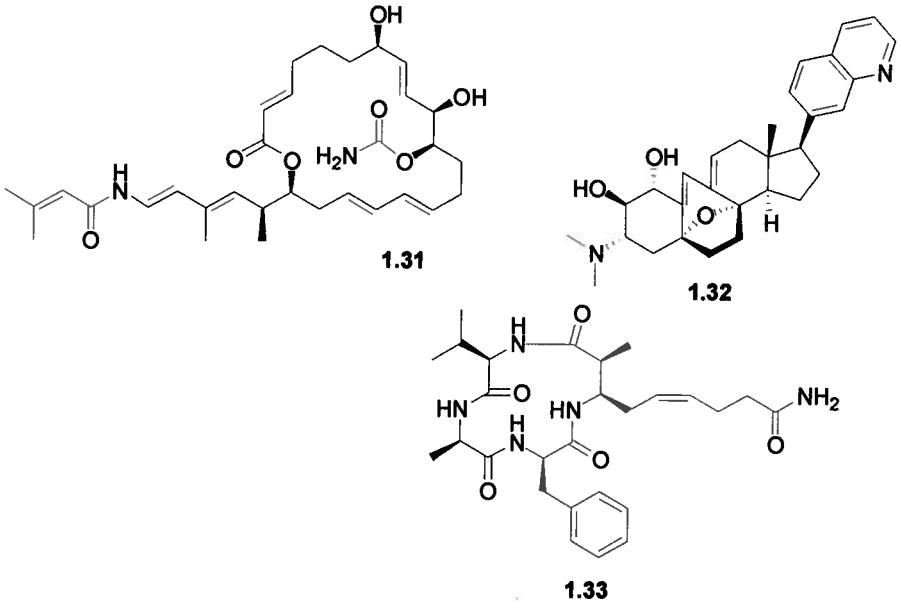

Figure 1.4.2. Promising marine natural products isolated in 2006.

1.5 Conclusions

The investigation of bioactive secondary metabolites from nature plays an important role in the medical sciences. First, bioactivity-guided natural product investigation can lead to the discovery of novel chemical entities, or the discovery of new biological activity for known compounds. Once a lead drug candidate is isolated, it may be modified synthetically to make it more efficacious or less toxic. Second, bioactive secondary metabolites may also be powerful biological tools to discover new drug targets. This was especially evident with camptothecin, where it was the first time inhibitors of DNA topoisomerase I were seen as drug

candidates against cancer.[11] Finally, searching for compounds in nature may also yield a source for a drug that may be very difficult or expensive to manufacture synthetically. This includes natural products produced from microorganisms where the fermentation of microbes may provide an industrial scale supply of the desired bioactive compound.[32]

Currently, it has been estimated that only one-third of diseases can be treated effectively.[33] Furthermore, with bacteria, cancer and viruses becoming resistant to the current therapeutic regimens, the need for novel drug candidates has never been greater. Despite the need for novel drug pharmacophores, major pharmaceutical companies in the last ten years have either abandoned, or drastically reduced funding for the research and development of novel bioactive compounds from nature.[34,35] Hopefully this trend will cease, as the majority of Earth's natural biological resources remain untapped for novel drug leads.

1.6. Preview of Thesis

This thesis focuses on the purification and structure elucidation of bioactive secondary metabolites from marine, terrestrial and microbial sources. The Andersen lab has access to a large library of extracts from organisms, which equates to a wide diversity of secondary metabolites. Furthermore, the Andersen lab also has access to a large number of novel biological assays. The combination of having access to unique biological assays, and a large library of extracts represents a unique opportunity to discover new bioactive small molecules.

The isolated bioactive natural products can serve various purposes in the biological sciences. Firstly, these compounds may be used as lead compounds to develop potential therapeutic agents. Secondly, the isolated small molecules may serve as biochemical tools to discover new drug targets, as well as to probe the molecular basis for diseases. Finally, the isolated molecules may assist in the development of novel biological assays and serve as a proof of principle that the biological screen may be used to search for bioactive compounds from biological extracts.[5]

The emphasis of the Andersen group is to use bioassay guided fractionation (Figure 1.6.1) to isolate the bioactive molecules from the crude extracts of organisms, and to use spectroscopic techniques to identify the structure of the bioactive compounds. In bioassay guided fractionation, a library of crude extracts are evaluated for a particular biological response.[4,33] The active crude extract is further separated using various chromatographic techniques to obtain semi-purified fractions, which are evaluated in a biological assay. Only the biologically active fractions are further separated and evaluated in the bioassay. This process is repeated until the biologically active components are purified (Figure 1.6.1). [4,33] The structures of the purified compounds are then determined using various spectroscopic techniques.

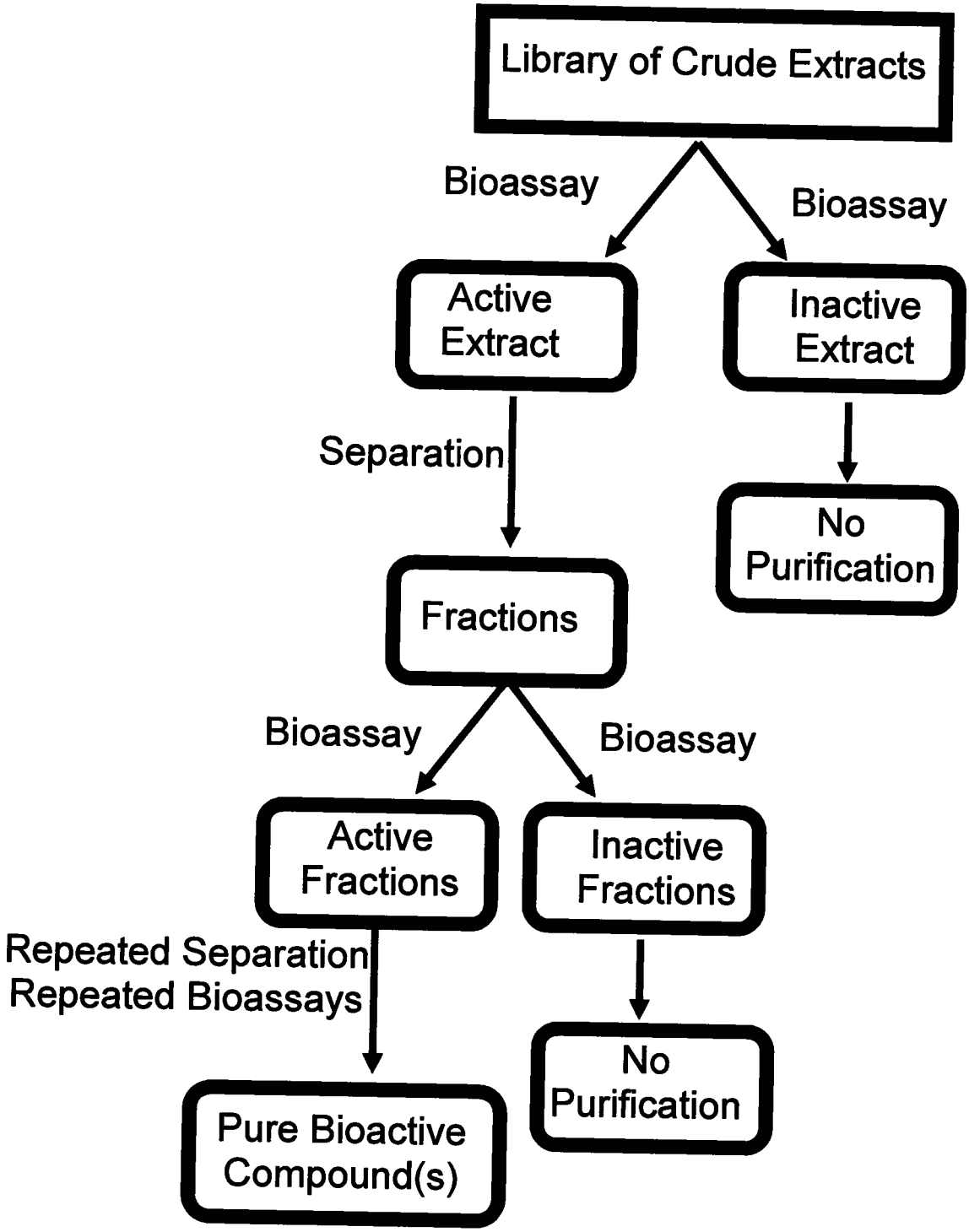

Figure 1.6.1. Procedure for bioassay guided fractionation.

The second chapter of the thesis will discuss the search for inhibitors for the enzyme indoleamine-2,3-dioxygenase (IDO). IDO is a protein that is expressed by many tumors in order to suppress the immune system, therefore, inhibitors of this enzyme have the potential to be used in cancer therapy. Bioassay-guided fractionation of the crude extract of the sponge *Neopetrosia exigua* yielded the novel alkaloids exiguamines A and B. Exiguamine A is one of the most active IDO inhibitors known to date.[36]

The third chapter will deal with the isolation and structure elucidation of compounds that induce neurite outgrowth. When there is an injury to the central nervous system, inhibitors are present that prohibit the spontaneous repair of axons. Compounds that stimulate neuronal outgrowth in the presence of these inhibitors have the potential to aid in the repair of the nervous system following traumatic spinal cord injury. Bioassay-guided fractionation of an extract from cultures of a marine *Bacillus* sp. yielded the diketopiperazine cyclo(S-Val-S-Phe) as the active component. Synthesis of all four diastereomers established that cyclo(R-Val-R-Phe) was also an axonal outgrowth activator.

The fourth chapter of the thesis will discuss the isolation of compounds that inhibit the G_2 checkpoint. Both the G_1 and the G_2 checkpoints are involved in repairing damaged DNA. It has been found that most tumors lack the G_1 checkpoint, so inhibitors of the G_2 checkpoint would make tumor cells more sensitive to DNA-damaging chemotherapeutics such as cisplatin. Bioassay guided fractionation of the MeOH extract of the plant *Duguetia odorata* yielded

oliveroline as the active compound and led to the isolation of three more alkaloids, including the new aporphine alkaloid, *N*-methylguatterine.[37]

The isolation of ligands for the sex hormone binding globulin will be the focus of the fifth chapter. Sex hormone-binding globulin (SHBG) is involved in regulating and binding steroids such as testosterone, estradiol, and 5α-dihydrotestosterone. Many conditions result in low levels of these steroids, so ligands that bind to SHBG may release bound steroids into the bloodstream. Bioassay-guided fractionation of the sponge *Myrmekioderma granulatum* yielded the known terpene (+)-curcudiol as the active component. Five additional inactive compounds were isolated, including a new glycolipid and two new terpenes.

1.7 References

(1) Mahdi J.G.; Mahdi A.J.; Mahdi A.J.; Bowen I.D. *Cell Proliferation* **2006**, *39*, 147-155.

(2) Newman D.J.; Cragg G.M.; Snader K.M. *Journal of Natural products* **2003**, *66*, 1022-1037.

(3) Ramawat K.G. *Biotechnology of Medicinal Plants*; Science Publishers, Inc.: Enfield, NH, 2004.

(4) Cseke L.J.; Kirakosyan A.; Kaufman P.B.; Warber S.L.; Duke J.A.; Brielmann H.L. *Natural Products From Plants*; 2nd ed.; Taylor & Francis: New York, 2006.

(5) Trignali C. *Bioactive Compounds from Natural Sources: Isolation, Characterisation and Biological Properties*; Taylor & Francis: New York, 2001.

(6) Wani M.C.; Taylor H.L.; Wall M.E.; Coggon P.; McPhail A.T. *Journal of the American Chemical Society* **1971**, *93*, 2325-2327.

(7) Schiff P.B.; Fant J.; Horwitz S.B. *Nature* **277**, 665-667.

(8) McGuire W.P.; Rowinsky E.K.; Rosenheim N.B.; Grubine F.C.; Ettinger D.S.; Armstrong D.K.; Donnehower R.C. *Annals of Internal Medicine* **1989**, 273-279.

(9) Holmes F.A.; Walters R.S.; Theriault R.L.; Forman A.D.; Newton L.K.; Raber M.N.; Buzdar A.U.; Fyre D.K.; Hortobagyi G.N. *Journal of the National Cancer Institute* **1991**, *83*, 1797-1805.

(10) Duffin J *Canadian Bulletin of Medical History* **2000**, *17*, 155-192.

(11) Oberlies N.H.; Kroll D.J. *Journal of Natural products* **2004**, *67*, 129-135.

(12) Heinrich M.; Teoh H.L. *Journal of Ethnopharmacology* **2004**, *92*, 147-162.

(13) Deleu D.; Hanssens Y.; Northway M.G. *Drugs and Aging* **2004**, *21*, 687-709.

(14) Demain A.L. *Journal of Industrial Microbiology & Biotechnology* **2006**, *33*, 486-495.

(15) Chin Y.W.; Balumas M.J.; Chai H.B.; Kinghorn A.D. *The APPS Journal* **2006**, *8*, E239-E253.

(16) Tanaka H.; Kuroda A.; Marusawa H.; Hatanaka H.; Kino T.; Goto T.; Hashimoto M. *Journal of the American Chemical Society* **1987**, *109*, 5031-5033.

(17) Endo A. *Journal of Lipid Research* **1992**, *33*, 1569-1582.

(18) Frommer W.; Junge B.; Muller L.; Schmidt D.; Truscheit E. *Planta Medica* **1979**, *35*, 195-217.

(19) Wang J.; Soisson S. M.; Young K.; W. Shoop; Kodali S.; Galgoci A.; Painter R.; G. Parthasarathy; Tang Y. S.; Cummings R.; Ha S.; K. Dorso; Motyl M.; Jayasuriya H.; Ondeyka J.; Herath K.; Zhang C.; Hernandez L.; Allocco J.; Basilio P.; Tormo J. R.; Genilloud O.; Vicente F.; Pelaez F.; Colwell L.; Lee S. H.; Michael B.; T. Felcetto; Gill C.; Silver L. L.; Hermes J. D.; Bartizal K.; Barrett J.; Schmatz D.; Becker J. W.; Cully D.; Singh S. B. *Nature* **2006**, *441*, 358-361.

(20) Kwon H.C.; Kauffman C.A.; Jensen P.R.; Fenical W. *Journal of the American Chemical Society* **2006**, *128*, 1622-1632.

(21) Scherlach K.; Patida-Martinez L.P.; Dahse H.M.; Hertwick C. *Journal of the American Chemical Society* **2006**, *128*, 11529-11536.

(22) Roberge M.; Cinel B.; Anderson H.J.; Lim L.; Jiang X.; Xu L.; Bigg C.M.; Kelly M.T.; Andersen R.J. *Cancer Research* **2000**, *60*, 5052-5058.

(23) Haefner B. *Drug Discovery Today* **2003**, *8*, 536-544.

(24) Newman D.J.; Cragg G.M. *Current Medicinal Chemistry* **2004**, *11*, 1693-1713.

(25) Simmons T.L.; Andrianasolo E.; McPhail K.; Flatt P.; Gerwick W.H. *Molecular Cancer Therapeutics* **2005**, *4*, 333-342.

(26) Markman M. *The Oncologist* **2007**, *12*, 186-190.

(27) Taraboletti G.; Poli M.; Dossi R.; Manenti L.; Borsotti P.; Faircoth G.T.; Broggini M.; D'Incalci M.; Ribatti D.; Giavazzi R. *British Journal of Cancer* **2004**, *90*, 2771-2784.

(28) Diyabalanage T.; Amsler C.D.; McClintock J.B.; Baker B.J. *Journal of the American Chemical Society* **2006**, *128*, 5630-5631.

(29) Jiang X.; Liu B.; Lebreton S.; DeBradander J.K. *Journal of the American Chemical Society* **2007**, ASAP.

(30) Aoki S.; Watanabe Y.; Sanagawa M.; Satiawan A.; Kotoku N.; Kobayashi M. *Journal of the American Chemical Society* **2006**, *128*, 3148-3149.

(31) Noako Y.; Yoshida S.; Matsunaga S.; Shindoh N.; Terada Y.; Nagai K.; Yamashita J.K.; Ganesa A.; Soest R.W.M. van; Fuesetani N. *Angewandte Chemie* **2006**, *45*, 7553-7557.

(32) Robbers J.E.; Speedie M.K.; Tyler V.E. *Phamacognosy and Pharmacobiotechnology*; Williams & Wilkins: Baltimore, 1996.

(33) Mulzer J.; Bohlman R. *The Role of Natural of Natural Products in Drug Discovery*; Springer: New York, 2000.

(34) Newman D.J.; Cragg G.M. *Journal of Natural products* **2007**, *70*, 461-477.

(35) Cordell G.A. *Phytochemistry Reviews* **2002**, *1*, 261-273.

(36) Brastianos H.C.; Vottero E.; Patrick B.O.; Soest R. van; Matainaho T.; Mauk A.G.; Andersen R.J. *Journal of the American Chemical Society* **2006**, *128*, 16046-16047.

(37) Brastianos H.C.; Sturgeon C.M.; Roberge M.; Andersen R.J. *Journal of Natural Products* **2007**, *70*, 287-288.

Chapter 2: Isolation of Inhibitors of Indoleamine-2,3-dioxygenase (IDO) from the Marine Sponge *Neopetrosia exigua*[a]

2.1. Preview of Chapter 2

Tumor cells express high levels of IDO and use this enzyme to gain protection from T-cell attack.[1] The rationale for using IDO inhibitors as anti-cancer drugs would be to prevent tumor cells from evading the immune system, therefore, this enzyme is an attractive target for treating cancer.[2] This chapter will discuss the isolation and structure elucidation of inhibitors of IDO from the marine sponge *Neopetrosia exigua*.

2.2 Biology of Indoleamine-2,3-dioxygenase (IDO)

The vital indole amino acid L-tryptophan is necessary for the biosynthesis of proteins and several important secondary metabolites. A small part of the ingested tryptophan is converted to serotonin and melatonin. The majority of tryptophan digested from food is metabolized by the kynurenine pathway (Figure 2.2.1) which synthesizes nicotinamide, a key component in several co-enzymes such as NAD^+ and $NADP^+$.[3] The first and rate limiting step in the kynurenine pathway is the oxidative cleavage of the indole ring. This is catalyzed by either tryptophan-2,3-dioxygenase (TDO), which is mainly found in the liver, or

[a]: Reproduced in part with permission from Brastianos H.C.; Vottero E.; Patrick B.O.; Soest R. van; Matainaho T.; Mauk A.G.; Andersen R.J. *Journal of the American Chemical Society* **2006**, *128*, 16046-16047. Copyright 2006 American Chemical Society.

indoleamine-2,3-dioxygenase (IDO), which is found in the epididymis, thymus, gut, lung, placenta and dendritic cells.[4]

It has been shown that IDO plays an immunological function. Interferon-γ activation in cells such as macrophages induces the activity of IDO. Tryptophan is an essential amino acid for protein synthesis. Induction of IDO depletes local extracellular concentrations of tryptophan causing pathogens sensitive to tryptophan concentrations to arrest in G_1 of the cell cycle.[3] Pathogens suppressed by the lack of tryptophan include: *Chlamydia psittaci, C. trachomatis, C. pneumoniae, Staphylococcus aureus* and the measles virus.[4]

Mann and co-workers showed that there was an increased inclination for pregnant mice to lose their fetus when they were exposed to an inhibitor of IDO (1-methyl tryptophan).[5] Loss of IDO function resulted in increased T-cell attack on the fetus, thus, causing pregnancy failure. These results suggest that the placenta expresses IDO to protect itself from the maternal T-cell attack.[6]

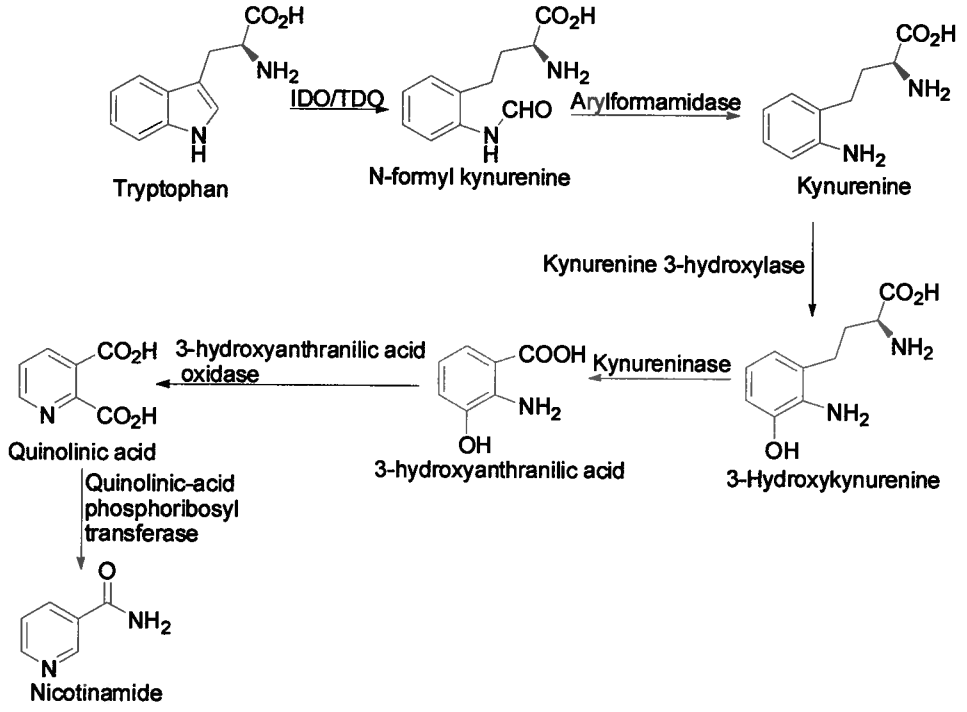

Figure 2.2.1. Kynurenine pathway (Adapted from Stone et al.).[7]

IDO also plays a critical role in the progression of cancer. Tumor cells expressing IDO are protected from attack by the killer T-cells of the host. Several molecular mechanisms explain the how tumors evade the immune system. One mechanism suggests that secondary metabolites in the kynurenine pathway are cytotoxic toward T-cells and are able to induce apoptosis.[8] T-cells are also sensitive to the local tryptophan concentration. IDO in cancer cells is able to deplete the concentration of tryptophan in the tumor environment, thus IDO is able to arrest T-cells in the G_1 phase of the cell cycle.[2] Tumor cells have adaptive mechanisms which are able to offset the low intracellular tryptophan concentrations and are able to continue to proliferate.[1] The importance of IDO in cancer stems from the fact that a large number of human tumors express IDO. Patients with tumors that express IDO in ovarian,[9] endometrial[10] and colorectal

cancer[11] have been found to have a poor prognosis for disease progression and overall survival.

The presence of IDO has also been confirmed in the lens of the eye.[12] Several key secondary metabolites that result from the kynurenine pathway are UV protection agents in the eye. The major UV filter is 3-hydroxykynurenine glucoside (3OHKG) which is specifically found in the lens of primates. Other UV filters from the kynurenine pathway include kynurenine (Kyn) and 3-hydroxykynurenine (3OHKyn). These small molecules protect the lens and the cornea by absorbing the harmful UV radiation between 300 and 400 nm.[13] Unfortunately, these compounds have also been found responsible for the undesirable yellowing of the lens and have been implicated in the formation of cataracts.[14] The mechanism that yields the coloration of the lenses begins with the spontaneous deamination of 3OHKG, Kyn or 3OHKyn to afford an α,β–unsaturated ketone. The cysteine residues in α–crystalin (the most abundant protein in the lens) covalently bind with the kynurenine metabolites in a Michael fashion. 3OHKyn oxidation, after forming adducts with α–crystalin, results in cross-linked and insoluble proteins which may play a role in the development of age-related nuclear cataracts (Figure 2.2.2).[15]

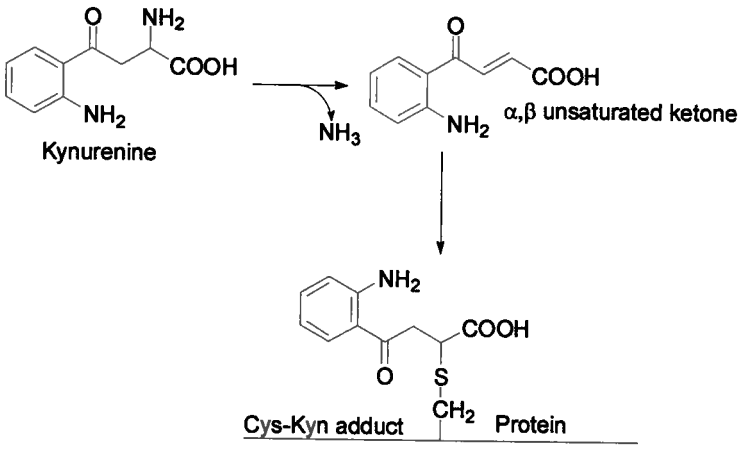

Figure 2.2.2. Mechanism of formation of adduct between α–crystalin and kynurenine (Adapted from Truscott).[15]

2.3 Inhibitors of IDO as Treatments for Cancer

Immune tolerance towards tumors is one of the hallmarks of cancer.[2] Cancer cells that express IDO are able to induce immune escape by inhibiting T-cell attack at the tumor site. Abrogators of IDO would enhance anti-tumor immunity by targeting the processes cancer cells use to evade T-cells. As a target for cancer, IDO is an attractive candidate. Knockout mice that have the gene for IDO removed are found to be viable and healthy, making it unlikely that IDO inhibitors will be highly toxic drugs.[2]

One strategy that was used to develop new inhibitors of IDO has involved synthesizing analogues of tryptophan or indole compounds. This is not surprising since the first step in the kynurenine pathway is the oxidative cleavage of the indole ring of tryptophan. The most common IDO inhibitors synthesized are compounds that have a substituent on the indole ring of tryptophan. These act as competitive inhibitors of IDO. Some of the more potent inhibitors with a

substituted indole ring include: 1-methyl tryptophan (**2.1**),[16] 7-fluoro tryptophan (**2.2**),[17] 5,7-difluoro tryptophan (**2.3**),[17] and methylthiohydantoin tryptophan (**2.4**).[18] All these inhibitors have K_i values ranging between 11-40 μM.

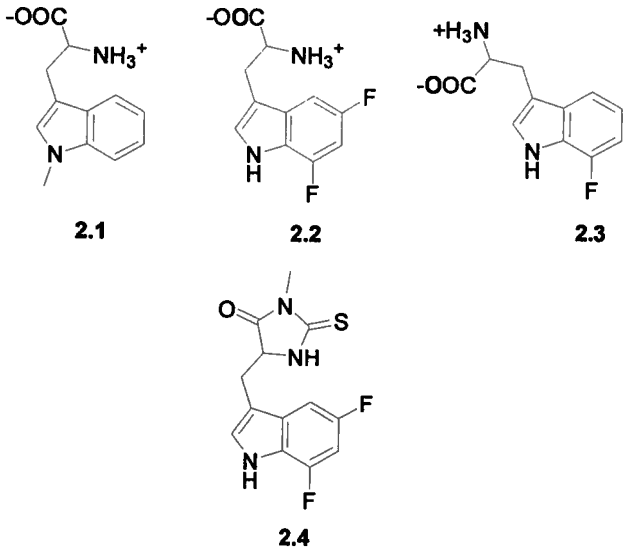

Figure 2.3.1. Analogs of tryptophan as competitive inhibitors of IDO.

Derivatives of β-carboline were found to be non-competitive inhibitors of IDO. The more active analogs of β-carboline include compounds **2.5** and **2.6**, which have K_i's of 3.3 and 7.4 μM, respectively.[19] Unfortunately, these compounds have unfavorable side effects in the central nervous system making them unlikely to be used for cancer treatment.[20]

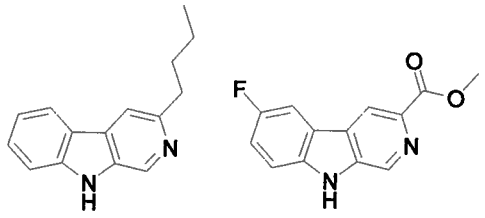

2.5 **2.6**

Figure 2.3.2. β-carbolines as inhibitors of IDO.

Among the most potent IDO inhibitors published to date are annulins A (**2.7**), B (**2.8**), and C (**2.9**) which have K_i's of 124, 140, and 690 nM, respectively. The annulins were isolated from a MeOH extract of the Northeastern Pacific marine hydroid *Garveia annulata*. These marine-derived polyketides contain a quinone moiety which appears to be essential for the activity.[21] The natural product brassinin (**2.10**) was identified as an IDO inhibitor and has a K_i of 97.7 μM.[22] A structure-activity relationship study was undertaken to determine which areas of the molecule are required for the inhibition of IDO. An unexpected finding was that the indole ring was not necessary to cause inhibition of IDO. It can be replaced with a wide range of aromatic substrates and still be able to prevent the activity of IDO. This may be a positive finding as indole compounds may cause neurological side effects.[22] Further synthetic experiments established that the dithiocarbamate moiety in brassinin was crucial for the biological activity. Finally, replacing the S-methyl group with an aromatic moiety such as naphthalene greatly increased the potency of brassinin.[22]

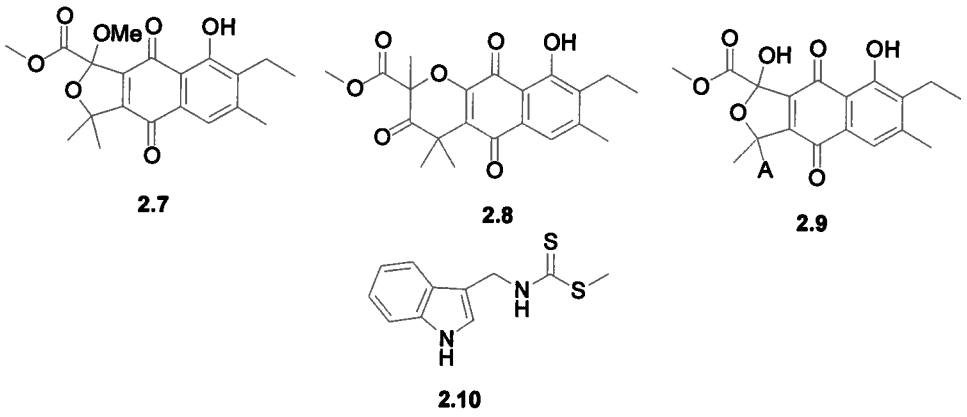

Figure 2.3.3. Isolated natural product IDO inhibitors.

The most widely used inhibitor of IDO is 1-methyl tryptophan (**2.1**). *In vitro* data show that 1-methyl tryptophan has a K_i of 34 μM. When 1-methyl tryptophan was used *in vivo* against the MMTV-Neu transgenic mouse model of breast cancer, very little inhibition of tumor growth was observed. Similarly, the use of paclitaxel did very little to slow down tumor growth in this particular mouse model.[18] Signficant tumor regression was observed when combining 1-methyl tryptophan with paclitaxel. This was also observed with other chemotherapeutic agents such as doxorubin, cisplatin and cyclophosphamide. Increased cytotoxicity towards cancer cells was not observed with other anti-cancer drugs such as 5-fluorouracil and methotrexate. These results indicate that IDO inhibitors can be used as adjuvants to enhance the efficacy of only certain chemotherapeutic drugs.[18] It is evident that combining IDO immunotherapy with chemotherapy is a potentially exciting new approach to cancer treatment.

Most of the studies done on 1-methyl tryptophan have used the racemic (R, S) mixture. One very recent study has compared the biological activity of the two enantiomers *in vitro* and *in vivo* to determine which of the two isomers would

be more effective in tumor regression.[23] The S-isomer of 1-methyl tryptophan was found to be more effective in inhibiting IDO *in vitro* using HeLa cells and the purified enzyme. The R-isomer was found to be significantly more effective than the S-isomer when combining IDO immunotherapy with chemotherapy in mouse models of melanoma and breast cancer. Because of the greater efficacy of the R-isomer *in vivo*, it is more likely that R-1-methyl tryptophan would be more appropriate for human clinical trials.[23]

2.4 Pyrroloquinones from Marine Sources

Marine derived alkaloids from the pyrroloiminoquinone family are characterized by their biological activity. The first example of this family from a marine source was discorhabdin C (**2.11**), which was isolated from a marine sponge of the genus *Latrunculia* collected in New Zealand. Discorhabdin C was found to be a potent cytotoxin toward P-388 murine leukemia cells with an IC_{50} of 40 ng/mL.[24] Furthermore, discorhabdin C was found to be an antibacterial agent with activity against both Gram-positive and Gram-negative bacteria.[25] The dischorhabdin family is characterized by an iminoquinone with a spiro cyclohexanone. Later, the structures of discorhabdin A (**2.12**), B (**2.13**), and D (**2.14**) were elucidated and these compounds were found to be potent cytotoxins against P-388 murine leukemia cells as well. These alkaloids had an additional sulfur containing ring.[25] More recently, the first discorhabdin dimer, discorhabdin W (**2.15**), was discovered and its biological activity was equivalent to that of discorhabdin B.[26] Epinardins A-D are very similar to the discorhabdins. However, the epinardins contain an allylic alcohol rather than an unsaturated

ketone. Epinardin C (**2.16**) displayed the most toxicity against murine leukemia cells with an IC_{50} of 0.32 μg/mL.[27]

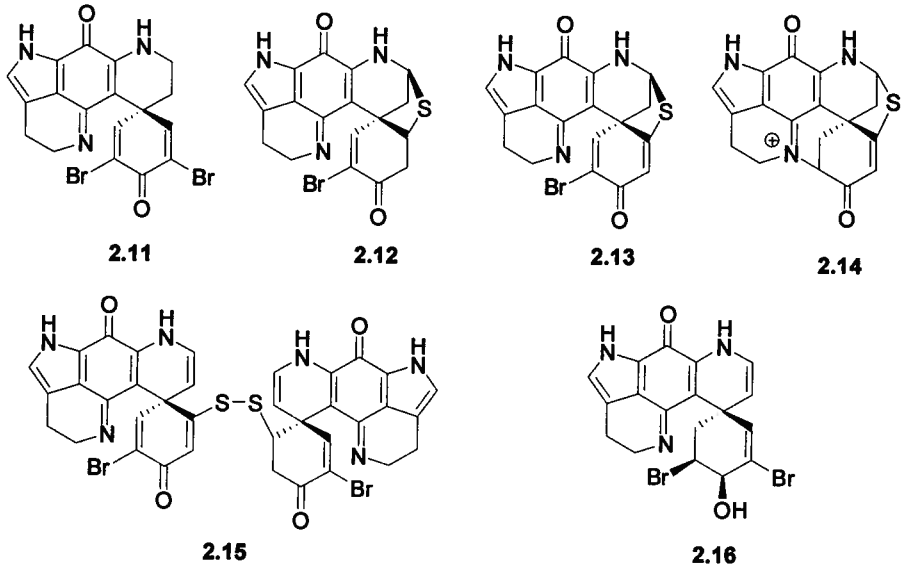

Figure 2.4.1. The discorhabdins and the epinardins.

Batzellines A (**2.17**), B (**2.18**) and C (**2.19**) were discovered in 1980 by Sakemi et al. from the sponge *Batzella* sp. collected in the Carribean.[28] Initially, no biological activity was found for these compounds, but later batzelline A was found to be cytotoxic against non-small cell lung carcinoma A-549 cells.[29] More recently, isobatzellines A-D (**2.20-2.23**) were discovered as being cytotoxic against P388 murine leukemia cells (IC_{50} = 0.42-20 μg/mL), and having anti-fungal activity against *Candida albicans* (MIC = 3.1-50 μg/mL).[30] Other structures related to the batzellines were the secobatzellines A (**2.24**) and B (**2.25**) isolated from *Batzella* sp.. Secobatzelline A was found to be a potent inhibitor of calcineurin and was one of the few known compounds to have nM potency against this target.[31] This particular group of secondary metabolites have a bicyclic core, while the batzellines and the isobatzellines are tricyclic. Damirones

A (**2.26**) and B (**2.27**) were isolated from the Palauan sponge *Damiria* sp. and have similar structures to the batzellines.[32]

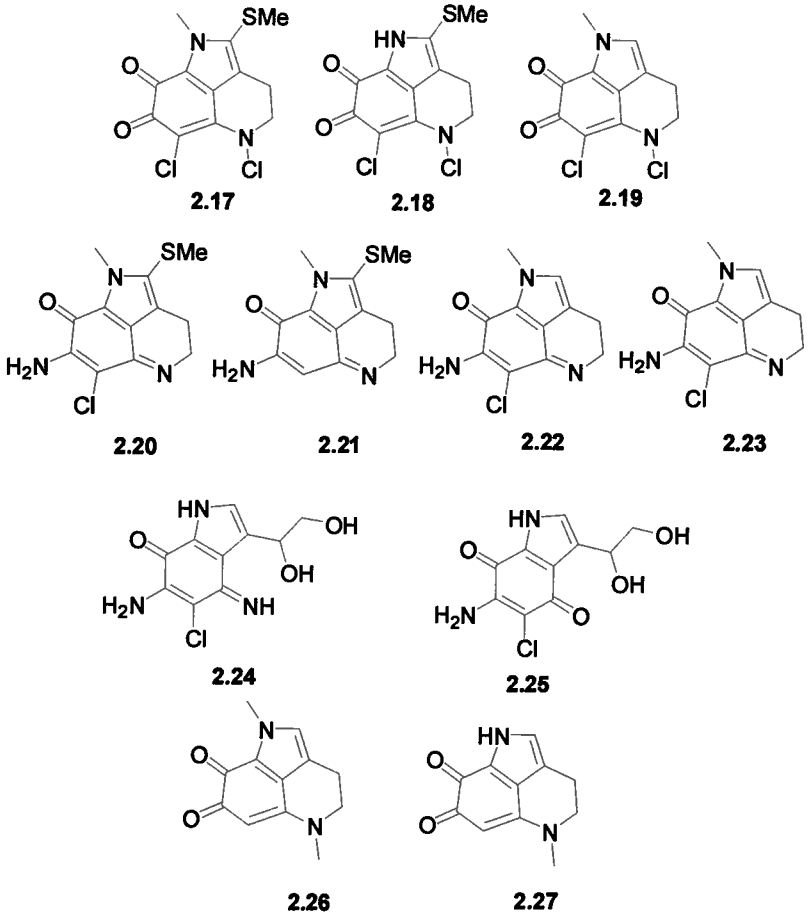

Figure 2.4.2. Batzelline family of natural products.

Makaluvamines A-F (**2.28-2.33**) were first isolated from *Zyzza fuliginosa*. These pyrroloiminoquinones have potent *in vitro* activity against the human colon tumor cell line HCT-116 and can inhibit topoisomerase II *in vitro*.[33] The makaluvamines were isolated along with the discorhabdins, indicating that a biosynthetic relationship may be present.[33] The pyrroloquinone veiutamine (**2.34**) along with makaluvamines A-D were isolated from *Zyzza fuliginosa* collected in Fiji.[34] Veiutamine (**2.34**) has a unique substitution pattern compared with

makaluvamine D, however, it was shown to be seven times more potent than makaluvamine D against the human colon tumor cell line HCT-116.[34]

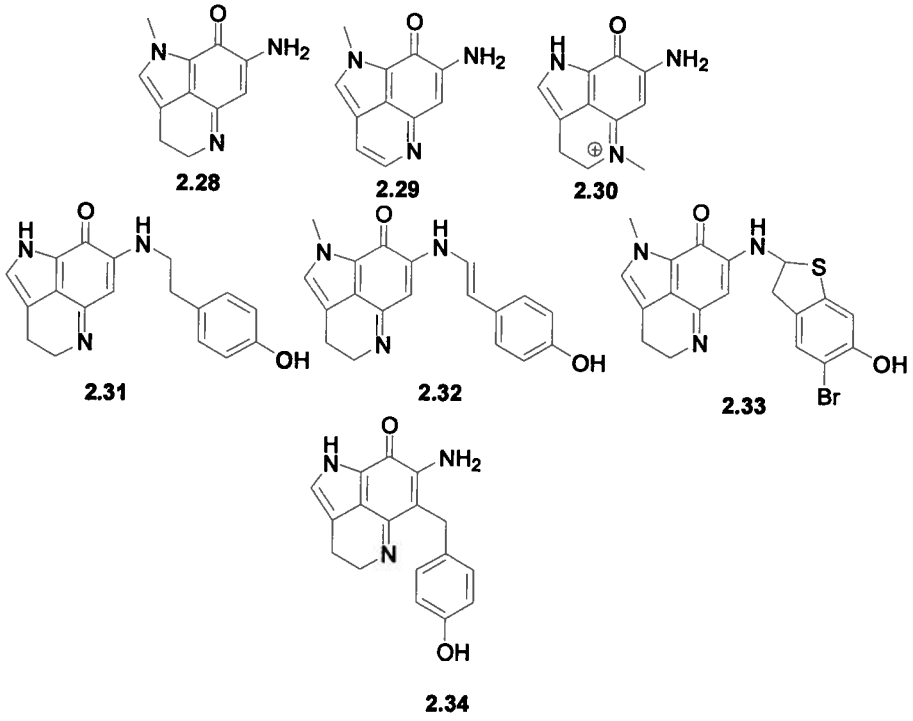

Figure 2.4.3. Makaluvamines and veiutamine.

Makaluvic acids A (**2.35**) and B (**2.36**) were first isolated from the sponge *Zyzzya fuliginosa*.[35] These compounds can be seen as the oxidation products of the batzellines, isobatzellines, and the makavulamines. Keyzers et al. isolated N-1-β-D-ribofuranosylmakaluvic acid C (**2.37**) from *Strongylodesma aliwaliensis* and it was found to have moderate activity against esophageal cancer cells (IC_{50} = 61 μg/mL).[36]

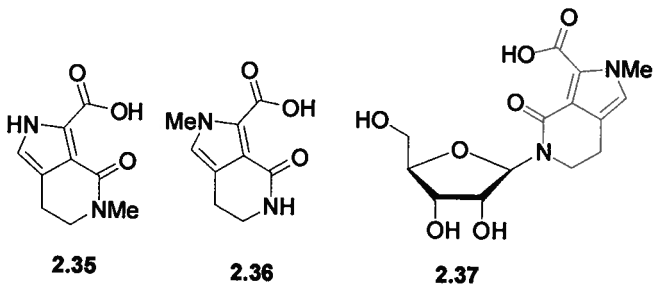

2.35 **2.36** **2.37**

Figure 2.4.4. Makaluvic Acids.

Wakayin (**2.38**), isolated from the ascidian *Clavelina* sp., is an example of a bispyrroloiminoquinone. It was reported to be cytotoxic against the human colon tumor cell line HCT-116 (IC_{50} = 0.5 μg/mL), an inhibitor of topoisomerase II, and a antimicrobial agent against *Bacillus subtillus* (MIC = 0.3 μg/mL).[37] Tsitsikammamines A (**2.39**) and B (**2.40**) were isolated from a South African Latrunculid sponge.[38] These compounds are also examples of bispyrroloquinones, but contain a phenol ring rather than the indole ring that is present in wakayin. Studies have shown that tsitsikammamines have antimicrobial activity, cytotoxicity to tumor cells, and antifungal activity, however, these compounds do not inhibit topoisomerase II.[38] More recently, the zyzzyanones A-D (**2.41-2.44**)[39,40] were isolated from the Australian sponge, *Zyzzya fuliginosa*. These bispyrroloquinones were found to lack the imine present in both the wakayins and the tsitsikammamines. All of the zyzzyanones were found to have moderate cytotoxicity against Ehrlich carcinoma cells (IC_{50} 25 μg/mL). This may indicate that the presence of the imine is vital for the cytotoxic activity of the pyrroloimminoquinones.[33,35]

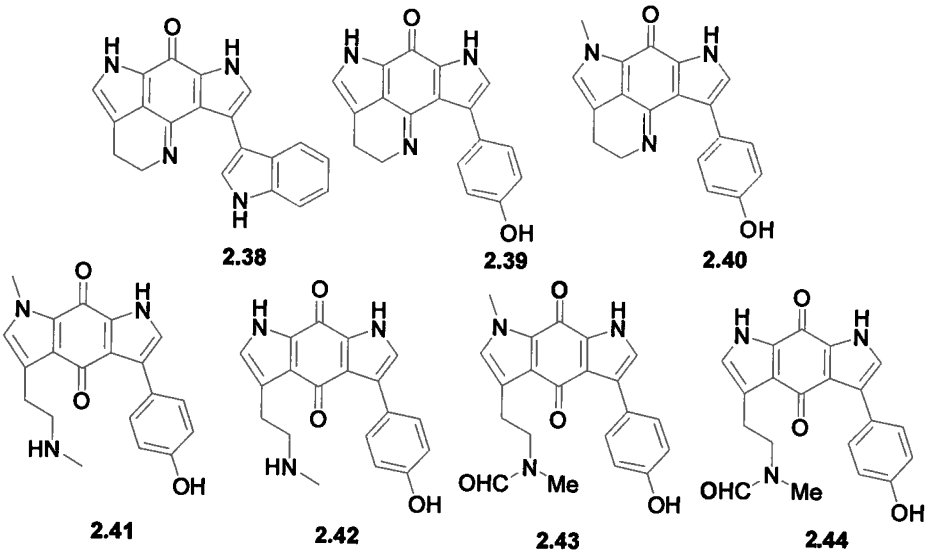

Figure 2.4.5. Bispyrroloquinones from marine sources.

2.5 Alkaloids isolated from *Neopetrosia* sp.

Neopetrosia and *Xestospongia* are two very similar genera of sponges with *Xestospongia* skeletons being composed of large spicules while *Neopetrosia* has smaller spicules.[41] In 2002, it was decided that *Xestospongia exigua* and *Neopetrosia exigua* were in fact the same species. *Xestospongia/Neopetrosia exigua* is a reddish brown sponge mainly found in the shallow tropical waters of the Indo-West Pacific. This species lives in colonies of up to 1 m^3 in size.[42,43]

The first alkaloids isolated from *Xestospongia/Neopetrosia exigua* were xestospongins A-D (**2.45-2.48**).[44] These quinolizidine alkaloids were isolated from a sponge collected in Australia. Their structures were determined using NMR and X-ray crystallography and they were found to be *in vivo* vasodilators.[44] Other similar quinolizidine alkaloids include the araguspongines A, C, K, and L (**49-52**) which were isolated from *N. exigua* collected in the Red sea. No

biological activity was reported for araguspongine K (**2.51**) and L (**2.52**), however, araguspongine C (**2.50**) had anti-parasitic activity against *Plasmodium falciparum*, as well as antituberculosis activity against *Mycobacterium tuberculosis*.[45] Araguspongine M (**2.53**) was isolated from *N. exigua* collected in Palau. This alkaloid showed cytotoxic activity against the human leukemia cell line HL-60 with an IC_{50} value of 5.5 μM, but did not show any anti-bacterial activity.[42] Xestosin A (**2.54**) was isolated from a *N. exigua* sample collected in Papua New Guinea. No biological activity was reported for this compound.[46]

Bioassay guided fractionation of a sample of a MeOH extract of *N. exigua* from Papua New Guinea yielded neoamphimedine (**2.55**) and 5-methoxyneoamphimedine (**2.56**).[47] These bisannulated acridines were found to be cytotoxic against murine cancer cells.[47] Other compounds isolated from *N. exigua* include the motuporamines. These heterocyclic alkaloids were isolated from an extract of *N. exigua* collected in Papua New Guinea. Biological studies revealed that these alkaloids are anti-angiogenic compounds with the most potent angiogenic inhibitor being motuporamine C (**2.57**).[48]

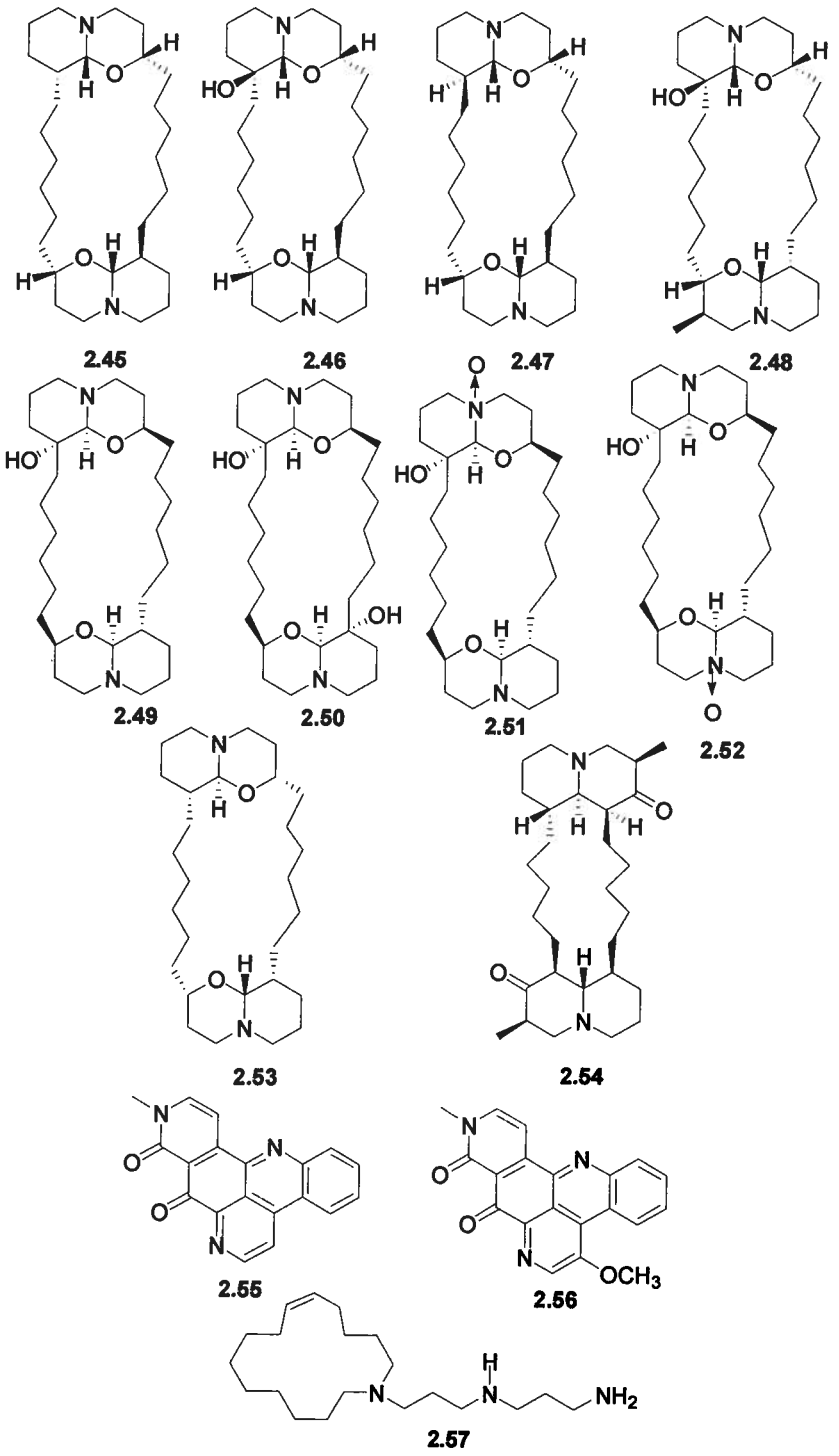

Figure 2.5.1. Alkaloids isolated from *Xestospongia/Neopetrosia exigua.*

2.6 Isolation of exiguamines A and B

Neopetrosia exigua (Figure 2.6.2) was collected by hand using SCUBA from Milne Bay in Papua New Guinea. A MeOH extract of the sponge was suspended in H_2O, and then sequentially partitioned with EtOAc and with *n*-butanol. The active butanol extract was subjected to size exclusion chromatography, flash reversed-phase column chromatography, gradient reversed-phase HPLC and isocratic reversed phase HPLC to yield exiguamine A (**2.58**) and exiguamine B (**2.59**) (Figure 2.6.1). For full experimental details, see Section 2.13.

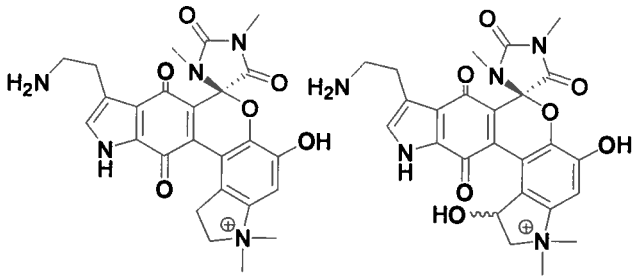

2.58 **2.59**

Figure 2.6.1. Secondary metabolites isolated from *Neopetrosia exigua*.

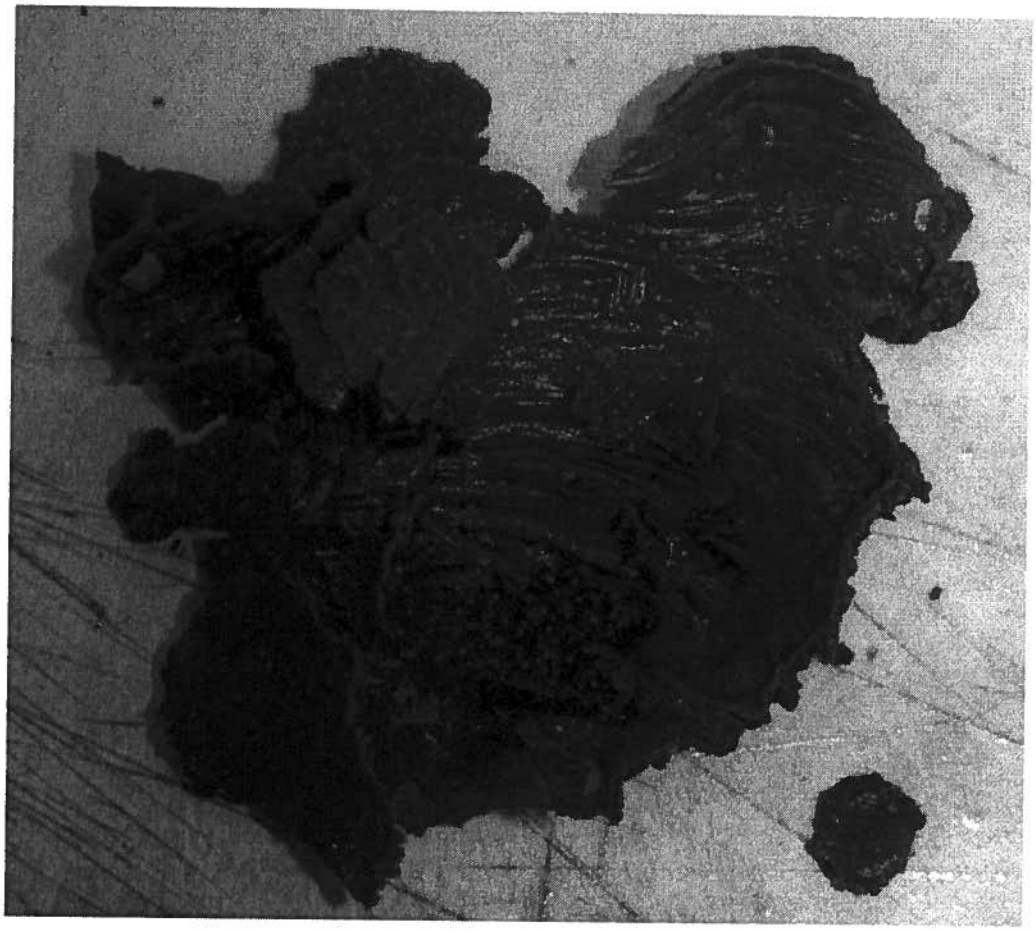

Figure 2.6.2 *Neopetrosia exigua* collected in Papua New Guinea.

2.7 Structure Elucidation of exiguamine A

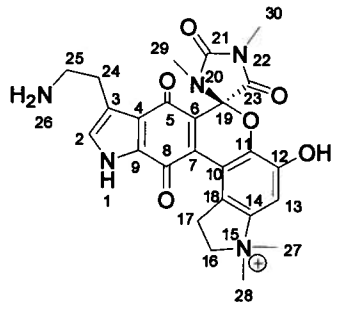

Figure 2.7.1. Numbering Scheme for exiguamine A.

Exiguamine A gave a $[M]^+$ ion at *m/z* 492.1883 in the HRESIMS indicating a molecular formula of $C_{25}H_{26}N_5O_6$ (calc'd 492.1883). The LRESIMS measurement in MeOH yielded a molecular ion peak at *m/z* 492.2, while the LRESIMS measurement in MeOD afforded a molecular ion peak at *m/z* 496.2, demonstrating that four exchangeable protons are present. The ^1H NMR spectrum (Figure 2.7.3) of exiguamine A acquired in DMSO-d_6 at 600 MHz displayed an indole proton (δ_H 13.10), a phenolic proton (δ_H 10.42), two amine protons (δ_H 7.82), two protons connected to sp^2 hybridized carbons (δ_H 7.52 and 7.30), and a series of methine and methyl protons connected to sp^3 hybridized carbons attached to either a nitrogen or an sp^2 hybridized carbon (δ_H 2.44-4.17). The ^{13}C NMR spectrum (Figure 2.7.4) indicated the presence of 25 carbons, confirming that no symmetry was present. The DEPT and the HMQC data (Figures 2.7.5 and 2.7.6) indicated four carbonyls (δ_C 179.7, 173.0, 168.4, 154.5), 11 quaternary carbons (δ_C 146.5, 142.8, 142.7, 138.8, 131.6, 130.5, 122.8, 121.3, 120.7, 114.7, 85.4), two methines (δ_C 126.5, 108.7), four methylenes (δ_C 67.4, 38.3, 28.5, 23.3), and four methyls (δ_C 54.3, 53.2, 26.0, 25.2). The ^1H, ^{15}N

LR-HMQC spectrum (Figure 2.7.9), which was referenced to an external standard of CH_3NO_2, revealed five nitrogens (δ_N -349, -310, -275, -248 and -218). After using HMQC to assign proton resonances to their respective carbon atoms (Table 2.7.1), it was possible to deduce three substructures (**I**, **II**, **III**, Figure 2.7.2) from the HMBC (Figure 2.7.7), COSY (Figure 2.7.8), and ^1H, ^{15}N LR-HMQC spectra.

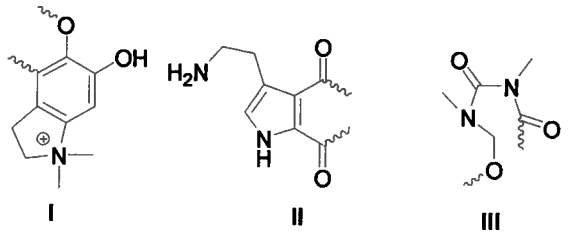

Figure 2.7.2. Three substructures of exiguamine A.

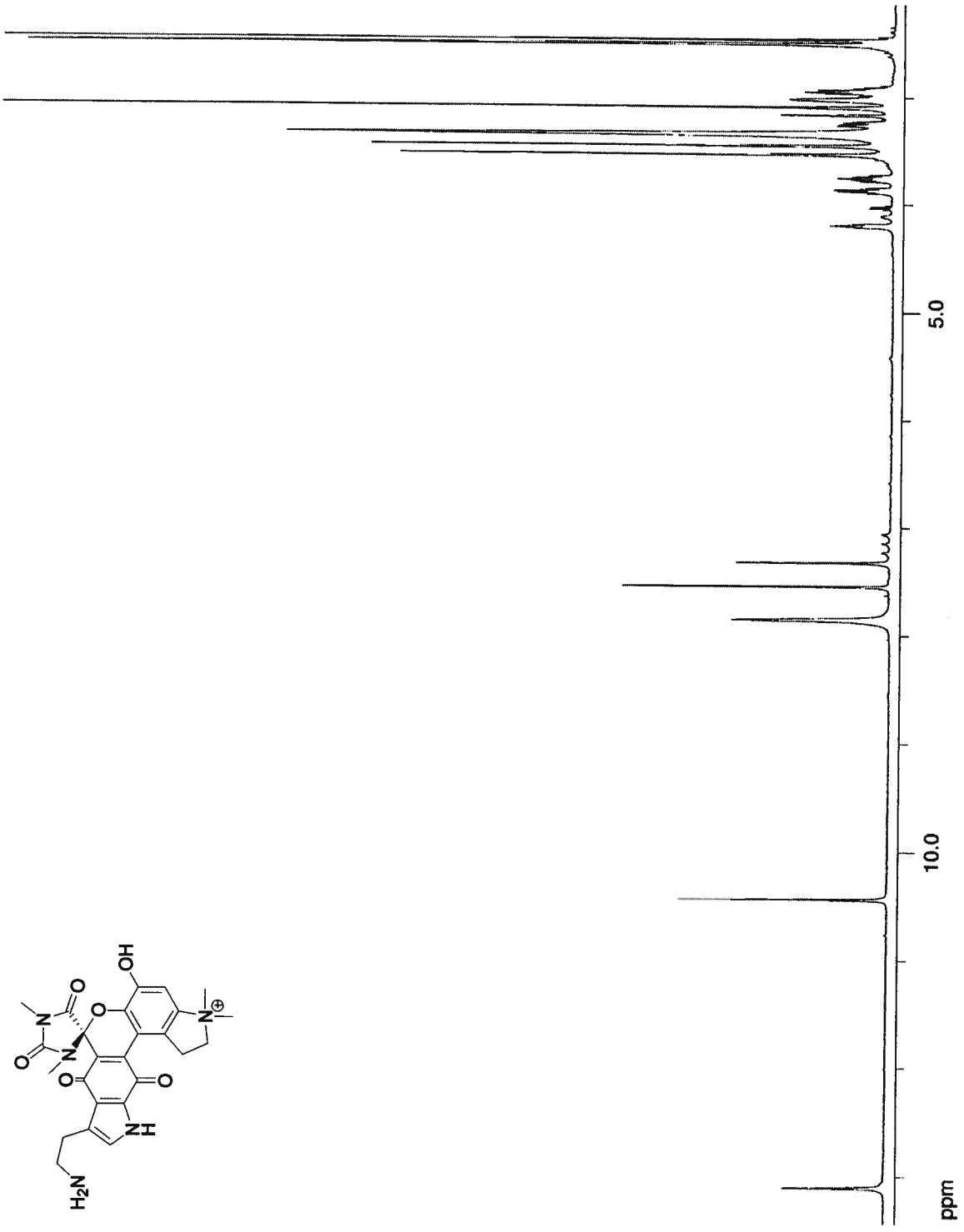

Figure 2.7.3. ^{1}H NMR spectrum of exiguamine A (**2.58**) acquired at 600 MHz in DMSO-d_6.

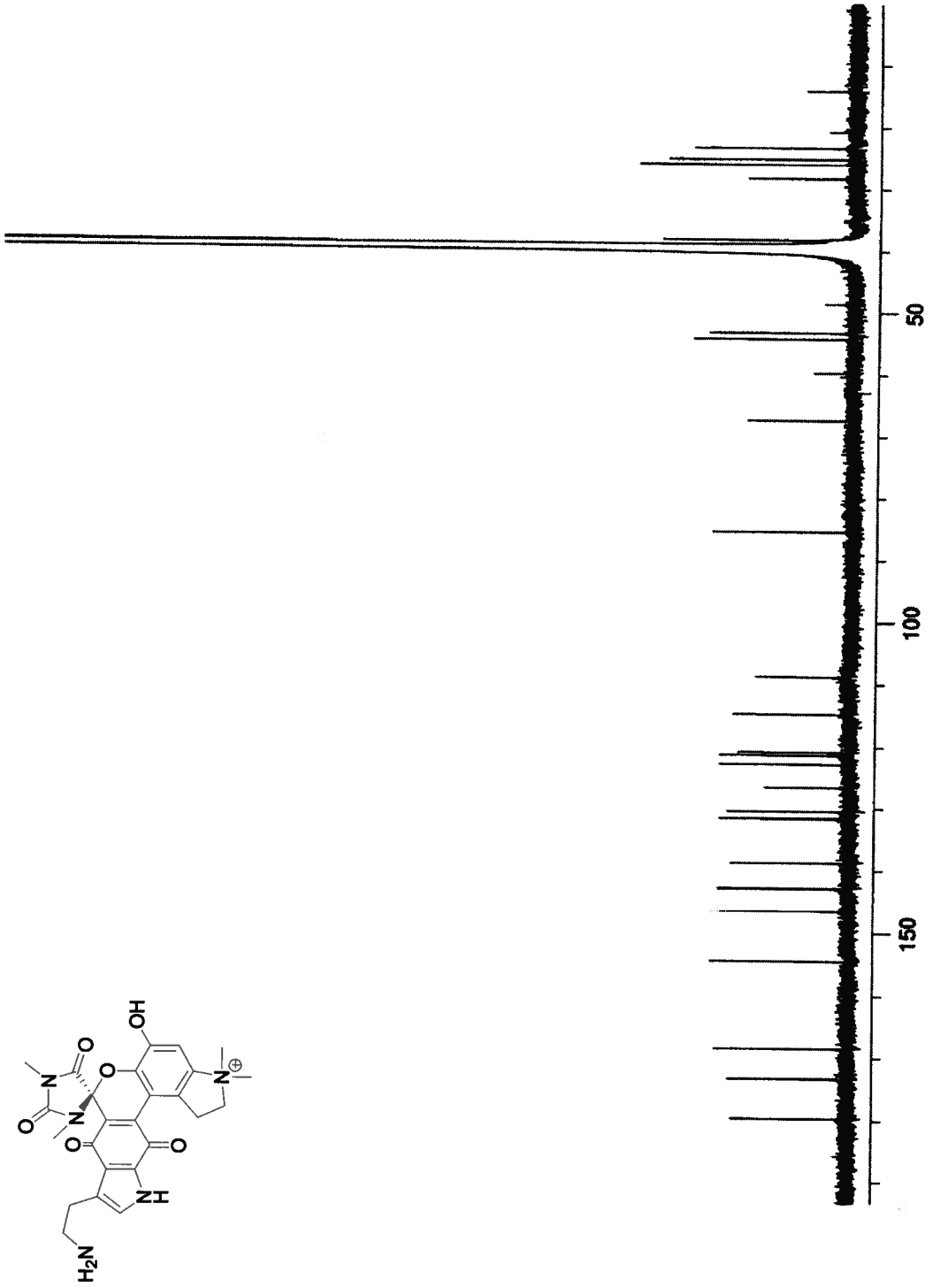

Figure 2.7.4. ^{13}C NMR spectrum of exiguamine A (**2.58**) acquired at 150 MHz in DMSO-d_6.

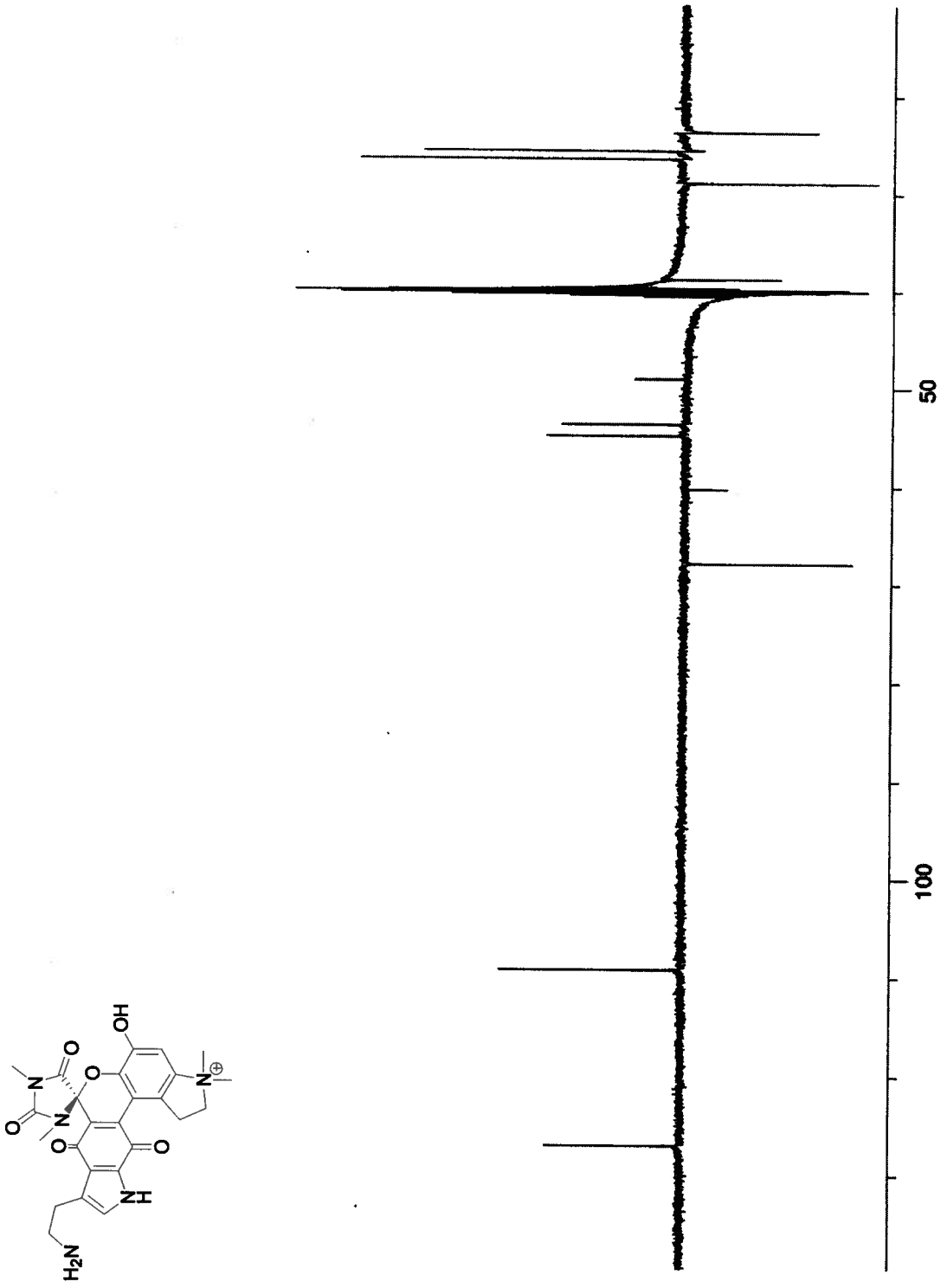

Figure 2.7.5. DEPT spectrum of exiguamine A (**2.58**) acquired at 150 MHz in DMSO-d_6

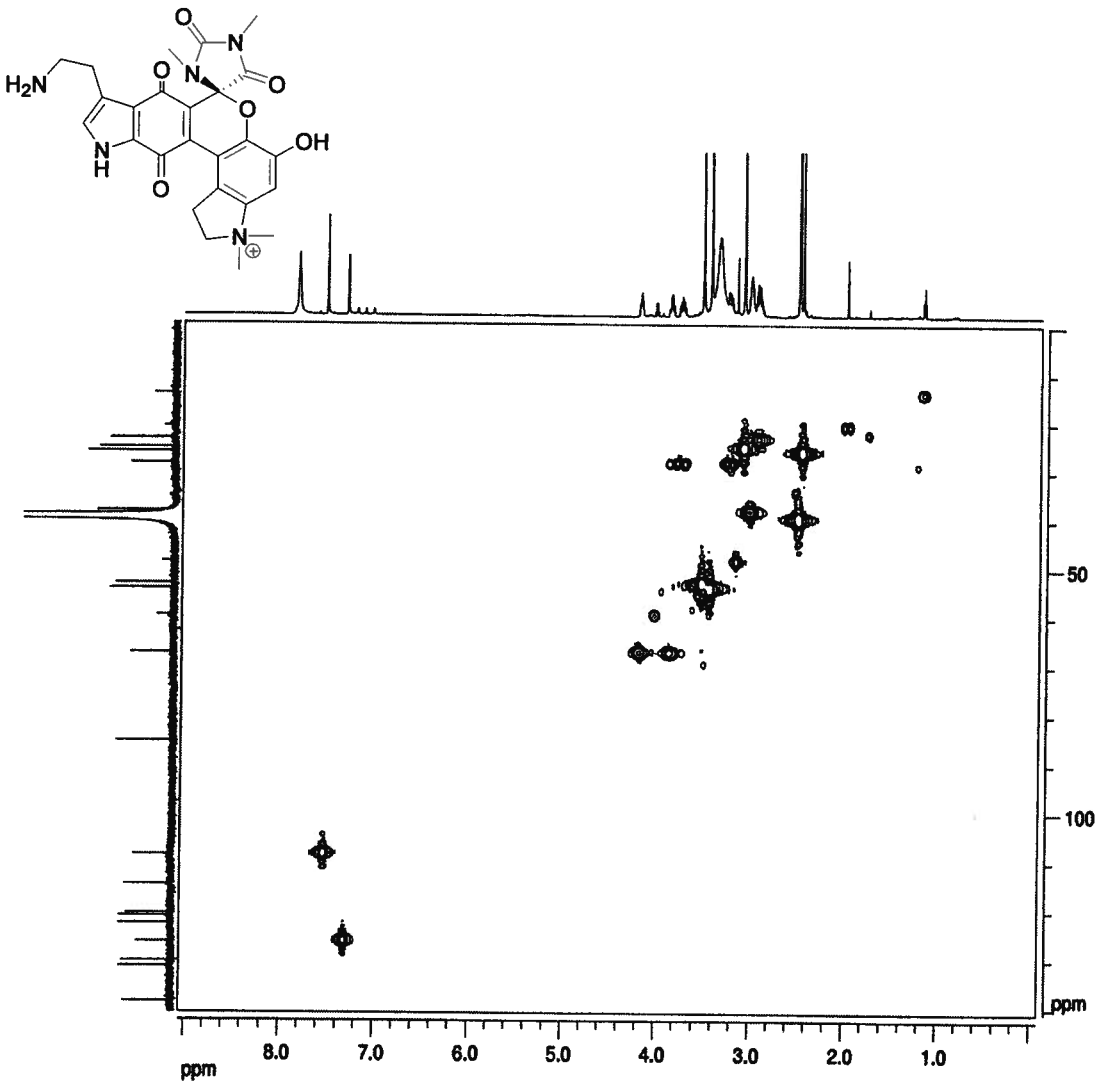

Figure 2.7.6. HMQC spectrum of exiguamine A (**2.58**) acquired at 600 MHz in DMSO-d_6.

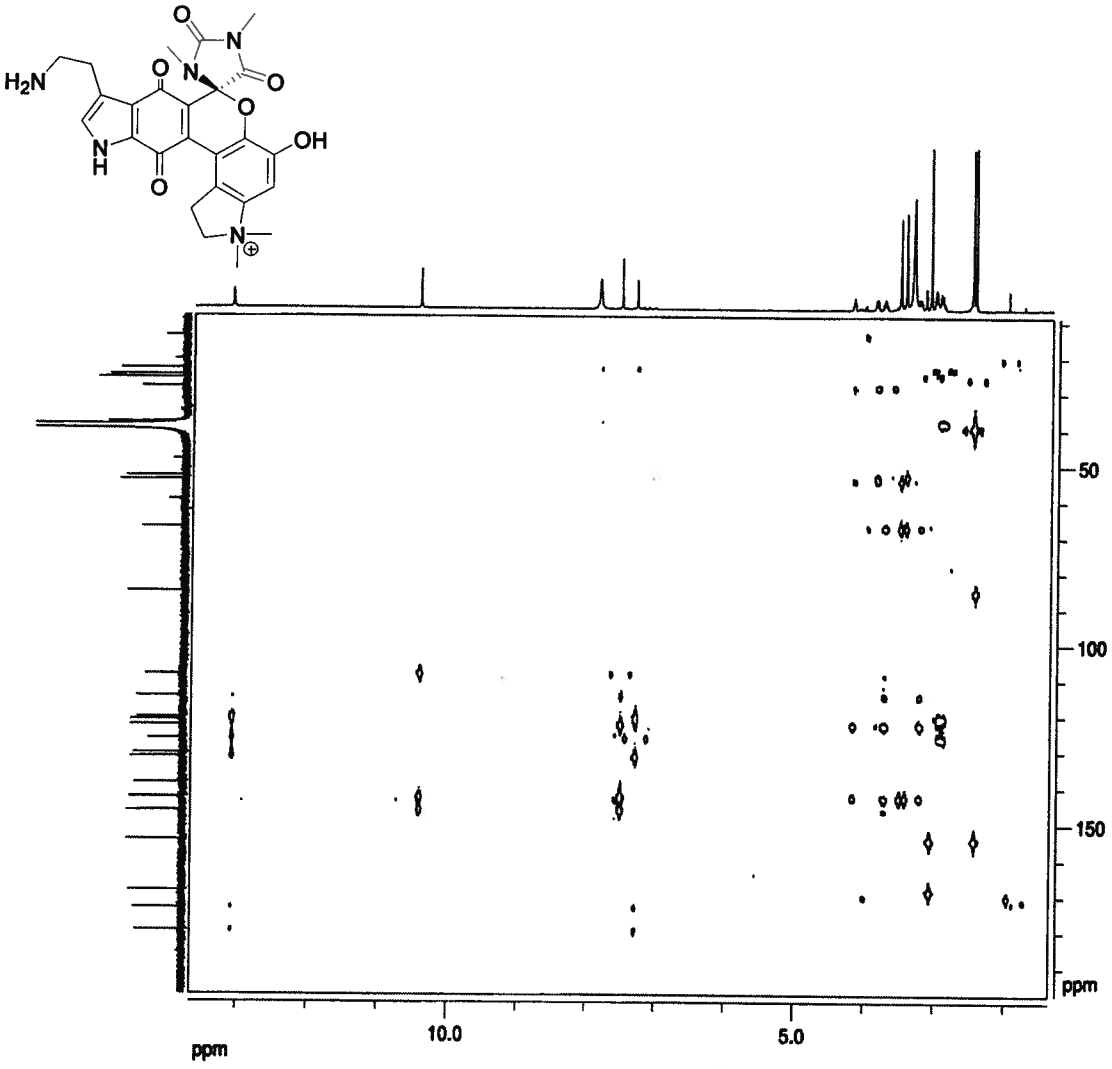

Figure 2.7.7. HMBC spectrum of exiguamine A (**2.58**) acquired at 600 MHz in DMSO-d_6.

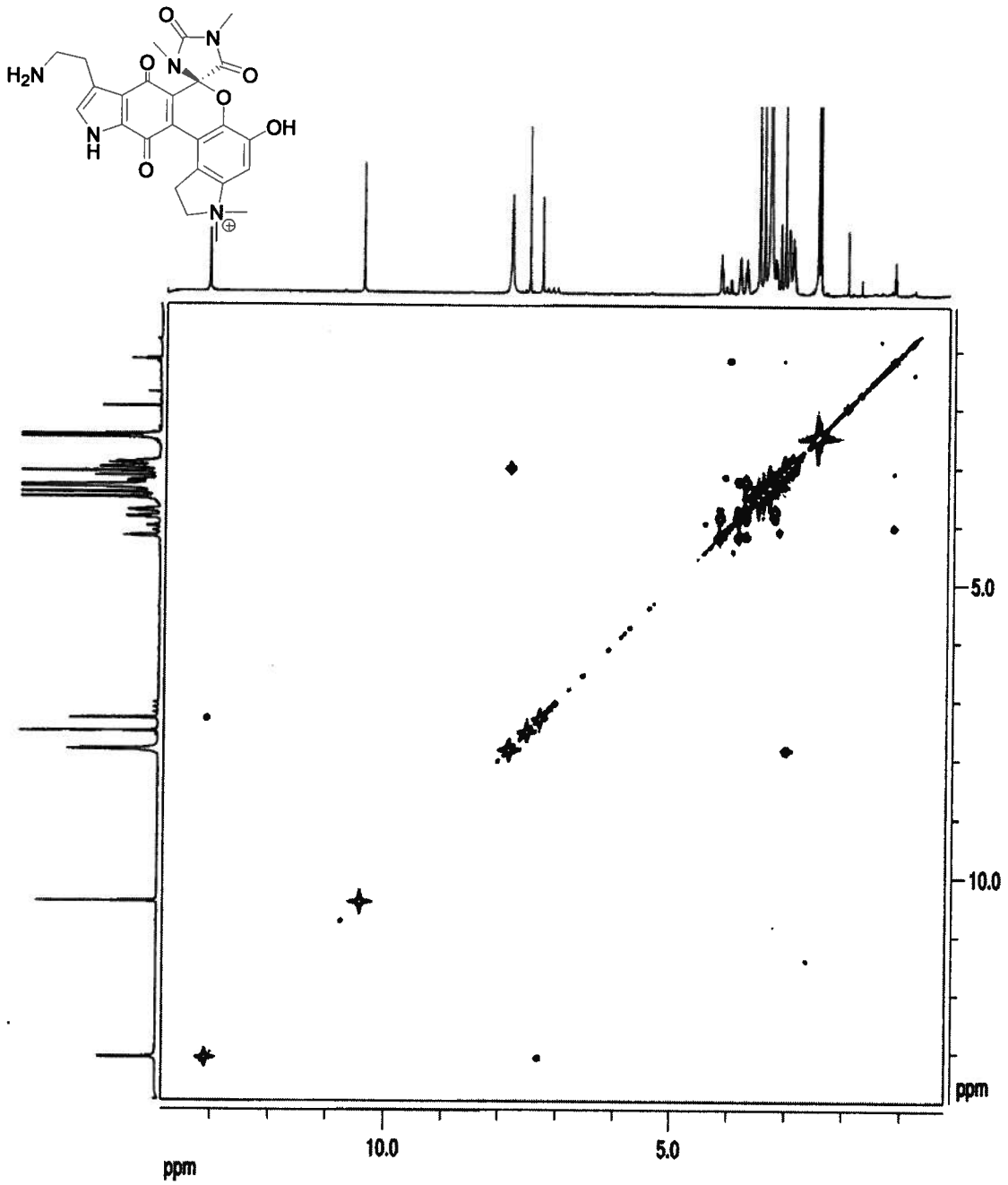

Figure 2.7.8. COSY spectrum of exiguamine A (**2.58**) acquired at 600 MHz in DMSO-d_6.

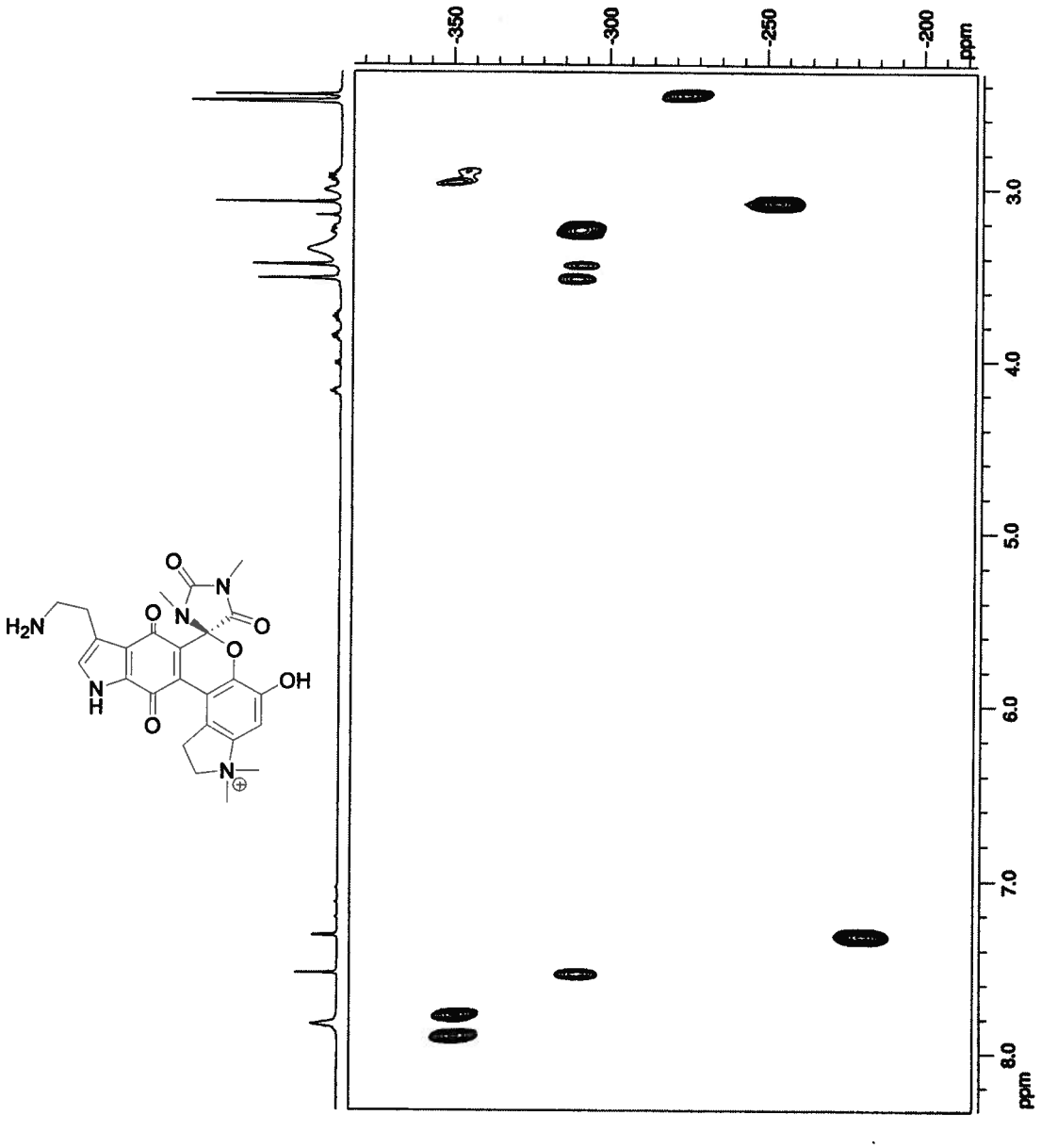

Figure 2.7.9. ^{1}H, ^{15}N LR-HMQC spectrum of exiguamine A (**2.58**) acquired at 600 MHz in DMSO-d_6.

Table 2.7.1. 1D and 2D NMR data for Exiguamine A. [a]

Position	δ_C	δ_N [b]	δ_H (*J* in Hz)	^1H, ^{13}C-HMBC	^1H, ^{15}N-HMQC	COSY
1		-218	13.10, brs	C-2, C-3, C-4 C-5, C-8, C-9		H-2
2	126.5		7.30, d, (2.2)	C-3, C-4, C-5, C-8, C-9, C-24	N-1	H-1
3	120.7					
4[c]	121.3					
5[d]	179.7					
6	126.5					
7	138.8					
8[d]	173.4					
9[c]	131.6					
10	114.7					
11	146.5					
12[e]	142.7					
13	108.7		7.52, brs	C-10, C-11, C-12, C-14, C-18	N-15	
14[e]	142.8					
15		-310				
16	67.4		3.84, q, (10.8)	C-17,C-18, C-27, C-28		H-16a, H-17b
16b			4.17, t, (8.6)	C-14, C-17, C-18, C-28		H-16b, H-17a
17	28.5		3.22, bdd (16.9, 7.5)	C-10, C-14, C-16, C-18	N-15	H-16a, H-17b

Position	δ_C	δ_N[b]	δ_H (*J* in Hz)	^1H, ^{13}C-HMBC	^1H, ^{15}N-HMQC	COSY
17b			3.73, m	C-10, C-13, C-14, C-16, C-18		
18	122.8					
19	85.4					
20		-275				
21	154.5					
22		-248				
23	168.6					
24a	23.3		2.92, m[f]	C-2, C-3, C-25	N-26	
24b			3.02, m[f]	C-2, C-3, C-25		
25	38.3		2.99, m	C-3, C-24	N-26	
26		-349	7.82, br			
27[g]	54.3		3.43, s	C-14, C-16, C-28	N-15	
28[g]	53.2		3.51, s	C-14, C-16,C-27	N-15	
29	26.0		2.44, s	C-19, C-21	N-20	
30	25.2		3.07, s	C-21, C-23	N-22	
12-OH			10.42, brs	C-11, C-12, C-13		

[a] ^1H and ^{13}C chemical shifts [ppm] are referenced to DMSO-d_6 (δ_H 2.50 and δ_C 39.51 ppm respectively)

[b] The ^{15}N spectrum was not calibrated with an external standard. The δ value has an accuracy of about 1ppm in reference to CH_3NO_2 (0 ppm).

[c] C4 and C9 are interchangeable signals

[d] C5 and C8 are interchangeable signals

[e] C12 and C14 are interchangeable signals

[f] H24a and H24b are interchangeable proton chemical shifts

[g] C27 and C28 are interchangeable signals

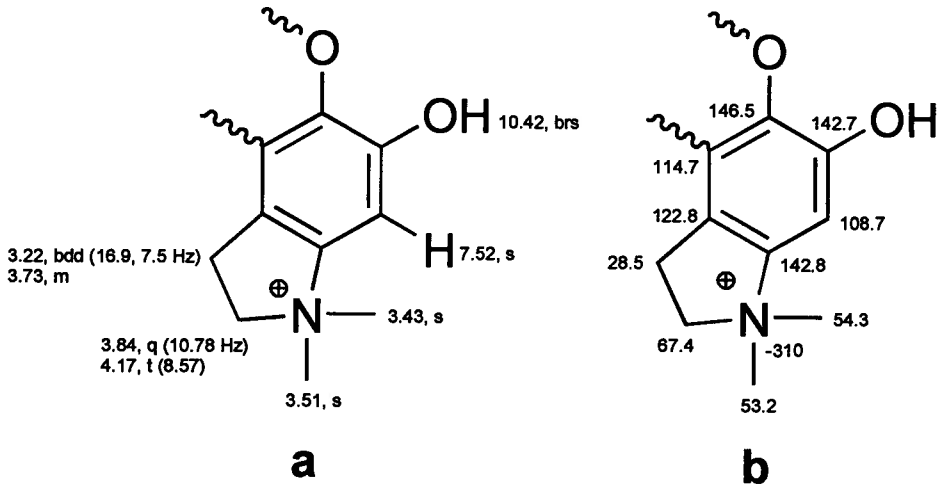

Figure 2.7.10. (**a**) ^{1}H and (**b**) ^{13}C and ^{15}N chemical shifts of substructure **I** of exiguamine A (**2.58**).

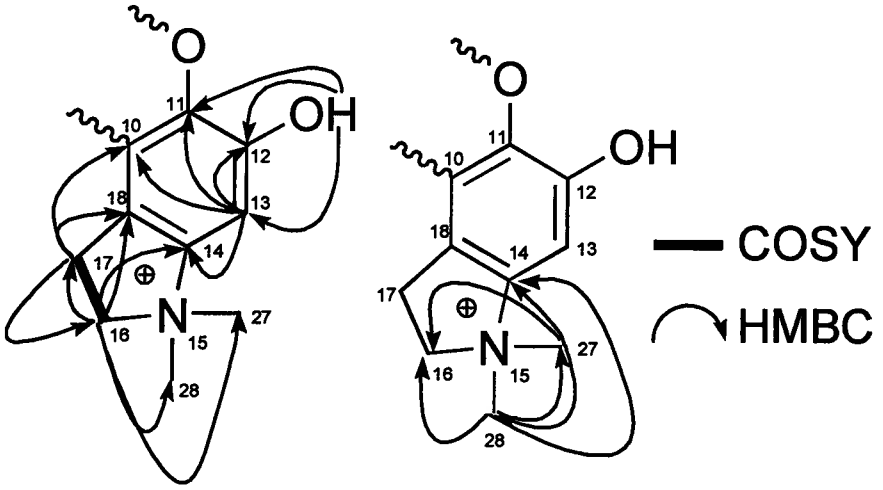

Figure 2.7.11. Key HMBC and COSY correlations of substructure **I** exiguamine A (**2.58**).

Two singlet proton resonances at δ_H 3.43 (H-27: HMQC to δ_C 54.3) and δ_H 3.51 (H-28: HMQC to δ_C 53.2) displayed ^{1}H, ^{15}N, LR-HMQC correlations to the nitrogen resonance at δ_N -310 (N-15) (Figure 2.7.12). HMBC correlations were observed between the proton resonance at δ_H 3.42 (H-27) and the carbon resonance at δ_C 53.2 (C-28). An additional HMBC correlation between the proton

resonance at δ_H 3.51 (H-28) and the carbon resonance at δ_C 53.2 (C-28) implied that Me-27 and Me-28 were geminal, and their chemical shifts indicated that they were attached to nitrogen (N-15). Both the proton resonances at δ_H 3.42 (H-27) and δ_H 3.51 (H-28) showed HMBC cross-peaks to the sp^2 hybridized carbon resonance at δ_C 142.8 (C-14), which confirmed the linkage between the C-14 (δ_C 142.8) and N-15 (δ_N -310) (Figures 2.7.10 and 2.7.11). Three bond HMBC correlations between the proton resonances at δ_H 3.42 (H-27) and δ_H 3.51 (H-28) and the methylene carbon resonance at δ_C 67.4 (C-16) established the bond between C-16 (δ_C 67.4) and N-15 (δ_N -310). Both methylene proton resonances at δ_H 3.84 (H-16a: HMQC to δ_C 67.4) and δ_H 4.17 (H-16b: HMQC to δ_C 67.4) showed COSY correlations to the proton resonances at δ_H 3.22 (H-17a: HMQC to δ_C 28.5) and δ_H 3.73 (H-17b: HMQC to δ_C 28.5), which assigned C-16 (δ_C 67.4) next to C-17 (δ_C 28.5) (Figure 2.7.13). All four proton resonances at δ_H 3.84 (H-16a), δ_H 4.17 (H-16b), δ_H 3.22 (H-17a) and δ_H 3.73 (H-17b) showed HMBC correlations to the aromatic carbon resonance at δ_C 122.8 (C-18). This determined the connectivity between C-17 (δ_C 28.5) and C-18 (122.8). Three proton resonances at δ_H 4.17 (H-16b), δ_H 3.22 (H-17a) and δ_H 3.73 (H-17b) showed HMBC cross-peaks to the carbon resonance at δ_C 142.8 (C-14). This assigned C-14 (δ_C 142.8) next to C-18 (δ_C 122.8) and established the presence of an *N,N*-dimethyldihydropyrrole moiety (Figures 2.7.10 and 2.7.11).

Both methylene proton resonances at δ_H 3.22 (H-17a) and δ_H 3.73 (H-17b) showed HMBC correlations with the carbon resonating at δ_C 114.7 (C-10), which

established the bond between C-10 (δ_C 114.7) and C-18 (δ_C 122.8). An aromatic methine proton resonance at δ_H 7.52 (H-13: HMQC to δ_C 108.7) displayed HMBC correlations with the carbon resonance at δ_C 142.8 (C-14) and ^{1}H, ^{15}N LR-HMQC correlations with the nitrogen resonance at δ_N -310 (N-15). This confirmed the linkage between C-13 (δ_C 108.7) and C-14 (δ_C 142.8). The chemical shift of the carbon resonating at δ_C 142.7 (C-12) was consistent for an oxygenated aromatic carbon. This was confirmed by HMBC correlations between the exchangeable phenolic proton resonance at δ_H 10.42 (12-OH) and the carbon resonance at δ_C 142.7 (C-12). The bond between C-12 (δ_C 142.7) and C-13 (δ_C 108.7) was deduced from a three bond HMBC correlation between the proton resonance at δ_H 10.42 (12-OH) and the carbon resonance at δ_C 108.7 (C-13). Both proton resonances at δ_H 10.42 (12-OH) and δ_H 7.52 (H-13) showed three bond HMBC correlations to the oxygenated carbon resonance at δ_C 146.5 (C-11), which allowed the determination of the linkage between C-11 (δ_C 146.5) and C-12 (δ_C 142.7). A four bond HMBC correlation was present between the aromatic methine proton resonance at δ_H 7.52 (H-13) and the quaternary aromatic carbon resonance at δ_C 114.7 (C-10) (Figure 2.7.14). This assigned C-10 next to C-11 and revealed substructure **I** (Figures 2.7.10 and 2.7.11).

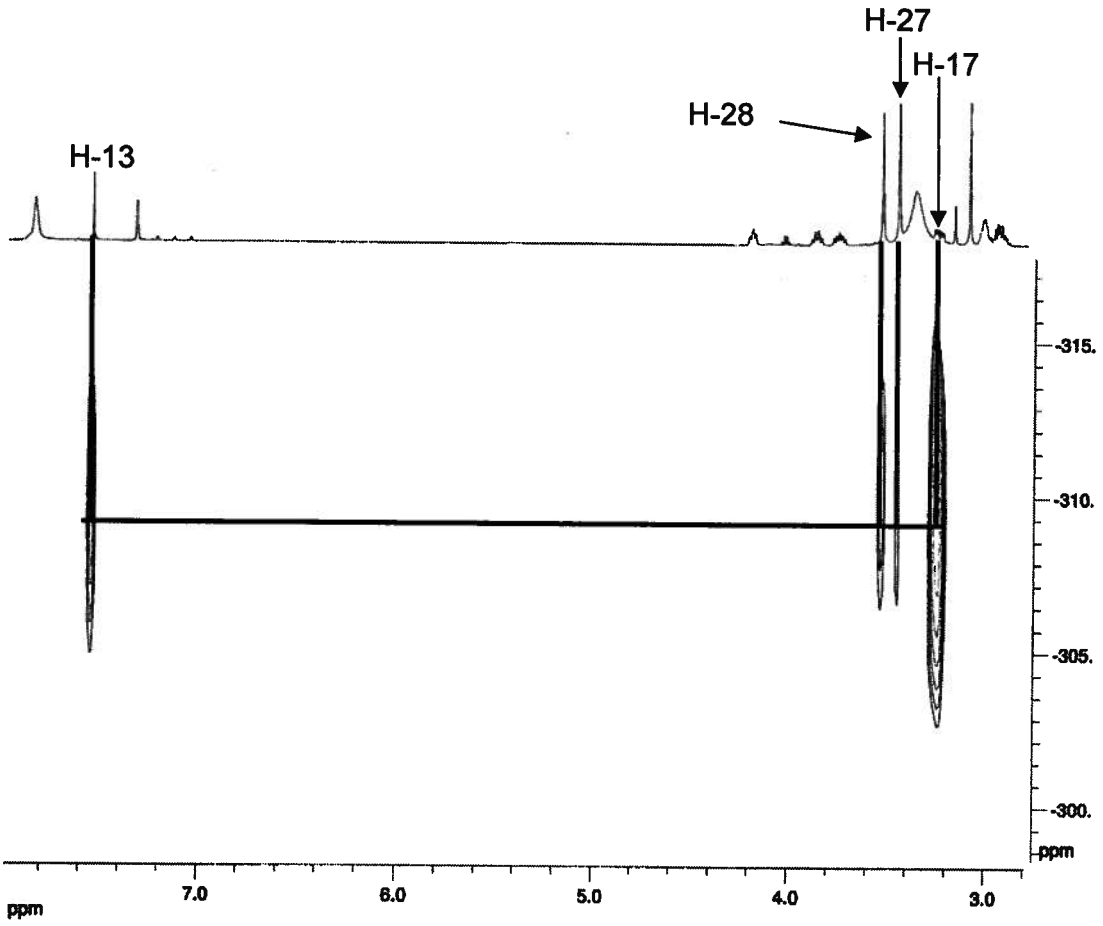

Figure 2.7.12. Expansion of the ^{1}H, ^{15}N LR-HMQC spectrum of the key correlations of substructure **I** of exiguamine A (**2.58**).

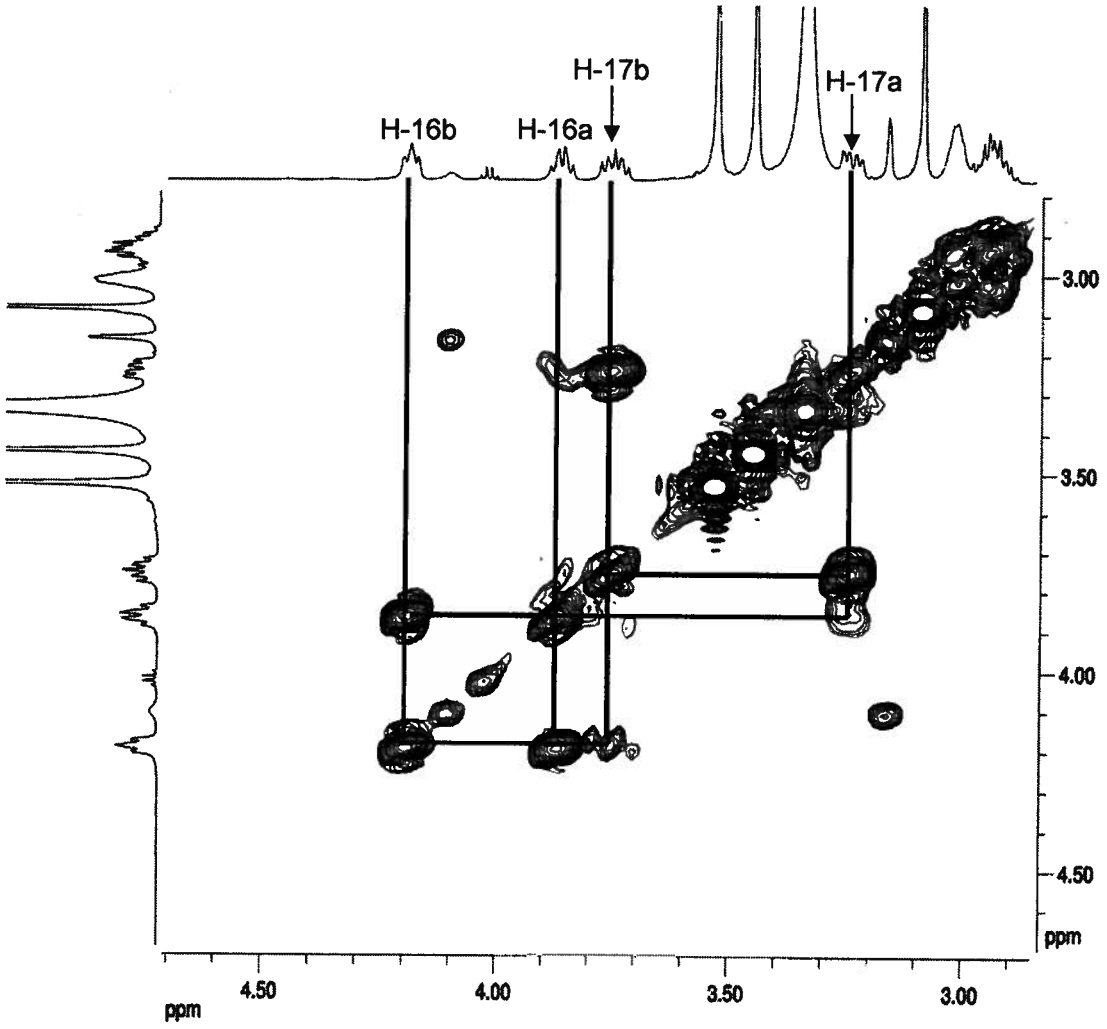

Figure 2.7.13. COSY expansion of the correlations for substructure **I** of exiguamine A (**2.58**).

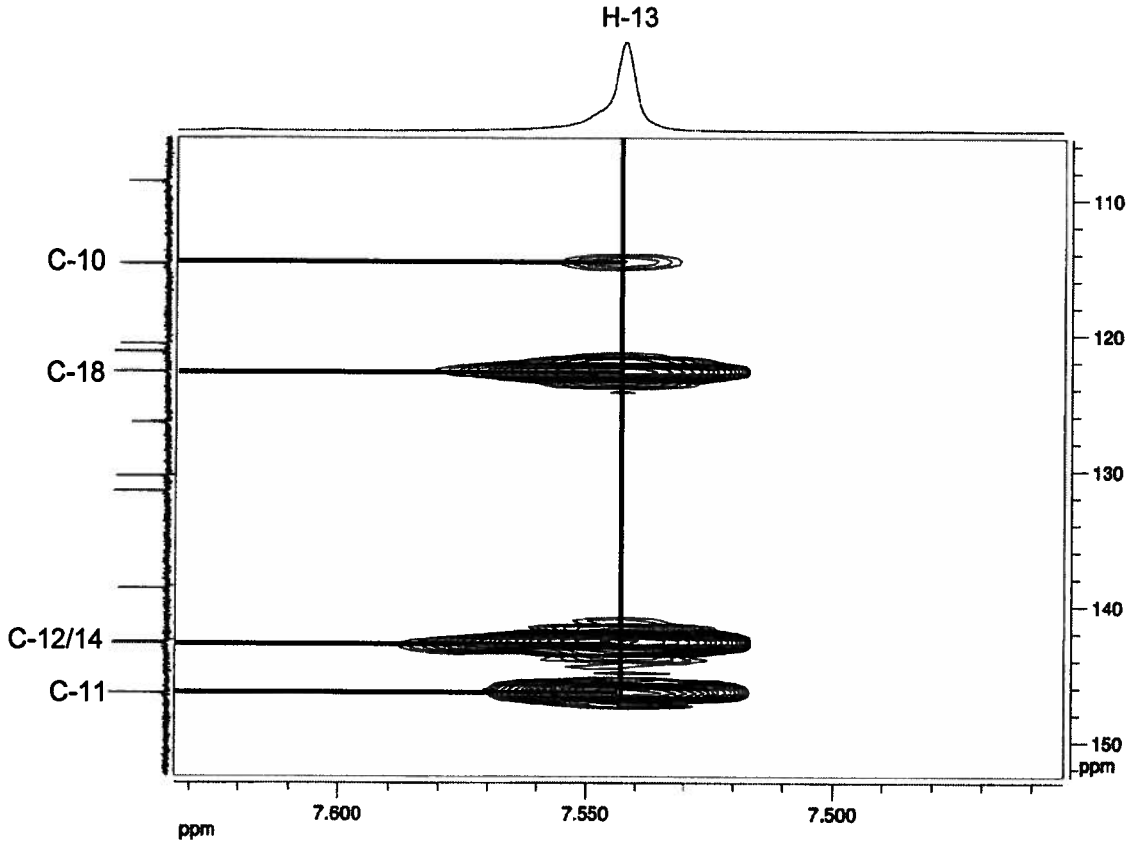

Figure 2.7.14. HMBC correlations observed for H-13 of substructure **I** of exiguamine A (**2.58**).

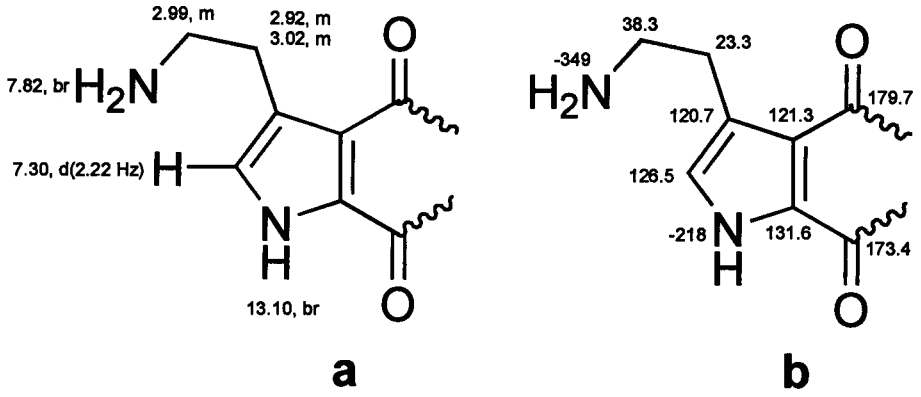

Figure 2.7.15. (**a**) ^{1}H and (**b**) ^{13}C and ^{15}N chemical shifts of substructure **II** of exiguamine A (**2.58**).

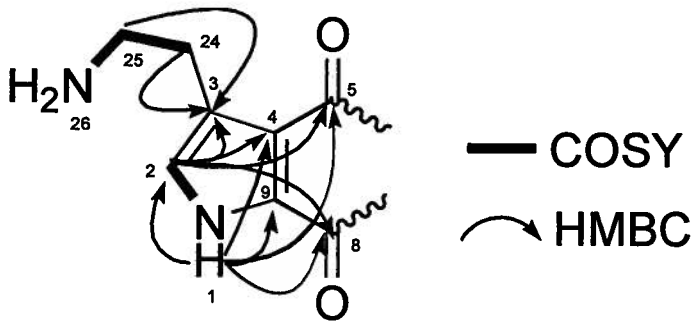

Figure 2.7.16. Key HMBC and COSY correlations of substructure **II** of exiguamine A (**2.58**).

The methylene proton resonance at δ_H 2.99 (H-25: HMQC to δ_C 38.3) showed COSY correlations to a broad exchangeable singlet at δ_H 7.82 (H-26) and LR-HMQC correlations to a nitrogen resonance at δ_N -349 (N-26). This confirmed C-25 (δ_C 38.3) was adjacent to an NH_2 moiety (N-26). The methylene proton resonance at δ_H 2.99 (H-25) displayed COSY correlations to both proton resonances at δ_H 3.02 (H-24a: HMQC to δ_C 23.3) and δ_H 2.92 (H-24b: HMQC to δ_C 23.3), which allowed the determination of the C-24 (δ_C 23.3) and C-25 (δ_C 38.3) linkage. All of the above is consistent for an ethylamine moiety.

All three proton resonances at δ_H 3.02 (H-24a), δ_H 2.92 (H-24b) and δ_H 2.99 (H-25) showed HMBC correlations to the sp^2 hybridized carbon resonance at δ_C 120.7 (C-3), thereby linking C-3 (δ_C 120.7) to C-24 (δ_C 23.3). The connection between C-2 (δ_C 126.5) and C-3 (δ_C 120.7) was deduced from three bond HMBC correlations between both methylene proton resonances at δ_H 3.02 (H-24a) and δ_H 2.92 (H-24b), and the methine carbon resonance at δ_C 126.5 (C-2). COSY correlations were observed between the methine proton resonance at

δ_H 7.30 (H-2: HMQC to δ_C 126.5) and the exchangeable proton resonance at δ_H 13.10 (H-1) (Figure 2.7.18). Additional ^1H, ^{15}N, LR-HMQC correlations were observed between δ_H 7.30 (H-2) and δ_N -218 (N-1), which confirmed that C-2 (δ_C 126.5) was linked to N-1 (δ_N -218) (Figure 2.7.17). The proton resonances at δ_H 13.10 (H-1) and δ_H 7.30 (H-2) showed HMBC correlations to the quaternary sp^2 hybridized carbon resonance at δ_C 131.6 (C-9), thereby, allowing the determination of the N-1 (δ_N -218) and C-9 bond (δ_C 131.6). Both proton resonances at δ_H 13.10 (H-1) and δ_H 7.30 (H-2) displayed additional HMBC cross-peaks to the carbon resonating at δ_C 121.3 (C-4). This established that C-3 (120.7) was connected to C-4 (δ_C 121.3), which in turn was bonded to C-9 (δ_C 131.6). All of the above is consistent for a tri-substituted pyrrole ring. Weak four bond HMBC correlations were observed between the proton resonance at δ_H 7.30 (H-2) and the two carbonyl carbon resonances at δ_C 179.7 (C-5) and δ_C 173.4 (C-8). Additional HMBC correlations were observed between the proton resonance at δ_H 13.10 (H-1) and the carbonyl resonances at δ_C 179.7 (C-5) and δ_C 173.4 (C-8) (Figure 2.7.19). This confirmed that both C-4 and C-9 were linked to carbonyls, thus completing substructure **II** (Figures 2.7.15 and 2.7.16).

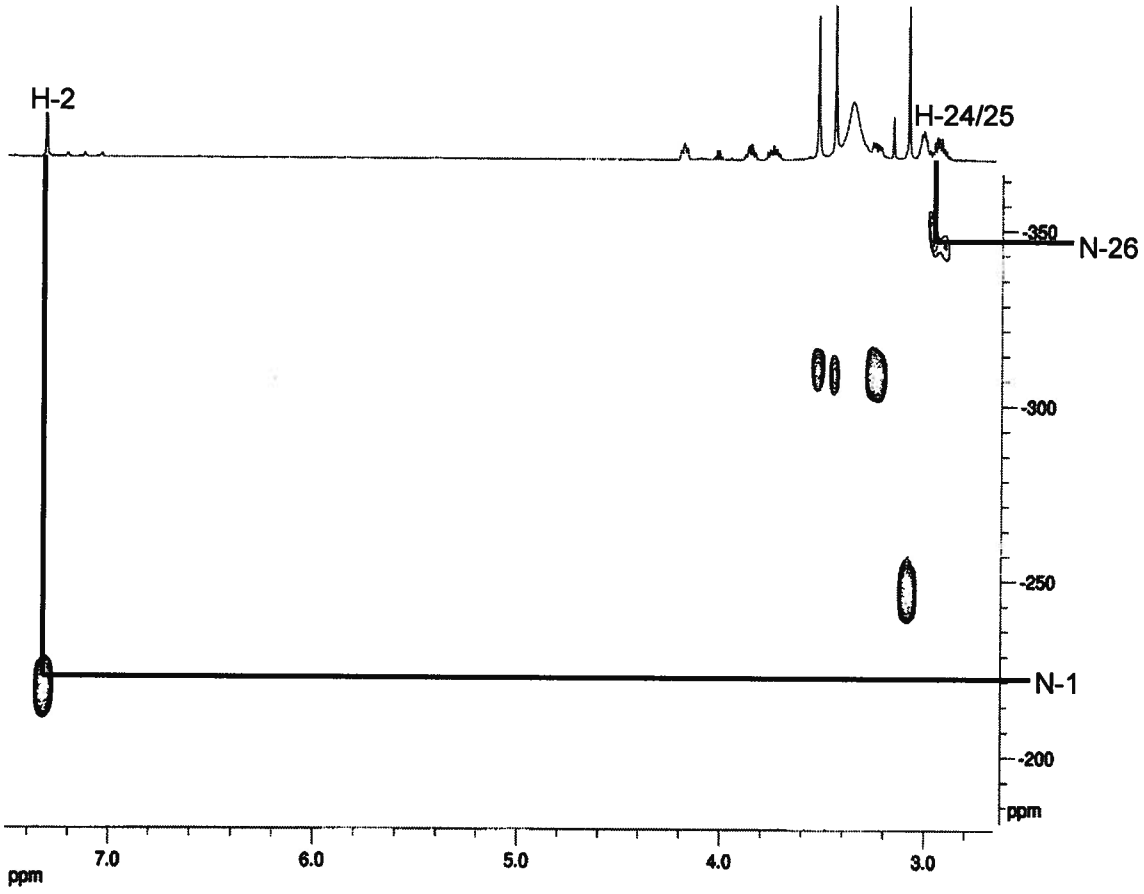

Figure 2.7.17. Expansion of the ^{1}H, ^{15}N LR-HMQC spectrum of the key correlations of substructure **II** of exiguamine A (**2.58**)..

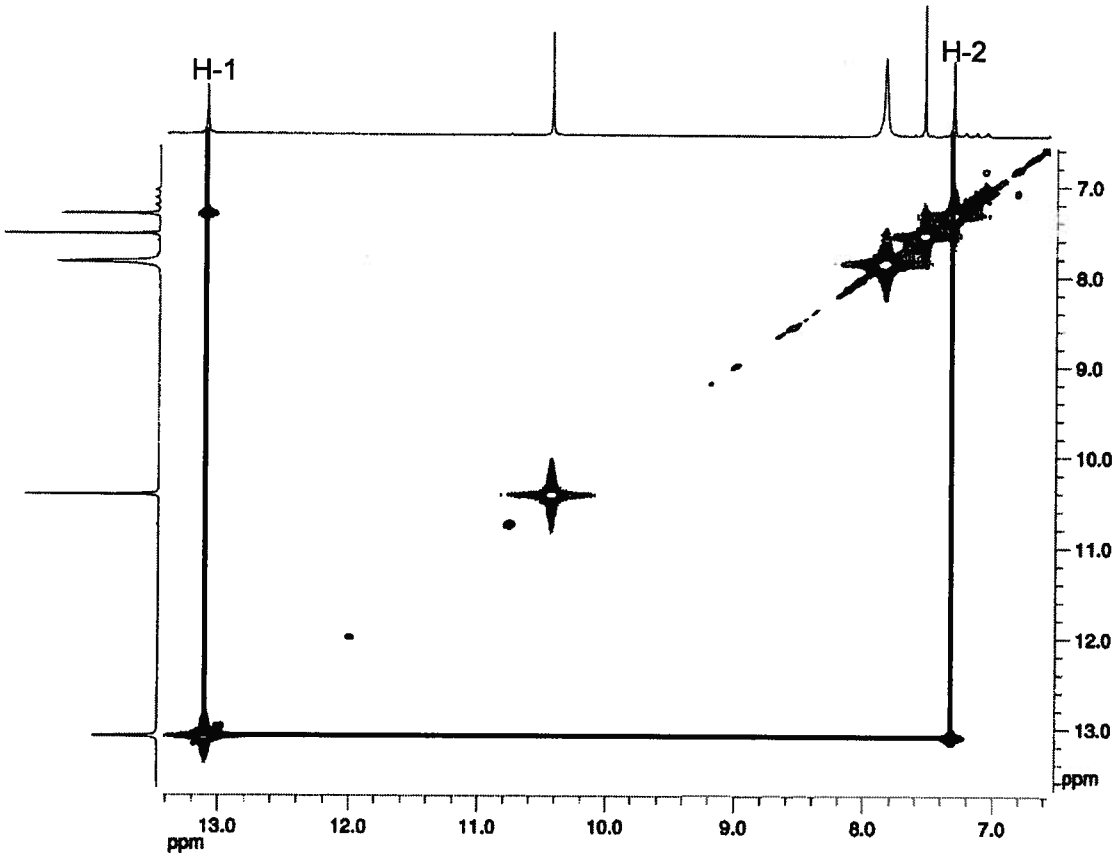

Figure 2.7.18. Key COSY correlation for substructure **II** of exiguamine A (**2.58**).

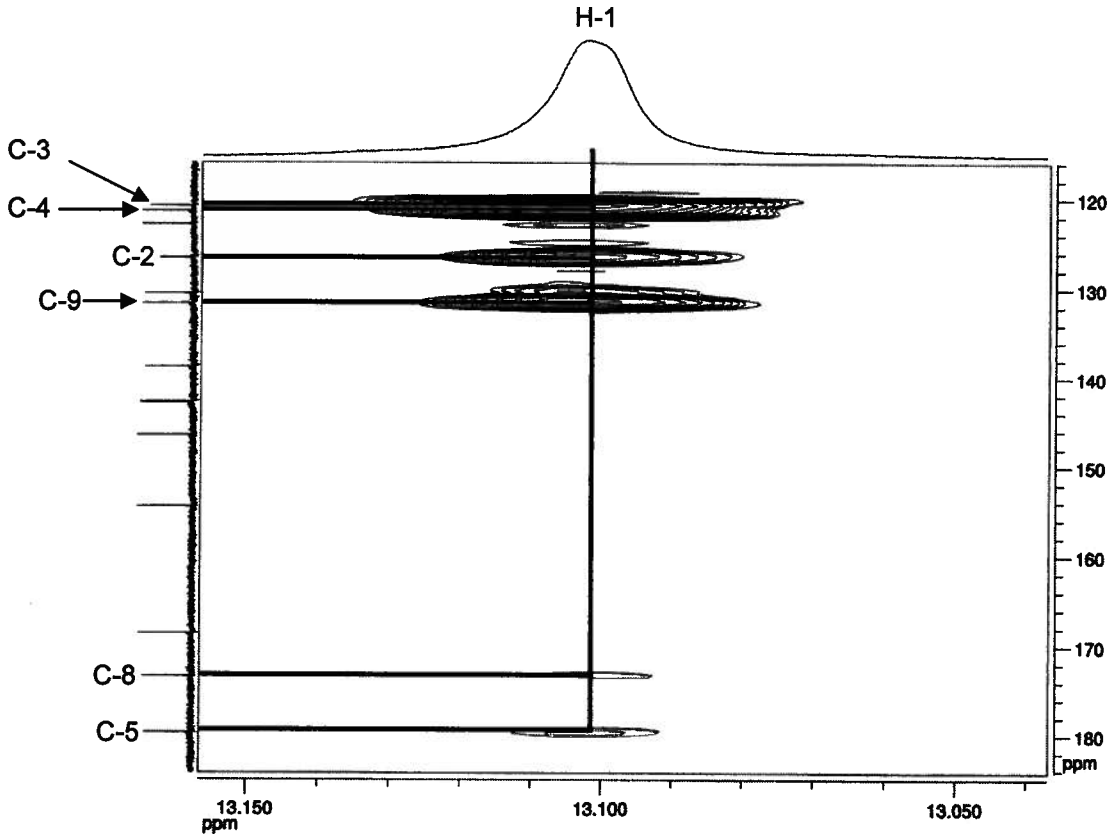

Figure 2.7.19. HMBC correlations observed for H-1 of substructure **II** of exiguamine A (**2.58**).

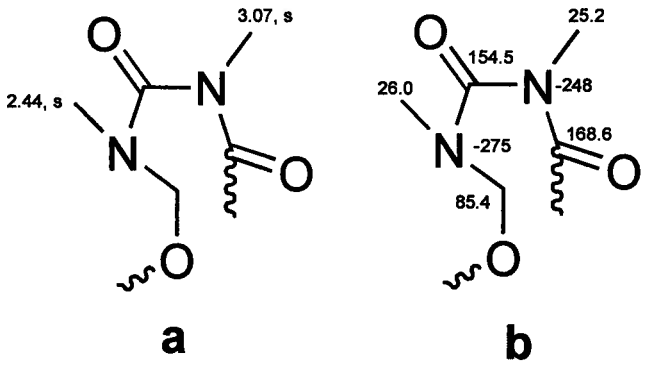

Figure 2.7.20. (**a**) ^{1}H and (**b**) ^{13}C and ^{15}N chemical shifts of substructure **III** of exiguamine A (**2.58**).

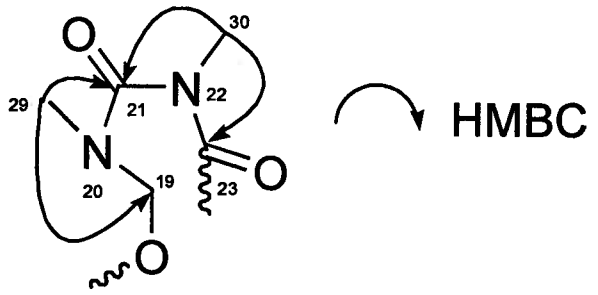

Figure 2.7.21. HMBC correlations of substructure **III** of exiguamine A (**2.58**).

The singlet methyl proton resonance at δ_H 3.07 (H-30: HMQC to δ_C 25.2) showed ^1H, ^{15}N LR-HMQC correlations to δ_N -248 (N-22), which established an *N*-methyl moiety (Figure 2.7.22). Three bond HMBC couplings between the methyl proton resonance at δ_H 3.07 (H-30) and the two carbonyl carbon resonances at δ_C 154.5 (C-21) and δ_C 168.6 (C-23) implies that N-22 (δ_N -248), is flanked by two carbonyls (Figures 2.7.21 and 2.7.23). This is further confirmed by observation of the chemical shift of N-22 (δ_N -248), which is consistent for an amide moiety.[49] Another *N*-methyl moiety was confirmed by a LR-HMQC correlation between δ_H 2.44 (H-29: HMQC to δ_C 26.0) and δ_N -275 (N-20). The HMBC spectrum revealed cross peaks between the proton resonance at δ_H 2.44 (H-29) and the carbonyl resonance at δ_C 154.5 (C-21), which yielded a second amide group. A three bond HMBC correlation between the proton resonance at δ_H 2.44 (H-29) and the carbon resonance at δ_C 85.4 (C-19) established the bond between C-19 (δ_C 85.4) and N-20 (δ_N -275) (Figures 2.7.21 and 2.7.23). The chemical shift of C-19 (δ_C 85.4) is typical for an sp^3 hybridized carbon connected to two heteroatoms. Since all the nitrogens of exiguamine A were accounted for,

the second heteroatom on C-19 was determined to be oxygen. All of the above data are consistent with substructure **III** (Figures 2.7.20 and 2.7.21).

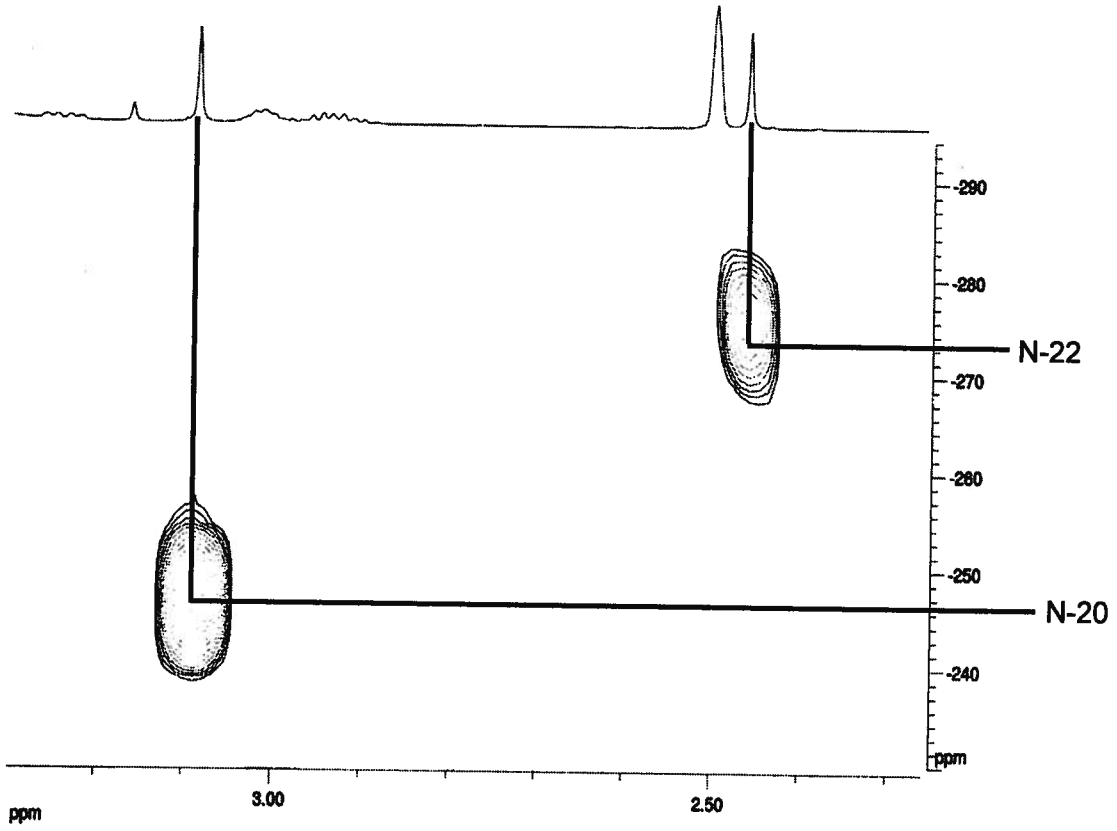

Figure 2.7.22. Expansion of the ^{15}N LR-HMQC spectrum of the key correlations of substructure **III** of exiguamine A (**2.58**).

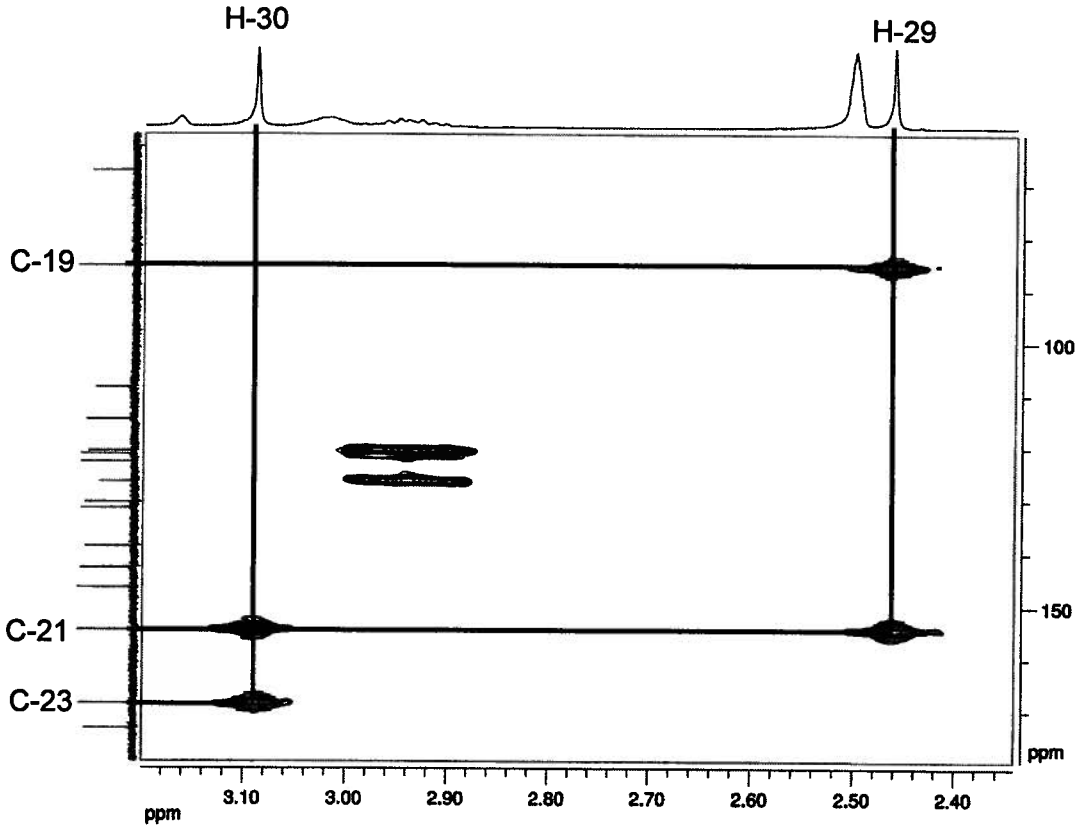

Figure 2.7.23. Expansion of the HMBC spectrum of the key correlations of substructure **III** of exiguamine A (**2.58**).

The NMR data of exiguamine A accounted for the fragments **I-III**. Unfortunately, due to the lack of proton resonances and the large number of quaternary carbons and hetero-atoms, the NMR data were inadequate for connecting fragments **I-III**. Therefore, x-ray crystallography was needed to establish the complete structure of exiguamine A. Exiguamine A was suspended in 1N HCl and the solution was evaporated *in vacuo*. This process was repeated four times to generate the HCl salt. Deep red crystals of exiguamine A were obtained by the slow evaporation of a methanol solution of the HCl salt. The crystals were appropriate for single crystal x-ray diffraction analysis. Dr. Brian Patrick from the department of chemistry at the University of British Columbia

performed the x-ray diffraction analysis and the structure was unequivocally established as that proposed for exiguamine A (Figure 2.7.24). For the full x-ray diffraction analysis parameters, see appendix I.

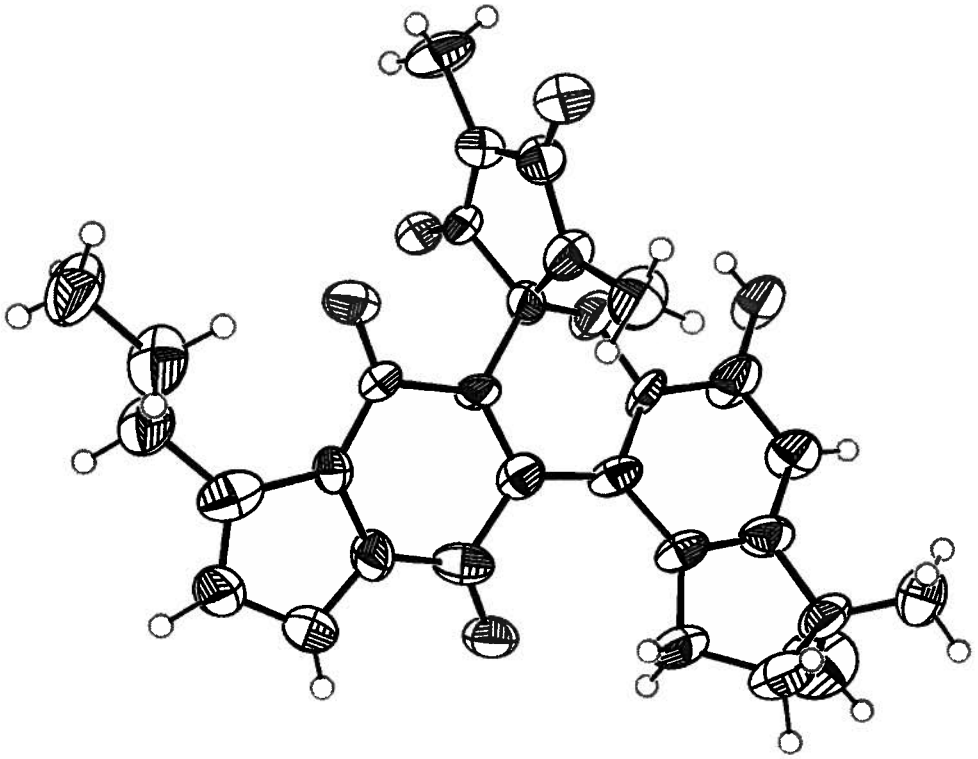

Figure 2.7.24. ORTEP diagram of exiguamine A (**2.58**). The x-ray diffraction analysis was performed by Dr. Brian Patrick.

2.8 Structure Elucidation of exiguamine B

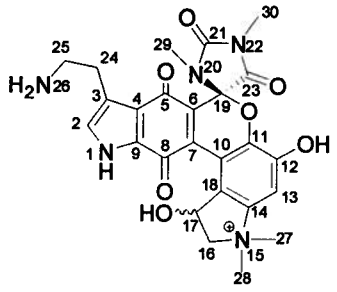

Figure 2.8.1. Numbering scheme of exiguamine B (**2.59**).

Exiguamine B (**2.59**) gave a [M^+] ion at *m/z* 508.1850 in the HRESIMS which afforded a molecular formula of $C_{25}H_{26}N_5O_7$ (calc'd 508.1832). This differs from the molecular formula of exiguamine A by the addition of one oxygen atom. The alkaloid, when subjected to LRESIMS in MeOH, was found to have a molecular ion peak at *m/z* 508.3. When the LRESIMS measurement was performed in MeOD, the molecular mass was determined to be 513.3, which is consistent with five exchangeable protons in the molecule. The ^{1}H NMR spectrum (Figure 2.8.3) of exiguamine B acquired in DMSO-d_6 at 600 MHz contained five exchangeable protons (δ_H 13.12, 10.71, 7.79, 6.07), two aromatic protons (δ_H 7.62 and 7.35), a deshielded oxymethine proton (δ_H 5.75), and a series of methines and methyl protons on carbons adjacent to either nitrogen, or an aromatic carbon (δ_H 2.44-4.45). The ^{13}C NMR spectra (Figure 2.8.4) run in DMSO-d_6 at 150 MHz contained 25 carbon resonances. Observation of the DEPT (Figure 2.8.5) and HMQC (Figure 2.8.6) data revealed four carbonyls (δ_C 179.4, 173.4, 168.6, 154.5), 11 quaternary carbons (δ_C 148.5, 143.7, 142.8, 138.7, 131.4, 130.7, 125.3, 121.9, 121.0, 113.8, 85.5), three methines (δ_C 126.9, 108.6, 69.1), three methylenes (δ_C 73.5, 38.3, 23.3), and four methyls (δ_C 57.3,

55.4, 26.2, 25.3). After assignment of all the protons to their respective carbons (Table 2.8.1), three independent spin systems (**I**, **II**, **III**, Figure 2.8.2) were deduced from the HMBC and the COSY data (Figures 2.8.7 and 2.8.8).

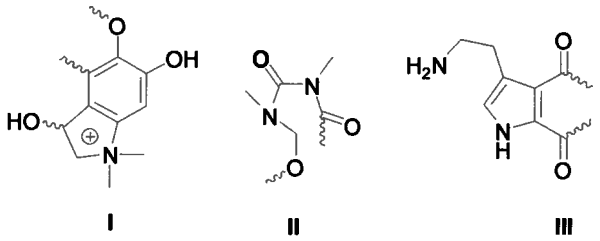

I II III

Figure 2.8.2. Three substructures of exiguamine B (**2.59**).

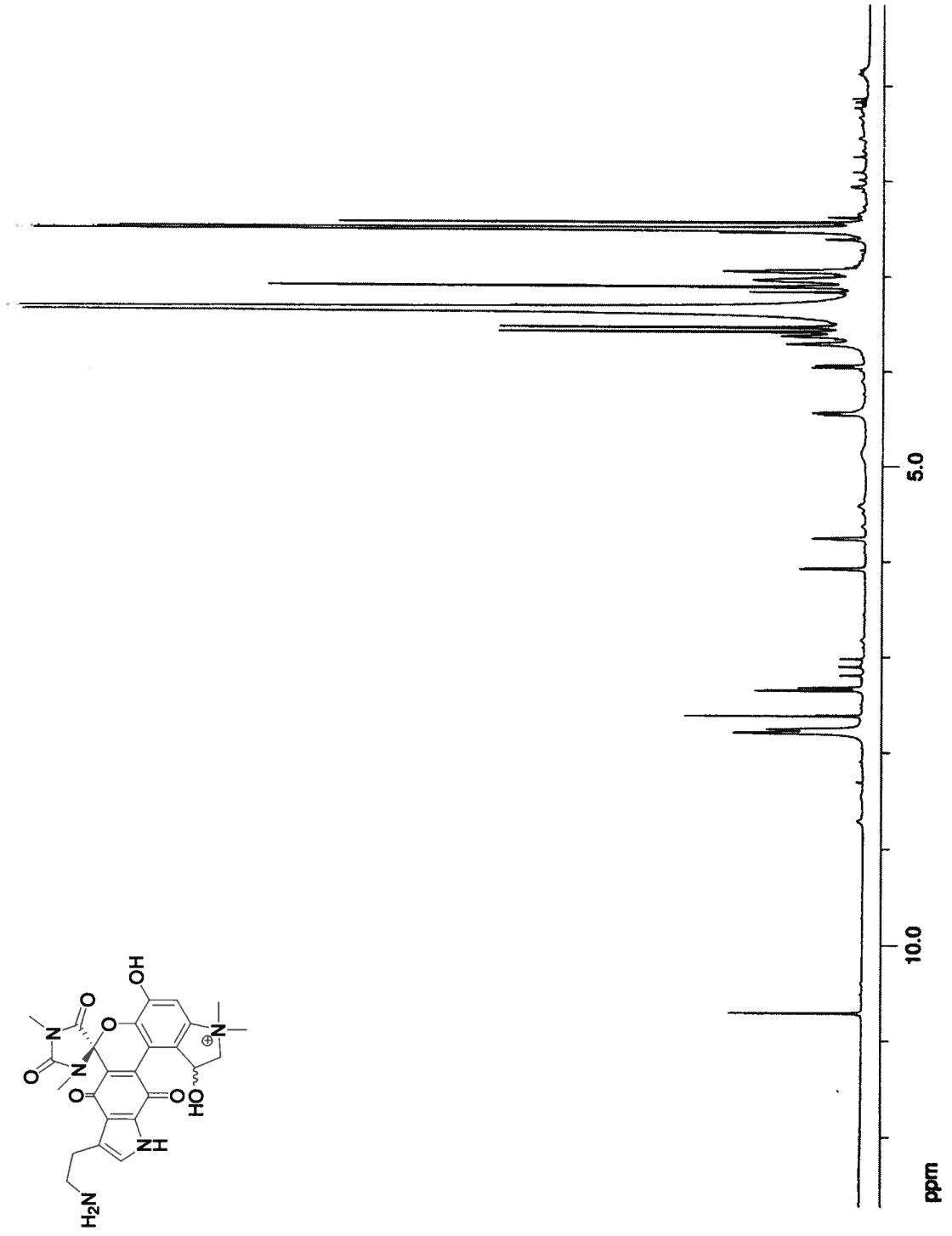

Figure 2.8.3. ^{1}H NMR spectrum of exiguamine B (**2.59**) run at 600 MHz in DMSO-d_6.

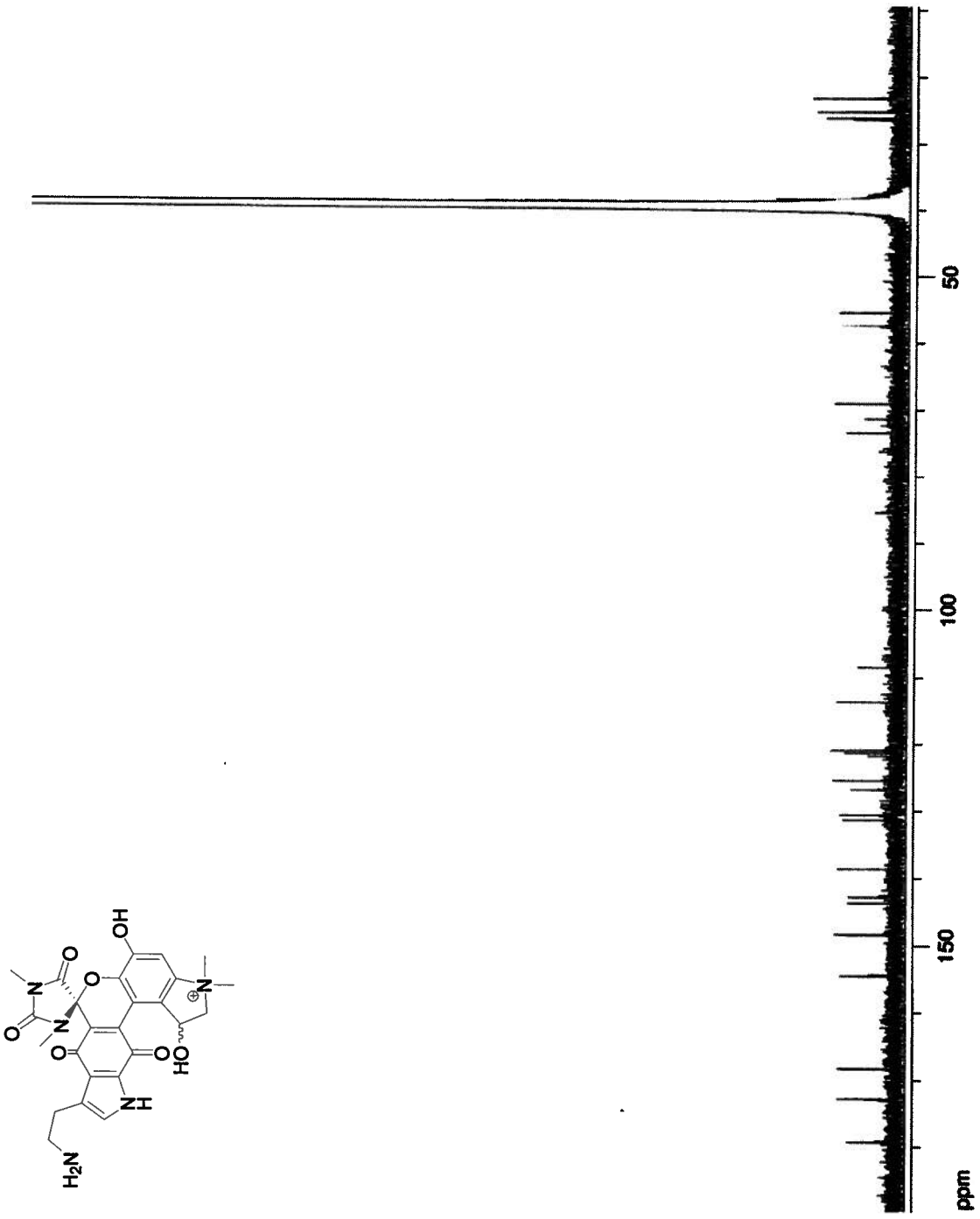

Figure 2.8.4. ^{13}C NMR spectrum of exiguamine B (**2.59**) run at 150 MHz in DMSO-d_6.

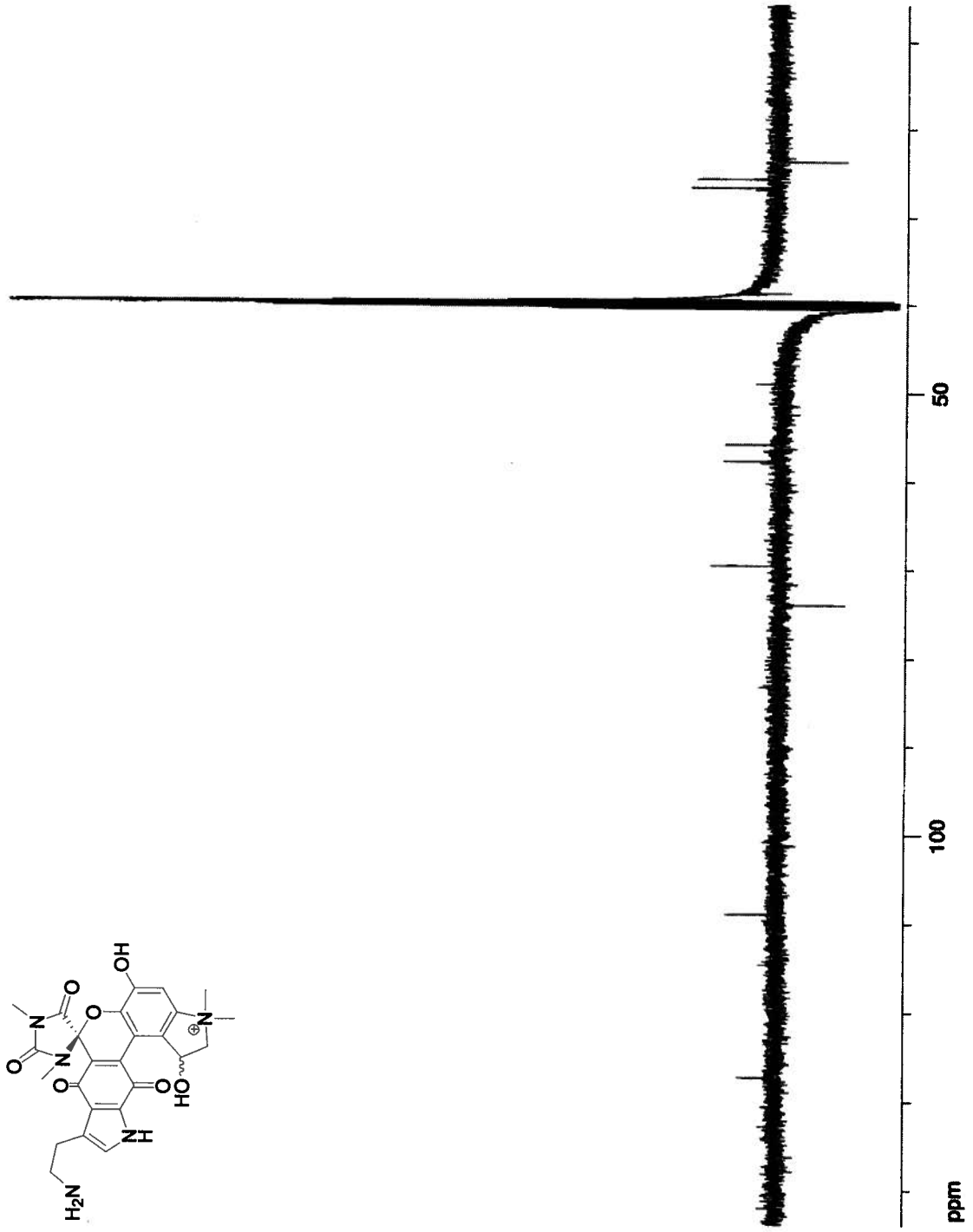

Figure 2.8.5. DEPT spectrum of exiguamine B (**2.59**) run at 150 MHz in DMSO-d_6.

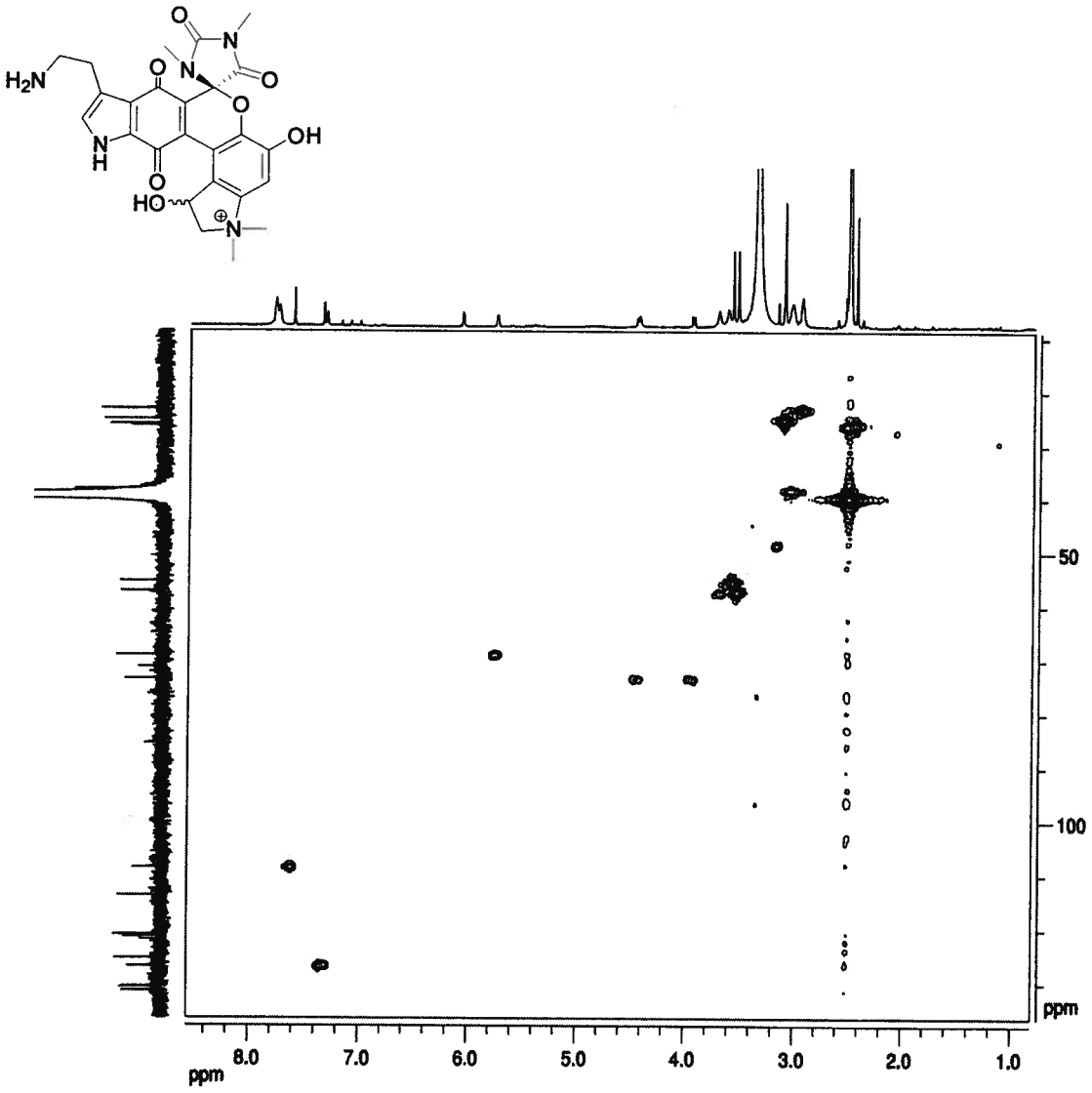

Figure 2.8.6. HMQC spectrum of exiguamine B (**2.59**) run at 600 MHz in DMSO-d_6.

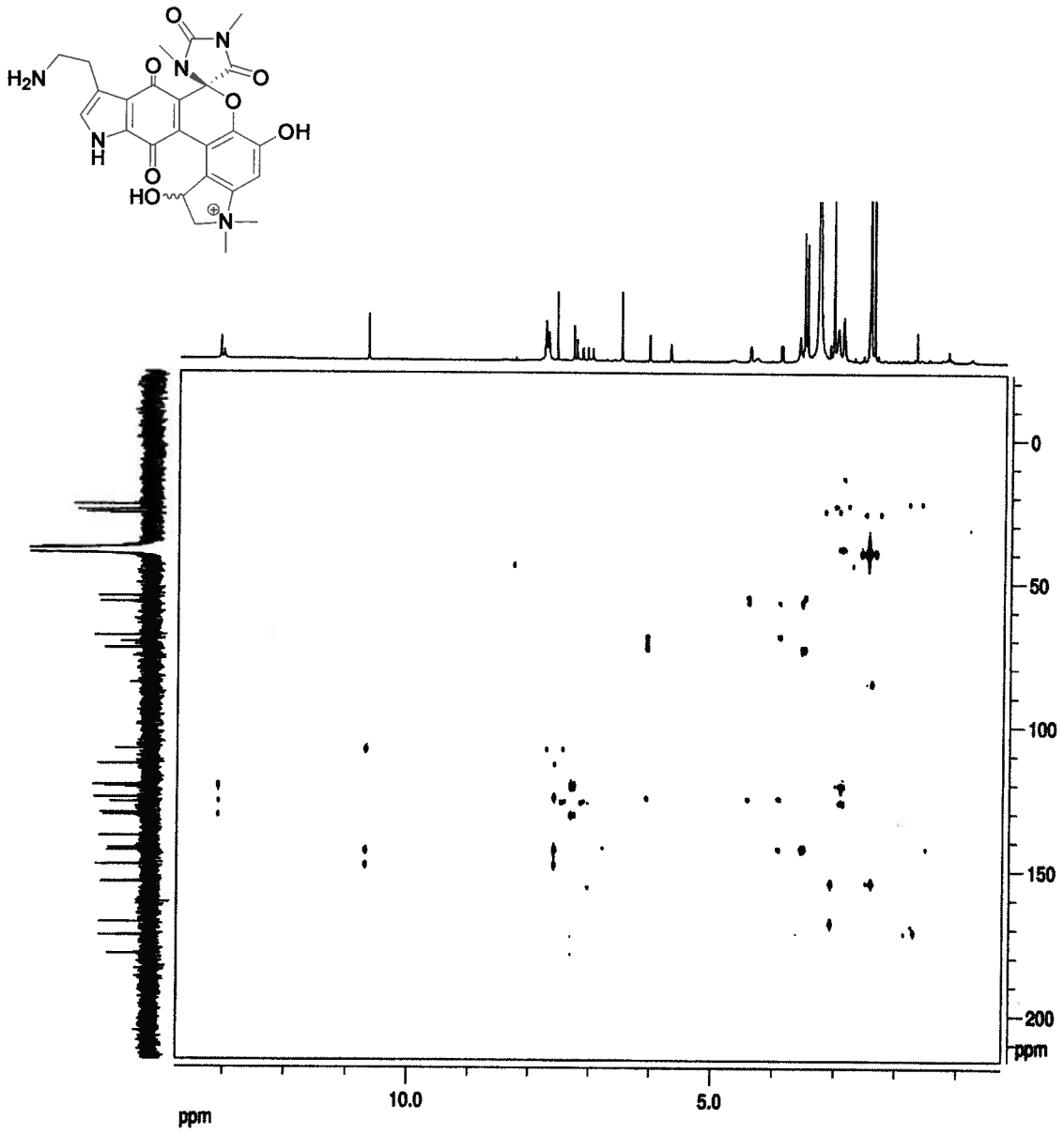

Figure 2.8.7. HMBC spectrum of exiguamine B (**2.59**) run at 600 MHz in DMSO-d_6.

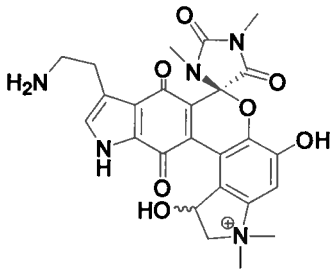

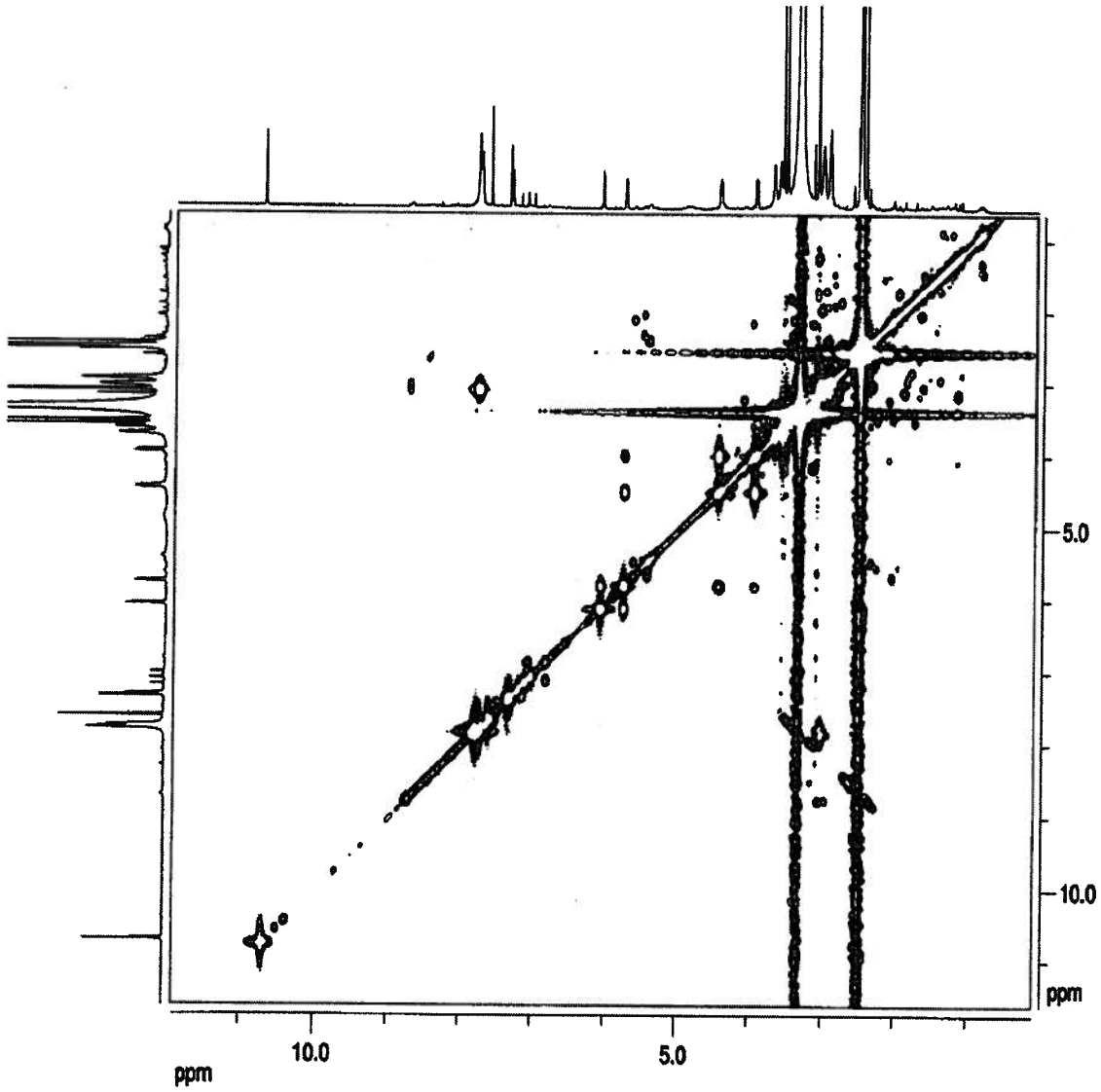

Figure 2.8.8. COSY spectrum of exiguamine B (**2.59**) run at 600 MHz in DMSO-d_6.

Table 2.8.1. 1D and 2D NMR data of Exiguamine B[a]

Position	δ_C	δ_H (J in Hz)	^1H, ^{13}C-HMBC	COSY
1		13.10, brs	C-2, C-3, C-4, C-9	H-2
2	126.9	7.35 ,d, (2.2)	C-3, C-4, C-9	H-2
3	121.0			
4[b]	121.9			
5[c]	173.0			
6	130.7			
7	138.7			
8[c]	179.4			
9[b]	131.4			
10	113.8			
11	148.5			
12	143.7			
13	108.6	7.62, s	C-10, C-11, C-12, C-14, C-18	
14	142.8			
15				
16a	73.5	4.45, dd, (12.4 Hz, 5.8)	C-14, C-18, C-27, C-28	H-16b, H-17
16b		3.95, dd, (12.4, 2.5)	C-14, C-18, C-17, C-28	H-16a, H-17
17	69.1	5.75, m		H-16a, H-16b, 17-OH
18	125.3			
19	85.5			
20				
21	154.5			
22				
23	168.4			
24	23.3	2.94, m	C-2, C-3, C-4, C-25	H-25
25	38.3	3.04, m	C-3, C-24	H-24, H-26
26		7.79, brs	C-24, C-25	H-25
27[d]	55.4	3.58, s	C-14, C-16, C-28	
28[d]	57.3	3.53, s	C-14, C-16, C-27	
29	26.2	2.44 , s	C-19, C-21	
30	25.3	3.10, s	C-21, C-23	
12-OH		10.71, brs	C-11, C-12, C-13	
17-OH		6.07, d, (5.0)	C-16, C-17, C-18	H-17

[a] ^1H and ^{13}C chemical shifts [ppm] are referenced to the DMSO-d_6 (2.50 and 39.51 ppm respectively)
[b] C4 and C9 are interchangeable signals
[c] C5 and C8 are interchangeable signals
[d] C27 and C28 are interchangeable signals

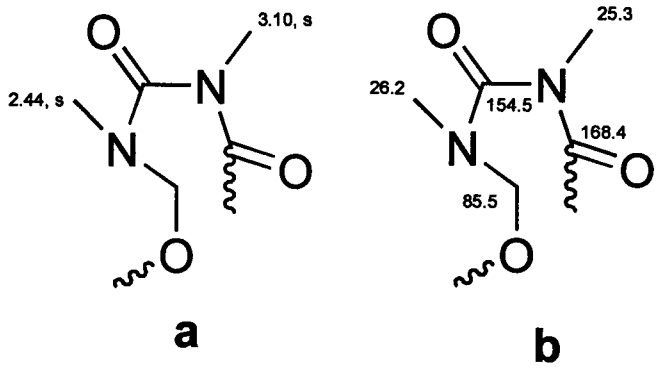

Figure 2.8.9. (**a**) ^{1}H NMR and (**b**) ^{13}C NMR assignments for substructure **I** of exiguamine B (**2.59**).

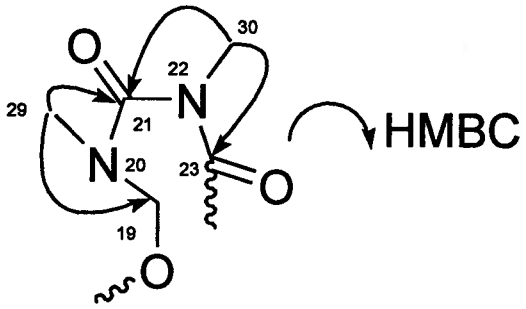

Figure 2.8.10. Key HMBC correlations observed for substructure **I** of exiguamine B (**2.59**).

The ^{1}H chemical shift of the methyl protons H-30 (δ_H 3.10, s) of exiguamine B (**2.59**) is very similar to that of H-30 (δ_H 3.07, s) for exiguamine A (**2.58**), which confirmed a nitrogen bearing methyl. HMBC correlations between the methyl proton resonance at δ_H 3.10 (H-30: HMQC to δ_C 25.3) and both the carbon resonances at δ_C 154.5 (C-21) and δ_C 168.4 (C-23) established an *N*-methyl moiety adjacent to two carbonyls (Figures 2.9.10 and 2.9.11). The ^{1}H chemical shift of the proton resonance H-29 (δ_H 2.44, s) of exiguamine B (**2.59**) is identical to the H-29 (δ_H 2.44, s) proton resonance of exiguamine A (**2.58**). This reveals an additional *N*-methyl moiety. Cross-peaks in the HMBC were present

between the methyl proton resonance at δ_H 2.44 (H-29: HMQC to δ_C 26.2) and the carbon resonance at δ_C 154.5 (C-21), thus yielding an additional amide moiety. A bond between C-19 (δ_C 85.5) and N-20 was deduced from an HMBC correlation between the methyl proton resonance at δ_H 2.44 (H-29) and the carbon resonance at δ_C 85.5 (C-19) (Figures 2.9.10 and 2.9.11). The ^{13}C chemical shift of carbon C-19 (δ_C 85.5) of exiguamine B is very similar to that of C-19 (δ_C 85.4) for exiguamine A, which allowed the determination of an aminal carbon. This confirmed substructure **I**, analogous to that found in exiguamine A (Figures 2.8.9 and 2.8.10).

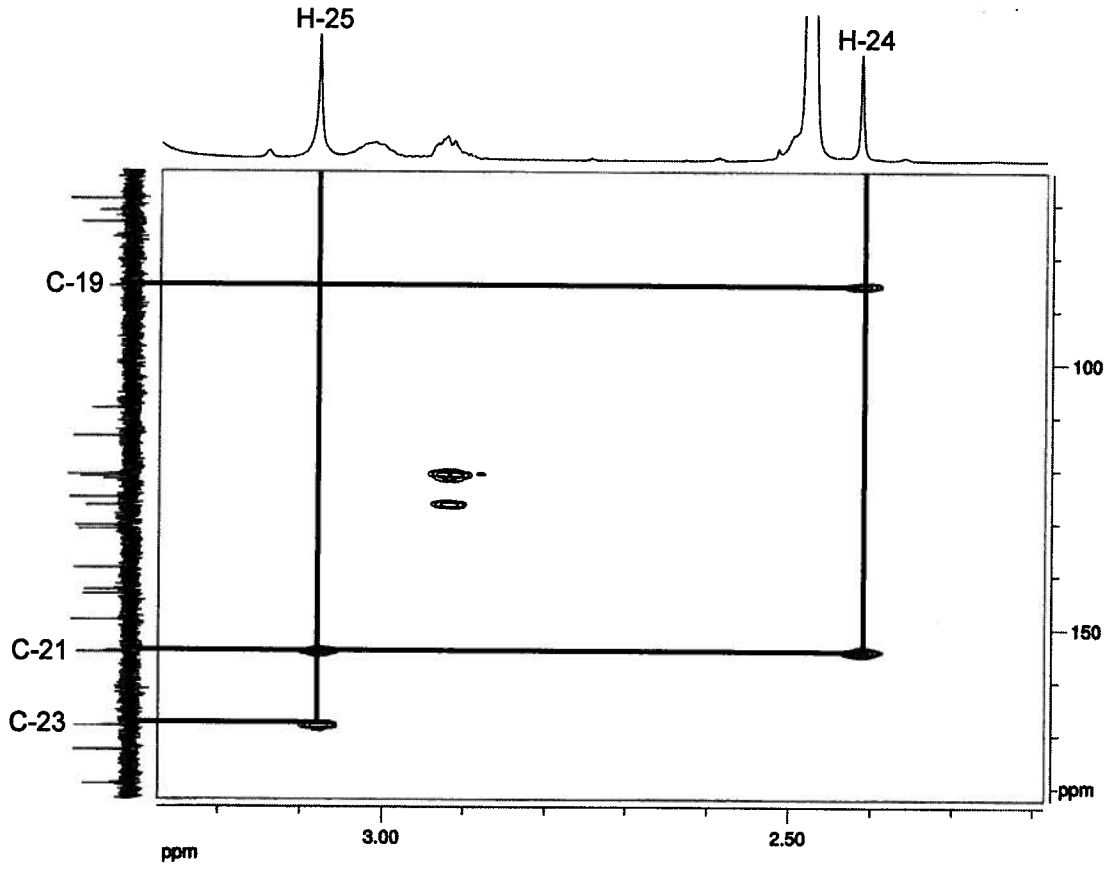

Figure 2.8.11. HMBC correlations observed for substructure **I** of exiguamine B (**2.59**).

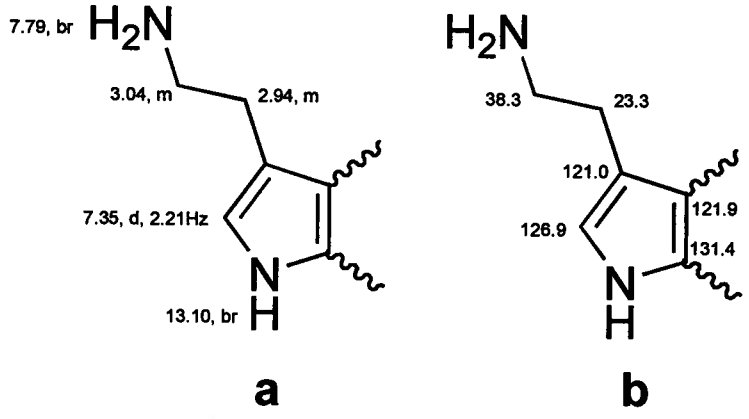

Figure 2.8.12. (**a**) ^{1}H NMR and (**b**) ^{13}C NMR assignments of substructure **II** of exiguamine B (**2.59**).

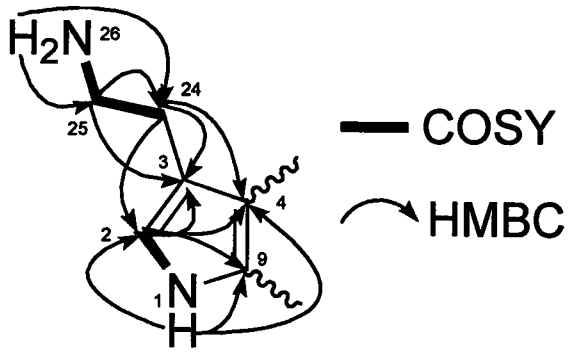

Figure 2.8.13. Key HMBC and COSY correlations observed for substructure **II** of exiguamine B (**2.59**).

The ^{1}H chemical shift of the exchangeable proton resonance H-26 (δ_H 7.79, brs) of exiguamine B (**2.59**) is very similar to the chemical shift found for H-26 (δ_H 7.82, brs) in exiguamine A (**2.58**). Therefore, one can establish the presence of a primary amine. The proton resonance at δ_H 7.79 (H-26) showed COSY correlations to the multiplet resonating at δ_H 3.04 (H-25: HMQC to δ_C 38.3), which, in turn, showed COSY correlations to the methylene proton resonance at δ_H 2.94 (H-24: HMQC to δ_C 23.3). This was consistent with an

ethylamine moiety, which was confirmed by key correlations in the HMBC data (Figure 2.8.13).

Both methylene proton resonances at δ_H 2.94 (H-24) and δ_H 3.04 (H-25) showed HMBC correlations to the quaternary sp^2 hybridized carbon resonating at δ_C 121.0 (C-3), thus assigning C-24 (δ_C 23.3) next to C-3 (δ_C 121.0). The linkage between C-2 (δ_C 126.9) and C-3 (δ_C 121.0) was deduced from three bond HMBC correlations between the multiplet resonating at δ_H 2.94 (H-24) and the sp^2 hybridized carbon resonance at δ_C 126.9 (C-2). Both proton resonances at δ_H 7.35 (H-2: HMQC to δ_C 126.9) and δ_H 2.94 (H-24) displayed HMBC correlations to the carbon resonance at δ_C 121.9 (C-4), thereby placing C-3 (δ_C 121.0) next to C-4 (δ_C 121.9). The exchangeable proton H-1 (δ_H 13.10, brs) of exiguamine B (**2.59**) had an identical chemical shift to H-1 (δ_H 13.10, brs) of exiguamine A (**2.58**), which is consistent for a proton on a pyrrole nitrogen. A proton resonance at δ_H 7.35 (H-2) showed a COSY correlation to the proton resonating at δ_H 13.10 (H-1), which confirms that C-2 (δ_C 126.9) is adjacent to an NH moiety (Figure 2.8.14). The proton resonances at δ_H 7.35 (H-2) and δ_H 13.10 (H-1) both showed HMBC correlations to the quaternary carbon resonating at δ_C 131.6 (C-9), thus allowing the determination of the N-1 and C-9 (δ_C 131.6) bond. A linkage between C-4 (δ_C 121.9) and C-9 (δ_C 131.6) was confirmed from a three bond HMBC correlation between the proton resonating at δ_H 13.10 (H-1), and the carbon resonance at δ_C 121.3 (C-4) (Figures 2.8.13 and 2.8.15). All of the above

data is consistent with a tri-substituted pyrrole moiety, and substructure **II** (Figures 2.8.12 and 2.8.13).

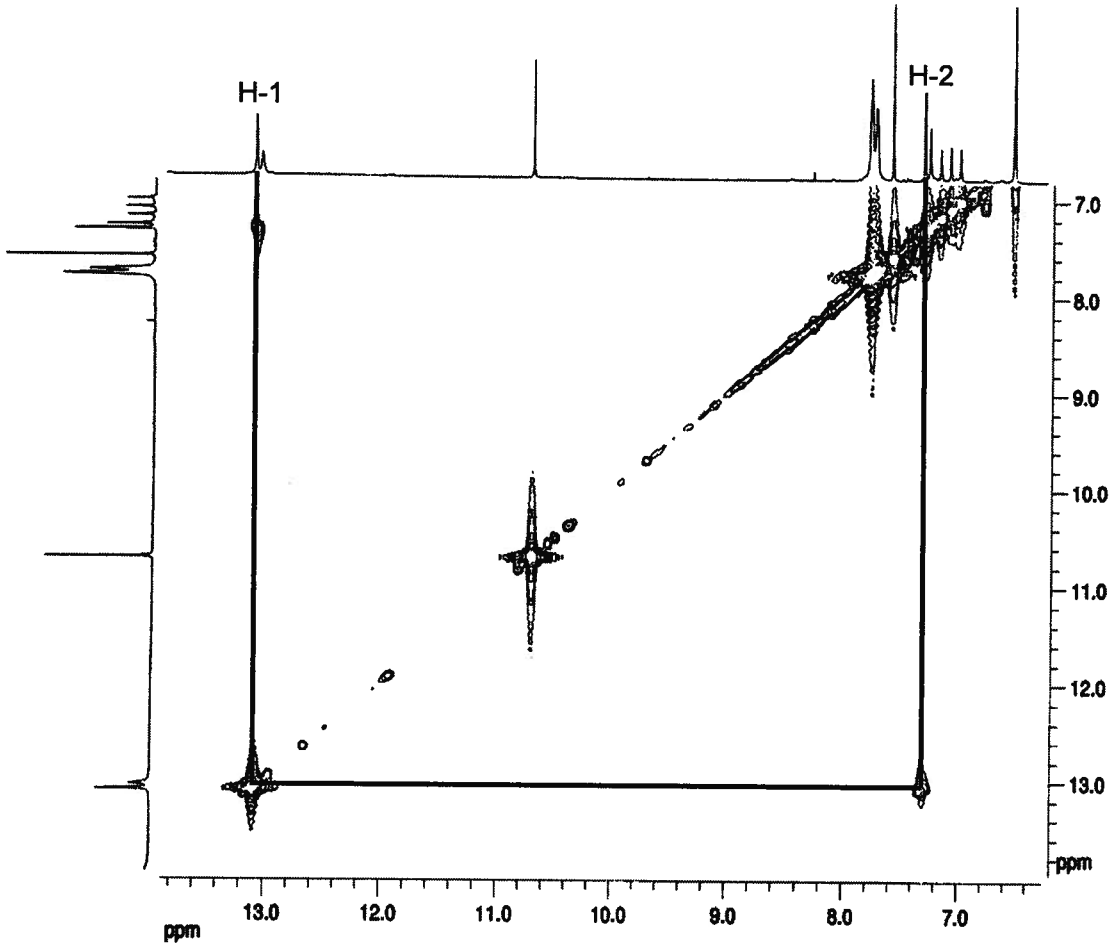

Figure 2.8.14. Key COSY correlation of substructure **II** of exiguamine B (**2.59**).

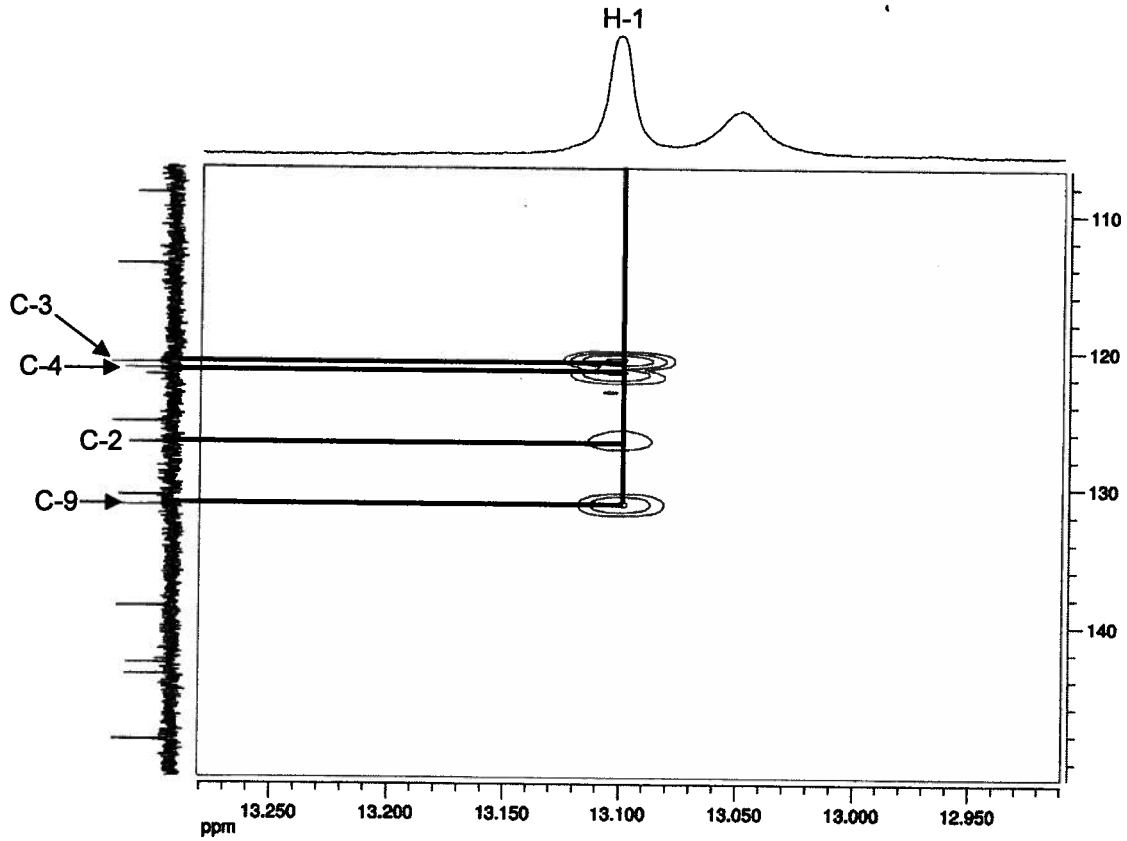

Figure 2.8.15. HMBC correlations for H-1 of substructure **II** of exiguamine B (**2.59**).

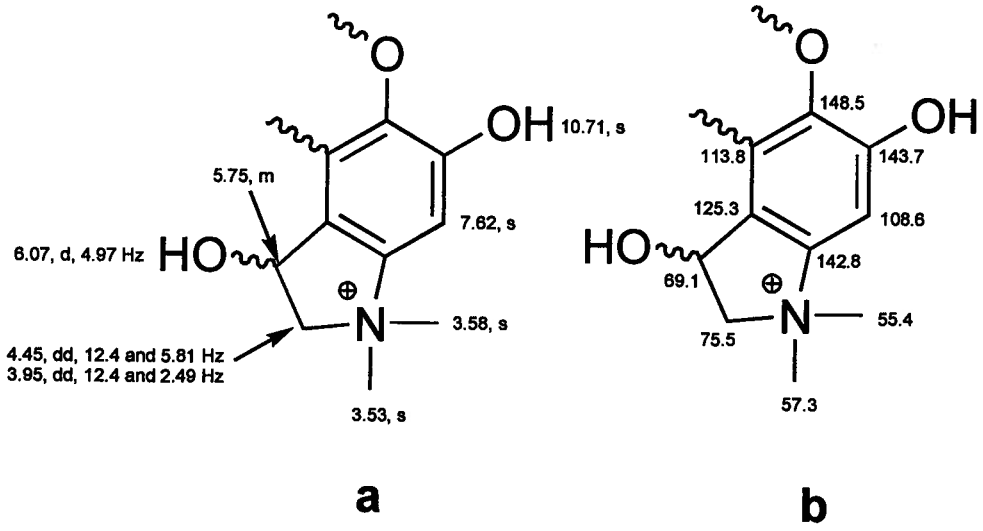

Figure 2.8.16. (**a**) ^{1}H NMR and (**b**) ^{13}C NMR of substructure **III** of exiguamine B (**2.59**).

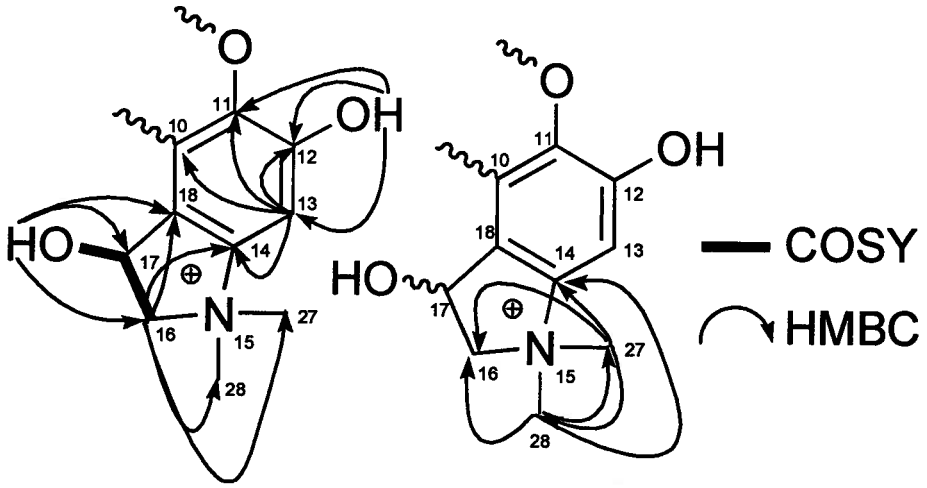

Figure 2.8.17. Key HMBC and COSY correlations of substructure **II** of exiguamine B (**2.59**).

HMBC cross-peaks were observed between the proton resonance at δ_H 3.58 (H-27: HMQC to δ_C 55.4) and the carbon resonance at δ_C 57.3 (C-28). A methyl proton resonance at δ_H 3.51 (H-28: HMQC to δ_C 57.3) showed HMBC correlations to δ_C 55.4 (C-27), which established that Me-27 and Me-28 were attached to the same nitrogen (N-15). Both methyl proton resonances at δ_H 3.58 (H-27) and 3.51 (H-28) showed HMBC correlations to the methylene carbon resonating at δ_C 73.5 (C-16), thereby placing C-16 (δ_C 73.5) next to the *N*-dimethyl moiety. All four proton resonances at δ_H 4.45 (H-16a: HMQC to δ_C 73.5), 3.95 (H-16b: HMQC to δ_C 73.5), δ_H 3.58 (H-27) and 3.51 (H-28) showed HMBC correlations to the quaternary sp^2 hybridized carbon resonating at δ_C 142.8 (C-14). This allowed the determination of the C-14 (δ_C 142.8) and N-15 bond. Observation of COSY correlations between the proton resonances at δ_H 4.45 (H-16a) and 3.95 (H-16b) and the methine proton resonating at δ_H 5.75 (H-17: HMQC to δ_c 69.1) established the connectivity between C-16 (δ_c 73.5) and C-

17 (δ_c 69.1) (Figure 2.8.18). Methine C-17 (δ_c 69.1) was linked to an alcohol moiety (17-OH) from observation of a COSY correlation between the proton resonating at δ_H 5.75 (H-17) and the exchangeable proton resonance at δ_H 6.07 (17-OH). The proton resonances at δ_H 4.45 (H-16a), 3.95 (H-16b) and δ_H 6.07 (17-OH) all showed HMBC correlations to the carbon resonance at δ_c 125.3 (C-18), which allowed the assignment of the C-17 (δ_c 69.1) and C-18 bond (δ_c 125.3) (Figure 2.8.17).

The chemical shift of the carbon at δ_c 143.7 (C-12) is indicative of an oxygenated aromatic carbon. This was confirmed from a two bond HMBC correlation between the phenolic proton resonating at δ_H 4.45 (12-OH) and the aromatic carbon resonance at δ_c 143.7 (C-12). The phenolic proton resonance at δ_H 4.45 (12-OH) showed three bond HMBC correlations to the carbon resonances at δ_c 148.5 (C-11) and δ_c 108.6 (C-13), thereby placing C-12 (δ_c 143.7) between C-11 (δ_c 148.5) and C-13 (δ_c 108.6). An aromatic methine proton resonating at δ_H 7.62 (H-13: HMQC to δ_c 108.6) had HMBC cross-peaks to the aromatic carbon resonance at δ_C 142.8 (C-14), thus linking C-13 (δ_c 108.6) to C-14 (δ_C 142.8) (Figures 2.8.17 and 2.8.19). The aromatic carbon C-14 (δ_C 142.8) was assigned next to C-18 (δ_c 125.3) from observation of a three bond HMBC correlation between the proton resonance at δ_H 7.62 (H-13) and the quaternary aromatic carbon resonance at δ_c 125.3 (C-18). Finally, a four bond HMBC correlation was present between the proton resonance at δ_H 7.62 (H-13) and the aromatic carbon resonance at δ_c 113.8 (C-10) (Figure 2.8.19). This established

that C-18 (δ_c 125.3) was linked to C-10 (δ_c 113.8), which, in turn, was linked to C-11 (δ_c 148.5). All of the above is consistent with substructure substructure **III** (Figures 2.8.16 and 2.8.17).

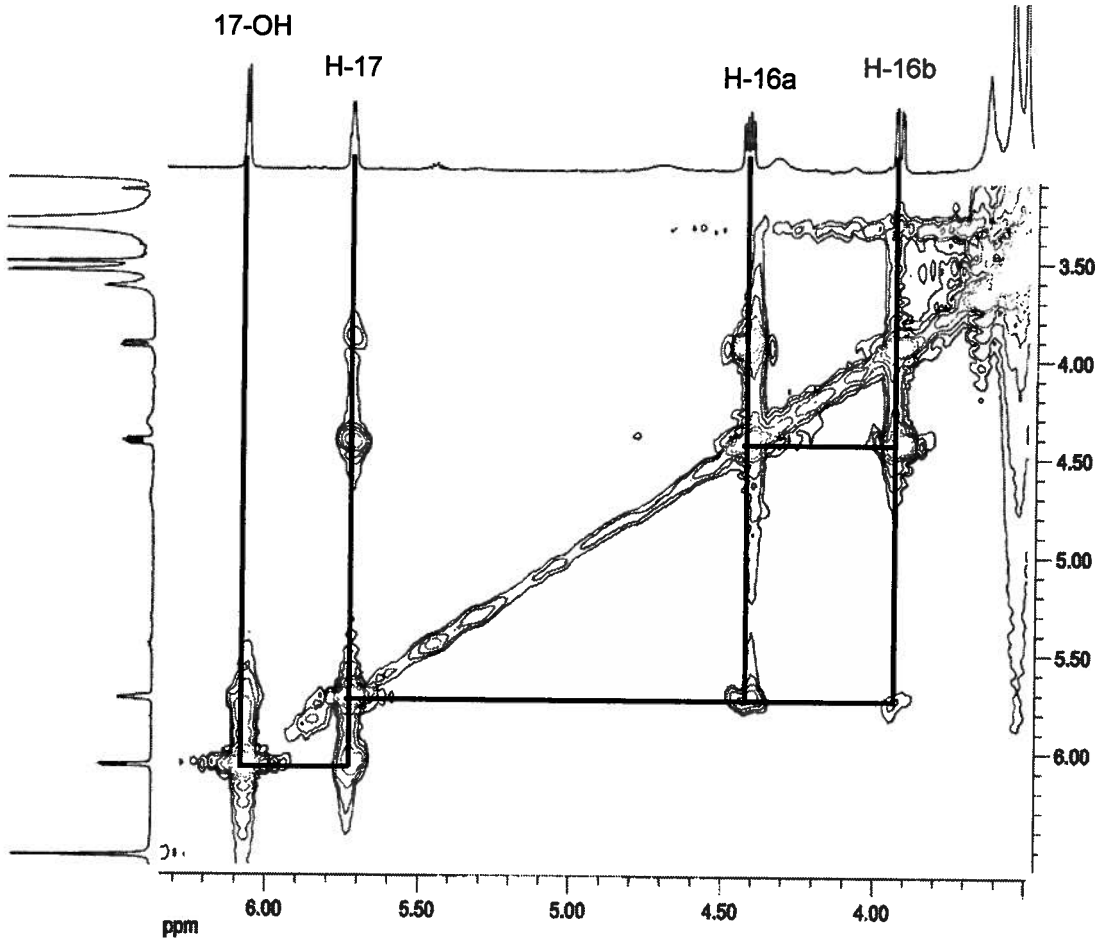

Figure 2.8.18. COSY correlations of substructure **III** of exiguamine B (**2.59**).

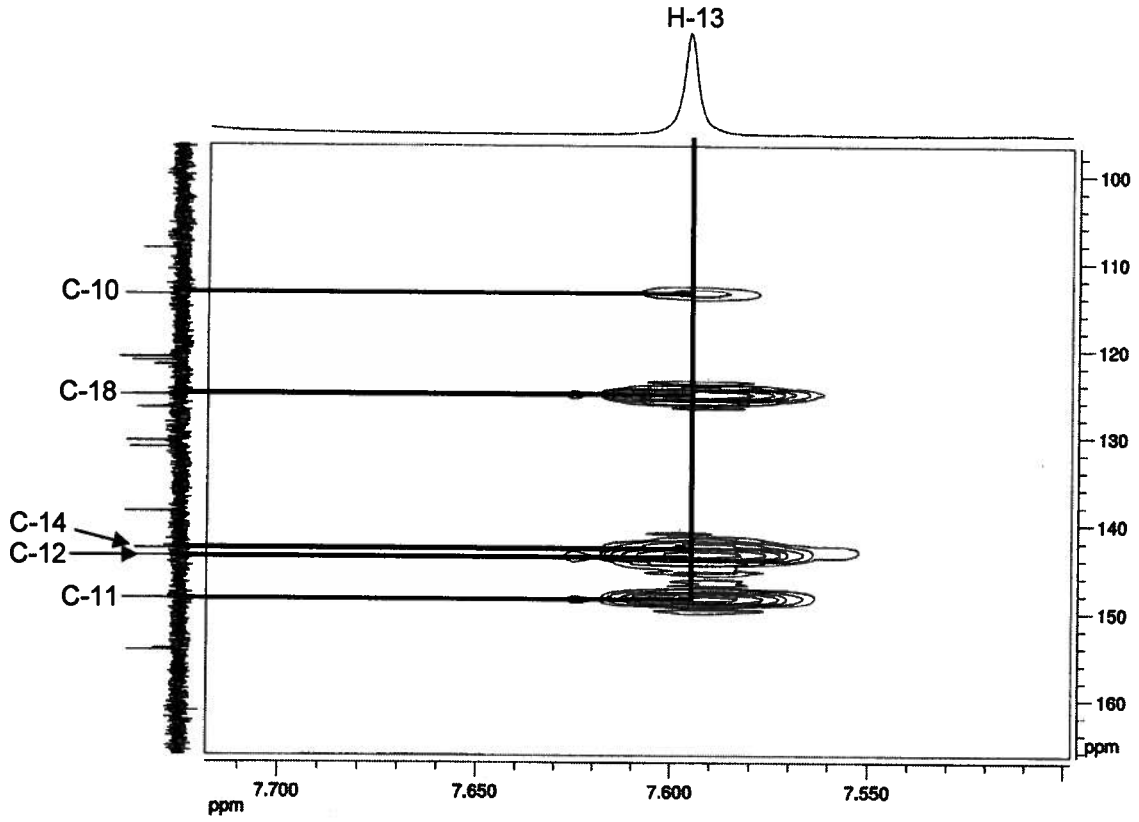

Figure 2.8.19. HMBC correlations observed for H-13 of substructure **III** of exiguamine B (**2.59**).

Unfortunately, there was insufficient NMR data to assign a constitution to exiguamine B. Attempts to crystallize exiguamine B by soaking in 1N HCl and crystallizing from methanol failed. However, comparison of the available NMR data between exiguamine A (**2.58**) and exiguamine B (**2.59**) showed that the only difference was in the placement of the hydroxyl group on C-17 (δ_c 69.1), consistent with the difference in the molecular formulae of the two natural products. Therefore, the structure of exiguamine B (**2.59**) was established based upon the comparison of the NMR data of exiguamine A (**2.58**) with those of B.

2.9 Proposed Biogenesis of Exiguamine A

A proposed biogenesis (Figure 2.9.1) of the skeleton of exiguamines involves tryptophan, DOPA, and a hydantoin moiety. Methylation of the two amides on the hydantoin (**2.60**) moiety occurs via S-adenosyl methionine to yield *N,N*-dimethylhydantoin (**2.61**). DOPA (**2.62**) undergoes a decarboxylation followed by an oxidation of the catechol ring to yield an ortho quinone moiety (**2.63**). The primary amine on **2.63** attacks in a Michael fashion to yield a bicyclic analog of DOPA (**2.64**). This is then followed by methylation via S-adenosyl methionine to afford **2.65**. A decarboxylation occurs on tryptophan (**2.66**), followed by a series of oxidations to yield tryptamine hydroquinone (**2.67**). The tryptamine analog (**2.67**) couples to the DOPA analog (**2.65**) in a Michael fashion followed by rearomatization and oxidation to yield **2.68**. Base catalyzed attack of the *N,N*-dimethylhydantoin followed by reformation of the quinone yields the exiguamine precursor **2.69**. Tautomerisation of **2.69** followed by a cyclization establishes the hexacyclic precursor to exiguamine A (**2.71**). Finally, oxidation of **2.71** affords exiguamine A (**2.58**) (Figure 2.9.1).

The exiguamines are novel alkaloids of the pyrroloquinone family of natural products. This family of natural products is characterized by having a pyrrole ring adjacent to a quinone moiety. As is evident in the biogenesis, the exiguamines contains dopamine, hydantoin, and tryptamine fragments. Even though these are very common biosynthetic elements, their connectivity yields an unprecedented hexacyclic skeleton.

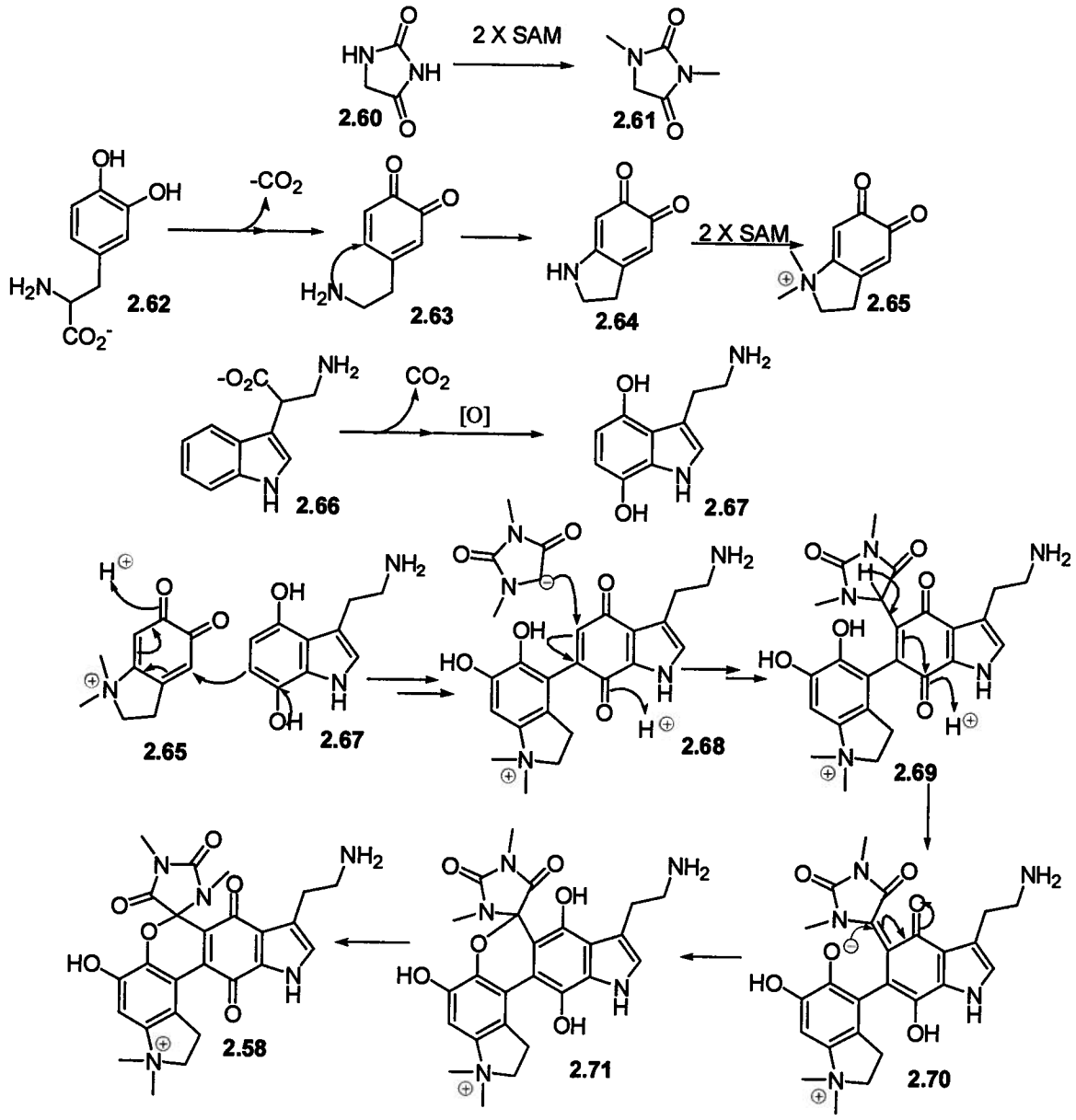

Figure 2.9.1. Proposed biogenesis of exiguamine A.

2.10 Stereochemistry of the exiguamines

From the x-ray diffraction analysis, it was discovered that exiguamine A was isolated as a racemic mixture. When exiguamine A crystallized, it belonged in the space group C2/c. The *c*-glide plane in this space group produces a symmetrical mirror relationship which means that a racemic mixture is present in

the unit cell. The lack of optical activity, as well as the lack of any peaks in the CD-spectrum (Figure 2.10.1) confirmed the racemate. When observing the biogenesis of the exiguamines, one could envisage that the oxygen on C-11 may attack from either face of the alkene, thus yielding a racemic mixture (Figure 2.10.2). Another explanation for the presence of a racemate is perhaps the exiguamines exist in equilibrium between the two enantiomers in an acidic solution (Figure 2.10.2). The purification of exiguamine A was performed using acidic solvent conditions. The acidic environment may have catalyzed the cleavage of the C-19/N-20 bond to yield a pentacyclic structure and an electrophilic imine. Nucleophilic attack of the phenol oxygen onto the electrophilic imine (C-11) from both faces yields the racemic mixture.

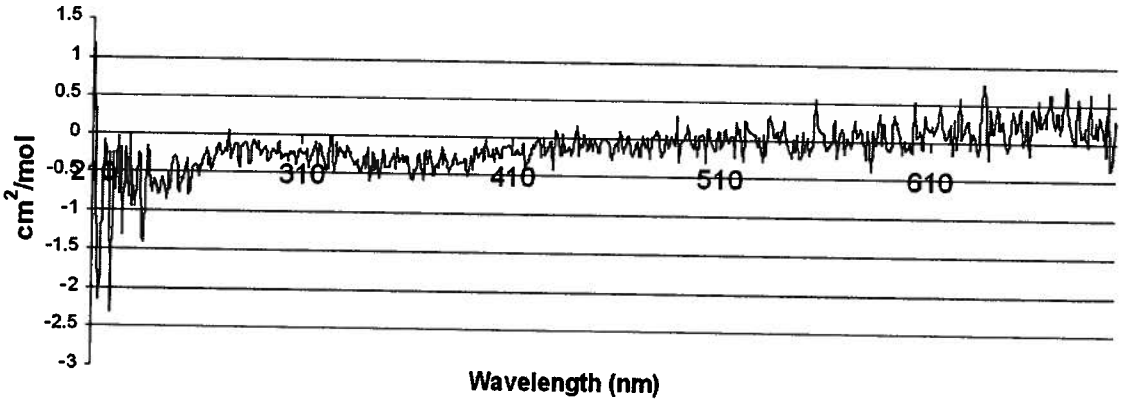

Figure 2.10.1. CD spectrum of exiguamine A.

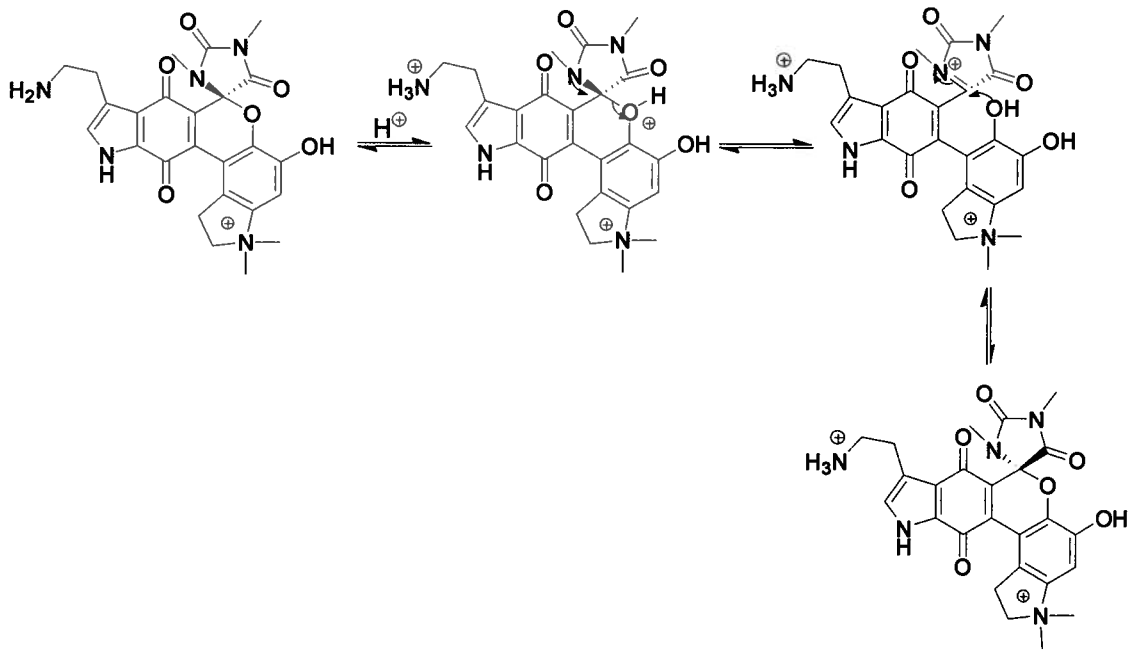

Figure 2.10.2. Possible equilibrium between the enantiomers of exiguamine A.

There are two chiral carbons in exiguamine B (**2.59**), C-17, and C-19. Similar to exiguamine A, **2.59** was purified in the presence of TFA, therefore, it is possible that a mixture of both configurations of C-19 are present. The optical rotation of exiguamine B was found to be zero and there were no peaks present in the CD-spectrum (Figure 2.10.3), suggesting the presence of equal quantities of four possible stereoisomers. Attempts to crystallize exiguamine B involved 1N HCl. The presence of the strong acid may have induced the isomerisation of the stereocentre on C-17, yielding a mixture of all four diastereomers (Figure 2.10.4). Another explanation for the lack of optical activity or a peak in the CD spectrum may be that the light emitted by the polarimeter or the CD spectrometer could not penetrate exiguamine B. The intense colour of the alkaloid may have prevented the measurement of a meaningful optical rotation or a CD curve.

Observing the ^1H NMR spectrum of exiguamine B, one could see the presence of minor peaks adjacent to the H-1, H-2, and H-26 resonances (Figure 2.10.5). The presence of these minor peaks may confirm that exiguamine B is present as a mixture of unequal quantities of diastereomers. There were no minor peaks present adjacent to either H-17 or 17-OH (Figure 2.10.6). This was unexpected as the largest deviations in chemical shift for diastereomers usually occur at the epimeric centre.

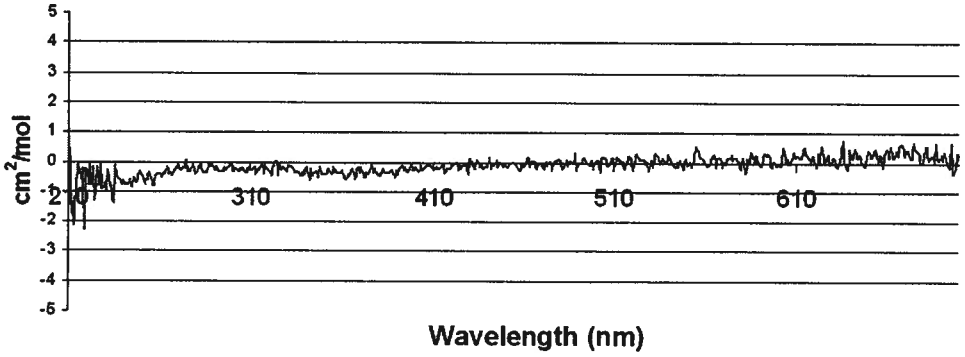

Figure 2.10.3. CD-spectrum of exiguamine B.

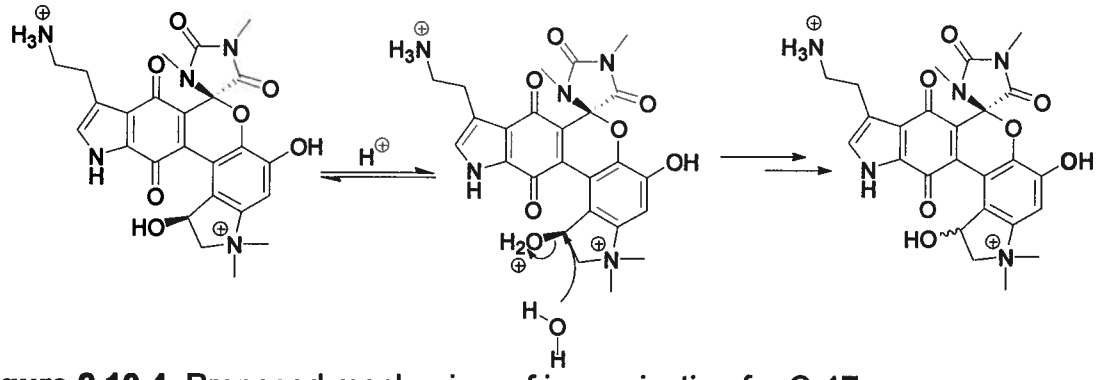

Figure 2.10.4. Proposed mechanism of isomerization for C-17.

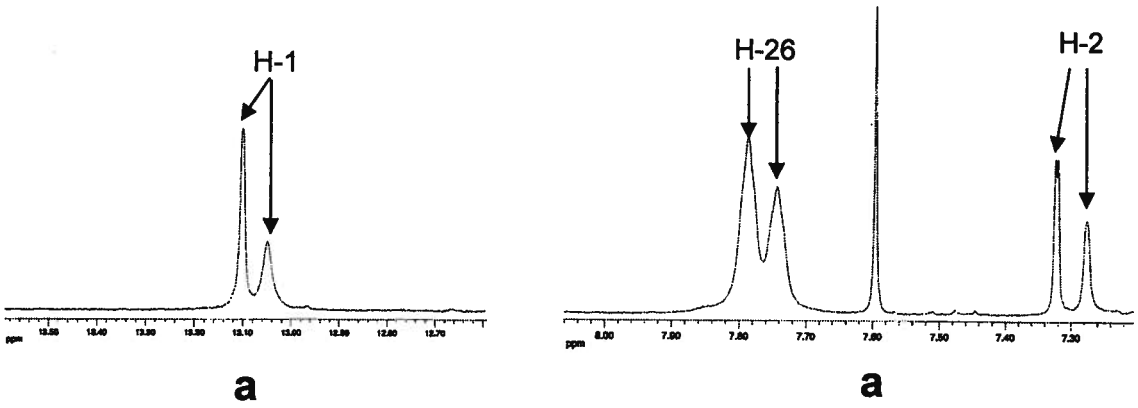

Figure 2.10.5. ^{1}H NMR expansions of exiguamine B. Minor peaks adjacent to (**a**) H-1 and (**b**) H-2 and H-26 confirm that exiguamine B was isolated as a diastereotopic mixture.

Figure 2.10.6. ^{1}H NMR of expansions of exiguamine B. No minor peaks were present adjacent to 17-OH and H-17, the proton on the epimeric carbon.

2.11 Biological activity of Exiguamine A

To screen for inhibitors against IDO, a high throughput assay was run by the laboratory of Professor Grant Mauk in the department of biochemistry at U.B.C.. IDO was added to a reaction mixture that contained tryptophan (**2.66**) and the desired extract to be tested for inhibition. A reaction was carried out for

30 minutes and stopped by the addition of trichloroacetic acid (TCA) which yields kynurerine (**2.73**). The reaction mixture was then heated at 65°C for 15 minutes, after which *p*-dimethylaminobenzaldehyde (**2.74**) was added to convert any kynurenine (**2.73**) present to the fluorescing kynurenine *N-p*-dimethylaminobenzylidene (**2.75**). The concentration of this compound was measured at 480 nm, and gave an indication of the activity of IDO.[50,51] A large concentration of **2.75** afforded an intense yellow color and indicated that the extract being tested did not inhibit IDO. Conversely, a small concentration of **2.75** yielded no color, and signified IDO inhibition. Exiguamine A was found to be a potent inhibitor of IDO in this assay, with a K_i of 210 nM, making it one of the most potent *in vitro* IDO inhibitors known to date.

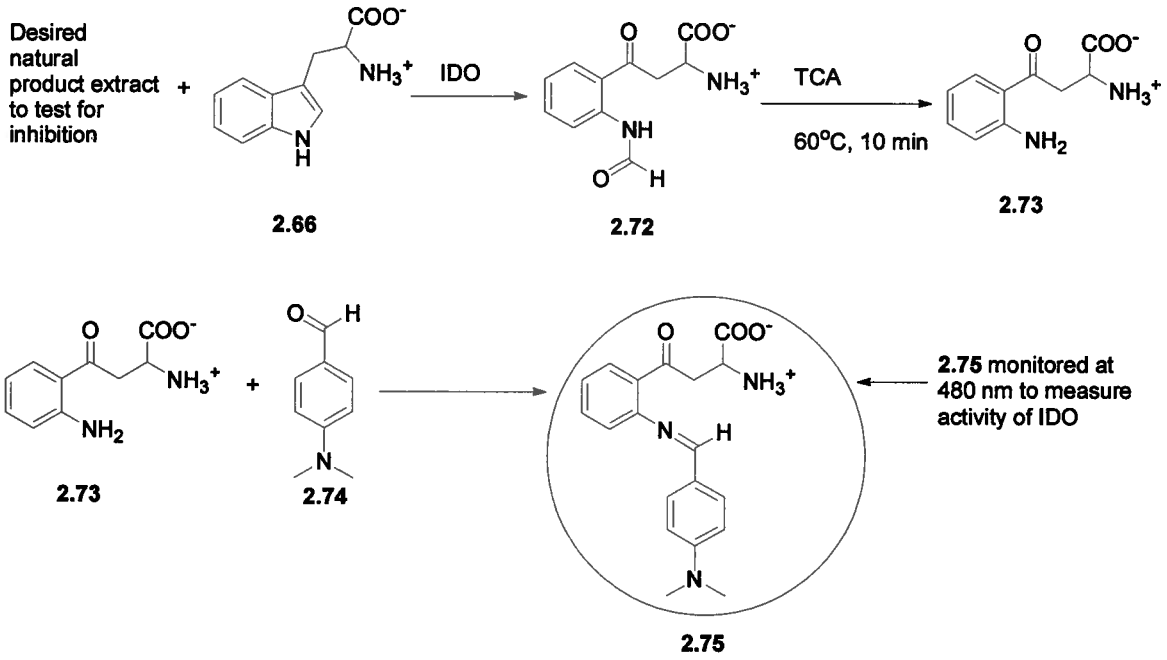

Figure 2.11.1. Description of the chemical reactions present in the *in vitro* IDO inhibition assay.

As mentioned previously, most IDO inhibitors are analogs of tryptophan. The most potent IDO inhibitors found have been the annulins,[21] which contain a quinone moiety that may be necessary for the potent activity. Exiguamines combine both of these elements of inhibition in that the proposed pharmacophore contains both an analog of trytophan, and a quinone moiety (Figure 2.12.2). We suggest that the presence of a substituted pyrroloquinone in the exiguamines is the reason these alkaloids are potent IDO abrogators. Currently, synthetic analogs of this pharmacophore are being developed to make novel inhibitors of IDO.

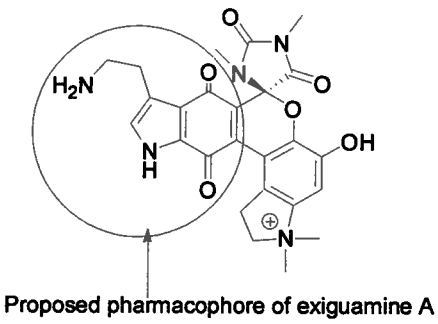

Figure 2.11.2. Proposed pharmacophore of the exiguamines.

2.12. General Experimental Methods

All solvents used (except for NMR solvents) were HPLC grade (Fisher) and no further purification was done on them unless for use on the HPLC. Those solvents were filtered through a 0.45 μm filter (Osmonics, Inc) before use. Reversed-phase C_{18} silica gel Sep Paks™ (10g) were purchased from Waters, Inc.. Separations on the HPLC was accomplished using either a Waters 2487 dual channel detector/system controller (Waters Series 515 pump; chart recorder, 0.25 cm/min), or a Waters 1500 series HPLC pump and a Waters 2487

dual channel detector. The HPLC column used was a Whatman Partisil 10 ODS-3 Magnum column. The conditions of the HPLC separation were 2.0 mL/min at 254 nm. Thin-layer chromatography (TLC) plates were Whatman MKC18F (reversed phase) and Kieselgel $60F_{254}$ (normal phase). TLC was visualized using either a dip solution of *p*-anisaldehyde (1% *p*-anisaldehyde, 2% H_2SO_4, 20% acetic acid and 77% ethanol) or under ultraviolet light (254 nm).

NMR spectra were recorded on a Bruker AV600 spectrometer fitted with a inverse triple resonance (^1H, ^{13}C, ^{15}N) cryoprobe. NMR solvents were purchased from Cambridge Isotope laboratories and were referenced to solvent peaks for DMSO-d_6 (δ_C 39.5 ppm and δ_H 7.24 ppm). Low resolution ESI mass spectra were recorded on a Bruker Esquire LC mass spectrometer. High resolution ESI mass spectra was obtained using a Micromass LCT mass spectrometer. Optical rotations were recorded with a JASCO J-1010 polarimeter equipped with a halogen lamp (589 nm) and a 10 mm micro cell. The CD spectra were determined using a JASCO J-710 spectropolarimeter with a 1 mm micro cell.

2.13. Isolation of exiguamines A and B

Neopetrosia exigua (138.5 g wet wt) was collected on Sept 17, 2003 in Milne Bay in Papua New Guinea, 10° 32.02' S, 150° 39.07' E. This is a red/brown smooth encrusting sheet sponge, 2 mm x 10 cm, collected from an overhang at 15 m depth. The sponge was identified by Dr. R. van Soest (University of Amsterdam) and a voucher sample has been kept at the Zoologisch Museum, Amsterdam (ref no ZMAPOR19113). The material was frozen and stored until workup. The frozen sponge was extracted four times with

MeOH (4 X 1L). The combined MeOH extracts were reduced *in vacuo* to give a brown solid (5.6 g). The brown solid was suspended in 400 mL of H_2O, and then sequentially partitioned with EtOAc (3 X 200 mL) and with *n*-butanol (3 X 200 mL). The active butanol fraction (1.2 g) was subjected to Sephadex ™ LH-20 size exclusion chromatography eluting with MeOH. Six hundred milligrams was further purified using gradient elution on a reversed phase Sep Pak™ (H_2O to MeOH) to attain 300 mg of the active fraction. The bioactive material was then subjected to gradient reversed phase HPLC (Inertsil C_{18}, 9.4 X 250 mm, H_2O to ACN in 0.1% TFA, UV detection at 254 nm) giving 98.3 mg. Finally, this material was purified by reversed phase HPLC (Inertsil C_{18}, 9.4 X 250 mm, 9:1:0.1 H_2O: ACN: TFA) to obtain exiguamine A (**58**, 20 mg), and exiguamine B (**59**, 4.5 mg).

2.14. Physical Data

Exiguamine A (2.58): UV (MeOH) λ_{max} (log ε) 212 (3.44), 263 (3.08), 330 (2.79) nm; $[\alpha]_D^{23}$ 0 (c 5.3, MeOH); CD (MeOH, 0.2 mg/mL) no absorption; HRESIMS $[M]^+$ *m/z* 492.1882 (calc'd for $C_{25}H_{26}N_5O_6$ 492.1883); ^1H and ^{13}C NMR data see **Table 2.7.1**.

Exiguamine B (2.59): UV (MeOH) λ_{max} (log ε) 215 (3.54), 267 (2.98), 332 (2.69) nm; $[\alpha]_D^{23}$ 0 (c 3.3, MeOH); CD (MeOH, 0.3 mg/mL) no absorption; HRESIMS $[M]^+$ *m/z* 508.1850 (calc'd for $C_{25}H_{26}N_5O_7$ 508.1832); ^1H and ^{13}C NMR data see **Table 2.8.1**.

2.15. References

(1) Munn, D. H.; Mellor, A. L. *Trends in Molecular Medicine* **2004**, *10*, 15-18.

(2) Muller, A.; Prendergast, G. C. *Cancer Research* **2005**, *65*, 8065-8068.

(3) Schrocksnadel, K.; Wirleitner, B.; Winkler, C.; Fuchs, D. *Clinica Chimica Acta* **2006**, *364*, 82 – 90.

(4) Takikawa, O. *Biochemical and Biophysical Research Communications* **2005**, *338*, 12-19.

(5) Munn, D. H.; Zhou, M.; Attwood, J. T.; Bondarev, I.; Conway, S. J.; Marshall, B.; Brown, C.; Mellor, A. L. *Science* **1998**, *281*, 1191-1193.

(6) Mellor, A. L.; Munn, D. H. *Journal of Reproductive Immunology* **2001**, *52*, 5-13.

(7) Stone, T. W.; Darlington, L. G. *Nature Reviews Drug Discovery* **2002**, *1*, 609-620.

(8) Mellor, A. *Biochemical and Biophysical Research Communications* **2005**, *338*, 20-24.

(9) Okamoto, A.; Nikaido, T.; Ochiai, K.; Takakura, S.; Saito, M.; Aoki, Y.; Ishii, N.; Yanaihara, N.; amada, K. Y.; Takikawa, O.; Kawaguchi, R.; Isonishi, S.; Tanaka, T.; Urashima, M. *Clinical Cancer Research* **2005**, *11*, 6030-6039.

(10) Ino, K.; Yoshida, N.; Kajiyama, H.; Shibata, K.; Yamamoto, E.; Kidokoro, K.; Takahashi, N.; Terauchi, M.; Nawa, A.; Nomura, S.; Nagasaka, T.; Takikawa, O.; Kikkawa, F. *British Journal of Cancer* **2006**, *95*, 1555-1561.

(11) Brandacher, G.; Perathoner, A.; Ladurner, R.; Schneeberger, S.; Obrist, P.; Winkler, C.; Werner, E. R.; G. Werner-Felmayer; Weiss, H. G.; Go, G.; Margreiter, R.; A. Konigsrainer; Fuchs, D.; Amberger, A. *Clinical Cancer Research* **2006**, *12*, 1144-1151.

(12) Malina, H. Z.; Martin, X. D. *Graefe's Archive for Clinical and Experimental Ophthalmology* **1993**, *231*, 482-486.

(13) Korlimbinis, A.; Truscott, R. J. W. *Biochemistry* **2006**, *45*, 1950-1960.

(14) Takikawa, O.; Truscott, R. J. W.; Fukao, M.; Miwa, S. *Advances in Experimental Medicine and Biology* **2003**, *527*, 277-285.

(15) Truscott, R. J. W. *The International Journal of Biochemistry & Cell Biology* **2003**, *35*, 1500-1504.

(16) Cady, S. G.; Sono, M. *Archives of biochemistry and biophysics* **1991**, 326-333.

(17) Sono, M.; Roach, M. P.; Coulter, E. D. *Chemical Reviews* **1996**, *96*, 2841-2888.

(18) Muller, A. J.; DuHadaway, J. B.; Donover, P. S.; Sutanto-Ward, E.; Prendergast, G. C. *Nature Medicine* **2005**, *11*, 312-319.

(19) Peterson, A. C.; Loggia, A. J. L.; Hamaker, L. K. *Medicinal chemistry research* **1993**, *4*, 473-482.

(20) Braestup, C.; Nielson, M.; Olsen, C. E. *Proceeding of the National Academy of Science* **1980**, *77*, 2288-2292.

(21) Pereira, A.; Vottero, E.; Roberge, M.; Mauk, A. G.; Andersen, R. J. *Journal of Natural Products* **2006**, *69*, 1496-1499.

(22) Gaspari, P.; Banerjee, T.; Malachowski, W. P.; Muller, A. J.; Prendergast, G. C.; DuHadaway, J.; Bennett, S.; Donovan, A. M. *Journal of Medicinal Chemistry* **2006**, *49*, 684-692.

(23) Hou, D. Y.; Muller, A. J.; Sharma, M. D.; DuHadaway, J.; Banerjee, T.; Johnson, M.; Mellor, A. I.; Prendergast, G. C.; Munn, D. H. *Cancer Research* **2007**, *67*, 792-801.

(24) Perry, N. B.; Blunt, J. W.; McCombs, J. D.; Munro, M. H. G. *Journal of the American Chemical Society* **1986**, *51*, 5476-5478.

(25) Copp, B. R.; Fulton, K. F.; Perry, N. B.; Blunt, J. W.; Munro, M. H. G. *Journal of Organic Chemistry* **1994**, *59*, 8233-8238.

(26) G. Lang; Pinkert, A.; Blunt, J. W.; Munro, M. H. G. *Journal of Natural Products* **2005**, *68*, 1796-1798.

(27) D'Ambrosio, M.; Guerriero, A.; Chiasera, G.; Pietra, F.; Tato, M. **1996**, *52*, 8899-8906.

(28) Sakemi, S.; Sun, H. H.; Jefford, C. W.; Berdardinelli, G. *Tetrahedron Letters* **1989**, *30*, 2517-2520.

(29) Longley, R. E.; McConnel, O. J.; Essich, E.; Harmony, D. *Journal of Natural Products* **1993**, *56*, 915-920.

(30) Sun, H. H.; Sakemi, S.; Burres, N.; McCarthy, P. *Journal of Organic Chemistry* **1990**, *55*, 4964-4966.

(31) Gunasekera, S. P.; McCarthy, P. J.; Longley, R. E.; Pomponi, S. A.; Wright, A. E. *Journal of Natural Products* **1999**, *62*, 1208-1211.

(32) Stierle, D. B.; Faulkner, D. J. *Journal of Natural Products* **1991**, *54*, 1131-1133.

(33) Radisky, D. C.; Radisky, E. S.; Barrows, L. R.; Copp, B. R.; Kramer, R. A.; Ireland, C. M. *Journal of the American Chemical Society* **1993**, *115*.

(34) Venables, D. A.; Barrows, L. R.; Lassota, P.; Ireland, C. M. *Tetrahedron Letters* **1997**, *38*, 721-711.

(35) Fu, X.; Ng, P. L.; Schmitz, F. J.; Hossain, M. B.; Helm, D. V. d.; Kelly-Borges, M. *Journal of Natural Products* **1996**, *59*, 1104-1106.

(36) Keyzers, R. A.; Arendse, C. E.; Hendricks, D. T.; Samaai, T.; Davies-Coleman, M. T. *Journal of Natural Products* **2005**, *68*, 506-510.

(37) Copp, B. R.; Ireland, C. M. *Journal of Organic Chemistry* **1991**, *56*, 4596-4597.

(38) Hooper, G. J.; Davies-Coleman, M. T.; Kelly-Borges, M.; Coetzee, P. S. *Tetrahedron Letters* **1996**, *37*, 7135-7138.

(39) Utkina, N. K.; Makrchenko, A. E.; Denisenko, V. A.; Dmitrenok, P. S. *Tetrahedron Letters* **2004**, *45*, 7491-7494.

(40) Utkina, N. K.; Makarchenko, A. E.; Denisenko, V. A. *Journal of Natural Products* **2005**, *68*, 1424-1427.

(41) Hooper, J. N. A.; Soest, R. W. M. V. *System Porifera A Guide to Classification of Sponges*; Kluwer Academic/Plenum Publishers: New York, 2002.

(42) Liu, H.; Mishima, Y.; Fujiwara, T.; Nagai, H.; Kitazawa, A.; Mine, Y.; Kobayashi, H.; Yao, X.; Yamada, J.; Oda, T.; Namikoshi, M. *Marine Drugs* **2004**, *2*, 154-163.

(43) Hildemann, W. H. *Transplantation* **1981**, *32*, 77-80.

(44) Nakagawa, M.; Endo, M. *Tetrahedron Letters* **1984**, *25*, 3227-3230.

(45) Orabi, K.; Sayed, K. A. E.; Hamann, M. T.; Dunbar, D. C.; Al-Said, M. S.; Higa, T.; Kelly, M. *Journal of Natural Products* **2002**, *65*, 1782-1785.

(46) Iwagawa, T.; Kaneko, M.; Okamura, H.; Nakatani, M.; Soest, R. W. M. v.; Shiro, M. *Journal of Natural Products* **2000**, *63*, 1310-1311.

(47) Thale, Z.; Johnson, T.; Tenney, K.; Wenzel, P. J.; Lobkovsky, E.; Clardy, J.; Media, J.; Pietraszkiewicz, H.; Valeriote, F. A.; Crews, P. *Journal of Organic Chemistry* **2002**, *67*, 9384-9391.

(48) Williams, D. E.; Craig, K. S.; Patrick, B.; McHardy, L. M.; Soest, R. v.; Roberge, M.; Andersen, R. J. *Journal of Organic Chemistry* **2002**, *67*, 245-258.

(49) Nelson, J. H. In *Nuclear Magnetic Spectroscopy*; Nelson, J. H., Ed.; Pearson Education, Inc.: Upper Saddle River, 2003.

(50) Sono, M.; Cady, S. G. *Biochemistry* **1989**, *28*, 5392-5399.

(51) Takikawa, O.; Kuroiwa, T.; Yamazaki, F.; Kido, R. J. *Journal of Biological Chemistry* **1988**, *263*, 2041-2048.

Chapter 3: Isolation of Compounds That Can Induce Neurite Outgrowth

3.1. Preview of Chapter 3

After an injury to the spinal cord, the axons within the lesion will attempt to repair the damage. Unfortunately, inhibitory components within the central nervous system prevent the spontaneous regeneration of axons.[1] Compounds that can activate neurite outgrowth and overcome the inhibitory cues of the central nervous system have the potential to be used to treat traumatic spinal cord injury.[1] This chapter will discuss the isolation and synthesis of compounds that can induce neurite outgrowth.

3.2. Inhibitions that Prevent Spinal Cord Repair

Traumatic spinal cord injuries (SCI) can result in severe disability. Patients may become either paraplegic or quadriplegic, lose their tactile sensation, lose the ability to coordinate voluntary movements and often have chronic pain issues and spasticity.[2] Unfortunately, treatment options are limited and damage to the spinal cord cannot be adequately treated by any therapy.[3] In 2004, it was estimated that 11,000 new cases of spinal cord injuries would be diagnosed per year in the United States.[4] The prevalence of SCI and the devastating effects it has on patients has led to considerable research to yield novel interventions that can repair the spinal cord.

Following a traumatic lesion in the spinal cord, the nerve fibers begin a brief attempt to repair the damage by sprouting over the area of damage. Unfortunately, the environment of the central nervous system (CNS) makes it difficult for axons to bypass the injury site.[1] One of the factors contributing to the lack of regeneration is the development of scar tissue at the lesion site. This tissue contains chondroitin-sulfate proteoglycans (CSPG) which inhibit axonal regeneration. The mechanism by which CSPGs inhibits neurite outgrowth is unclear.[1]

The lack of regeneration in the CNS is also due to the presence of inhibitory compounds within myelin, which is the electrically insulating layer that surrounds the axons of many neurons.[5] After damage to the spinal cord, myelin is disrupted, which leaves a high concentration of inhibitory molecules present in the lesion. Three proteins from myelin have been identified as the major inhibitors of axon regeneration. These are Nogo-A, myelin-associated glycoprotein (MAG), and oligodendrocyte-myelin glycoprotein (OMgp).[5] All of these proteins bind to the Nogo receptor (NgR), which then activates the RhoA GTP-ase. RhoA then serves to trigger the ROCK (RhoA associated coiled-coil-containing protein kinase) serine-threonine protein kinase which leads to the inactivation of neurite outgrowth (Figure 3.2.1).[6]

Compounds that induce axonal regeneration might be used to treat the dysfunctions brought on by spinal cord injury. Inhibitors of the ROCK kinase are compounds that can potentially induce neurite outgrowth by overcoming the inhibitory proteins of myelin. The two most studied inhibitors of the ROCK kinase

are the isoquinoline alkaloid fasudil (**3.1**, Figure 3.2.2) and Y-27632 (**3.2**, Figure 3.2.2). Fasudil inhibits the ROCK kinase with a K_i of 330 nM,[7] but unfortunately, fasudil is a non-specific kinase inhibitor and is unlikely to be used to treat spinal cord injuries.[8] Y-27632 has a K_i of 140 nM and is more potent at inhibiting ROCK than fasudil,[7] but this amino-pyridine is not a promising drug candidate to treat spinal cord injuries because it too is a non-specific kinase inhibitor.[8]

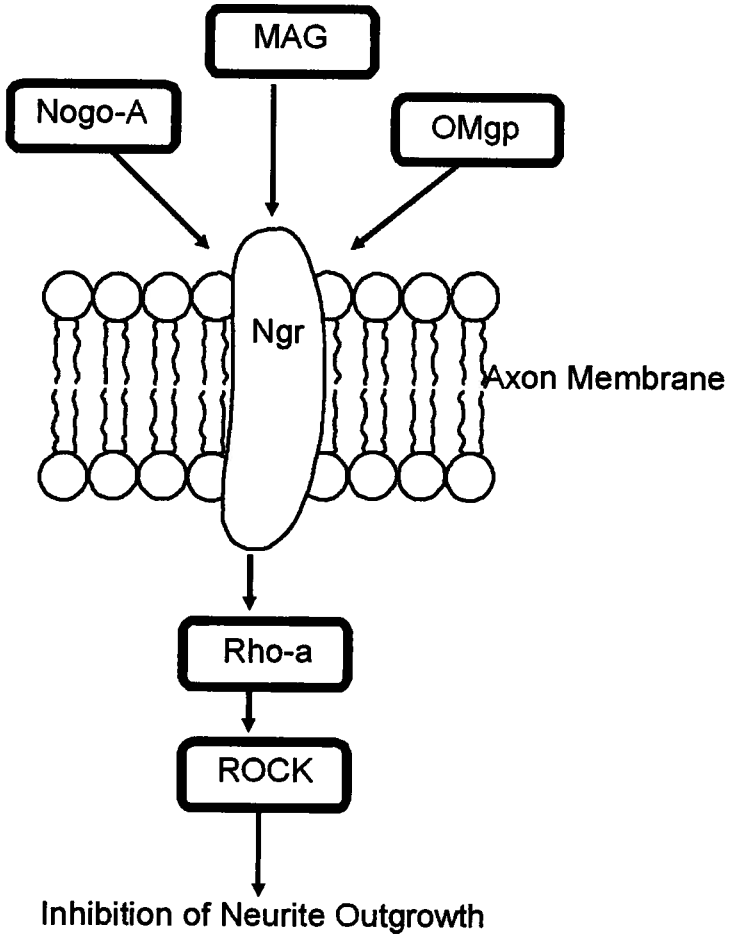

Figure 3.2.1. Nogo-A, MAG, and OMgp are inhibitory proteins found in myelin. These bind to the Nogo receptor (Ngr) which activates the RhoA GTPase. This then triggers ROCK which inhibits neurite outgrowth.

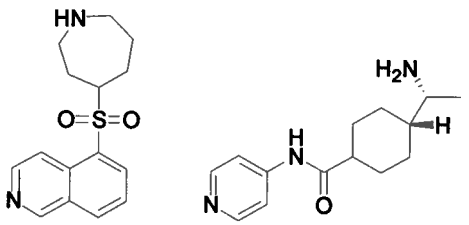

3.1 3.2

Figure 3.2.2. Inhibitors of ROCK as potential axonal outgrowth activators.

3.3. Neuroprotective Properties of Diketopiperazines

The thyrotropin-releasing hormone (TRH) (**3.3**, Figure 3.3.1) is a tri-peptide hormone that is produced by the hypothalamus. It is distributed throughout the CNS and has many neurological functions including regulating changes in temperature, and also interacting with opioid receptors.[9] TRH is metabolized in the central nervous system and in the blood into the diketopiperazine cyclo(S-His-S-Pro) (**3.4**, Figure 3.3.1). This diketopiperazine is also present throughout the CNS and has significant neurological roles. Levels of cyclo(S-His-S-Pro) increase in the presence of alcohol in the brain. Studies have revealed that **3.4** assists in diminishing the sedative effects of alcohol. Other behavioral effects of cyclo(S-His-S-Pro) include acting on the hypothalamus to reduce the intake of food.[10]

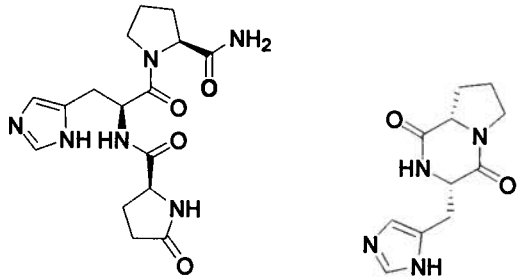

3.3 3.4

Figure 3.3.1. TRH (**3**) and Cyclo(S-His-S-Pro).

In the presence of a spinal cord injury, it has also been shown that the thyrotopin-releasing hormone has neuroprotective effects. TRH increases cerebral blood flow as a neuroprotective mechanism. In a small clinical trial, twenty patients with spinal cord injuries were treated with TRH. Examination of these patients after four months of treatment revealed significant increases in motor and sensory functions.[11] Unfortunately, TRH would be a poor drug candidate to treat spinal cord injuries due to the large number of physiological processes this hormone is involved in.[12]

As mentioned above, TRH is also metabolized to the bioactive diketopiperazine cyclo(S-His-S-Pro) (**3.4**) which has similar biological properties. Synthesis of diketopiperazines may provide compounds that can potentially provide similar neuroprotective effects to that of TRH.[9] Based on this fact, a series of cyclized dipeptides were synthesized and evaluated for their neuroprotective actions. One diketopiperazine similar to cyclo(S-His-S-Pro) was synthesized in which the histidine functionality was replaced by a 3,5-di-*tert*-butyltyrosine. Evaluation of its neuroprotective properties established that cyclo((di-*tert*-Bu)Tyr-Pro) (**3.5**, Figure 3.3.2) protected neurons from free-radical mediated death.[9]

The most promising cyclized dipeptide is the compound referred to as 35b (**3.6**, Figure 3.3.2). *In vitro* studies have revealed that 35b provides neuroprotection against apoptotic and mechanical cell death.[13] Administering 35b to rats and mice with brain injuries reduced their lesions and improved cognitive and motor outcomes. This compound displayed no harmful effects

even at 100 times the optimal therapeutic dosage. Furthermore, 35b did not have any endocrine effects, nor did it interact with any TRH receptors. The specificity of 35b makes it a promising drug candidate.[12] Other diketopiperazines with neuroprotective properties include **3.7** and **3.8**, however these two cyclic dipeptides are less potent neuroprotective agents.[12]

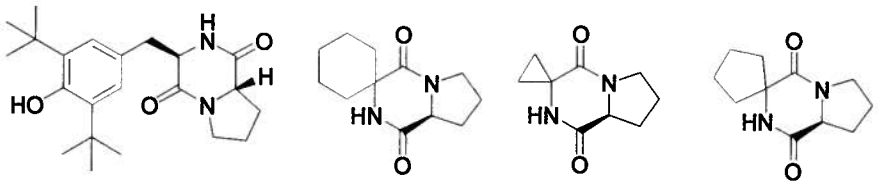

3.5 3.6 3.7 3.8

Figure 3.3.2. Neuroprotective Diketopiperazines.

3.4. Isolation of Neurite Outgrowth Activator from *Bacillus* sp.

A MeOH extract of a *Bacillus* sp. collected in Dominica was suspended in a 9:1 MeOH: H_2O mixture and then partitioned with hexanes. The MeOH/H_2O partition showed axonal outgrowth activity and was subjected to size exclusion chromatography, flash reversed-phase column chromatography and reversed-phase HPLC to yield pure cyclo(S-Val-S-Phe) (**3.9**). The structure of the known diketopiperazine was confirmed by comparing the optical rotation, NMR, and MS data to the literature values.[14] For full experimental details, see Section 3.10.

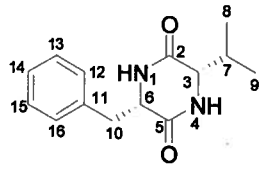

3.9

Figure 3.4.1. Cyclo(S-Val-S-Phe) (**3.9**), a compound promoting axonal outgrowth.

3.5. Stucture Elucidation of Cyclo(S-Val-S-Phe)

Cyclo(S-Val-S-Phe) (**3.9**) was isolated as a white powder that gave a $[M + Na]^+$ ion at *m/z* 269.1269 in the HRESIMS, appropriate for a molecular formula of $C_{14}H_{14}O_{14}Na$ (calc'd for 269.1266) and requiring seven degrees of unsaturation. The ^1H NMR spectrum was acquired in DMSO-d_6 at 600 MHz. Examination of the ^1H NMR spectrum (Figure 3.5.1) revealed two exchangeable protons (δ_H 8.11 and 7.91), five aromatic protons (δ_H 7.17-7.25), four protons on carbons adjacent to either a heteroatom or an aromatic ring (δ_H 4.21, 3.52, 3.15, 2.86), and two methyl doublets (δ_H 0.64 and 0.25). Analysis of the ^{13}C NMR (Figure 3.5.2) and the HMQC spectra indicated the presence of two carbonyls (δ_C 166.5 and 166.3), one quaternary carbon (δ_C 136.2), six methine carbon resonances (δ_C 130.2, 127.9, 126.4, 59.0, 54.9, 30.9), one methylene (δ_C 37.7) and two methyls (δ_C 18.2 and 16.0). The planar structure of **3.9** was determined as cyclo(Val-Phe) by extensive examination of the 1D and 2D NMR data. Comparison of the ^1H NMR data of **3.9** to previously published data of cyclo(S-Val-S-Phe)[14] and cyclo(S-Val-R-Phe)[15] established a cis-diketopiperazine (Table 3.6.1). The optical rotation of **3.9** ($[\alpha]_D^{22}$ -45.82 (c 0.3, DMSO)) was similar to that found for cyclo(S-Val-S-Phe) ($[\alpha]_D^{22}$ -43.30 (c 0.3, DMSO)) in the literature,[15] which established the absolute configuration as 3S and 6S.

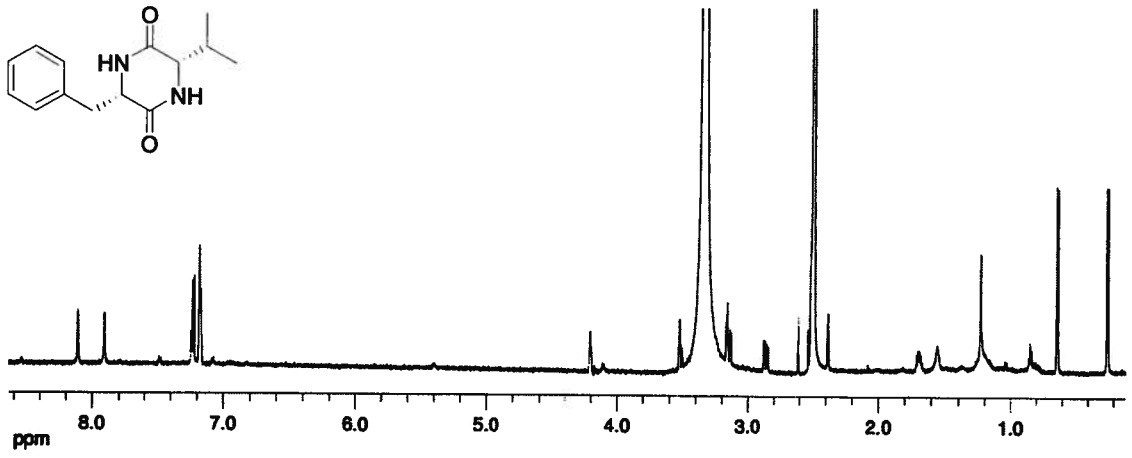

Figure 3.5.1. ^{1}H NMR spectrum of cyclo(S-Val-S-Phe) (**3.9**) acquired at 600 MHz in DMSO-d_6.

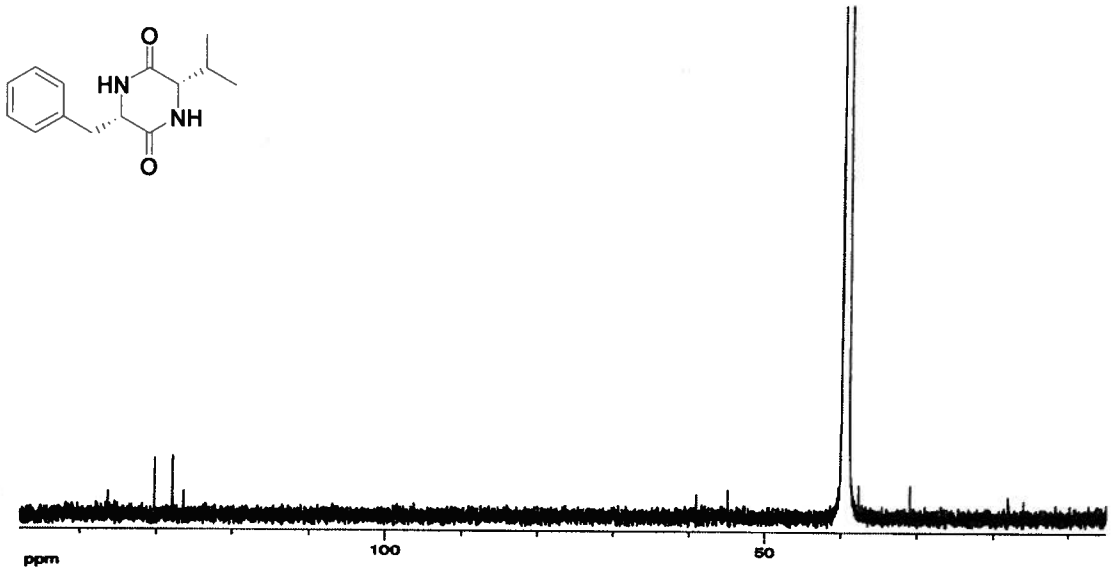

Figure 3.5.2. ^{13}C NMR spectrum of cyclo(S-Val-S-Phe) (**3.9**) acquired at 150 MHz in DMSO-d_6.

Table 3.5.1. ^{1}H chemical shift values for **3.9**, and the literature ^{1}H chemical shift values for both cyclo(S-Val-S-Phe) and cyclo(S-Val-R-Phe).[a]

	Chemical shift values of **3.9**	Literature chemical shift values of cyclo(S-Val-S-Phe)[14]	Literature chemical shift values of cyclo(S-Val-R-Phe)[15]
Position	δ_H (*J* in Hz)	δ_H (*J* in Hz)	δ_H (*J* in Hz)
1	8.11, bs	8.14, bs	8.14, bs
2			
3	3.52, m	3.52, m	3.38, m
4			
5	7.91, brs	7.92, brs	7.93, brs
6	4.21, m	4.22, m	4.16, m
7	1.69, m	1.71, m	2.00, m
8[b]	0.64, d, (7.2)	0.66, d, (7.1)	0.79, d, (7.0)
9[b]	0.25, d, (7.2)	0.27, d, (6.8)	0.72, d, (7.0)
10a	3.15, m	3.16, dd, (13.5, 4.5)	3.14, dd, (13.6, 3.7)
10b	2.86, m	2.88, dd, (13.5, 5.0)	2.86, dd, (13.6, 3.7)
11-16	7.17-7.25, m	7.16-7.28, m	7.05-7.30, m

[a] ^{1}H chemical shifts [ppm] were all referenced to DMSO-d_6 (2.50 ppm)
[b] H-8 and H-9 are interchangeable signals

3.6. Synthesis of Cyclo(S-Val-S-Phe) and its Diastereomers

Isolation and structure elucidation of the active component from the *Bacillus* sp. extract had established that cyclo(S-Val-S-Phe) was inducing axonal outgrowth. Further biological studies were necessary, so cyclo(S-Val-S-Phe) was generated by employing the synthesis developed by Bull *et. al.* (Scheme 3.6.1).[14,16] To analyze if the stereochemistry played a role in the biological activity of **3.9**, the three other diastereomers were also synthesized (Schemes 3.6.1 and 3.6.2).

The commercially available diketopiperazine (S)-(+)-3-isopropyl-2,5-piperazinedione (**3.10**, Scheme 3.6.1) was added to a solution of sodium hydride and DMF and stirred at 0°C. *p*-methoxybenzyl chloride was added and the reaction was stirred for 4 h. The reaction was quenched and purified by flash

silica gel chromatography to afford the protected diketopiperazine **3.11** (α_D^{22}: -49.8 (c 0.8, $CHCl_3$)) with an overall yield of 75% (Scheme 3.6.2). To a stirring solution of LHMDS in THF, **3.11** was added and allowed to stir at -78°C for 1 h. To the solution, benzyl bromide was added and the reaction stirred for an additional 3 h at -78°C. The solution was quenched with ammonium chloride and the (3S, 6R) benzylated diketopiperazine **3.12** (65% yield) (Scheme 3.6.2) was separated from the reaction mixture via flash silica gel chromatography.

Molecular modeling studies have shown that **3.15** (enolate of **3.11**) prefers a conformation where the (3S)-isopropyl group is syn to the N-1 protecting group, and anti to the N-4 protecting group (Figure 3.6.1). This conformation sterically inhibits benzylation at the Si face of enolate **3.15.** Benzylation occurs anti to both the N-1 protecting group and the isopropyl moiety which yields the (3S, 6R) benzylated diketopiperazine **3.12.**[16,17] Treatment of **3.12** with ceric ammonium nitrate followed by separation with a reversed phase Sep Pak™ afforded the diastereomerically pure cyclo(S-Val-R-Phe) (**3.14**, α_D^{21}: -65.4 (c 0.25, DMSO); 65%) (Scheme 3.6.1). The structure and absolute stereochemistry of **3.14** was confirmed by comparing the optical rotation, MS and NMR data to the literature values.[16]

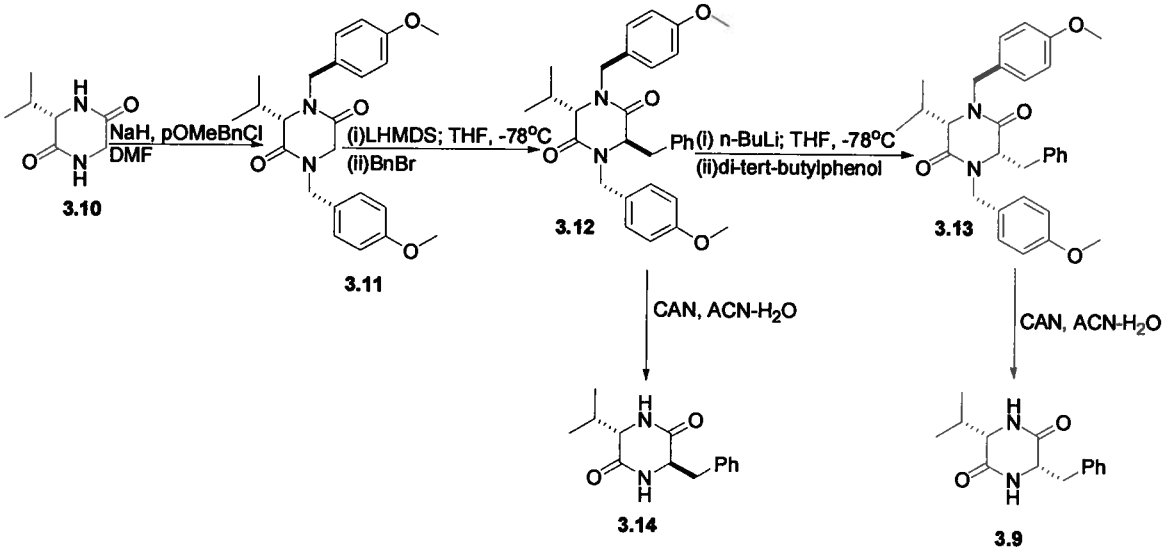

Scheme 3.6.1. Synthesis of cyclo(S-Val-S-Phe) (**3.9**) and cyclo(S-Val-R-Phe) (**3.14**)

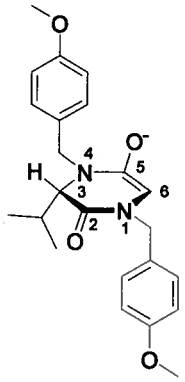

3.15

Figure 3.6.1. Preferred conformation of enolate **3.15**.

To obtain the other diastereomer, **3.12** was added to a solution of *n*-BuLi in THF and allowed to stir for 1 h at -78°C. The reaction was quenched with 2,6-di-*tert*-butylphenol, and flash silica chromatography afforded the (3S, 6S) benzylated diketopiperazine **3.13** (Scheme 3.6.1) in an 80% yield. The preferred conformation of **3.12** has the isopropyl group syn to the N-1 protecting group and anti to the N-4 protecting group. The branched isopropyl group and the N-4 protecting group provide steric hindrance to *n*-BuLi. This results in selective

deprotonation at C-6 to obtain the enolate **3.16**. When **3.13** was treated with *n*-BuLi and deuterated with MeOD, there was no deuterium incorporation on C-3. Therefore, only the proton on C-6 was abstracted by *n*-BuLi (Figure 3.6.2).[17] When a bulky proton source such as 2,6-di-*tert*-butylphenol is used, the C-3 alkyl group and the N-1 protecting group provide enough steric hindrance, which results in selective reprotonation trans to both the C-3 and N-1 allyl substituents to obtain the (3S, 6S) diketopiperazine **3.13**. Deprotection of **3.13** was accomplished by the oxidative removal of the *p*-methoxybenzyl groups using ceric ammonium nitrate. Chromatographic purification of the reaction mixture with a reversed phase Sep Pak™ and reversed phase HPLC obtained the diastereomerically pure cyclo(S-Val-S-Phe) (**3.9**) in 70% yield (α_D^{22}: -45.82 (c 0.3, DMSO)). The structure and absolute stereochemistry of diketopiperazine **3.9** was confirmed by comparing the optical rotation, MS and NMR data to the literature values.[14]

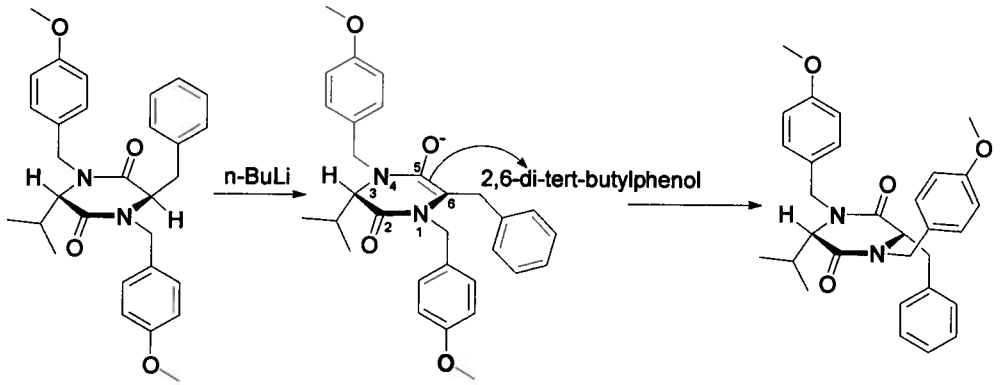

3.12 **3.16** **3.13**

Figure 3.6.2. Preferred conformations of **3.12**, **3.16**, **3.13**.

Cyclo(R-Val-S-Phe) (**3.21**) was prepared in a similar fashion to cyclo(S-Val-R-Phe) (**3.14**) (Scheme 3.6.2). Comparison of the NMR data of

diketopiperazine **3.21** to both diketopiperazine **3.14** and the literature established the structure and relative stereochemistry of **3.21**.[16] The optical rotation of diketopiperazine **3.21** (α_D^{21}: 69.3, (c 0.3 DMSO)) was similar, but opposite in sign, to diketopiperazine **3.14** (α_D^{21}: -65.4, (c 0.25 DMSO)).[16] This confirmed that these two molecules are enantiomers and the absolute stereochemistry of cyclo(R-Val-S-Phe) was determined.

To prepare cyclo (R-Val-R-Phe) (**3.22**), a similar synthesis was employed to that of its enantiomer, cyclo(S-Val-S-Phe) (**3.9**) (Scheme 3.6.2). The NMR data of cyclo(R-Val-R-Phe) (**3.22**) was compared to those of both **3.9** and the literature to obtain the structure and relative stereochemistry of **3.21**.[16] The diketopiperazine **3.22** (α_D^{22}: 43.45 (c 0.29, DMSO)) had an optical rotation that was similar but opposite in sign to that of **3.9** (α_D^{22}: -45.82 (c 0.3, DMSO)). This established that both molecules are enantiomers; thus, the absolute stereochemistry of cyclo(R-Val-R-Phe) was confirmed.

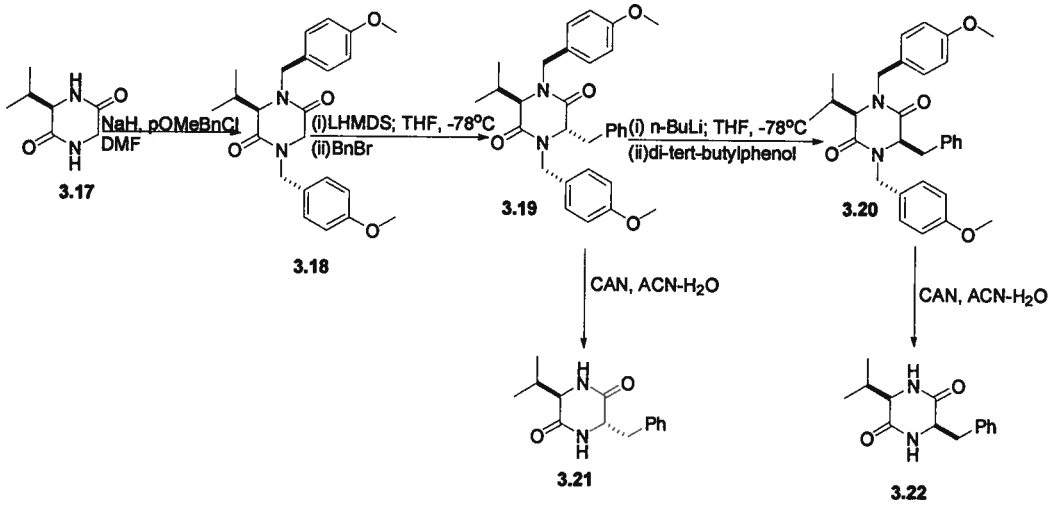

Scheme 3.6.2. Synthesis of cyclo(R-Val-S-Phe) (**3.21**) and cyclo(R-Val-R-Phe) (**3.22**).

3.7. Biology of Diketopiperazines

Actin is an abundant protein in cells that polymerizes to form actin filaments. These filaments are dispersed throughout the cell and are critical for cell motility. Cell migration and neurite outgrowth are very similar processes in that they both require the organized polymerization of actin filaments.[18] Because of the parallels that exist between cell migration and neurite outgrowth, Dr. Tim O'Connor from the Department of Anatomy at the University of British Columbia has developed a novel high-throughput assay to look for compounds that are able to promote cell migration. In this screen, HEK293 cells are cultured in 96-well plates and allowed to grow to confluency. A 96-pin Biogrid robot then scratches the middle of each well and natural product extracts are added. The treated cells are incubated for 18 hours and then evaluated for their ability to reenter the scratch. Positive candidates stimulate migration into the scratch, while cells exposed to inactive compounds will not reinvade the scratch (Figures 3.7.1 and 3.7.2). Bioassay guided fractionation of the *Bacillus* sp. extract led to the discovery of cyclo(S-Val-S-Phe) (**3.9**) as a promoter of cell migration at a concentration range of 20-40 μM. The synthetic enantiomer, cyclo(R-Val-R-Phe) (**3.22**), was also found to be active in the cell migration assay at a similar concentration range. The other two synthetic diastereomers, cyclo(S-Val-R-Phe) (**3.14**) and cyclo(R-Val-S-Phe) (**3.21**), were found to be inactive. These results indicate that the cyclo(cis-Val-Phe) will promote neurite outgrowth while the cyclo(trans-Val-Phe) is not active.

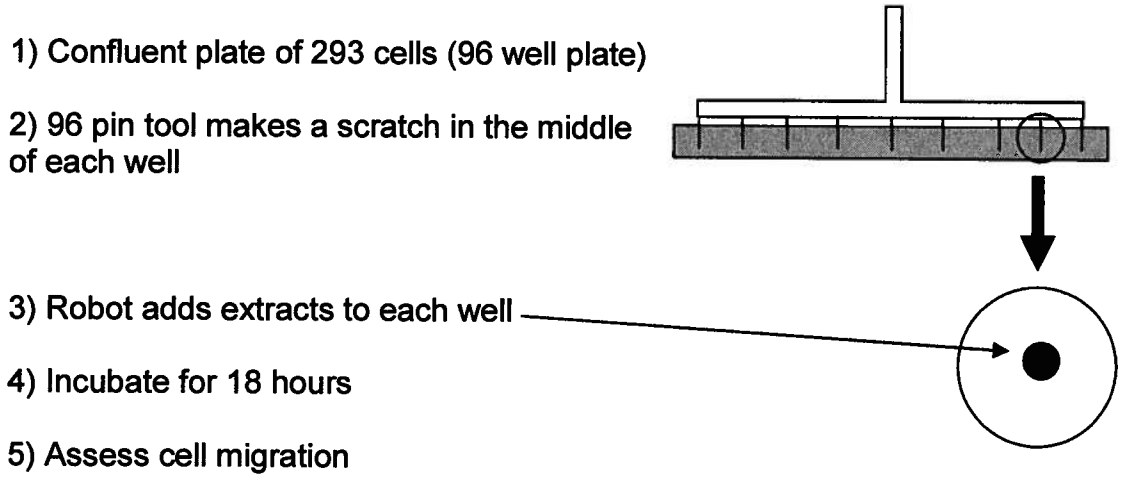

Figure 3.7.1. The procedure of the cell migration assay to isolate neurite outgrowth activators.

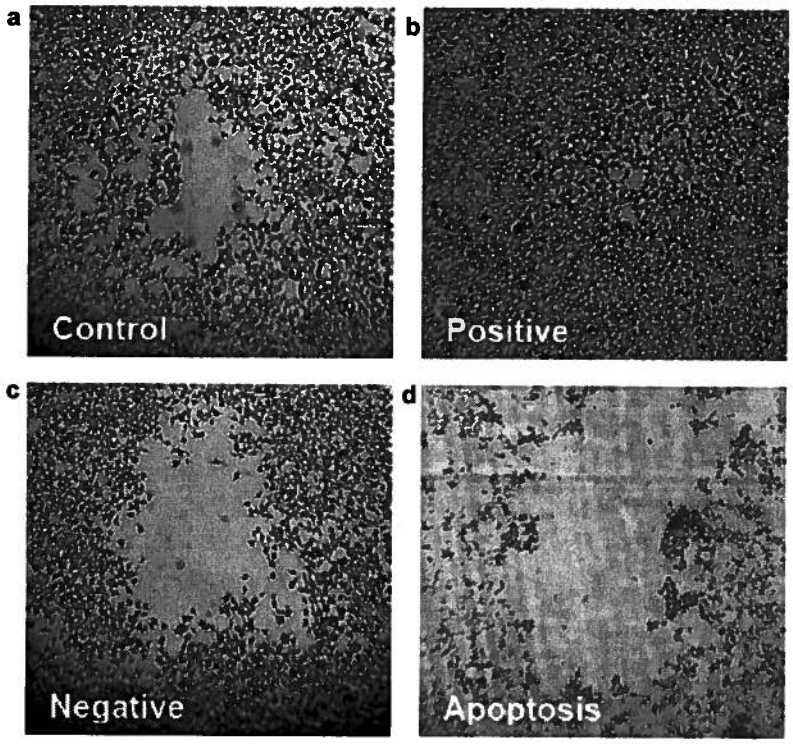

Figure 3.7.2. To evaluate the ability of the extracts to promote cell migration, each well is viewed under a microscope. These images were generated by Jennifer Wong of the O'Connor lab. As is evident in **b**, when compounds induce cell migration, the scratch becomes inhabited. Extracts may also inhibit cell migration (**c**), or promote apoptosis (**d**). In the last two cases, cells do not enter the scratch.

To further assess the ability of cyclo(S-Val-S-Phe) to act as an activator of neurite outgrowth, a secondary assay was performed. In this assay, day eight dorsal root ganglia isolated from chick embryos were cultured on glass coverslips coated with 100 μg/mL poly-L-lysine (PLL). The dorsal root ganglia were incubated on the coverslips for 2 h and the natural product candidates were added. Increases in the neurite length measurements establish an activator of axonal outgrowth. Hence, addition of 32 μM of cyclo(S-Val-S-Phe) enhanced neurite length. To analyze the ability of cyclo(S-Val-S-Phe) to induce axonal outgrowth in a physiological environment, the secondary assay was done in the presence of inhibitors present in the lesion site. Day 8 dorsal root ganglia from chick embryos were cultured with both 20 μg/mL of poly-L-lysine and 4 μg/mL of CSPG. These neurons showed axonal outgrowth when 32 μM of cyclo(S-Val-S-Phe), was added. Similar results were present when 32 μM of cyclo(S-Val-S-Phe) was added to day 14 dorsal root ganglia from chick embryos cultured in 20 μg/mL of PLL and 40 μg/mL of myelin (Figures 3.7.3 and 3.7.4).

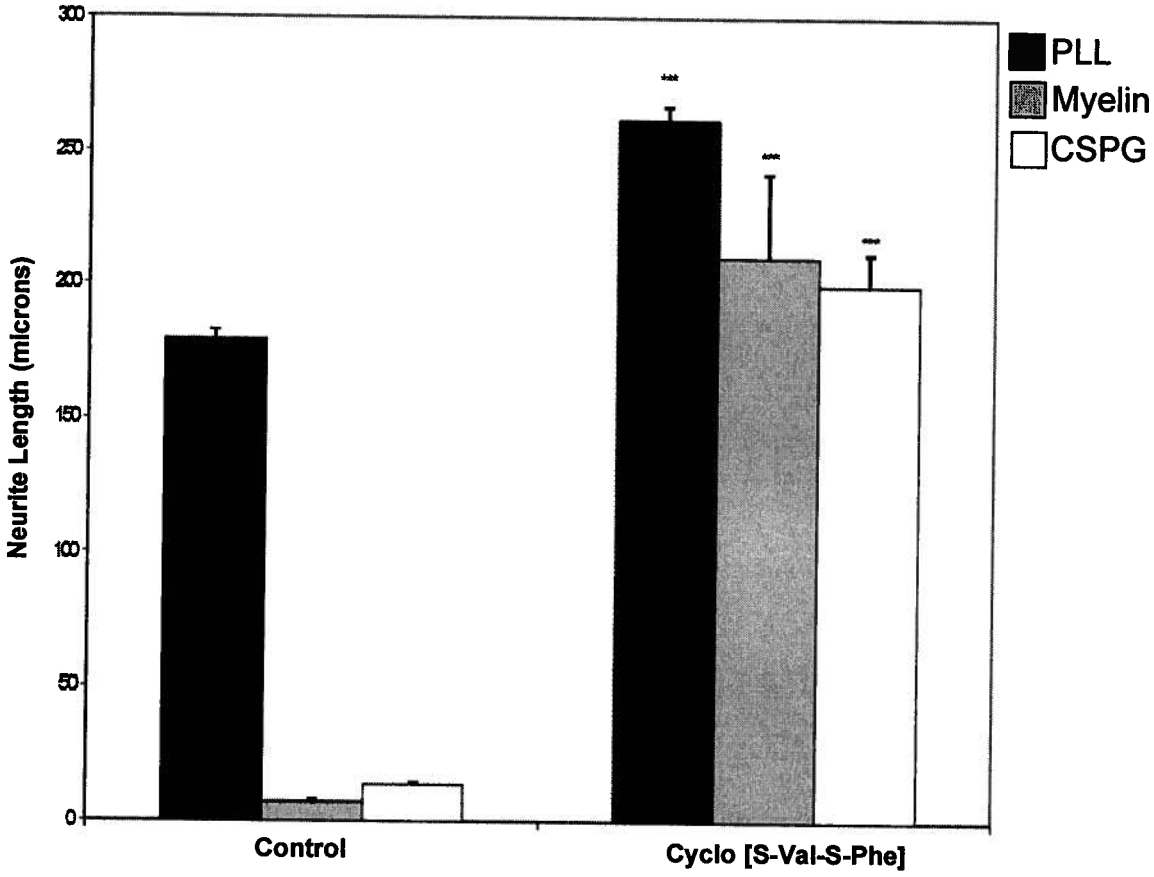

Figure 3.7.3. Addition of 32 μM of cyclo(S-Val-S-Phe) increases the neurite length even in the presence of inhibitors present in the central nervous system. This data was obtained by Jennifer Wong of the O'Connor lab.

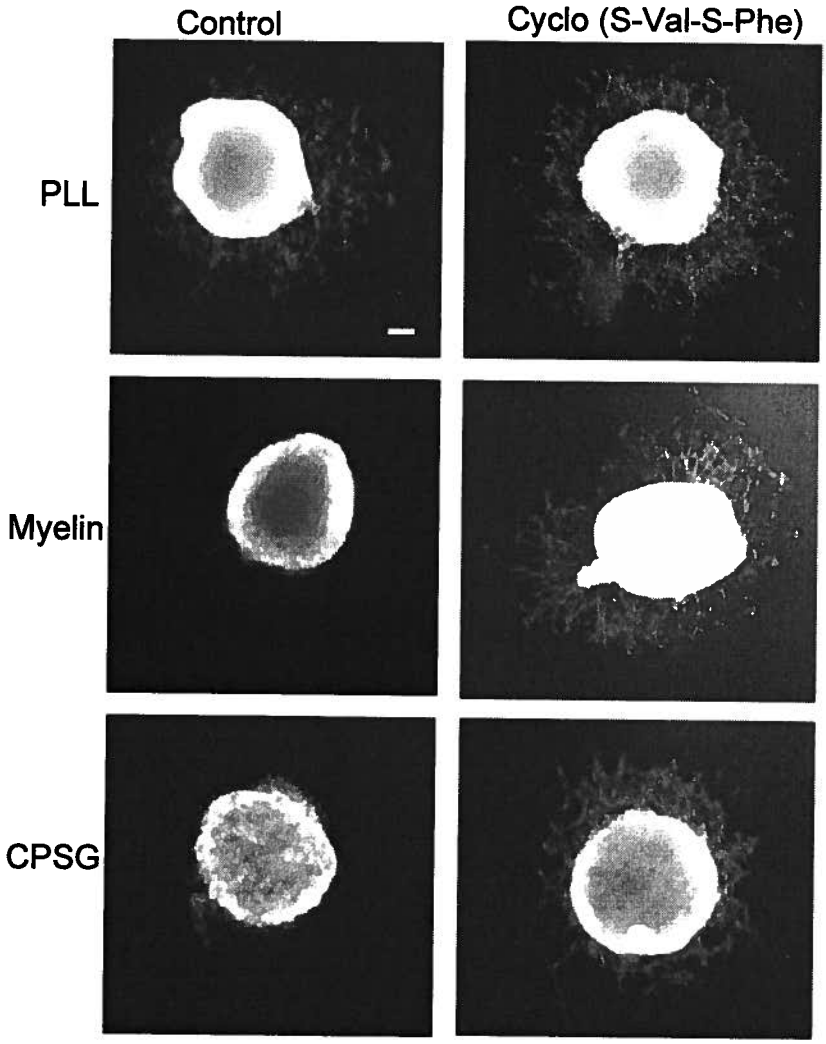

Figure 3.7.4. Addition of cyclo(S-Val-S-Phe) (**3.9**) enhances the neurite length of axons even in the presence of inhibitory substrates from the central nervous system. These images were generated by Jennifer Wong of the O'Connor lab.

Further studies were done to analyze the *in vivo* effects of cyclo(S-Val-S-Phe). Sprague Dawley rats underwent a septuptle dorsal rhizotomy. This was then followed by addition of either DMSO or 32 μM of cyclo(S-Val-S-Phe) intrathecally via a cannula attached to a subcutaneously implanted osmotic pump. The presence of cyclo(S-Val-S-Phe) produced an increase in both the

serotonergic and adrenergic axons sprouting in both injured and uninjured dorsal horns (Figure 3.7.5).

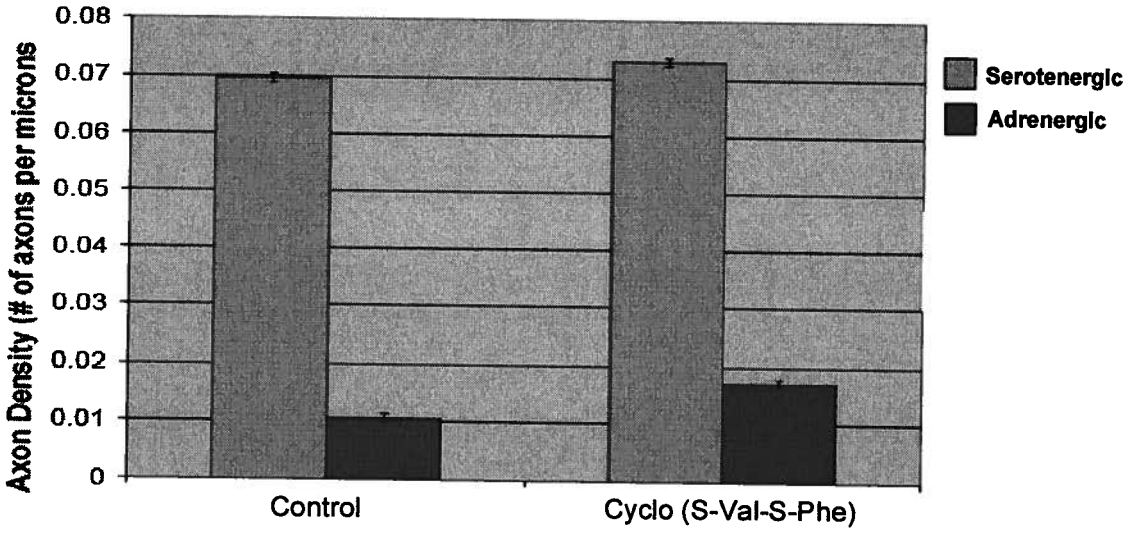

Figure 3.7.5. Addition of cyclo(S-Val-S-Phe) increased the axon sprouting in both serotonergic and adrenergic sprouting in the dorsal horn. This data was obtained by Jennifer Wong of the O'Connor lab.

3.8. Concluding Remarks

The two diketopiperazines, cyclo(S-Val-S-Phe) (**3.9**) and cyclo(R-Val-R-Phe) (**3.22**) were *in vitro* activators of neurite outgrowth. More importantly though, *in vitro* studies showed that these compounds are able to promote axonal outgrowth even in the presence of inhibitory substrates naturally found in the nervous system. *In vivo* tests also revealed that following a dorsal rhizotomy, cyclo(S-Val-S-Phe) promoted sprouting of uninjured dorsal roots over the injured site.

The two enantiomers, cyclo(S-Val-S-Phe) and cyclo(R-Val-R-Phe) both showed equivalent biologically activity. This was unexpected because one assumes that there should be a difference in biological activity between two enantiomers. Comparison of the chemical structures of the two enantiomers

reveals that there is pseudosymmetry between the two compounds (Figure 3.8.1). Due to their similar structure, both compounds are able to induce neurite outgrowth.

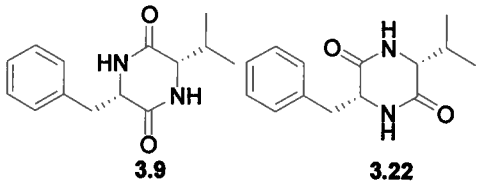

3.9 3.22

Figure 3.8.1. Comparison of the structures of cyclo(S-Val-S-Phe) (**3.9**) and cyclo(R-Val-R-Phe) (**3.22**).

3.9. General Experimental Section

All solvents used for extraction and chromatography were HPLC grade. When used for HPLC, solvents were filtered through a 0.45 µm filter (Osmonics, Inc). Reversed-phase C_{18} silica gel Sep Paks™ (10 g) and normal-phase Si gel Sep Paks™ (2 g) were purchased from Waters, Inc.. HPLC separations were carried out on a Waters 2487 dual channel detector/system controller (Waters Series 515 pump; chart recorder, 0.25 cm/min), or a Waters 600 controller and Waters 486 Tunable Absorbance Detector. A 5 µm Inertsil column from Chromatography Sciences (Montreal, PQ) was used for reversed phase HPLC, and separations were carried out at 2.0 mL/min, monitoring with UV absorption at 220 nm. Thin-layer chromatography (TLC) plates were Whatman MKC18F (reversed phase) and Kieselgel $60F_{254}$ (normal phase). TLC spots were visualized using either a dip solution of *p*-anisaldehyde (1% *p*-anisaldehyde, 2% H_2SO_4, 20% acetic acid and 77% ethanol) or under ultraviolet light (254 nm). All synthetic reagents were purchased from Aldrich Canada.

NMR spectra were recorded on a Bruker AV600 spectrometer fitted with a inverse triple resonance (^{1}H, ^{13}C, ^{15}N) cryoprobe. NMR solvents were purchased from Cambridge Isotope laboratories and were referenced to solvent peaks for DMSO-d_6 (δ_H 2.49 ppm and δ_C 39.5 ppm) and $CDCl_3$ (δ_H 7.24 ppm and δ_C 77.0 ppm). Low resolution ESI mass spectra were recorded on a Bruker Esquire LC mass spectrometer. High resolution ESI mass spectra was obtained using a Micromass LCT mass spectrometer. Optical rotations were recorded with a JASCO J-1010 polarimeter equipped with a halogen lamp (589 nm) and a 10 mm micro cell.

3.10. Bacterial Culture

The *Bacillus sp.* culture was isolated from a sediment sample collected by Mike LeBlanc in Dominica in June 2003. It was originally grown on M1 agar and subsequent pans were also made of this agar. To make M1 agar, 10 g of soluble starch, 2 g of bacto-peptone and 18 g of agar were immersed in 1L of sterile seawater (30 g/L NaCl in distilled H2O) and then autoclaved. The autoclaved agar was dispensed into large stainless steel pans at 400 mL per pan and was subsequently incubated for seven days before harvest. The cells and the agar were freeze dried before extraction with MeOH.

3.11. Identification of bacterial culture from sediment

Identification of the bacterial species was performed by Helen Wright of the biological services laboratory at the UBC department of Chemistry. The pure culture of the sediment bacterial strain was grown at room temperature on M1

plates. Extraction of genomic DNA was then performed by using the DNeasy Tissue Kit (QIAGEN, Mississauga, ON, Canada) in accordance with the manufacturer's instructions.

PCR reactions were performed in 25 µL reaction volumes that contained 12.5 µL of iQ Master mix (BioRad Laboratories), and a mixture of 0.2 µM each *1387r* (reverse) and *27f* forward primers, and 6.5 µL of sterile distilled H_2O. Primers were synthesized by the NAPS (Nucleic Acids and Protein Services, UBC). The PCR reactions were set up as follows: 95°C for 3 min, 30 cycles of 95°C for 15 sec (denaturation), 60°C for 15 sec (annealing) and 72°C for 15 sec (elongation). The amplification product was cut from the 0.1% agarose gel and a sequencing reaction was performed by NAPS. The results of the BLAST search of the GenBank database (National Center for Bioinformatics, website http://www.ncbi.nih.gov) confirmed that the PCR product had a sequence corresponding to the 16s rRNA of the *Bacillus* sp.

3.12. Isolation of Cyclo(S-Val-S-Phe) from Bacillus sp.

The bacterial species (coll no 101516) was collected from a sediment sample off the coast of Dominica and identified by the Biological Services at UBC as *Bacillus* sp. Twenty pans of the freeze dried *Bacillus sp.* were extracted five times with MeOH (5 X 1.5L). The MeOH extracts were combined and reduced *in vacuo* to give a golden brown solid (6 g). The crude extract was then dissolved in 500 mL of a 9:1 MeOH: H_2O mixture which was then partitioned with hexanes (3 X 200mL). The active MeOH/H_2O fraction (800 mg) was then subjected to Sephadex ™ LH-20 size exclusion chromatography eluting with MeOH which

afforded an active fraction of 122.3 mg. This material was further purified using a stepped gradient reversed phase Sep Pak™ (H_2O to MeOH) where the active fraction eluted with 6:4 MeOH: H_2O (7.6 mg). The crude brown solid was further purified using reversed phase HPLC (Inertsil C_{18}, 9.4 X 250 mm, 1:1 H_2O: MeOH, UV detection at 220 nm) to yield 1.3 mg of the cyclic dipeptide cyclo(S-Val-S-Phe) (**3.9**, Figure 3.3.1) as the bioactive compound. The structure of the known diketopiperazine was confirmed by comparing the optical rotation, NMR and MS data to the literature values.[14]

3.13. Physical Data of Isolated Diketopiperazine from Bacillus sp.

(3*S*,6*S*)-3-Benzyl-6-isopropyl-2,5-piperazinedione (3.9): white powder. $[\alpha]_D^{22}$: -45.82 (c 0.3, DMSO); ^{1}H NMR (600 MHz, DMSO-d_6): δ_H 8.11 (1H, bs, NH), 7.91 (1H, bs, NH), 7.22-7.25 (2H, m, ArH), 7.17-7.18 (3H, m, ArH), 4.21 (1H, m, H-6), 3.52 (1H, m, H-3), 3.15 (1H, m, H-10a), 2.86 (1H, dd, *J* = 13.4, 4.9 Hz, H-10b), 1.69 (1H, m, H-7), 0.64 (3H, d, *J* = 7.2, H-8 or H-9), 0.25 (3H, d, *J* = 7.2 Hz, H-9 or H-8); ^{13}C NMR (150 MHz, DMSO-d_6): δ_C 166.5 (C, C-4), 166.3 (C, C-1), 136.2 (C, C-11), 130.2 (CH, C-12, C-16), 127.9 (CH, C-13, C-15), 126.4 (CH, C-14), 59.0 (CH, C-3), 54.9 (CH, C-6), 37.7 (CH_2, C-10), 30.9 (CH, C-7), 18.2 (CH_3, C-8 or C-9), 16.0 (CH_3, C-8 or C-9); LRESIMS *m/z* 269.1; HRESIMS *m/z* 269.1269 (calc'd for $C_{14}H_{18}N_2O_2Na$ 269.1266).

3.14. Synthetic Experimental Section

Preparation of (*S*)-*N*,*N*'-bis(*p*-methoxybenzyl)-3-isopropylpiperazine-2,5-dione (3.11)

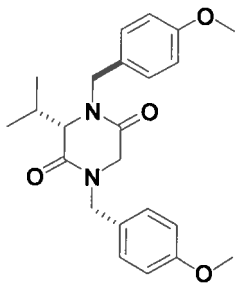

To 30 mL of dimethyl formamide, 20 mg (0.75 mmol) of NaH was added and the mixture was subsequently cooled to 0°C. The addition of 43 mg (0.3 mmol) of (*S*)-3-isopropylpiperazine-2,5-dione (**3.10**) was followed by the slow addition of *p*-methoxybenzyl chloride (100 μL; 0.75 mmol) over a period of 1 h. After the reaction mixture was stirred for 4 h, the solution was quenched with H_2O (5 mL), followed by the addition of excess NH_4Cl. Extraction of the mixture was accomplished with EtOAc (3 X 10 mL) and dried with $MgSO_4$, filtered through Celite™ and concentrated to dryness *in vacuo*. Purification of the reaction mixture was accomplished using flash chromatography (40 X 2 cm; 1:1 EtOAc: Hexanes) and removal of trace solvents (vacuum pump) provided 96 mg (75% yield) of the protected diketopiperazine (**3.11**) as a white solid.

(*S*)-*N*,*N*'-bis(*p*-methoxybenzyl)-3-isopropylpiperazine-2,5-dione (3.11): white powder. $[\alpha]_D^{22}$: -49.8 (c 0.8, $CHCl_3$); ^1H NMR (600 MHz, $CDCl_3$) δ_H 6.79-7.15 (8H, m), 5.26 (1H, d, J = 14.8 Hz), 4.84 (1H, d, J = 14.2 Hz), 4.27 (1H, d, J = 14.2 Hz), 3.99 (1H, d, J = 16.5 Hz), 3.89 (1H, d, J = 14.8 Hz), 3.85 (3H, s), 3.85 (3H, s), 3.81 (1H, d, J = 16.5 Hz), 3.77 (1H, d, J = 4.8 Hz), 2.24 (1H, m), 1.05 (3H, d, J

= 7.2 Hz), 0.90 (3H, d, *J* = 7.2 Hz); ^{13}C NMR (150 MHz, $CDCl_3$): δ_C 167.2, 165.8, 158.5, 132.1, 130.7, 128.4, 115.8, 65.7, 55.1, 50.5, 47.2, 46.5, 32.3, 20.1, 18.5; LRESIMS *m/z* 379.2; HRESIMS *m/z* 379.2321 (calc'd for $C_{23}H_{28}N_2O_4$ 379.2324).

Preparation of (3*S*,6*R*)-*N*,*N*'-Bis(*p*-methoxybenzyl)-3-isopropyl-6-benzylpiperazine-2,5-dione (3.12).

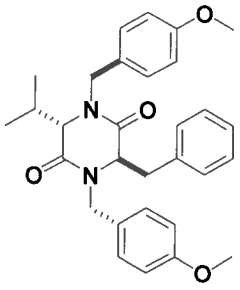

n-BuLi (237 μL; 0.379 mmol) was added to a cold (-78°C) stirred solution of hexamethyldisilizane (131 μL; 0.625 mmol) in dry THF (10 mL) under an argon atmosphere. The resulting solution was then warmed to 0°C before being added to a solution of **3.11** (96 mg; 0.253 mmol) in dry THF at -78°C under an argon atmosphere. The reaction mixture was stirred for 1 h at -78°C which was then followed by the addition of benzyl bromide (55 μL; 0.506 mmol). After the solution was stirred for 3 h, the reaction mixture was quenched by the addition of excess saturated NH_4Cl. The volatiles were removed *in vacuo* and the solution was subsequently extracted with EtOAc (10 mL), dried with $MgSO_4$, and concentrated *in vacuo*. Purification of the reaction mixture was accomplished using flash chromatography (40 X 2 cm; 1:4 EtOAc: Hexanes) and removal of trace solvents (vacuum pump) provided 80 mg (65%) of the protected diketopiperazine (**3.12**) as a white solid.

(3*S*,6*R*)-*N*,*N*'-Bis(*p*-methoxybenzyl)-3-isopropyl-6-benzylpiperazine-2,5-dione (3.12): $[\alpha]_D^{22}$: + 49.4 (c 0.76, $CHCl_3$); ^1H NMR (600 MHz, $CDCl_3$) δ_H 6.63-7.60 (13H, m), 5.71 (1H, d, *J* = 14.7 Hz), 4.34 (1H, t, *J* = 4.2 Hz), 3.98 (1H, d, *J* = *14.5*), 3.90 (3H, s), 3.86 (3H, s), 3.77 (1H, d, *J* = 14.7 Hz), 3.50 (1H, dd, *J* = 13.9, 4.2), 3.42 (1H, dd, *J* = 13.9, 4.2), 3.29 (1H, d, *J* = 3.0 Hz) , 2.22 (1H, m), 1.05 (3H, d, *J* = 7.0 Hz), 0.69 (3H, d, *J* = 7.0 Hz); ^{13}C NMR (150 MHz, $CDCl_3$): δ_C 168.5, 166.1, 161.5, 159.6, 136.2, 131.7, 130.9, 130.1, 129.3, 128.5, 127.6, 127.1, 115.7, 114.9, 61.7, 59.1, 55.3, 47.1, 45.8, 34.9, 31.3, 18.9, 16.0; LRESIMS *m/z* 487.2597; HRESIMS *m/z* 487.2597 (calc'd for $C_{30}H_{35}N_2O_4$ 487.2597).

Preparation of 3*S*,6*S*-*N*,*N*'-Bis(*p*-methoxybenzyl)-3-isopropyl-6-benzylpiperazine-2,5-dione (3.13):

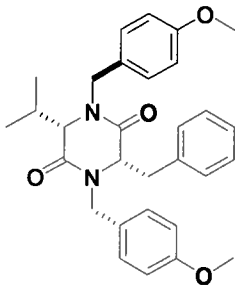

n-BuLi (140 μL; 0.22 mmol) was added to a cold (-78°C) stirred solution of **3.12** (54 mg; 0.11 mmol) in dry THF (5mL) under an argon atmosphere. After the solution was stirred for 3 h at -78°C, the reaction mixture was quenched by the addition of an excess of a solution of 2,6-di-*tert*-butylphenol in THF at -78°C. The volatiles were removed *in vacuo* and the solution was subsequently extracted with EtOAc (5 mL), dried with $MgSO_4$, and concentrated *in vacuo*. Purification of the reaction mixture was accomplished using flash chromatography (40 X 2 cm;

1:4 EtOAc: Hexanes) and removal of trace solvents (vacuum pump) provided 43 mg (80%) of the protected diketopiperazine (**3.13**) as a white solid.

(3*S*,6*S*-*N*,*N*'-Bis(*p*-methoxybenzyl)-3-isopropyl-6-benzylpiperazine-2,5-dione (3.13): white powder; $[\alpha]_D^{22}$: -199 (c 0.85, $CHCl_3$); ^1H NMR (600 MHz, $CDCl_3$) δ_H 7.21–7.32 (3H, m), 7.16–7.20 (2H, m), 6.89–6.95 (2H, m), 6.65–6.73 (2H, m), 5.38 (1H, d, *J* = 14.8), 5.15 (1H, d, *J* = 14.6), 4.10 (1H,dd, *J* = 7.9, 4.0), 3.76 (1H, d, *J* = 14.8), 3.69 (3H, s), 3.67 (3H, s), 3.49 (1H, d, *J* = 7.9), 3.37 (1H, dd, *J* = 14.3, 4.1), 3.00 (1H, dd, *J* = 14.3, 4.1), 2.98 (1H, d, *J* = 14.6), 1.86 (1H, m), 1.07 (3H, d, *J* = 7.0), 1.01 (3H, d, *J* = 7.0); ^{13}C NMR (150 MHz, $CDCl_3$): δ_C 167.9, 166.5, 160.1, 159.7, 138.2, 129.6, 129.4, 129.2, 129.0, 128.8, 127.6, 127.1, 126.9, 115.1, 114.7, 64.1, 61.2, 55.4, 55.3, 49.2, 47.2, 41.2, 33.8, 21.1, 20.0; LRESIMS *m/z* 509.2; HRESIMS *m/z* 509.2423 (calc'd for $C_{30}H_{35}N_2O_4Na$ 509.2416).

Preparation of (3*S*,6*R*)-3-Benzyl-6-isopropyl-2,5-piperazinedione (3.14):

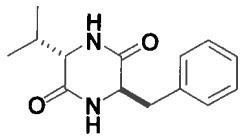

To a solution of **3.12** (26 mg; 0.05 mmol) in ACN-H_2O (1:1; 5 mL), ceric ammonium nitrate (54 mg; 0.1 mmol) was added and stirred for 4 h. Reversed-phase silica gel was added and the solvent was removed *in vacuo*, and the residue was purified using a 10 g reversed-phase Sep Pak™ (eluent: 1:9 MeOH: H_2O) to afford 10 mg of **3.14** (75 % yield).

(3*S*,6*R*)-3-Benzyl-6-isopropyl-2,5-piperazinedione (3.14): white powder. $[\alpha]_D^{21}$: -65.4 (c 0.25, DMSO); ^1H NMR (600 MHz, DMSO-d_6) δ_H 8.10 (1H, br s), 8.00

(1H, br s), 7.10-7.34 (5H, m), 4.22 (1H, m), 3.15 (1H, dd, *J* = 13.4, 3.9 Hz), 2.95 (1H, m), 2.90 (1H, dd, *J* = 13.4, 3.9 Hz), 1.95 (1H, m), 0.81 (3H, d, *J* = 6.8 Hz), 0.72 (3H, d, *J* = 6.8 Hz); ^{13}C NMR (150 MHz, $CDCl_3$): δ_C 167.0, 166.1, 134.9, 129.6, 126.1, 125.7, 59.1, 55.1, 38.1, 31.3, 18.1, 16.4; LRESIMS *m/z* 269.1; HRESIMS *m/z* 269.1266 (calc'd for $C_{14}H_{18}N_2O_2Na$ 269.1266).

Preparation of (3*S*,6*R*)-3-Benzyl-6-isopropyl-2,5-piperazinedione (3.9):

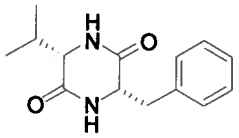

To a solution of **3.13** (43 mg; 0.08 mmol) in ACN-H_2O (1:1; 5 mL), ceric ammonium nitrate (87.7 mg ; 0.16 mmol) was added and the solution stirred for 4 hours. Reversed-phase silica gel was added and the solvent was removed *in vacuo*, and the residue purified using a reversed-phase Sep Pak™ (10 g)(eluent: 9:1 MeOH:H_2O) to afford 15 mg of **3.9** (70% yield).

(3*S*,6*S*)-3-Benzyl-6-isopropyl-2,5-piperazinedione (3.9): white powder. $[\alpha]_D^{23}$: -47.32 (c 0.5, DMSO); ^1H NMR (600 MHz, DMSO-d_6): δ_H 8.11 (1H, bs, NH), 7.91 (1H, bs, NH), 7.22-7.25 (2H, m), 7.17-7.18 (3H, m), 4.21 (1H, m), 3.52 (1H, m), 3.15 (1H, m), 2.86 (1H, dd, *J* = 13.4, 4.9 Hz), 1.69 (1H, m), 0.64 (3H, d, *J* = 7.2), 0.25 (3H, d, *J* = 7.2 Hz); ^{13}C NMR (150 MHz, DMSO-d_6): δ_C 166.5, 166.3, 136.2, 130.2, 127.9, 126.4, 59.0, 54.9, 37.7, 30.9, 18.2, 16.0; LRESIMS *m/z* 269.1; HRESIMS *m/z* 269.1269 (calc'd for $C_{14}H_{18}N_2O_2Na$ 269.1266).

Preparation of (*R*)-*N*,*N*'-bis(*p*-methoxybenzyl)-3-isopropylpiperazine-2,5-dione (3.18)

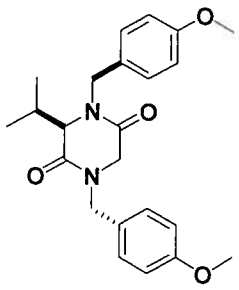

To 50 mL of dimethyl formamide, 20 mg (0.92 mmol) of NaH was added and the mixture was subsequently cooled to 0°C. The addition of (*R*)-3-isopropylpiperazine-2,5-dione (57 mg; 0.37 mmol) was then followed by the slow addition of *p*-Methoxybenzyl chloride (124 μL; 0.92 mmol) over a period of 1 h. After the reaction mixture was stirred for 4 h, the solution was quenched with H_2O (6 mL), followed by the addition of excess NH_4Cl. Extraction of the mixture was accomplished with EtOAc (3 X 5 mL) and was dried with $MgSO_4$, filtered through Celite™ and concentrated to dryness *in vacuo*. Purification of the reaction mixture was accomplished using flash chromatography (40 X 2 cm; 1:1 EtOAc: Hexanes) and removal of trace solvents (vacuum pump) provided 100 mg (70% yield) of the protected diketopiperazine (**3.18**) as a white solid.

(*R*)-*N*,*N*'-bis(*p*-methoxybenzyl)-3-isopropylpiperazine-2,5-dione (3.18): white powder. $[\alpha]_D^{22}$: 44.6 (c 0.76, $CHCl_3$); ^1H NMR (600 MHz, $CDCl_3$) δ_H 6.79-7.15 (8H, m), 5.26 (1H, d, *J* = 14.8 Hz), 4.84 (1H, d, *J* = 14.2 Hz), 4.27 (1H, d, *J* = 14.2 Hz), 3.99 (1H, d, *J* = 16.5 Hz), 3.89 (1H, d, *J* = 14.8 Hz), 3.85 (3H, s), 3.85 (3H, s), 3.81 (1H, d, *J* = 16.5 Hz), 3.77 (1H, d, *J* = 4.8 Hz), 2.24 (1H, m), 1.05 (3H, d, *J* = 7.2 Hz), 0.90 (3H, d, *J* = 7.2 Hz); ^{13}C NMR (150 MHz, $CDCl_3$): δ_C

167.2, 165.8, 158.5, 132.1, 130.7, 128.4, 115.8, 65.7, 55.1, 50.5, 47.2, 46.5, 32.3, 20.1, 18.5; LRESIMS *m/z* 379.2; HRESIMS *m/z* 379.2321 (calc'd for $C_{23}H_{28}N_2O_4$ 379.2322).

Preparation of (3*R*,6*S*)-*N*,*N*'-Bis(*p*-methoxybenzyl)-3-isopropyl-6-benzylpiperazine-2,5-dione (3.19).

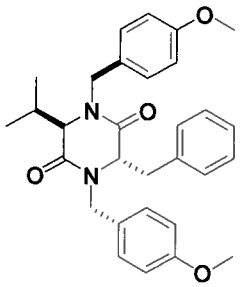

n-BuLi (62 μL; 0.39 mmol) was added to a cold (-78°C) stirred solution of hexamethyldisilizane (135 μL; 0.52 mmol) in dry THF (10 mL) under an argon atmosphere. The resulting solution then was warmed to 0°C before being added to a solution of **3.18** (100 mg; 0.26 mmol) in dry THF at -78°C under an argon atmosphere. The reaction mixture was stirred for 1 h at -78°C which was then followed by the addition of benzyl bromide (62 μL; 0.52 mmol). After the solution was stirred for 3 h, the reaction mixture was quenched by the addition of excess saturated NH_4Cl. The volatiles were removed *in vacuo* and the solution was subsequently extracted with EtOAc (3 X 5 mL), dried with $MgSO_4$, and concentrated *in vacuo*. Purification of the reaction mixture was accomplished using flash chromatography (40 X 2 cm; 1:4 EtOAc: Hexanes) and removal of trace solvents (vacuum pump) provided 79 mg (60% yield) of the protected diketopiperazine (**3.19**) as a white solid.

(3*R*,6*S*)-*N*,*N*'-Bis(*p*-methoxybenzyl)-3-isopropyl-6-benzylpiperazine-2,5-dione (3.19): $[\alpha]_D^{22}$: - 46.2 (c 0.71, $CHCl_3$); ^1H NMR (600 MHz, $CDCl_3$): δ_H 6.63-7.60 (13H, m), 5.71 (1H, d, *J* = 14.7 Hz), 4.34 (1H, t, *J* = 4.2 Hz), 3.98 (1H, d, *J* = 14.5 Hz), 3.90 (3H, s), 3.86 (3H, s), 3.77 (1H, d, *J* = 14.7 Hz), 3.50 (1H, dd, *J* = 13.9, 4.2 Hz), 3.42 (1H, dd, *J* = 13.9, 4.2 Hz), 3.29 (1H, d, *J* = 3.0 Hz) , 2.22 (1H, m), 1.05 (3H, d, *J* = 7.0 Hz), 0.69 (3H, d, *J* = 7.0 Hz); ^{13}C NMR (150 MHz, $CDCl_3$): δ_C 168.5, 166.1, 161.5, 159.6, 136.2, 131.7, 130.9, 130.1, 129.3, 128.5, 127.6, 127.1, 115.7, 114.9, 61.7, 59.1, 55.3, 47.1, 45.8, 34.9, 31.3, 18.9, 16.0; LRESIMS *m/z* 487.3; HRESIMS *m/z* 487.2590 (calc'd for $C_{30}H_{35}N_2O_4$ 487.2597).

Preparation of 3R,6R-*N*,*N*'-Bis(*p*-methoxybenzyl)-3-isopropyl-6-benzylpiperazine-2,5-dione (3.20):

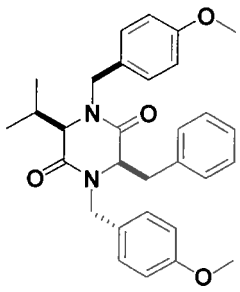

n-BuLi (295 μL; 0.18 mmol) was added to a cold (-78°C) stirred solution of **3.19** (45 mg; 0.092 mmol) in dry THF (5 mL) under an argon atmosphere. After the solution was stirred for 3 h at -78°C, the reaction mixture was quenched by the addition of an excess of a solution of 2,6-di-*tert*-butylphenol in THF at -78°C. The volatiles were removed *in vacuo* and the solution was subsequently extracted with EtOAc (3 X 5mL), dried with $MgSO_4$, and concentrated *in vacuo*. Purification of the reaction mixture was accomplished using silica gel flash chromatography (40 x 2 cm; 1:4 EtOAc: Hexanes) and removal of trace solvents (vacuum pump)

provided 31 mg (69% yield) of the protected diketopiperazine (**3.20**) as a white solid.

(3*R*,6*R*-*N*,*N*'-Bis(*p*-methoxybenzyl)-3-isopropyl-6-benzylpiperazine-2,5-dione (3.20): white powder; $[\alpha]_D^{22}$: 189 (c 0.79, $CHCl_3$); ^1H NMR (600 MHz, $CDCl_3$) δ_H 7.21–7.32 (3H, m), 7.16–7.20 (2H, m), 6.89–6.95 (2H, m), 6.65–6.73 (2H, m), 5.38 (1H, d, *J* = 14.8 Hz), 5.15 (1H, d, *J* = 14.6 Hz), 4.10 (1H, dd, *J* = 7.9, 4.0 Hz), 3.76 (1H, d, *J* = 14.8 Hz), 3.69 (3H, s), 3.67 (3H, s), 3.49 (1H, d, *J* = 7.9 Hz), 3.37 (1H, dd, *J* = 14.3, 4.1 Hz), 3.00 (1H, dd, *J* = 14.3, 4.1 Hz), 2.98 (1H, d, *J* = 14.6 Hz), 1.86 (1H, m), 1.07 (3H, d, *J* = 7.0 Hz), 1.01 (3H, d, *J* = 7.0 Hz); ^{13}C NMR (150 MHz, $CDCl_3$): δ_C 167.9, 166.5, 160.1, 159.7, 138.2, 129.6, 129.4, 129.2, 129.0, 128.8, 127.6, 127.1, 126.9, 115.1, 114.7, 64.1, 61.2, 55.4, 55.3, 49.2, 47.2, 41.2, 33.8, 21.1, 20.0; LRESIMS *m/z* 487.3; HRESIMS *m/z* 487.2588 (calc'd for $C_{30}H_{35}N_2O_4$ 487.2597).

Preparation of (3*R*,6*S*)-3-Benzyl-6-isopropyl-2,5-piperazinedione (3.21):

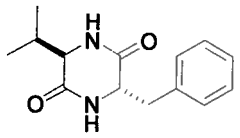

To a 5 mL solution of **3.19** (34 mg; 0.41 mmol) in ACN-H_2O (1:1), ceric ammonium nitrate (0.45 mg; 0.82 mmol) was added and the solution was stirred for 4 h. Reversed-phase silica was added and the solvent was removed *in vacuo*, and the residue was purified using a reversed-phase Sep Pak™ (9:1 H_2O: MeOH) to afford 13 mg (65% yield) of **3.21**.

(3*R*,6*S*)-3-Benzyl-6-isopropyl-2,5-piperazinedione (3.21): white powder. $[\alpha]_D^{21}$: 69.3 (c 0.27, DMSO); ^1H NMR (600 MHz, DMSO-d_6) δ_H 8.10 (1H, br s), 8.00 (1H,

br s), 7.10-7.34 (5H, m), 4.22 (1H, m), 3.15 (dd, J = 13.4, 3.9 Hz), 2.95 (1H, m), 2.90 (1H, dd, J = 13.4, 3.9 Hz), 1.95 (1H, m), 0.81 (3H, d, J = 6.8 Hz), 0.72 (3H, d, J = 6.8 Hz); ^{13}C NMR (150 MHz, $CDCl_3$): δ_C 167.0, 166.1, 134.9, 129.6, 126.1, 125.7, 59.1, 55.1, 38.1, 31.3, 18.1, 16.4; LRESIMS *m/z* 269.1; HRESIMS *m/z* 269.1268 (calc'd for $C_{14}H_{18}N_2O_2Na$ 269.1266).

Preparation of (3*R*,6*R*)-3-Benzyl-6-isopropyl-2,5-piperazinedione (3.22):

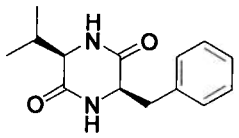

To a 5 mL solution of **3.20** (31 mg; 0.06 mmol) in ACN-H_2O (1:1), 65 mg of ceric ammonium nitrate was added and stirred for 4 hours. Reversed-phase silica was added and the solvent was removed *in vacuo*, and the residue purified using a reversed-phase Sep Pak™ (10 g)(eluent: 9:1 MeOH:H_2O) to afford 12 mg (70 % yield) of **3.22**.

(3*R*,6*R*)-3-Benzyl-6-isopropyl-2,5-piperazinedione (3.22): white powder. $[\alpha]_D^{22}$: 43.45 (c 0.29, DMSO); ^1H NMR (600 MHz, DMSO-d_6): δ_H 8.11 (1H, bs, NH), 7.91 (1H, bs), 7.22-7.25 (2H, m), 7.17-7.18 (3H, m), 4.21 (1H, m), 3.52 (1H, m), 3.15 (1H, m), 2.86 (1H, dd, J = 13.4, 4.9 Hz), 1.69 (1H, m), 0.64 (3H, d, J = 7.19), 0.25 (3H, d, J = 7.2 Hz); ^{13}C NMR (150 MHz, DMSO-d_6): δ_c 166.5, 166.3, 136.2, 130.2, 127.9, 126.4, 59.0, 54.9, 37.7, 30.9, 18.16, 16.0; LRESIMS *m/z* 269.1; HRESIMS *m/z* 269.1267 (calc'd for $C_{14}H_{18}N_2O_2Na$ 269.1266).

3.15 References

(1) Fawcett J.F. *Journal of Neurotrama* **2006**, *23*, 371-383.

(2) Ditunno J.F.; Formal C.S. *New England Journal of Medicine* **1994**, *330*, 550-556.

(3) Bradbury E.J.; McMahon S.B. *Nature Reviews Neuroscience* **2006**, *7*, 644-653.

(4) Lim P.A.C.; Tow A.M. *Annals of the Academy of Medicine, Singapore* **2007**, *36*, 49-57.

(5) Skaper S.D. *Annals of the New York Academy of Sciences* **2005**, *1053*, 376-385.

(6) Lee D.H.S.; Strittmatter S.M.; Sah D.W.Y. *Nature Reviews Drug Discovery* **2003**, *2*, 1-7.

(7) Uehata M.; Ishizaki T.; Satoh H.; Ono T.; Kawahara T.; Morishita T.; Tamakawa H.; Yamgami K.; Inui J.; Maekawa M.; Narumiya S. *Nature* **1997**, *30*, 990-994.

(8) Mueller B.K.; Mack H.; Teusch N. *Nature Reviews Drug Discovery* **2005**, *4*, 387-398.

(9) Prakash K. R. C.; Tang Y.; Kozikowski A.P.; Flippen-Anderson J.L.; Knoblachc S.M.; Fadenc A.I. *Bioorganic and Medicinal Chemistry* **2002**, *10*, 3043-3048.

(10) Prasad C. *Peptides* **1995**, *16*, 151-164.

(11) Baptiste D.C.; Fehlings M.G. *Journal of Neurotrama* **2006**, *23*, 318-334.

(12) Faden A.I.; Knoblack S.M.; Movsesyan V.A.; IV P.M. Lea; Cernak I. *Annals of the New York Academy of Science* **2005**, *1053*, 472-481.

(13) Faden A.I.; Knoblach S.M.; Movseyan V.A.; Cernak I. *Journal of Alzheimer's Disease* **2004**, *6*, S93-S97.

(14) Bull S.D.; Davies S.G.; Garner A.C.; O'Shea M.D. **2001**, *J. Chem. Soc., Perkin Trans. 1*, 3281-3287.

(15) Lopez-Cobenas A.; Cledera P.; Sanchez J.D.; Lopez-Alvarado P.; Ramos M.T.; Avendano C.; Menedez J.C. *Synthesis* **2005**, *19*, 3412-3422.

(16) Bull S.D.; Davies S.G.; Epstein S.W.; Leech M.A.; Ouzman J.V.A. *Journal of the Chemical Society, Perkin Trans. 1* **1998**, *2321-2330*.

(17) Bull S.D.; Davies S.G.; Epstein S.W.; Ouzman J.V.A. *Tetrahedron: Assymmetry* **1998**, *9*, 2795-2798.

(18) Meyer G.; Feldman E.L. *Journal of Neurochemistry* **2002**, *83*, 490-503.

Chapter 4: Structure Elucidation of G_2 Checkpoint inhibitors from *Duguetia Odorata*[a]

4.1. Preview of Chapter 4

High-throughput screening of plant extracts from the U.S. National Cancer Institute's Open Repository collection identified the South American plant *Duguetia odorata* as having activity in the G_2 checkpoint inhibition assay. Bioassay guided fractionation of the plant extract led to the discovery of oliveroline (**4.32**) as an abrogator of G_2 arrest. This investigation also yielded the new aporphine alkaloid *N*-methylguatterine (**4.33**), as well as the known alkaloids dehydrodiscretine (**4.34**) and pseudopalmatine (**4.35**).

4.2. The Cell cycle

The cell cycle (Figure 4.2.1) is a process the cell undergoes until it has reproduced itself. Interphase is the first part of cell division, where the cell grows, prepares for cell division and metabolism take place. It is divided into the G_1, S, and G_2 phases. The G_1 phase is where metabolism takes place. At the end of G_1, centrioles replicate and prepare for cell division. Before progressing to the S-phase, sensors scan to check the fidelity of the DNA. Should there be any anomalies present on the DNA, the G_1 checkpoint would stall the cell cycle to allow the damage to be repaired. In the S-phase, DNA synthesis and chromosome replication take place. Critical proteins and enzymes required for

[a]: Reproduced with permission from Brastianos H.C.; Sturgeon C.M.; Roberge M.; Andersen R.J. *Journal of Natural Products* **2007**, *70*, 287-288. Copyright 2007 American Chemical Society.

cell division are synthesized in the G_2 phase of interphase. Similar to the G_1 checkpoint, the G_2 checkpoint halts the cell cycle to repair any damaged DNA. The M-phase is the second part of cell division which consists of both mitosis and cytokinesis. Mitosis is where the cell divides the duplicated chromosomes to obtain identical sets and is divided into four stages. The first stage of mitosis is prophase where the chromosomes condense and the centrioles move toward the opposite poles of the cell. This is then followed by metaphase, where the chromosomes line up at the equator of the cell. During anaphase, the two sets of chromosomes split and move towards the opposite poles of the cell. The final step of mitosis is telophase where the nuclear envelope forms around each chromosome. Cytokinesis is the final part of the cell cycle where division of the cytoplasm takes place and two independent cells are obtained.[1]

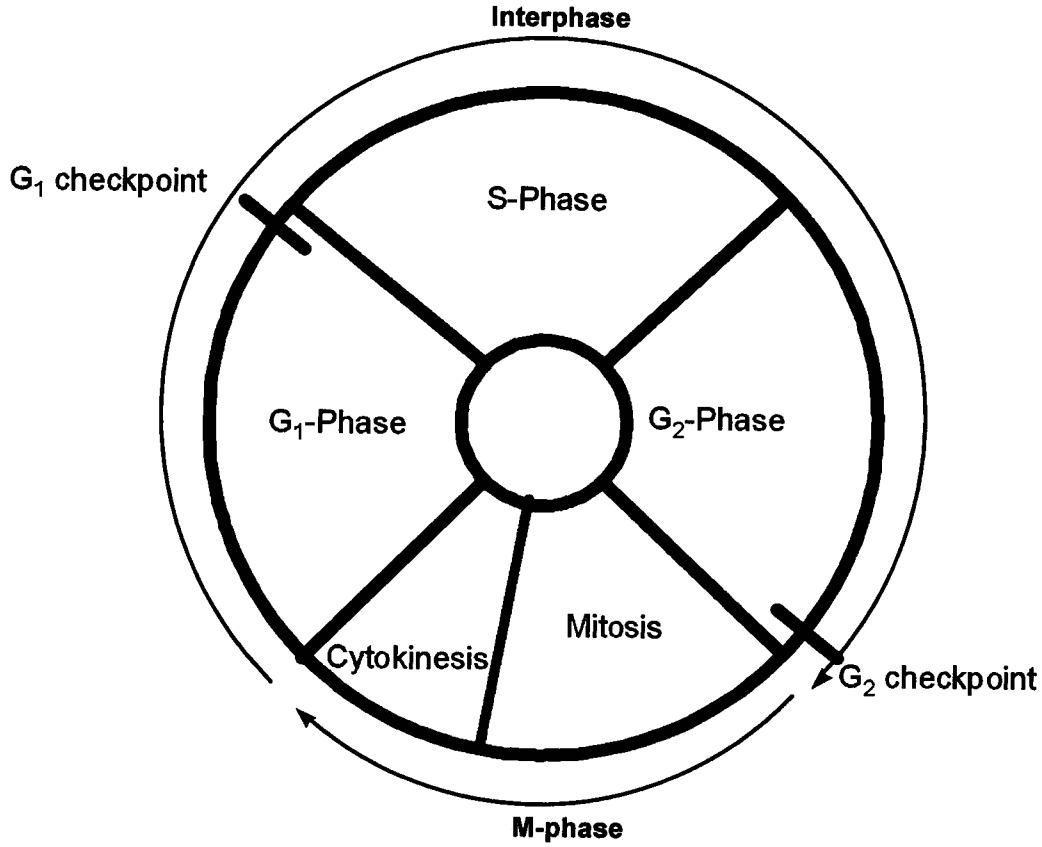

Figure 4.2.1. The cell cycle consists of interphase and the M-phase (Adapted from Voet & Voet).[1] Interphase is the first part of the cell cycle and it consists of the G_1, S, and G_2 phases of the cell cycle. The M-phase consists of mitosis where the chromosomes are divided, and cytokinesis where two separate cells are obtained.

4.3. G_2 to M Transition

The formation of the cyclinB/cdc2 complex is crucial for cells to enter mitosis. This complex is known as the M-phase promoting factor. Throughout mitosis and G_1, the levels of cyclinB are low. At the end of the S-phase however, cyclinB is synthesized, which leads to the formation of the cylcinB/cdc2 complex. During G_2, the cyclinB/cdc2 complex is held inactive by inhibitory phosphorylations on cdc2. These phosphorylations are carried out by Wee1. Cdc25c acts as a positive regulator of the cdc2/cyclin B complex by

dephosphorylating cdc2. Dephosphorylation of cdc2 activates the complex and triggers mitosis (Figure 4.3.1).[2-4]

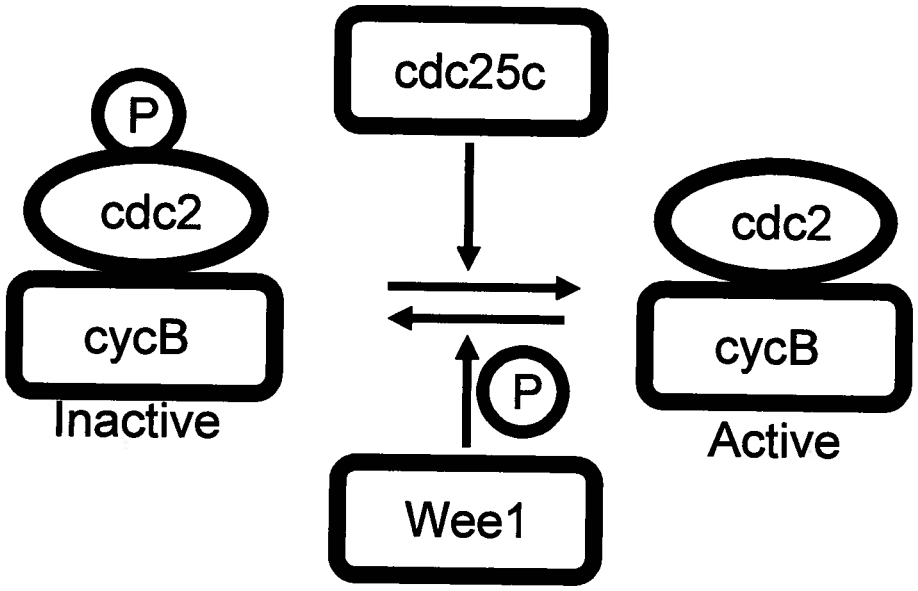

Figure 4.3.1. G_2/M transition (adapted from Foijer).[4]

It is vital for the DNA not to be damaged before entering mitosis. This is ensured by the G_2 checkpoint pathway. This checkpoint's purpose is to prohibit cdc25c from activating the cyclinB /cdc25c complex, therefore, the checkpoint arrests the onset of mitosis to repair any damaged DNA. Upon DNA damage, ATM/ATR induces the activation of Chk1/Chk2, which goes on to phosphorylate cdc25c. The phosphorylation on cdc25c also creates a binding site for the 14-3-3σ proteins. The 14-3-3σ/cdc25c complex is then sequestered out of the nucleus. Since cdc25c is not present to activate the cyclinB/cdc2 complex, the cell cycle is arrested (Figure 4.3.2).[5,6]

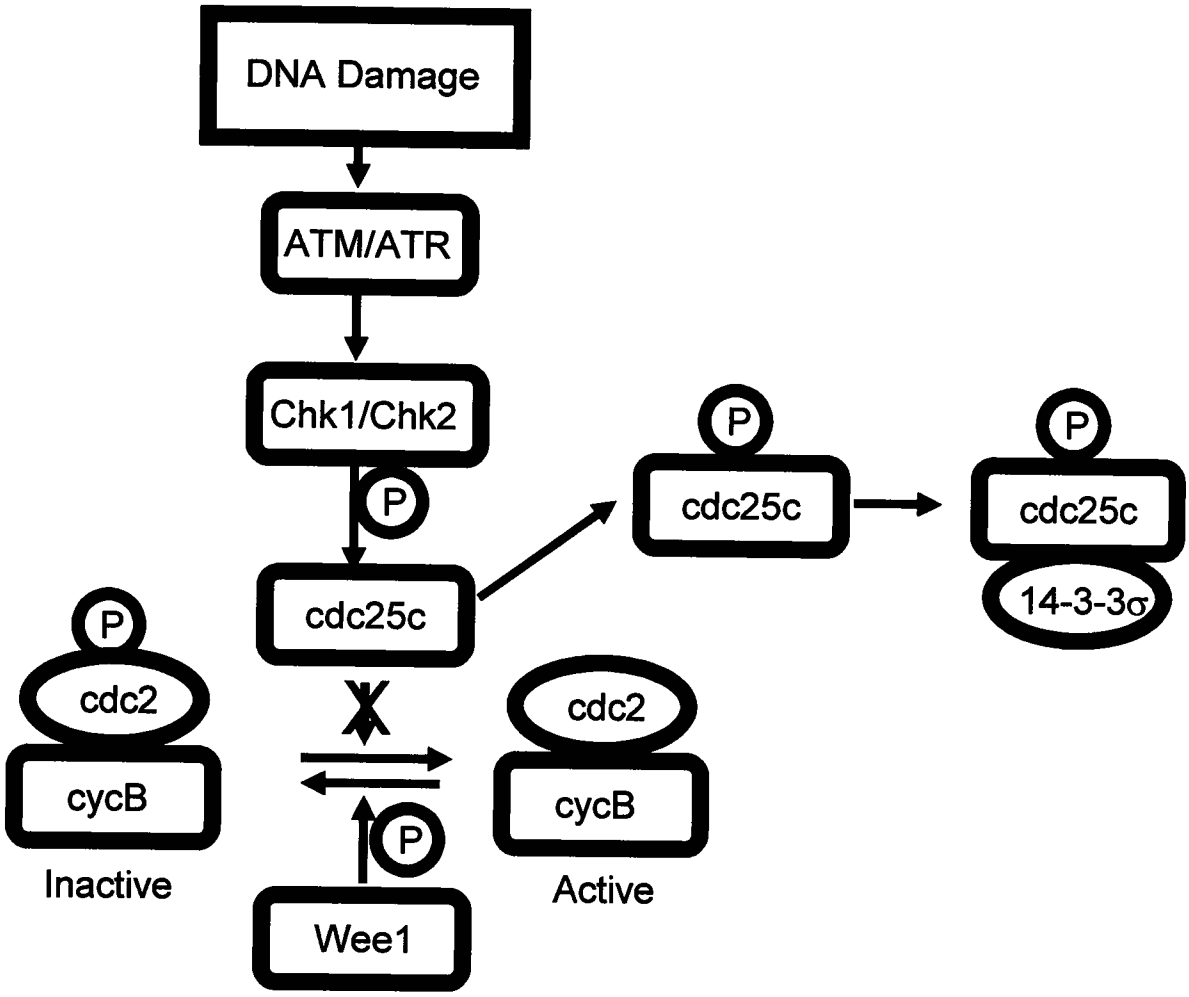

Figure 4.3.2. G_2 checkpoint pathway (Adapted from Samuel et al.).[6]

4.3. Rationale for using G_2 Checkpoint Inhibitors

The p53 protein is critical for protecting against cellular damage. It is a tumor suppressor protein that is significant in cell-cycle control, apoptosis, and maintaining genetic stability. A critical role of p53 is to activate the G_1 checkpoint to allow time to repair any lesions in the DNA. It has been found, however, that at least 60% of tumors lack p53 and in the presence of DNA damage, mp53 cells fail to arrest at G_1 to repair their DNA. The mp53 cells may then either die, or continue to proliferate with a blemished genome.[7]

Due to their genetic instability, it had been thought that mp53 cells would be more sensitive to treatments that involved DNA damaging agents. It has been found, however, that there is no correlation between p53 function and radiosensitivity. An explanation may lie in the fact that cells still arrest at the G_2 checkpoint. This allows tumor cells time to recover and repair their DNA.[8,9] Tumor cells lacking p53 may also have a growth advantage over wild type cells because the mp53 cells do not arrest at the G_1 checkpoint.[7]

DNA damaging agents such as cisplatin are often used to treat tumors. Upon DNA damage, the wild type cells activate both the G_1 and the G_2 checkpoints, but mp53 cells activate only the G_2 checkpoint. If a G_2 checkpoint inhibitor is used, the wild type cell is still able to arrest at G_1, but mp53 cells would not have any mechanism to repair their DNA. Tumor cells would enter mitosis with a large portion of their genome damaged, which is a lethal event (Figure 4.4.1).[10]

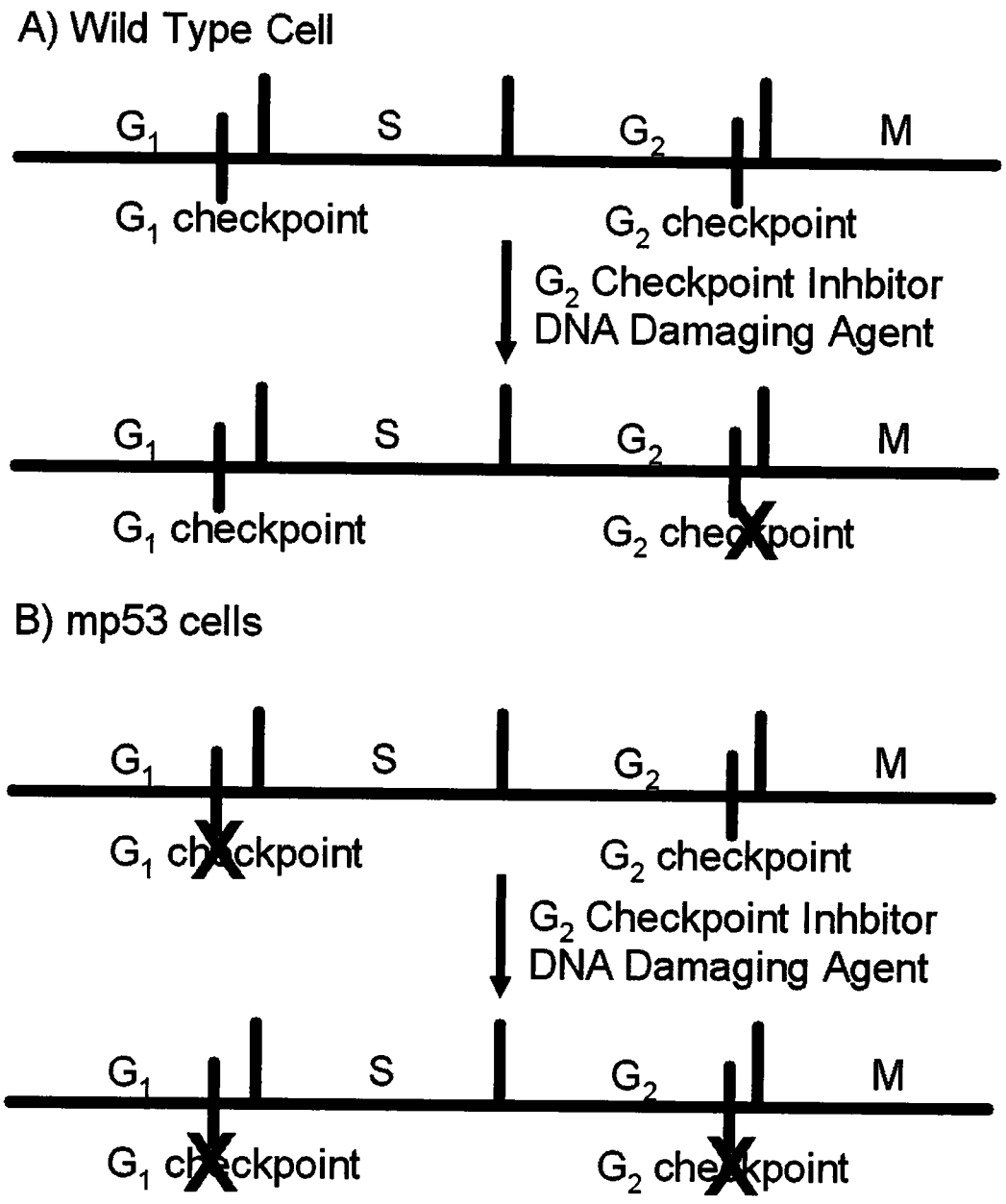

Figure 4.4.1. Rationale for using G_2 checkpoint inhibitors.

4.5. Known G_2 Checkpoint Inhibitors

There have been numerous G_2 checkpoint inhibitors that have been discovered. The first G_2 checkpoint inhibitor found was caffeine (**4.1**), and it was found to inhibit ATM/ATR mediated phosphorylation of Chk1. Unfortunately, caffeine is not practical to use in the clinic due to its numerous pharmacological activities and its cytotoxicity to cells at millimolar concentrations.[10] Other compounds that can inhibit ATM/ATR include the polyketide kinase inhibitor wortmannin (**4.2**), which has been found to be a strong G_2 checkpoint abrogator at 10 μM.[11,12]

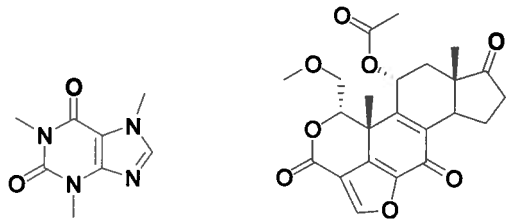

4.1 4.2

Figure 4.5.1. ATM/ATR inhibitors of the G_2 checkpoint pathway.

Staurosporine (**4.3**) is a very potent G_2 checkpoint inhibitor (IC_{50} 0.2 nM).[10,12] Unfortunately, this indole alkaloid is a non-specific kinase inhibitor and is highly toxic.[13] In efforts to find staurosporine analogs, UCN-01 (**4.4**) (7-hydroxystaurosporine) has been found to be a potent kinase inhibitor, a G_2 checkpoint inhibitor (IC_{50} 50-100 nM),[14] and an *in vitro* inhibitor of Chk1 (IC_{50} 10-25 nM).[15] UCN-01's promising biological activities allowed it to undergo clinical trials in both Japan and the U.S. One case report found that a patient with lymphoma chemotherapeutically resistant to EPOCH II (etoposide, prednisone, vincristine, cyclophosphamide, doxorubicin) had complete remission after one

cycle of UCN-01 proceeded by an EPOCH II dosage.[16] As evidenced by this study, further trials with this promising compound need to be done. SB-218078 (**4.5**) has also been shown as a compound that can inhibit G_2 arrest. This indole alkaloid was discovered by testing a series of Ser/Thr kinase inhibitors for their ability to inhibit Chk1 *in vitro*. It is a potent Chk1 inhibitor that can inhibit G_2 arrest with an IC_{50} of 15 nM. Paradoxically, SB-218078 was found to induce G_2 arrest at higher concentrations.[17]

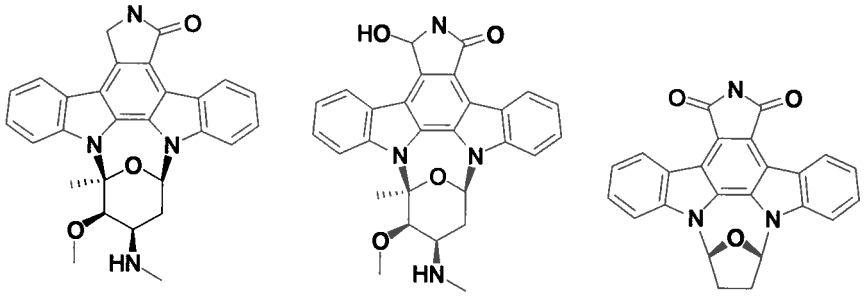

4.3 **4.4** **4.5**

Figure 4.5.2. Indole alkaloids inhibiting the G_2 checkpoint through Chk1.

Bioassay-guided fractionation of the Brazilian ascidian *Didemnum granulatum* led to the isolation of two G_2 checkpoint inhibitors: granulatimide (**4.6**) and isogranulatimide (**4.7**). Each of these alkaloids inhibited G_2 arrest with an IC_{50} of 6 μM.[10] Isogranulatimide was able to inhibit Chk 1 with an IC_{50} of 0.432 μM, while granulatimide was more potent (IC_{50} 0.081 μM).[18] Other marine G_2 checkpoint inhibitors discovered include the alkaloids hymenialdisine (**4.8**) and debromohymenialdisine (**4.9**) isolated from a MeOH extract of the marine sponge *Stylissa flabeliformis.* Both of these alkaloids were able to inhibit G_2 arrest (IC_{50} 6-8 μM) and were found to be *in vitro* inhibitors of Chk1 (IC_{50} 3 μM).[19]

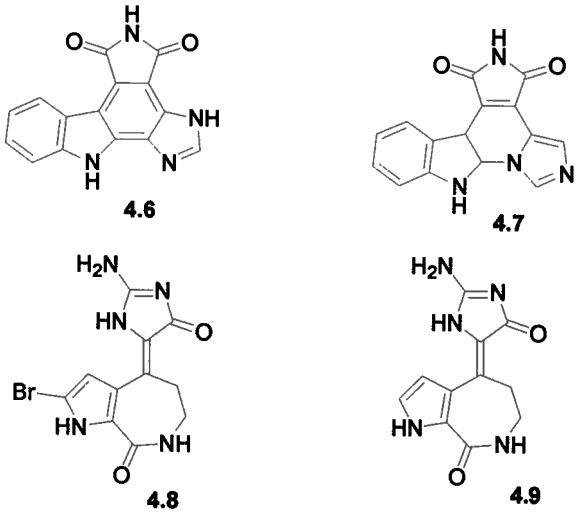

Figure 4.5.3 Alkaloids inhibiting the G_2 checkpoint through Chk1

Other inhibitors of the G_2 checkpoint include 13-hydroxy-15-oxozoapatlin (**4.10**), which was isolated from a MeOH extract of *Parinari curatellifona* bark obtained from the NCI Natural Products Repository. This compound was able to inhibit the G_2 checkpoint (IC_{50} 5-7 μM), however, the target of this small molecule is unknown, as it was found to be neither an inhibitor of ATM or of Chk1.[20] One hypothesis for the biological activity is that the presence of the α, β-unsaturated ketone makes it reactive to thiols in proteins. Other polyketide derived G_2 checkpoint abrogators include okadaic acid (**4.11**), which has an IC_{50} of 0.5 μM. Unfortunately, okadaic acid is a carcinogen and a food poison, so it is unlikely to be used in the clinic.[21] Fostriecin (**4.12**) is an anti-tumor drug that has activity against lung, breast, and colon cancer. This polyketide was shown to inhibit the G_2 checkpoint pathway with an IC_{50} of 3.2 μM.[21]

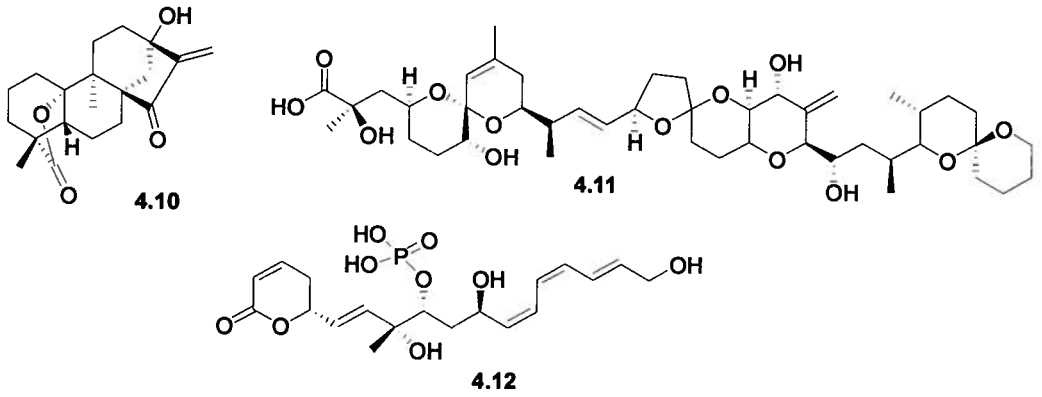

Figure 4.5.4. G_2 checkpoint inhibitors

4.6. Description of the G_2 Checkpoint Assay

Dr. Michel Roberge has developed the first assay to search for G_2 checkpoint inhibitors in crude extracts.[10] In the assay, MCF-7 mp53 cells are cultured and allowed to grow for 24 hours. The cells are then irradiated and after 16 hours, extracts are added to the cells along with nocodazole. Caffeine is used as a positive control in this assay. Cells are incubated for eight hours after adding the crude extracts, and cells that enter mitosis are measured by ELISA. The TG-3 antibody used in the ELISA assay recognizes a phosphorylated form of nucleolin present only in mitotic cells (Figure 4.6.1).[10]

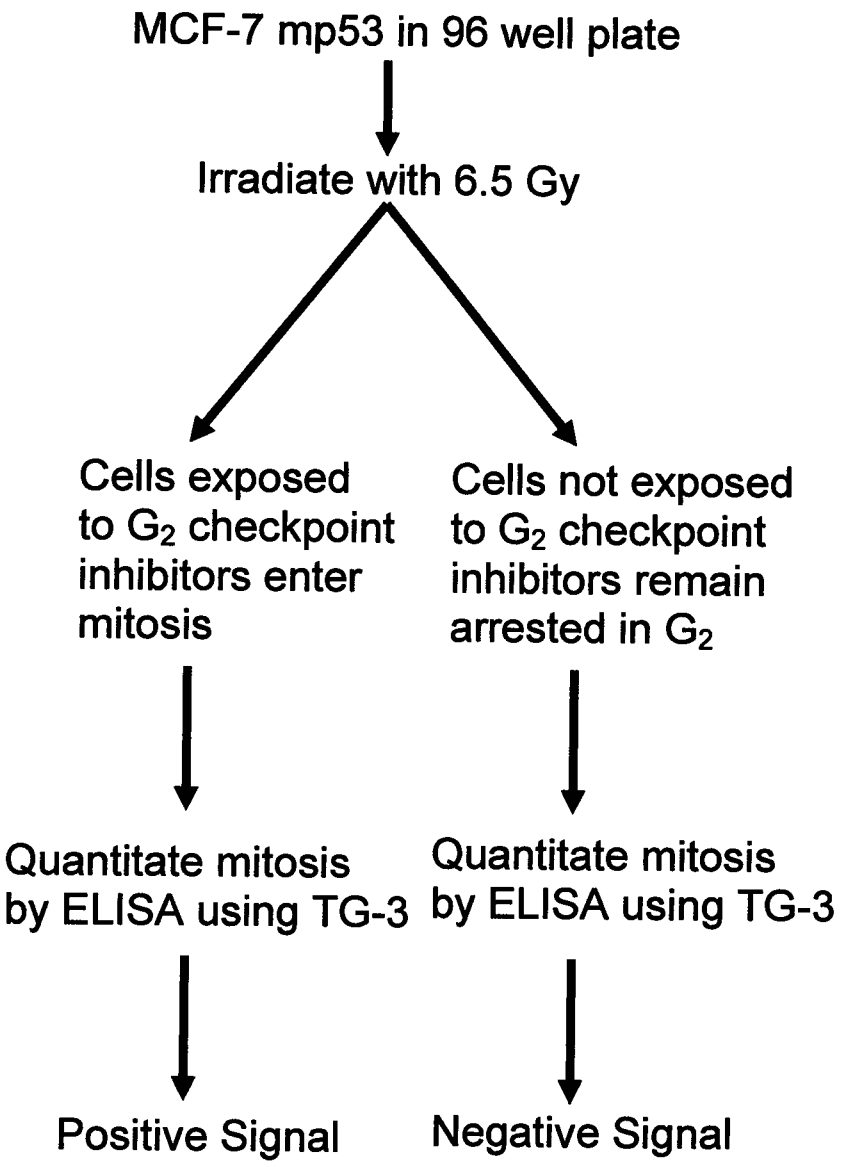

Figure 4.6.1. Description of the G_2 checkpoint inhibition assay.

4.7. Chemistry of Duguetia sp.

The Annonaceae family contains numerous shrubs, trees, and lianas, and is distributed in the tropics of South America, Africa, and Asia. This particular family is known for the acetogenins, a group of chemical compounds that have been discovered to have potent anti-tumor, cytotoxic, and anti-microbial

properties.[22] *Duguetia* is a genus within the Annonaceae family and contains approximately 80 species. Even though numerous chemical studies have been done on the *Duguetia* genus, biological studies have not been as detailed.[23] Plants in the genus *Duguetia* have medicinal potential as components of *D. glabriuscula* have been found to have anti-neoplastic activity,[24] and extracts of *D. furfuracea* and *D. lanceolata* have anti-parasitic activity.[25]

Three aporphinoid alkaloids, R-(-) dicentrine (**4.13**), duguetine (**4.14**) and norglaucine (**4.15**), were the first natural products isolated from a *Duguetia* sp. collected in Brazil.[23] Aporphine alkaloids that were first discovered from the bark of *D. spixiana* include reomerolidine (**4.16**), nornuciferidine (**4.17**), rurrebanine (**4.18**), and rurrebanidine (**4.19**). None of these natural products were reported to have any biological activity.[26] More recently, an ethanol extract of *D. furufuracea* collected in Brazil afforded *N*-nitrosoanonaine (**4.20**) and *N*-nitrosoxylopine (**4.21**). Their structures were determined using both NMR spectroscopy and X-ray crystallography.[23]

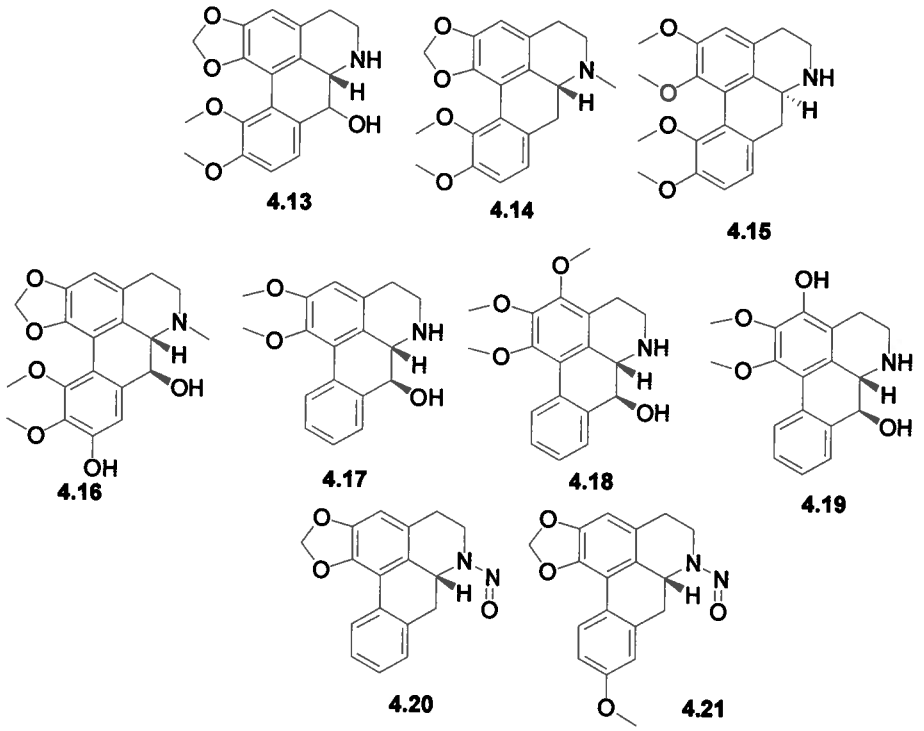

Figure 4.7.1. Aporphine alkaloids from *Duguetia.*

Chemical studies of an extract of *D. eximia* led to the isolation of several known oxoaporphines including *O*-methylmoschatoline (**4.22**) and oxostephanine (**4.23**), and the first report of oxo-*O*-methylpukateine (**4.24**).[27] Later, biological studies on *O*-methylmoschatoline revealed this oxoaporphine to have moderate antiparasitic activity against *Leishmania braziliensis*, and *Leishmania guyanesis* as well as cytotoxicity in the brine shrimp assay with an IC_{50} of 3.80 μg/mL.[28,29] Oxostephanine was discovered to have promising activity against the *Herpes simplex* virus.[30] More recently, duguevaline (**4.25**) was isolated from a CH_2Cl_2 extract of *D. vallicola* collected in Columbia.[31] Other isoquinoline alkaloids isolated from the bark of *D. spixiana* include codamine-*N*-oxide (**4.26**), spiguetine (**4.27**), and spiguetidine (**4.28**).[26,32] An EtOH extract of *D. hadrantha* has also yielded a series of bioactive alkaloids. Hadranthine A (**4.29**), sampangine (**4.30**)

and 1-methoxysampangine (**4.31**) were found to display *in vitro* antimalarial activity against *Plasmodium falciparum* (IC_{50} 120, 68, 95 ng/mL). Sampangine was also cytotoxic towards human malignant melanoma cells (IC_{50} 370 ng/mL).

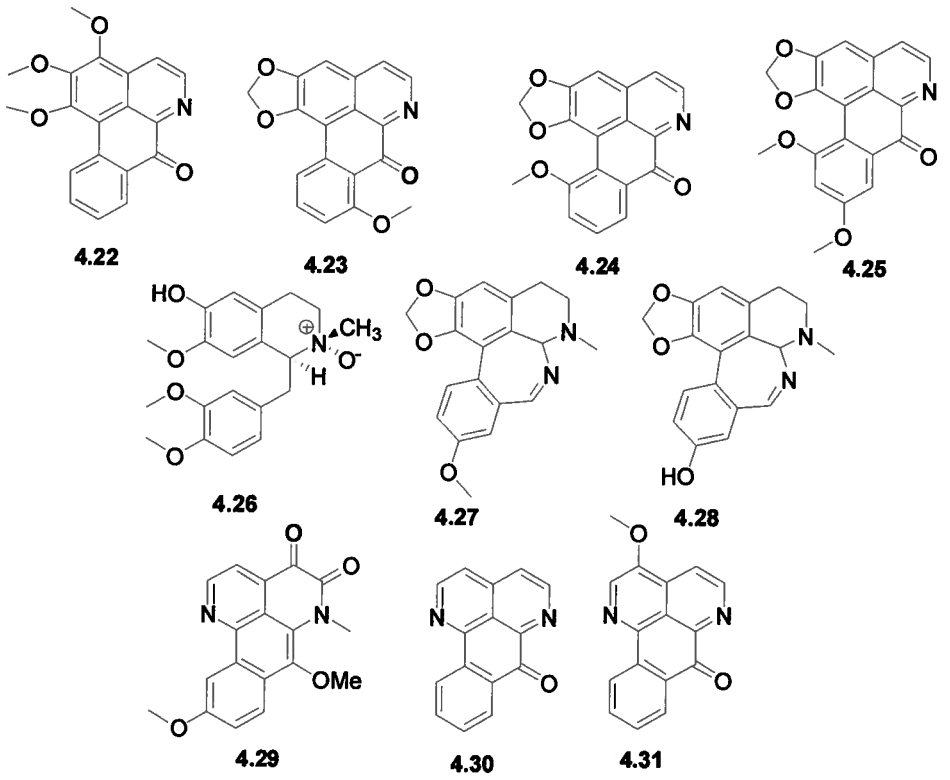

Figure 4.7.2 Alkaloids from *Duguetia* sp..

4.8. Isolation of alkaloids from Duguetia odorata

A MeOH extract of *D. odorata* (MacBride 1929) (Annonaceae) was obtained from the NCI repository of natural products and found to have bioactivity in the G_2 checkpoint assay. The MeOH extract was suspended in H_2O, and then sequentially partitioned with hexanes, CH_2Cl_2, EtOAc and *n*-butanol. The active *n*-butanol extract was subjected to size exclusion chromatography, flash reversed-phase column chromatography and reversed-phase HPLC to obtain oliveroline (**4.32**), a new alkaloid *N*-methylguatterine (**4.33**), dehydrodiscretine

(**4.34**), and pseudopalmatine (**4.35**). The structures of the known alkaloids oliveroline (**4.32**),[33,34] dehydrodiscretine (**4.34**), [35,36] and pseudopalmatine (**4.35**) [37] were all confirmed by comparing their NMR and MS data to the literature values. For full experimental details, see section 4.12.

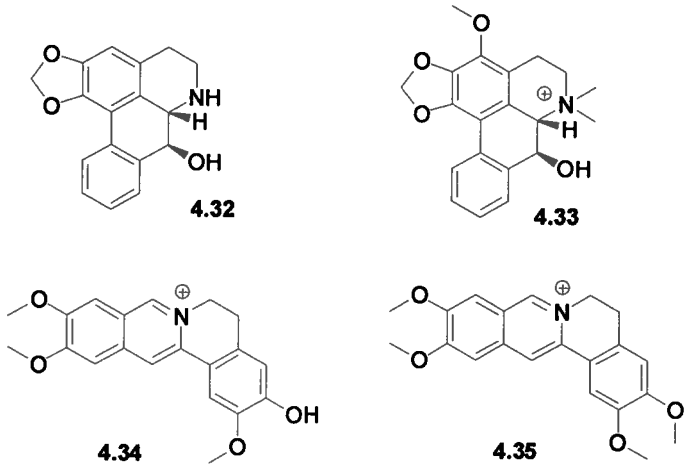

Figure 4.8.1. Alkaloids isolated from *D. odorata*.

4.9. Structure Elucidation of N-methylguatterine

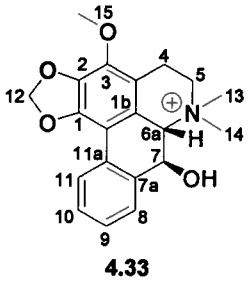

Figure 4.9.1. Numbering scheme of *N*-methylguatterine.

N-methylguatterine (**4.33**) was isolated as an optically active colorless solid that gave a $[M]^+$ ion at *m/z* 340.1534 in the HRESIMS, which is consistent with a molecular formula of $C_{20}H_{22}NO_4$ (calc'd for 340.1549). The ^1H NMR spectrum (Figure 4.9.3) was acquired in DMSO-d_6 at 500 MHz and was found to be similar to the ^1H NMR spectrum of oliveroline, suggesting that **4.33** was an

aporphine alkaloid. Examination of the ^1H NMR spectrum revealed four aromatic protons (δ_H 7.42-7.87), an exchangeable proton (δ_H 6.95), two deshielded protons (δ_H 6.25 and 6.07), a series of protons on carbons attached to a heteroatom (δ_H 3.17-5.02) and two protons on a carbon attached to an sp^2-hybridized carbon (δ_H 2.93). Analysis of the ^{13}C NMR spectra (Figure 4.9.4) and the HMQC data (Figure 4.9.5) identified 12 sp^2 hybridized carbons (δ_C 145.1, 138.9, 136.9, 135.9, 128.0, 127.9, 127.6, 125.4, 123.9, 119.2, 116.3, 109.5), an acetal carbon (δ_C 101.7), six sp^3 hybridized carbons attached to heteroatoms (δ_C 70.8, 68.2, 61.8, 59.4, 56.8, 42.1) and one shielded sp^3-hybridized carbon (δ_C 18.6). The HMQC data allowed the assignment of the proton resonances to their respective carbons (Table 4.9.1). It was possible to deduce four substructures (Figure 4.9.2) using the HMBC and COSY data ((Figures 4.9.6 and 4.9.7).

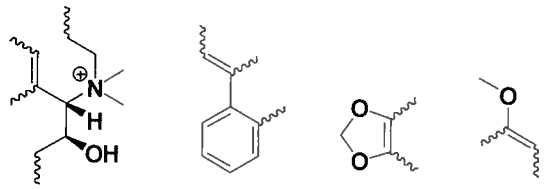

Figure 4.9.2. Substructures of *N*-methylguatterine deduced from the COSY and HMBC spectra.

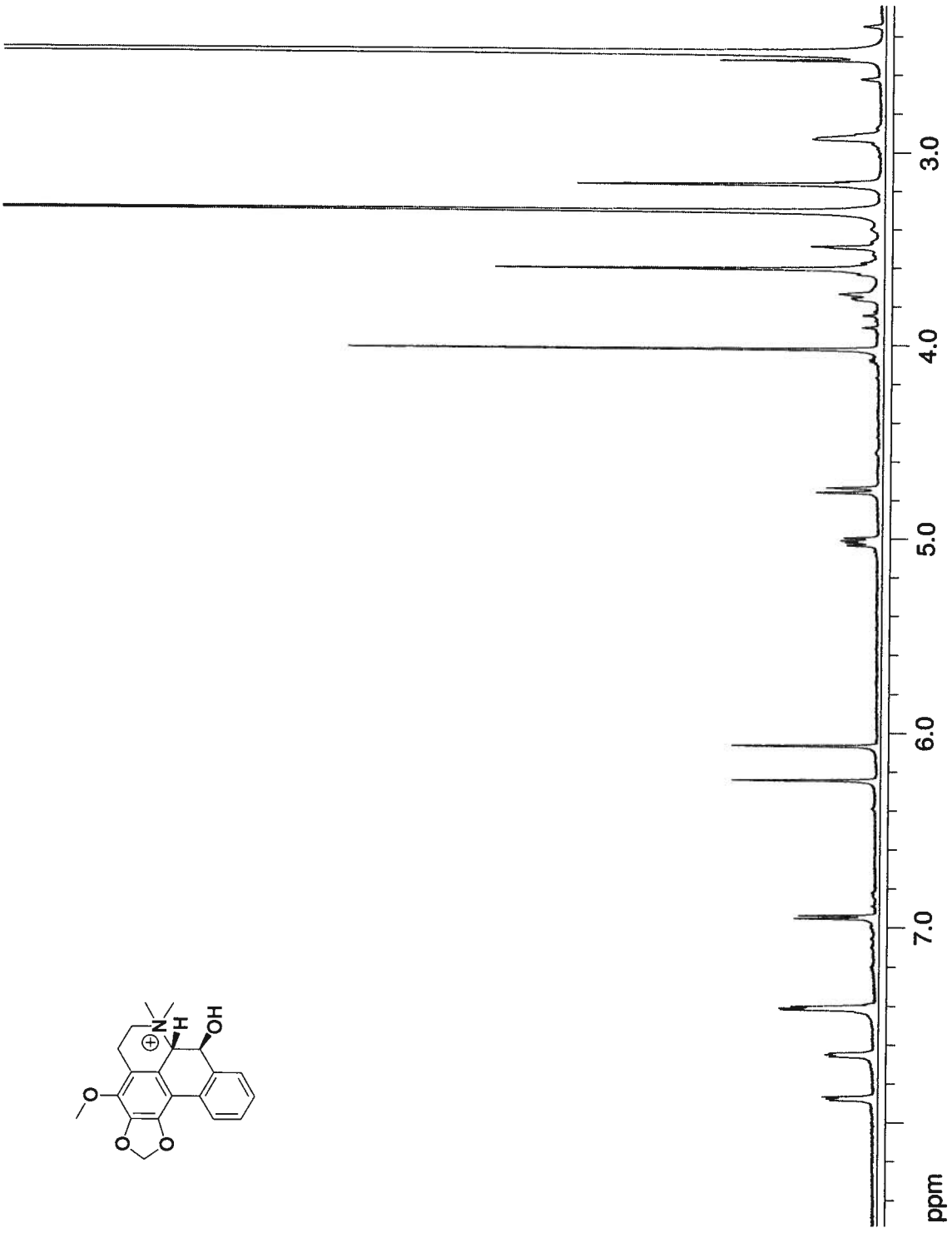

Figure 4.9.3. ^{1}H NMR spectrum of *N*-methylguatterine at 500 MHz in DMSO-d_6.

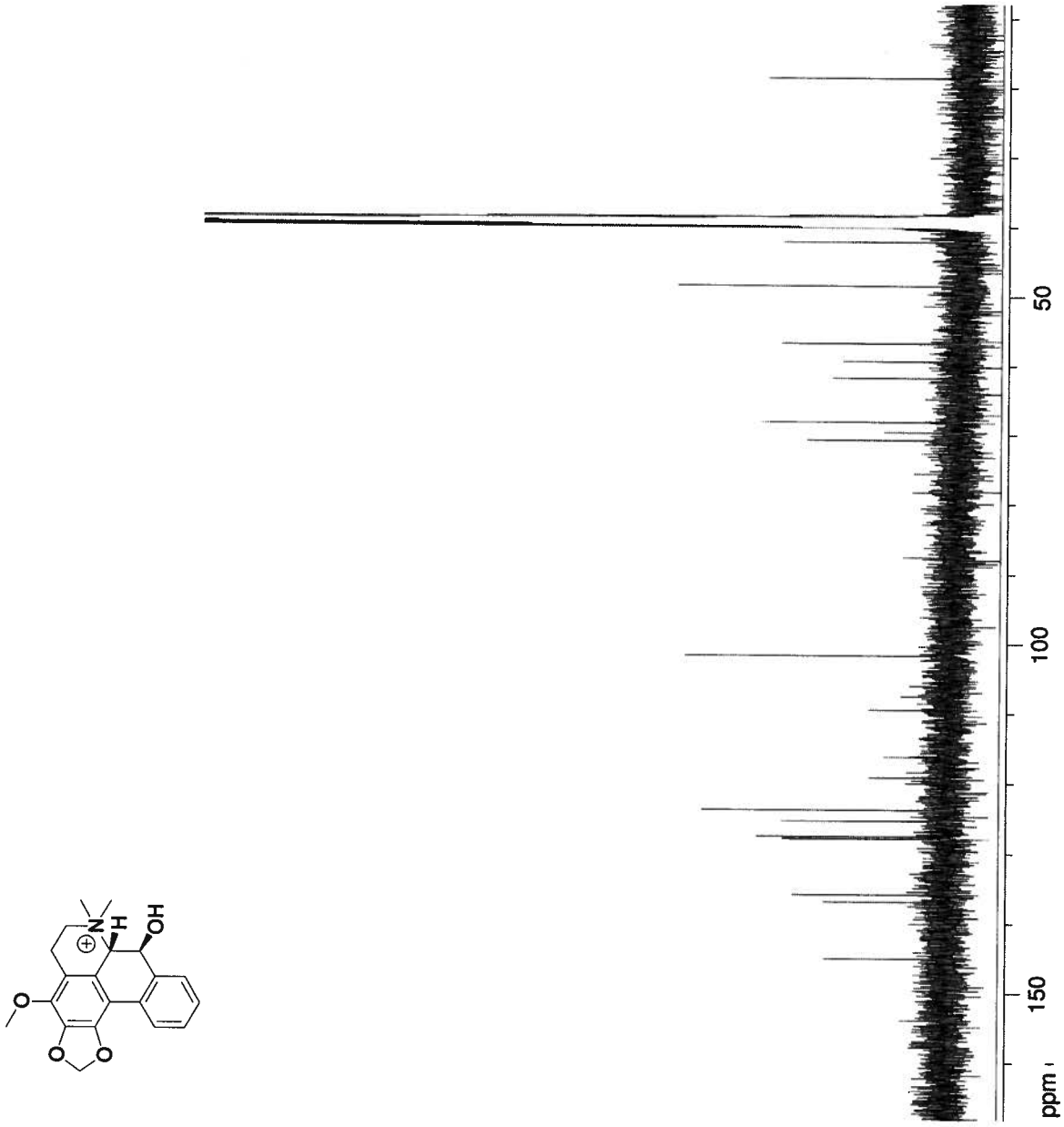

Figure 4.9.4. ^{13}C spectrum NMR of *N*-methylguatterine at 100 MHz in DMSO-d_6.

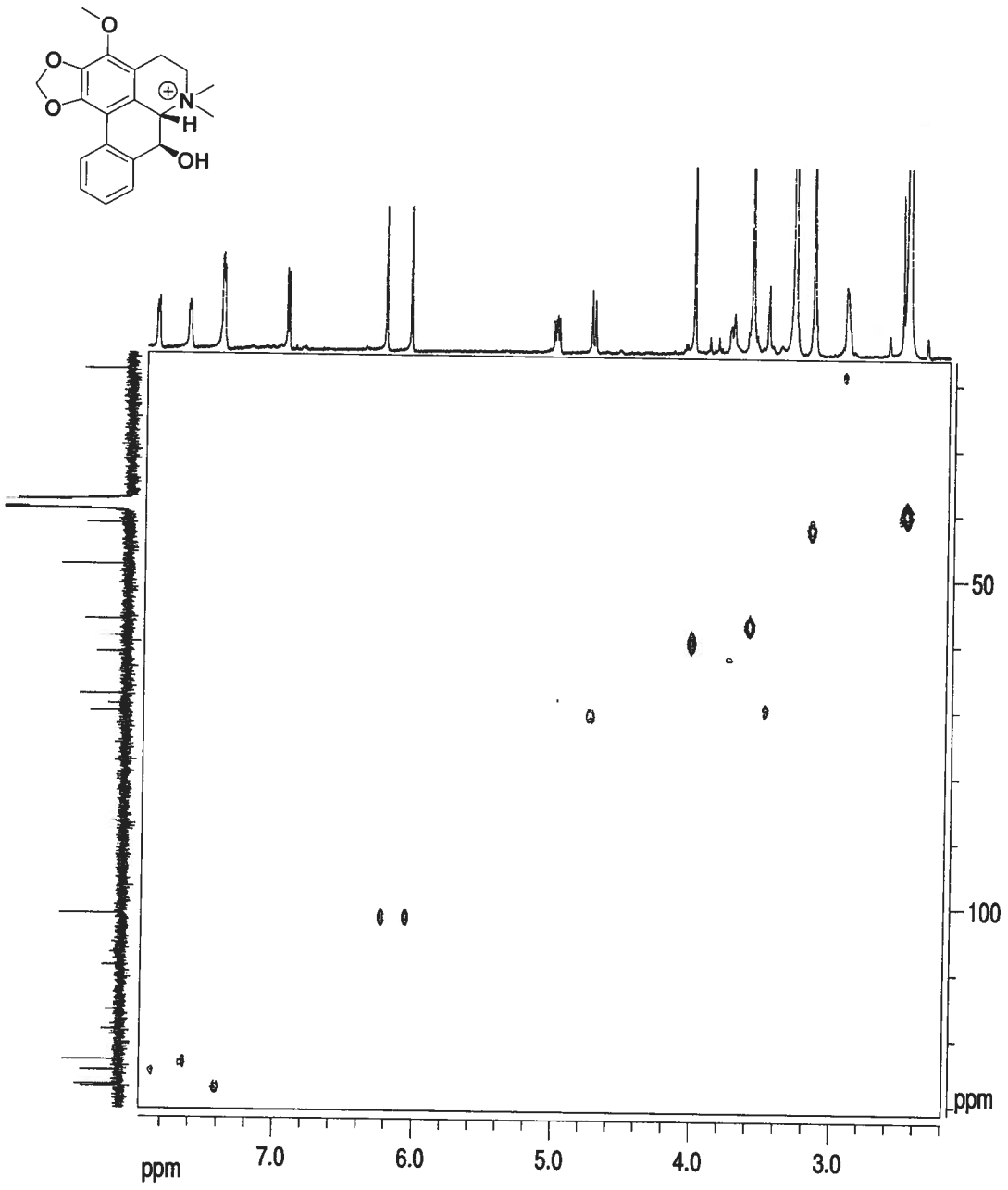

Figure 4.9.5. HMQC spectrum of *N*-methylguatterine at 500 MHz in DMSO-d_6.

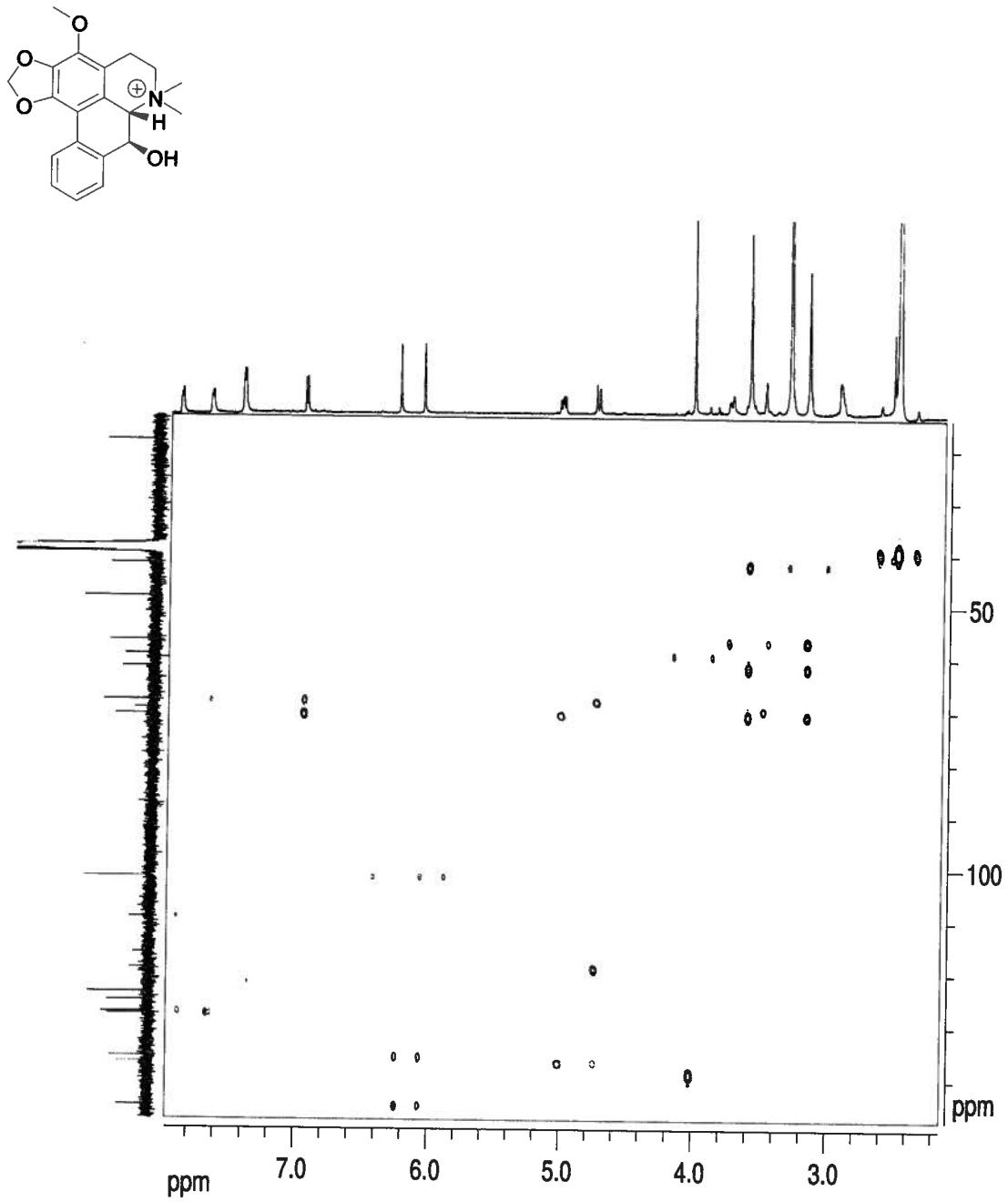

Figure 4.9.6. HMBC spectrum of *N*-methylguatterine at 500 MHz in DMSO-d_6.

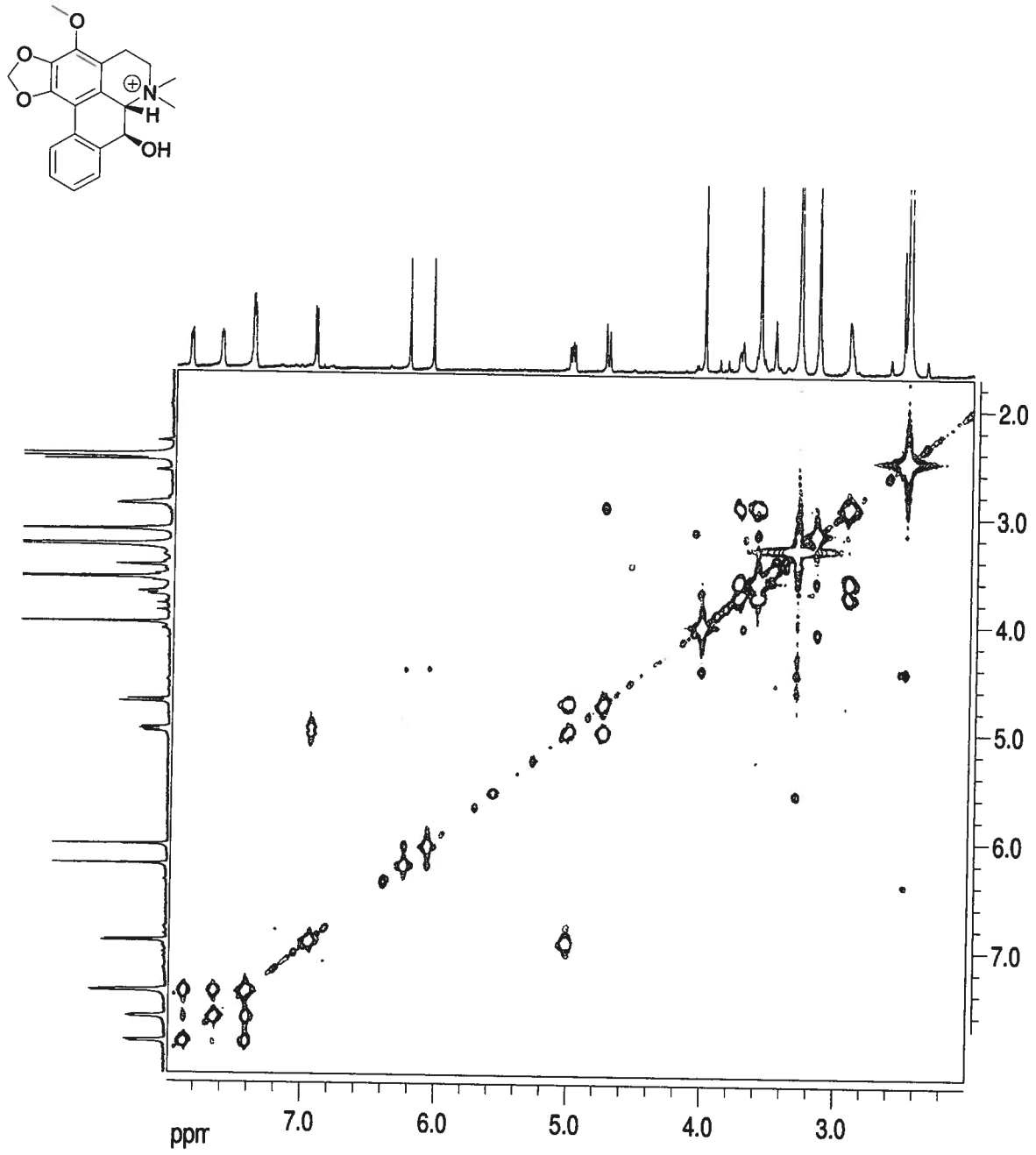

Figure 4.9.7. COSY spectrum of *N*-methylguatterine at 500 MHz in DMSO-d_6.

Table 4.9.1. 1D and 2D NMR data of *N*-methylguatterine.[a]

Position	δ_C	δ_H (*J* in Hz)	^1H, ^{13}C-HMBC	COSY
1	145.1			
1a	109.5			
1b	119.2			
2	135.9			
3	138.9			
3a	116.3			
4	18.6	2.93, m		H-5a, H-5b
5a	61.8	3.61, m	C-14	H-4, H-5b
5b		3.75, m	C-4	H-4, H-5a
6				
6a	70.8	4.74, d, (12.0)	C-1b, C-7, C-7a, C-13, C-14	H-7
7	68.2	5.02,dd, (12.0, 7.0)	C-1b, C-6a, C-7a	7-OH, H-6a
7a	136.9			
8	123.9	7.65, m	C-7, C-9, C-10	H-9
9[b]	127.9	7.41, m	C-11	H-8, H-10
10[b]	128.0	7.42, m	C-8	H-9, H-11
11	125.4	7.87, m	C-11a, C-1a	H-10
11a	127.6			
12	101.7	6.25 (a), s	C-1, C-2	H-12b
		6.07 (b), s	C-1, C-2	H-12a
13	42.1	3.17, s	C-5, C-6a, C-14	H-14
14	56.8	3.61, s	C-5, C-6a, C-13	H-13
15	59.4	4.02, s	C-3	
7-OH		6.95, d, (7.0)	C-6a, C-7	H-7

[a:] ^1H and ^{13}C chemical shifts [ppm] are referenced to DMSO-d_6 (δ_H 2.50 and δ_C 39.51 respectively)

[b:] Signals may be interchanged

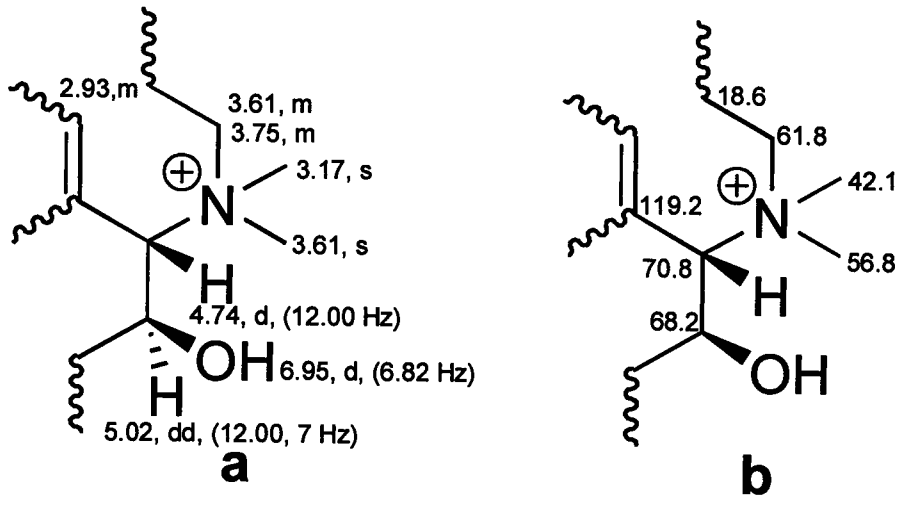

Figure 4.9.8. (**a**) ^{1}H chemical shifts and coupling constants for substructure **I** and (**b**) ^{13}C chemical shifts for substructure **I**.

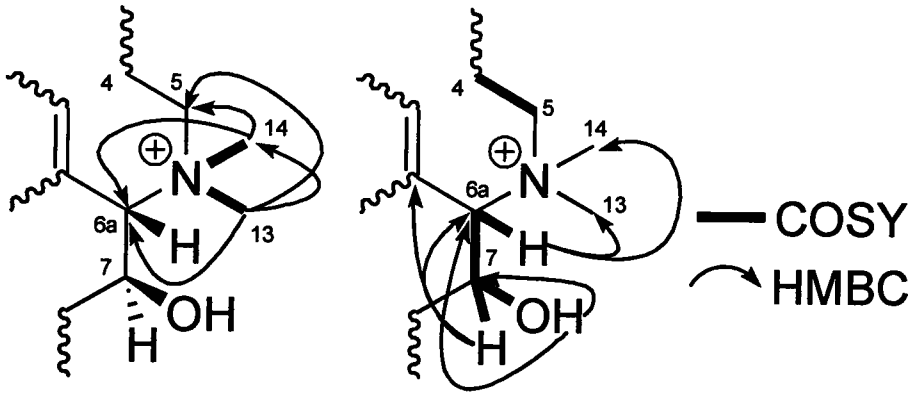

Figure 4.9.9. Key COSY and HMBC correlations observed for substructure **I** of **33**.

A singlet methyl proton resonance at δ_H 3.17 (H-13: HMQC to δ_C 42.1) showed HMBC correlations to a methyl carbon resonance at δ_C 56.8 (C-14). HMBC cross-peaks were also observed between the methyl proton resonance at δ_H 3.61 (H-14: HMQC to δ_C 56.8) and the methyl carbon resonance at δ_C 42.1 (C-13). This implied that Me-13 and Me-14 were geminal, and their chemical shifts indicated that they were attached to nitrogen (N-6) (Figure 4.9.11). Both the methyl proton resonances at δ_H 3.17 (H-13) and δ_H 3.61 (H-14) showed HMBC

correlations to the carbon resonance at δ_C 61.8 (C-5). Further HMBC correlations between the proton resonance at δ_H 3.61 (H-5a: HMQC to δ_C 61.8) and the carbon resonance at δ_C 56.8 (C-14) established the bond between C-5 and N-6 (Figures 4.9.8 and 4.9.11). The downfield chemical shift of the methylene carbon C-5 (δ_C 61.8) confirmed the attachment to the *N*-dimethyl moiety (Figure 4.9.8). Both methylene proton resonances at δ_H 3.61 (H-5a) and δ_H 3.75 (H-5b) displayed COSY cross-peaks with the methylene proton resonance at δ_H 2.93 (H-4), which established the connectivity between C-4 and C-5 (Figure 4.9.9 and 4.9.10).

Both the proton resonances at δ_H 3.17 (H-13) and δ_H 3.61 (H-14) displayed HMBC correlations to the methine carbon resonance at δ_C 70.8 (C-6a). A methine proton resonance at δ_H 4.74 (H-6a: HMQC to δ_C 70.8) displayed HMBC correlations to the methyl resonances at δ_C 56.8 (C-14) and δ_C 42.1 (C-13), which established the connectivity between C-6a and N-6 (Figure 4.9.8). Observation of the carbon chemical shift of C-6a (δ_C 70.8) also confirmed this linkage (Figure 4.9.8). The proton resonance at δ_H 4.74 (H-6a) contained a COSY correlation to the methine proton resonance at δ_H 5.02 (H-7: HMQC to δ_C 68.2), which indicated a linkage between C-6a (δ_C 70.8) and C-7 (δ_C 68.2) (Figures 4.9.8 and 4.9.9). No HMQC correlations were present for the proton resonance at δ_H 7.95 (7-OH), which indicated the presence of an exchangeable alcohol proton. COSY correlations between the exchangeable proton resonance at δ_H 7.95 (7-OH), with the methine proton resonance at δ_H 5.02 (H-7) placed the

alcohol moiety on C-7 (δ_C 68.2) (Figures 4.9.8 and 4.9.9). The chemical shift of C-7 (δ_C 68.2) is typical of an alcohol moiety attached to a carbon. Both methine proton resonances at δ_H 4.74 (H-6a) and δ_H 5.02 (H-7) showed HMBC correlations to δ_H 119.2 (C-1b), which indicated that H-6a was neighboring an sp^2-hybridized carbon. All of the above data was consistent with substructure **I** (Figures 4.9.8 and 4.9.9).

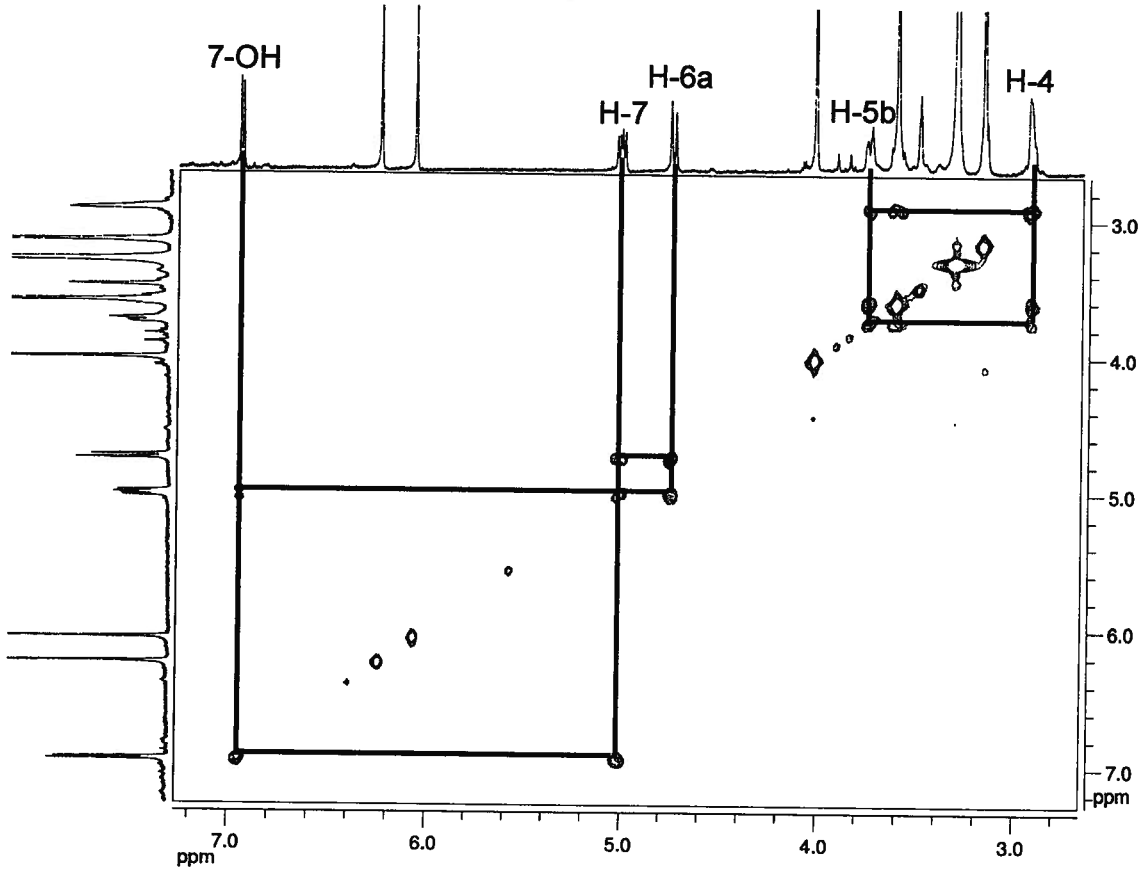

Figure 4.9.10. COSY correlations for substructure **I** of **4.33**.

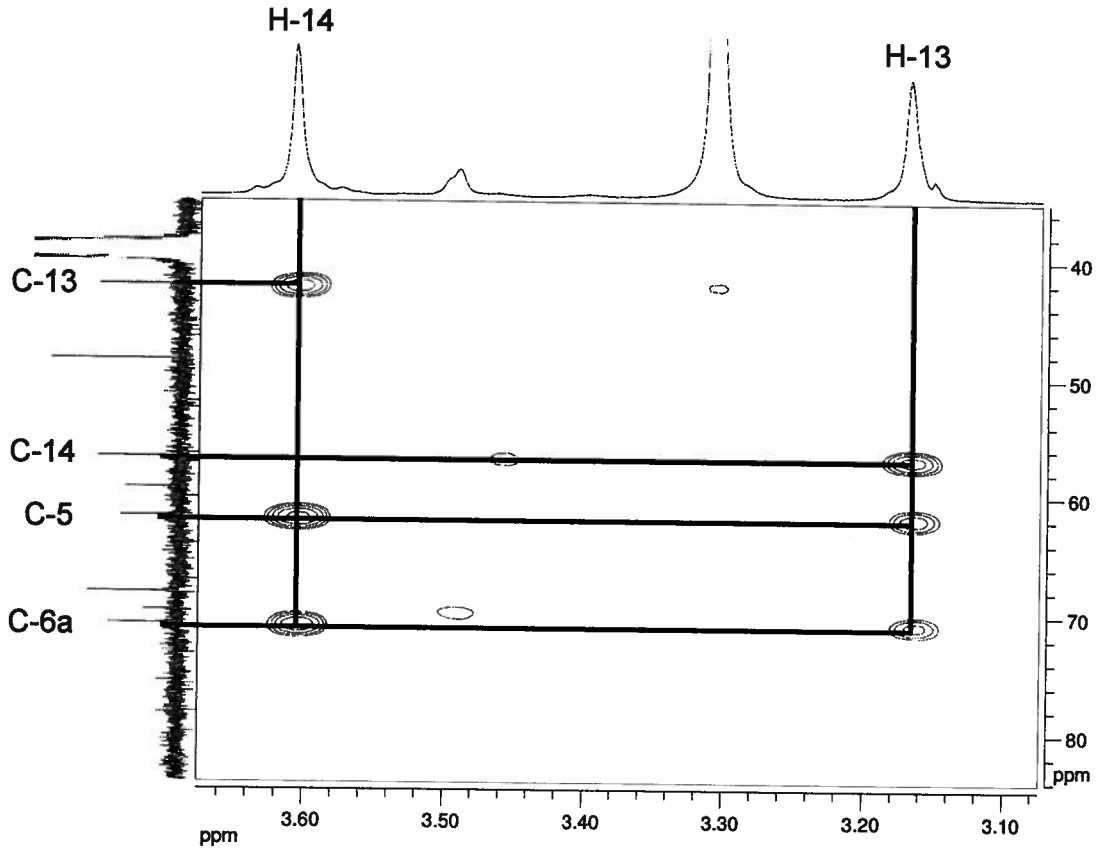

Figure 4.9.11. HMBC correlations observed for H-13 and H-14 for substructure **I** of **4.33**.

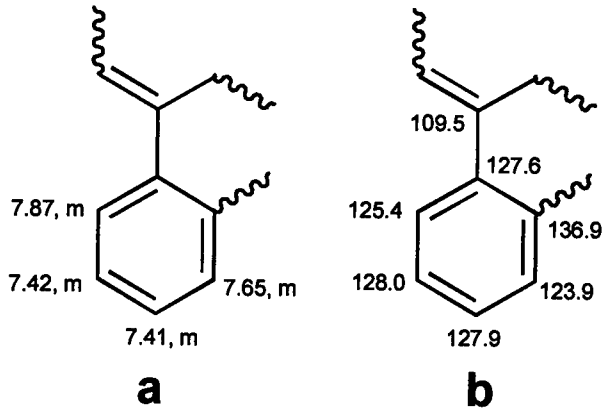

Figure 4.9.12. (**a**) ^{1}H chemical shifts and (**b**) ^{13}C chemical shifts for substructure **II**.

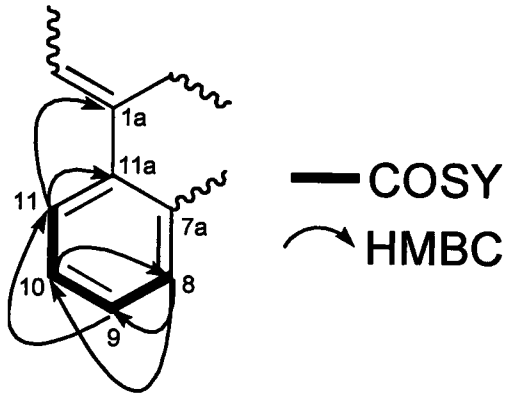

Figure 4.9.13. Key HMBC and COSY correlations observed for substructure **II** of **4.33**.

The aromatic proton resonance at δ_H 7.65 (H-8: HMQC to δ_C 123.9) showed COSY correlations to the proton resonance at δ_H 7.41 (H-9: HMQC to δ_C 127.9), which in turn had COSY correlations to the proton resonance at δ_H 7.42 (H-10: HMQC to δ_C 128.0). Additional COSY cross-peaks were observed between the proton resonance at δ_H 7.42 (H-10) and the proton resonance at δ_H 7.87 (H-11: HMQC to δ_C 125.4) (Figures 4.9.13 and 4.9.14). All of the above data are consistent with four contiguous aromatic methines (C-8 to C11) and the presence of a 1,2 disubstituted benzene ring. This was also confirmed by observation of the HMBC data (Figure 4.9.13). The proton resonance at δ_H 7.87 (H-11) showed HMBC correlations to the quaternary aromatic carbon resonance at δ_C 109.5 (C-1a), thus establishing substructure **II** (Figures 4.9.12 and 4.9.13).

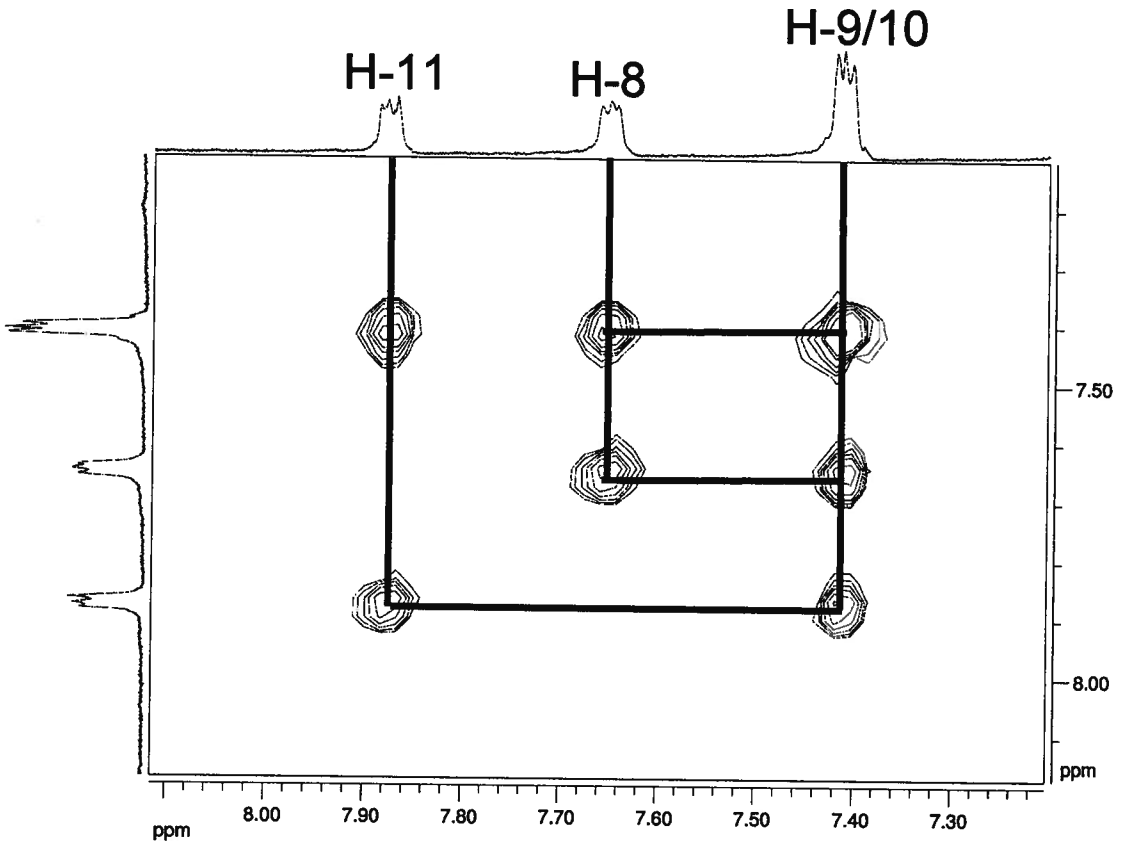

Figure 4.9.14. Expansion of the aromatic region of the COSY spectrum for **4.33**.

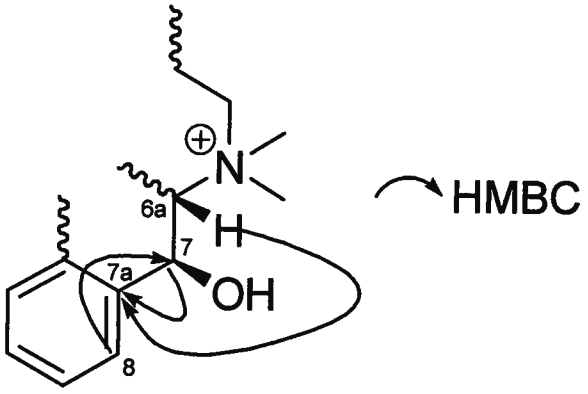

Figure 4.9.15. HMBC correlations linking substructures **I** and **II** for **4.33**.

Both methine proton resonances at δ_H 4.74 (H-6a), and δ_H 5.02 (H-7) showed HMBC correlations to the quaternary aromatic carbon resonance at δ_C 136.9 (C-7a). This indicated that carbon resonances C-7 (δ_C 68.2) and C-7a (δ_C

136.9) were linked. Finally, HMBC correlations between the aromatic methine proton resonance at δ_H 7.65 (H-8) and the oxygenated carbon methine resonance at δ_C 68.2 (C-7) confirmed that substructure **I** was adjacent to substructure **II** (Figure 4.9.15).

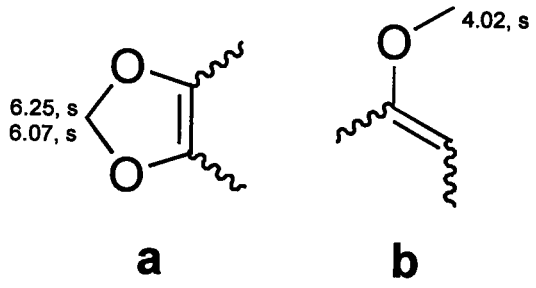

Figure 4.9.16. ^{1}H NMR of substructures **III** (**a**) and **IV** (**b**)

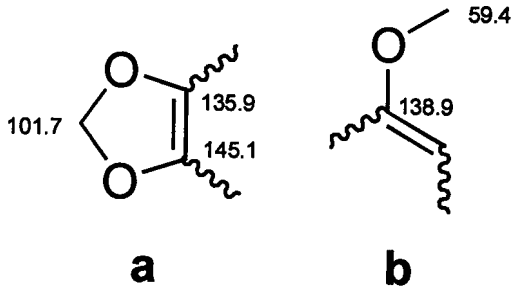

Figure 4.9.17. ^{13}C NMR of substructures **III** (**a**) and **IV** (**b**)

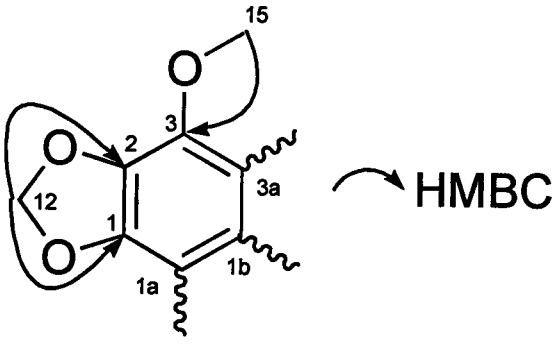

Figure 4.9.18. HMBC correlations for substructure **III** and **IV** for **4.33**.

The chemical shift of the resonance at δ_C 101.7 (C-12) is consistent for that of a methylene-dioxy carbon. The methylene proton resonances at δ_H 6.25 (H-12a: HMQC to δ_C 101.7) and δ_H 6.07 (H-12b: HMQC to δ_C 101.7) showed three bond HMBC couplings to the sp^2-hybrizided carbon resonances at δ_C 145.1 (C-1) and δ_C 135.9 (C-2) (Figure 4.9.18). All of the above is consistent with substructure **III** (Figures 4.9.16 and 4.9.17). The ^1H NMR spectrum of **4.33** lacked a proton resonance that belonged to C-3. HMBC correlations between the proton resonance at δ_H 4.02 (H-15) and the carbon resonating at δ_C 138.9 (C-3) placed the methyl ether on C-3 (substructure **IV**) (Figures 4.9.16, 4.9.17, and 4.9.18). Closely related aporphine alkaloids with a methyl ether on C-3 display similar ^{13}C chemical shifts.[34,38] Finally, comparison of the ^{13}C chemical shifts of **4.33**, to that of the related aporphine alkaloid guatterine (**4.36**),[39] confirmed the constitution of *N*-methylguatterine (Figure 4.9.19).

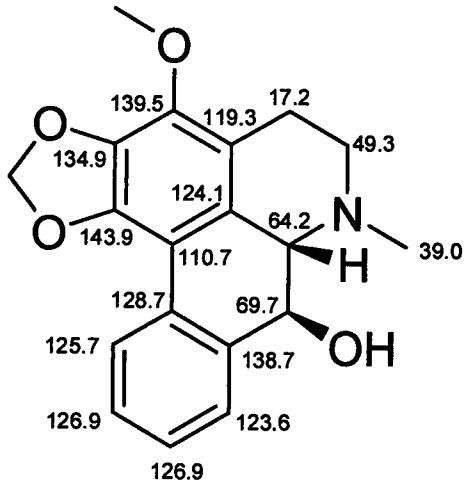

4.36

Figure 4.9.19. ^{13}C chemical shifts for guatterine (**4.36**), an aporphine alkaloid related to **4.33**.

Observation of the scalar coupling constant between H-6a and H-7 (J = 12.0 Hz) in **4.33** revealed a trans-relationship between the two protons. The scalar coupling of **4.33** was very similar to the scalar coupling present in oliveroline between H-6a and H-7 (J = 13.0 Hz) which indicated that the relative configurations of C-6a and C-7 were identical. The CD-spectra (Figure 4.9.20) of both oliveroline and *N*-methylguatterine were similar. This established that *N*-methylguatterine had S configurations on both stereocentres.

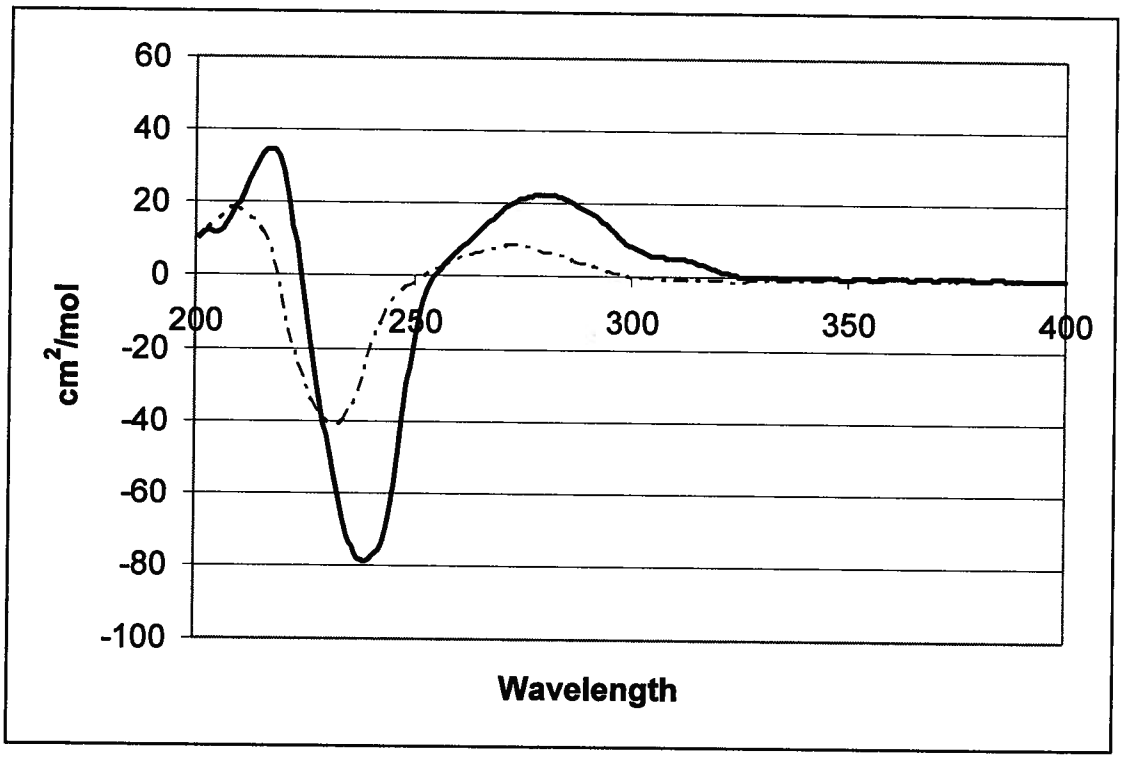

Figure 4.9.20. CD spectrum of *N*-methylguatterine (dashed line) and oliveroline (solid line).

4.10. Biology of the Alkaloids Isolated from Duguetia odorata

Oliveroline was found to be active in the G_2 checkpoint assay at concentrations above 10 μM (Figure 4.10.2). There were insufficient amounts of *N*-methylguatterine to biologically test this molecule, while dehydrodiscretine and

pseudopalmatine were all found to be inactive. To test if a structure activity relationship was present, the known alkaloids boldine (**4.37**), apomorphine (**4.38**), berberine (**4.39**) and palmatine (**4.40**) were also tested and no biological activity was found (Figures 4.10.2 and 4.10.3). Flow cytometry analysis indicated that 43 +/- 12% of cells entered mitosis in the presence of 10 μM of the known G_2 checkpoint inhibitor isogranulatimide (**B,** Figure 4.10.1), while 50 μM of oliveroline was required to induce the same activity (**C,** Figure 4.10.1). In the presence of the drug carrier DMSO, 16% of cells had escaped G_2 arrest (**A,** Figure 4.10.1). Oliveroline, dehydrodiscretine and pseudopalmatine were found to be moderate inhibitors of cell proliferation with IC_{50}'s of 45, 250, and 75 μM respectively, but were 2-3 times more potent when cells were irradiated with 6.5 Gy (IC_{50} 20, 80, 50 μM respectively). Oliveroline is an efficacious but moderate inhibitor of the G_2 checkpoint. It was discovered that oliveroline is not an inhibitor of Chk1, which means that this compound is a potential biological tool that can be used to discover new targets in the G_2 checkpoint pathway.

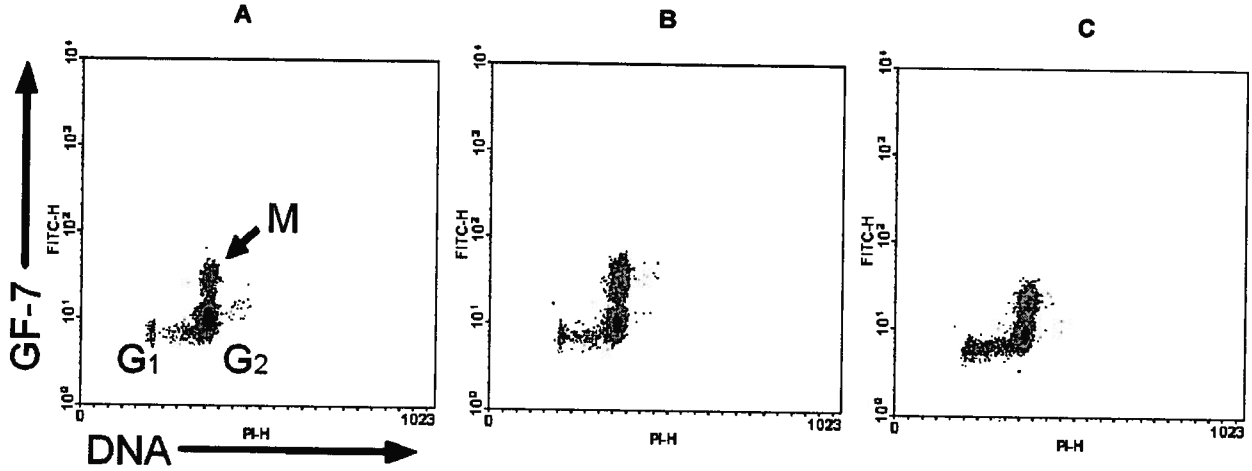

Figure 4.10.1 Flow cytometry analysis of **A** DMSO, **B** isogranulatimide and **C** oliveroline. These graphs were obtained by Dr. Chris Sturgeon of the Roberge laboratory.

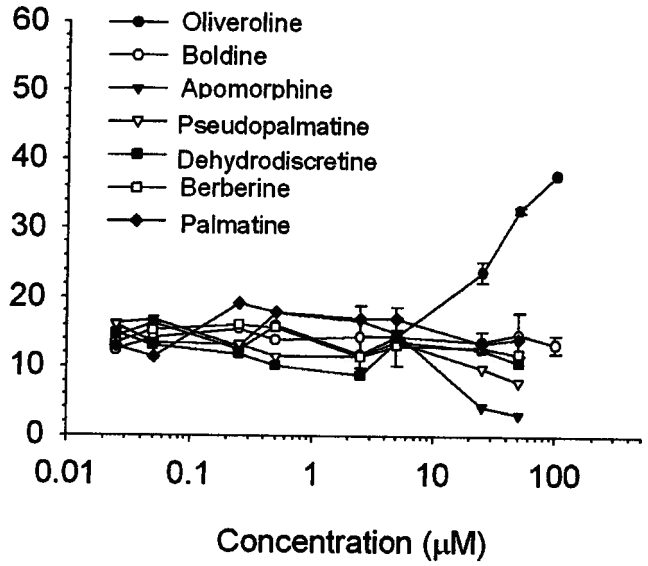

Figure 4.10.2. Concentration dependence of checkpoint inhibition activity of oliveroline and the other alkaloids. The graph was obtained by Dr. Chris Sturgeon of the Roberge laboratory.

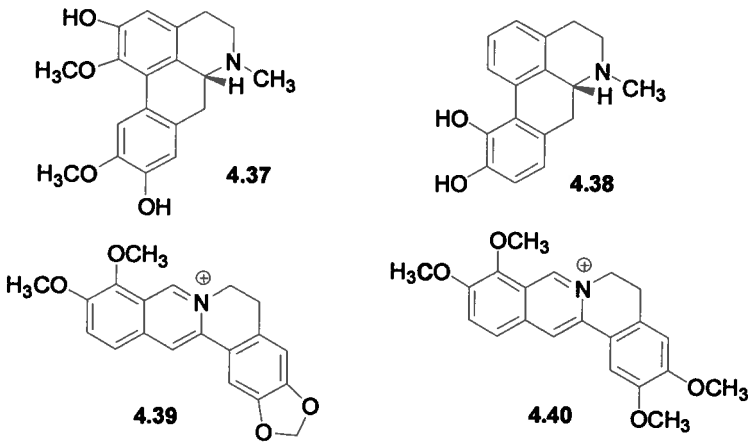

Figure 4.10.3. Other alkaloids tested in the G_2 checkpoint assay

4.11. General Experimental Methods

All solvents used (except for NMR solvents) were HPLC grade (Fisher) and no further purification was done on them unless for use on the HPLC. Solvents for HPLC were filtered through a 0.45 μm filter (Osmonics, Inc) before use. Pure alkaloids screened in the G_2 checkpoint assay (boldine (**4.37**), apomorphine (**4.38**), berberine (**4.39**) and palmatine (**4.40**)) were purchased from Aldrich. Reversed-phase C_{18} silica gel Sep Paks™ (10 g) were purchased from Waters, Inc.. Separations on the HPLC were accomplished using either a Waters 2487 dual channel detector/system controller (Waters Series 515 pump; chart recorder, 0.25 cm/min), or a Waters 1500 series HPLC pump and a Waters 2487 dual channel detector. The HPLC column used was a Whatman Partisil 10 ODS-3 Magnum column. The conditions of the HPLC separation were as follows: 2.0 mL/min with UV observation at 220 nm. Thin-layer chromatography (TLC) plates were Whatman MKC18F (reversed phase) and Kieselgel $60F_{254}$ (normal phase). TLC was visualized using either a dip solution of *p*-anisaldehyde

(1% *p*-anisaldehyde, 2% H_2SO_4, 20% acetic acid and 77% ethanol) or under ultraviolet light (254 nm).

The ^{13}C spectra were obtained with the Bruker AM400 spectrometer. ^1H spectra and 2-D data sets were taken with Bruker AMX500, and Bruker AV400 spectrometers. NMR solvents were purchased from Cambridge Isotope laboratories and were referenced to solvent peaks for DMSO-d_6 (δ_C 39.5 ppm and δ_H 2.50 ppm). Low resolution ESI mass spectra were recorded on a Bruker Esquire LC mass spectrometer. High resolution ESI mass spectra were obtained using a Micromass LCT mass spectrometer. Optical rotations were recorded with a JASCO J-1010 polarimeter equipped with a halogen lamp (589 nm) and a 10 mm micro cell. The CD spectra were determined using a JASCO J-710 spectropolarimeter with a 1 mm micro cell.

4.12. Isolation procedure of the alkaloids from Duguetia odorata

A sample of *D. odorata* was obtained from Peru in February 1992 by the New York Botanical Gardens as part of a contract with the NCI. A voucher specimen is found at the National Herbarium in Washington, D.C. (0CKH0164). A crude MeOH extract of *Duguetia odorata* (MacBride 1929) (Annonaceae) was obtained from the NCI repository (N075679-Z/3) of natural products and found to have bioactivity in the G_2 checkpoint assay. The crude extract (4 g) was first suspended in 100 mL of H_2O, and then sequentially partitioned with hexanes (3 X 50 mL), CH_2Cl_2 (3 X 50 mL), EtOAc (3 X 50 mL) and butanol (3 X 50 mL). Four hundred milligrams of the bioactive butanol fraction was subjected to Sephadex ^{TM} LH-20 size exclusion chromatography eluting with 100% MeOH.

This was followed by further purification on a gradient reverse phase Sep Pak™ (eluent: H_2O to MeOH) to yield one biologically active fraction. This fraction was subjected to repeated reversed phase HPLC (Inertsil C_{18}, 9.4 X 250 mm, 6:4:0.1 H_2O: MeOH: TFA, UV detection at 220 nm) to yield oliveroline (**4.32**, 1.7 mg), *N*-methylguatterine (**4.33**, 1.3 mg), dehydrodiscretine (**4.34** 3.3 mg), and pseudopalmatine (**4.35**, 2.6 mg).

4.13. Checkpoint inhibitor activity

Cells were seeded at 2 x 10^5 cells/dish in 35 mm-diameter dishes and subsequently cultured for 24 h. Cells were then irradiated with 6.5 Gy using a ^{60}Co source (1.2 Gy/min, Gammacell 220, Atomic Energy Commission of Canada). Sixteen hours later, when 90% of cells were arrested in G_2,[10] drugs were added with 100 ng/mL nocodazole, and cells were cultured for another 8 h. Cells were then collected in SAB (phosphate buffered saline with 1% fetal bovine serum and 0.1% sodium azide) and fixed in 10 volumes of 70% ethanol at 4°C overnight. Cells were washed in 0.5% Tween-20 in SAB and incubated with a mitosis-specific antibody GF-7[20] for 1 h, washed twice, and suspended with 1:500 diluted Alexa 488-conjugated goat anti-rabbit (Molecular Probes A-11029) antibody for 30 min. Following two more washes, cells were suspended in RNase A (Roche Diagnostics, 500 units/mL in 4 mM sodium citrate buffer, pH 8.4) for 30 min at 37°C. An equal volume of 50 µg/mL propidium iodide prepared in 4 mM sodium citrate pH 8.4 was added and incubated for an additional 20 min. Cells were resuspended at a final concentration of 1x10^6 cells/mL in 25 µg/mL propidium iodide solution and stored in the dark overnight. Cells were analyzed

with a Becton-Dickson FACSCalibur, collecting 20,000 events per sample. All data was analyzed using WinMDI freeware.

4.14. Description of the Cell Viability Assay

MCF-7 mp53 cells were seeded at 1000 cells/well in 96-well plates, grown overnight, and treated or not treated with compound for 24 h, immediately followed by irradiation or not. DMSO carrier did not exceed 1% final concentration. The drug was removed, and cells were allowed to grow in fresh medium until those not treated with the drug approached confluence, which was typically 4-6 days. Cell proliferation was measured as follows: 25 μL of a 5 mg/mL solution of 3(4,5-dimethylthiazol-2-yl)-2,5-diphenyltetrazolium bromide in phosphate-buffered saline was added to cells in the presence of 100 μL of cell culture medium. After a 2 h incubation at 37°C, 100 μL of 20% sodium dodecyl sulfate dissolved in DMF/H_2O (1:1), pH 4.7, was added, and the absorbance at 570 nm was measured after overnight incubation.

4.15. Physical Data of Alkaloids From Duguetia odorata

(-)-Oliveroline (4.32): Brown oil. $[\alpha]_D^{23}$: -16.9 (c 0.3, MeOH) UV (MeOH) λ_{max} (log ε): 233 (3.91), 271 (3.88), 315 (3.39); CD (MeOH) λ_{max} ($\Delta\varepsilon$) 232 nm (-314.36); ^{1}H NMR (500 MHz, DMSO-d_6): δ_H 8.00 (1H, d, J = 6.7 Hz, H-11), 7.43 (1H, m, H-9 or H-10), 7.43 (1H, m, H-10 or H-9), 6.89 (1H, s, H-3), 6.82 (1H, d, 5.90 Hz, 7-OH), 6.24 (1H, s, H-12a or H-12b), 6.06 (1H, s, H-12b or H-12a), 4.92 (1H, dd, J = 12.4, 5.9 Hz, H-7), 4.62 (1H, d, J = 12.4 Hz, H-6a), 3.51 (2H, m, H-5), 3.16 (1H, m, H-4a or H-4b), 2.90 (1H, m, H-4 or H-4a), 2.83 (1H, s, H-13); ^{13}C

NMR (100 MHz, DMSO-d_6): δ_C 148.1 (C, C-2), 143.1 (C, C-1), 136.9 (C, C-7a), 128.4 (CH, C-9 or C-10), 128.1 (C, C-1b), 127.9 (CH, C-9 or C-10), 126.2 (CH, C-11), 124.2 (CH, C-8), 116.5 (C, C-1a), 115.1 (C, C-11a), 107.9 (CH, C-3), 101.5 (CH_2, C-12), 65.6 (CH, C-7), 62.5 (CH, C-6a), 49.5 (CH_2, C-5), 32.1 (CH_3, C-13), 21.3 (CH_2, C-4); LRESIMS *m/z* 295; HRESIMS *m/z* 295.12029 $[M+H]^+$ (calc'd for $C_{18}H_{17}NO_3$ 295.12084).

(+)-*N, N*-methylguatterine (4.33): Brown oil. $[\alpha]_D^{21}$: 6.17 (c 0.13, MeOH); UV (MeOH) λ_{max} (log ε): 242 (3.48), 279 (3.42); CD (MeOH) λ_{max} ($\Delta\varepsilon$) 239 nm (-162.82); ^1H NMR and ^{13}C NMR see Table 4.9.1; LRESIMS *m/z* 295; HRESIMS *m/z* 295.12029 $[M^+]$ (calc'd for $C_{18}H_{17}NO_3$ 295.12084).

Dehydrodiscretine (4.34): Yellow powder. UV (MeOH) λ_{max} (log ε): 289 (3.81), 242 (3.59), 340 (3.52), 378 (3.15); ^1H NMR (400 MHz, DMSO-d_6): δ_H 10.05 (1H, s, OH-3), 9.48 (1H, s, H-8), 8.79 (1H, s, H-13), 7.68 (1H, s, H-9), 7.65 (1H, s, H-9), 7.58 (1H, s, H-12), 6.84 (1H, s, H-4), 4.74 (2H, t, J = 6.4 Hz, H-6), 4.07 (3H, s, OMe-10), 4.00 (3H, s, OMe-11), 3.93 (3H, s, OMe-2), 3.22 (2H, m, H-5); ^{13}C NMR (100 MHz, DMSO-d_6): δ_C 157.3 (C, C-10), 152.0 (C, C-11), 150.0 (C, C-3), 147.7 (C, C-2), 138.7 (C, C-14), 136.6 (C, C-8a), 128.7 (C, C-4a), 121.8 (C, C-12a), 117.6 (C, C-14a), 117.5 (CH, C-13), 114.9 (CH, C-4), 109.2 (CH, C-1), 56.5 (CH_3, OMe-10), 56.2 (CH_3, OMe-11), 56.0 (CH_3, OMe-2), 54.6 (CH_2, C-6), 25.8 (CH_2, C-5); LRESIMS *m/z* 338; HRESIMS *m/z* 338.1394 $[M^+]$ (calc'd for $C_{18}H_{17}NO_3$ 338.1392).

Pseudopalmatine (4.35): Yellow powder. UV (MeOH) λ_{max} (log ε): 287 (4.02), 239 (3.75), 338 (3.65), 373 (3.24); ^{1}H NMR (400 MHz, DMSO-d_6): δ_H 9.52 (1H, s, H-8), 8.84 (1H, s, H-13), 7.71 (1H, s, H-9), 7.67 (1H, s, H-1), 7.60 (1H, s, H-12), 7.10 (1H, s, H-4), 4.78 (2H, t, J = 6.1 Hz, H-6), 4.07 (3H, s, OCH_3-10), 4.00 (3H, s, OMe-11), 3.93 (3H, s, OMe-3), 3.86 (3H, s, OMe-2), 3.21 (2H, t, J = 6.1 Hz, H-5); ^{13}C NMR (100 MHz, DMSO-d_6): δ_C 157.5 (C, C-10), 151.5 (C, C-11), 151.5 (C, C-2), 151.5 (C, C-3), 145.5 (C, C-H), 138.4 (C, C-14), 136.6 (C, C-8a), 128.6 (C, C-4a), 122.0 (C, C-12a), 117.9 (CH, C-13), 111.3 (C, C-4), 108.6 (CH, C-1), 106.5 (CH, C-9), 56.6 (CH_3, OMe-10), 56.3 (CH_3, OMe-11), 56.0 (CH_3, OMe-3), 55.8 (CH_3, OMe-2), 54.7 (CH_2, C-6), 26.0 (CH_2, C-5); LRESIMS *m/z* 353; HRESIMS *m/z* 352.1541 [M^+] (calc'd for $C_{21}H_{22}NO_4$ 352.1549).

4.16. References

(1) Voet D.; Voet J.G. In *Biochemistry*; 3 ed.; Wiley: New Jersey, 2004.

(2) Molinari M. *Cell Proliferation* **2000**, *33*, 261-274.

(3) Hwang A.; Muschel R.J. *Radiation Research* **1998**, *150*, S52-S59.

(4) Foijer F.; Riele H. te *Cell Cycle* **2006**, *5*, 831-836.

(5) Pientenpol J.A.; Steward Z.A. *Toxicology* **2002**, *181*, 475-481.

(6) Samuel T.; Weber H.O.; Funk J.O. *Cell Cycle* **2002**, *1*, 162-168.

(7) Greenblat M.S.; Bennet W.P.; Hollstein B.M.; Harris C.C. *Cancer Research* **1994**, *54*, 4855-4878.

(8) McIlwrath A.J.; Vasey P.A.; Ross G.M.; Brown R. *Cancer Research* **1994**, *53*, 3667-3699.

(9) Slichenmeyer W.J.; Nelson W.G.; Slebos R.J.; Kastan M.B. *Cancer Research* **1993**, *53*, 4164-4168.

(10) Roberge M.; Berlink R.G.; Xu L.; Anderson H.J.; Lim L.Y.; Curman D.; Stringer C.M.; Friend S.H.; Davies P.; Vincent I.; Haggarty S.J.; Kelly M.T.; Britton R.; Piers E.; Andersen R.J. *Cancer Research* **1998**, *58*, 5701-5706.

(11) Sarkaria J.N.; Tibbets R.S.; Busby E.C.; Kennedy A.P.; Hill D.E.; Abrahm R.T. *Cancer Research* **1998**, *58*, 4375-4382.

(12) Blasina A.; Weyer I. van de; Laus M.C.; McGowan C. *Current Biology* **1999**, *9*, 1-10.

(13) Tamaoki T. *Methods in Enzymology* **1991**, *201*, 340-347.

(14) Bunch R.T.; Eastman A. *Clinical Cancer Research* **1996**, *2*, 791-797.

(15) Busby E.C.; Leistritz D.F.; Abraham R.T.; Karnitz L.M.; Sarkaria J.N. *Cancer Research* **2000**, *60*, 2108-2112.

(16) Wilson W.H.; Sorbara L.; Figg W.D.; Mont E.K.; Sausville E.; Warren K.E.; Balis F.M.; Bauer K.; Raffeld M.; Senderowicz A.M.; Monks A. *Clinical Cancer Research* **2000**, *6*, 415-421.

(17) Jackson J.R.; Gilmartin A.; Imburgia C.; Winkler J.D.; Marshall L.A.; Roshak A. *Cancer Research* **2000**, *60*, 566-572.

(18) Hénon H.; Messaoudi S.; Anizon F.; Aboab B.; Kucharczyk N.; Léonce S.; Golsteyn R.M.; Pfeiffer B.; Prudhomme M. *European Journal of Pharmacology* **2007**, *554*, 106-112.

(19) Curman D.; Cinel B.; Williams D.E.; Rundle N.; Block W.D.; Goodarz A.A.; Hutchins J.R.; Clarke P.R.; Zhou B.B.; Lees-Miller S.P.; Andersen R.J.; Roberge M. *Journal of Biological Chemistry* **2001**, *276*, 17914-17919.

(20) Rundle N.T.; Xu L.; Andersen R.J.; Roberge M. *Journal of Biological Chemistry* **2001**, *276*, 48231-48326.

(21) Anderson H.J.; Andersen R.J.; Roberge M. *Progress in Cell Cycle Research* **2003**, *5*, 423-430.

(22) Bermejo A.; Figadere B.; Zafra-Polo M.C.; Barrachina I.; Estornell E.; Cortes D. *Natural Product Reports* **2005**, *22*, 269-303.

(23) Carollo C.A.; Siqueira J.M. de; Garcez W.S.; Diniz R.; Fernandes N.G. *Journal of Natural Products* **2006**, *69*.

(24) Matos M.F.C.; Leite L.I.S.P.; Brustolim D.; Siqueira J.M. de; Carollo C.A.; Hellmann A.R.; Pereira N.F.G.; Silva D.B. da *Fitoterapia* **2006**, *77*, 227–229.

(25) Tempone A.G.; Borborema S.E. Treiger; Jr. H.F. de Andrade; Gualda N.C. de Amorim; Yogi A.; Carvalho C. Salerno; Bachiega D.; Lupo F.N.; Bonotto S.V.; Fischer D.C.H. *Phytomedicine* **2005**, *12*, 382-390.

(26) Ramasamizafy S.; Hocquemiller R.; Cave A. *Journal of Natural Products* **1987**, *50*, 674-679.

(27) Gottlieb O.R.; Magalhaes A.F.; Maia J.G.S.; Marsioli A.J. *Phytochemistry* **1978**, *17*, 837-838.

(28) Costa E.V.; Piheiro M.L.B.; Xavier C.M.; Silva J.F.R.; Amaral A.C.F.; Souza A.D.L; Barison A.; Campos F.R.; Ferreira A.G.; Machado G.M.C.; Leon L.L.P. *Journal of Natural Products* **2006**, *69*, 292-294.

(29) Rahman M.M.; Lopa S.S.; Sadik G.; Rashid H.O.; Islam R.; Khondkar P.; Alam A.H.M.K.; Rashid M.A. *Fitoterapia* **2005**, *76*, 758-761.

(30) Montanha J.A.; Amoros M.; Boustie J.; Girre L. *Plant Medica* **1995**, *61*, 419-424.

(31) Perez E.; Saez J.; Blair S.; Franck X.; Figadere B. *Letters in Organic Chemistry* **2004**, *1*, 102-104.

(32) Debourges D.; Roblot F.; Hocquemiller R.; Cave A. *Journal of Natural Products* **1987**, *50*, 852-859.

(33) Hamonniere M.; Leboeuf M.; Cave A. *Phytochemistry* **1977**, *16*, 1029-1034.

(34) Shamma M.; Stephens R.L.; Wenkert E.; Leboeuf M.; Cave A.J. *Journal of Natural Products* **1979**, *42*, 437-439.

(35) Duah F.K.; Owusu P.D.; Slatkin D.J.; Schiff P.L. *Phytochemistry* **1983**, *22*, 321-322.

(36) Chen C.H.; Chen T.M.; Lee. C.J. *Journal of Pharmaceutical Sciences* **1980**, *69*, 1061-1065.

(37) Patra A.; Montgomery C.T.; Freyer A.J.; Guinaudeau H.; Shamma M.; Tantisewie B.; Pharidai K. *Phytochemistry* **1987**, *26*, 547-549.

(38) Marsaioli A.J.; Reis F.A.M.; Maglhaes A.F.; Ruveda E.A.; Kuck A.M. *Phytochemistry* **1979**, *18*.

(39) Jackman L.M.; Trewella J.C.; Moniot J.L.; Shamma M.; Stephens R.L.; Wenkert E. *Journal of Natural Products* **1979**, *42*, 437-449.

Chapter 5: Isolation of ligands for the Human Sex Hormone Binding Globulin

5.1. Preview of Chapter 5

Sex hormone-binding globulin (SHBG) is a protein that is vital in the transport of unbound steroids such as testosterone, estradiol, and 5α-dihydrotestoterone. Furthermore, SHBG also plays a role in regulating the concentration of these hormones in the blood.[1] Elevated SHBG levels are present in various disorders including anorexia, osteoporosis and hypogonadal men.[2] Many of these pathological conditions are associated with a lower plasma concentration of hormones. Ligands that bind to SHBG can release steroids into the blood, so these ligands can be viewed as potential drug candidates.[3] This chapter will deal with the isolation and structure elucidation of ligands for SHBG from the marine sponge *Myrmekioderma granulatum.*

5.2. Biology of the Sex-Hormone Binding Globulin Protein

The sex-hormone binding gobulin (SHBG) is a homodimeric glycoprotein primarily synthesized in the liver.[1] SHBG found in the testes is commonly referred to as the androgen binding protein (ABP).[2] Monomeric SHBG contains 373 amino acid residues and 3 carbohydrate side chains mainly composed of sialic acid and *N*-glucosamine.[4] SHBG strongly binds to planar steroids that have a 17β hydroxyl group through Van der Waals forces and polar attractions.

Several examples of steroids that bind to SHBG include estradiol, testosterone, and 5α-dihydrotestosterone.[5]

SHBG interacts with hormones and has a key role in regulating their distribution and biological function. It has been estimated that less than two percent of steroids circulate freely in the blood, with the remainder sequestered in SHBG.[4] Free steroids diffuse into the cells altering cellular function, so a role of SHBG is to regulate the concentration of unbound hormone in the plasma. SHBG may also directly transport steroids to the plasma membranes of some tissues to induce intracellular signaling pathways.[2] The ABP synthesized in the testes is subsequently taken to the epididymis where it is thought to aid in transporting androgens vital for sperm maturation.[5]

Various pathological conditions have higher levels of SHBG which results in a lower concentration of free steroids in the blood. Hypogonadal males have higher concentrations of SHBG which leads to decreased plasma testosterone levels. This results in testicular failure and defective gonadotropin secretion.[6] Other conditions with elevated SHBG levels include anorexia nervosa where low estradiol concentrations prevent women from ovulating.[7] Lower plasma concentrations of estradiol due to increased SHBG levels have also been associated with an increased rate of bone loss and osteoporosis.[8]

It is evident that ligands capable of binding to SHBG could release bound steroids into the bloodstream. Therefore, SHBG could represent an attractive drug target for conditions where a hormone insufficiency is present. The first potent ligand discovered was (-)-3,4-divanillyltetrahydrofuran (**5.1**),[3] which has an

IC_{50} of 2.6 μM. Other ligands developed include compounds **5.2** and **5.3**, which have IC_{50}'s of 13.6 and 1 μM, respectively.[9,10]

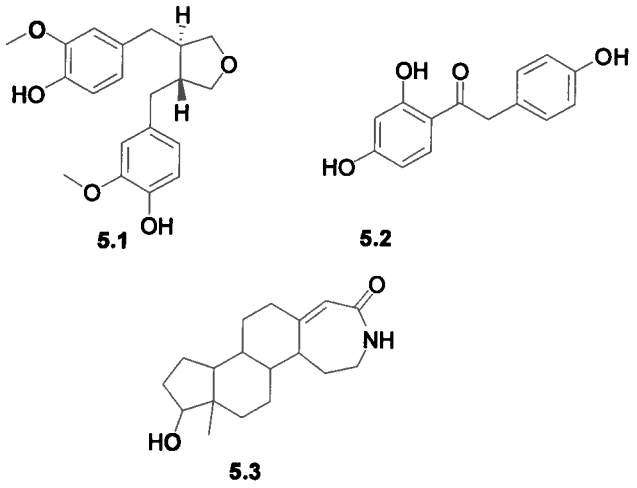

Figure 5.2.1. Several examples of ligands that bind to SHBG.

5.3. Compounds Isolated from the genus Myrmekioderma

Sponges in the genus *Myrmekioderma* (family Heteroxyidae) are distributed in the shallow oceans of the Indo-Pacific.[11] In 1992, the first secondary metabolites from a *Myrmekioderma* sp. were discovered when Faitorusso and co-workers isolated four oxygenated linear diterpenes from the sponge *M. styx.*[12] All four diterpenoids were active in the brine shrimp assay with styxenol (**5.4**) and **5.5** showing the most cytotoxicity (LC_{50}= 154 μg/mL and 3 μg/mL respectively). [12]

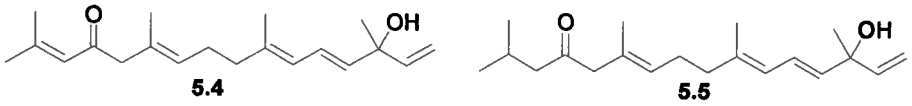

Figure 5.3.1. Linear diterpenes from *M. styx.*

The cyanthiwigin family of diterpenoids play a predominant role in the chemistry of the genus *Myrmekioderma*. Cyanthiwigin C (**5.6**) was the first of this

family of 5,6,7 tricarbocyclic diterpenoids to be isolated from the *Myrmekioderma*.[13] In 2002, Peng *et al.* reported the isolation of twenty-seven previously unreported cyanthiwigins from *M. styx*.[14] The most biologically active cyanthiwigins isolated from this study include the cytotoxins cyanthiwigin D (**5.7**) and cyanthiwigin F (**5.8**), which had IC_{50}'s of 5 μg/mL and 3 μg/mL, respectively, against human primary tumor cells.[14] In 2003, Hamann and co-workers isolated several unreported diterpenoids of the cyanthiwigin class from *M. styx*.[15] Cyanthiwigin AC (**5.9**) was found to contain a six-membered spiro ring rather than a seven-membered ring, while cyanthiwigin AD (**5.10**) was found to have a 5,6,6 tricarbocyclic structure rather than the 5,6,7 tricarbocyclic ring formation. No biological screening was done on these compounds due to the very small quantities that were isolated from the sponge.[15]

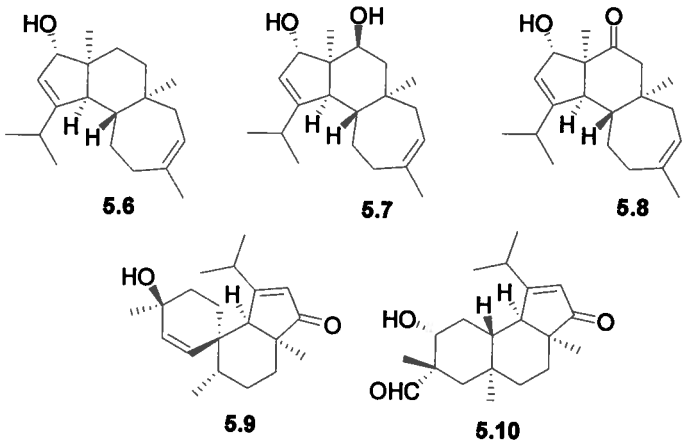

Figure 5.3.2. Cyanthiwigins isolated from *Myrmekioderma* sp..

Several bisabolane sesquiterpenes have been isolated from sponges of the genus *Myrmekioderma*. The bisabolanes (+)-curcuphenol (**5.11**) and (+)-curcudiol (**5.12**) were isolated from *M. dendyi*, and were found to have antifouling activity against the cypris larvae of the barnacle *Balanus amphitrite* with EC_{50}'s of

2.5 and 2.8 μg/mL, respectively.[16] Compounds (**5.13**), (**5.14**) and (**5.15**) are three biologically inactive bisabolane sesquiterpenes that were first isolated from *M. dendyi.*[17] Styxone A (**5.16**) and B (**5.17**) are other biologically inactive sesquiterpenes that were first discovered from *M. styx.*[18]

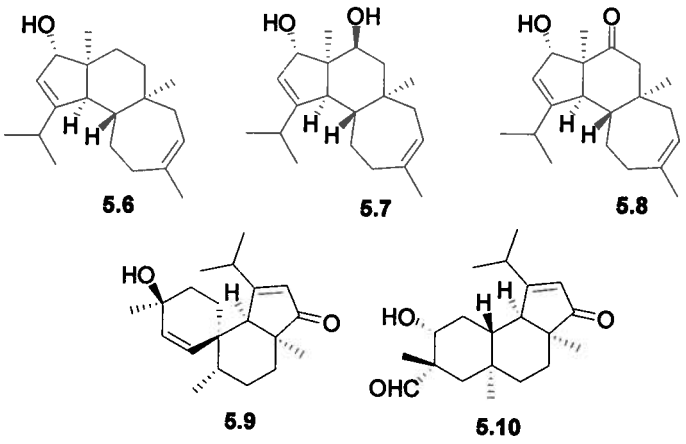

Figure 5.3.3. Sesquiterpenoids isolated from *Myrmekioderma* sp..

Other biologically active natural products that have been discovered from *Myremekioderma* are myrmekiosides A (**5.18**) and B (**5.19**).[19] These glycolipids have been found to alter the tumor cell morphology of H-Ras transformed NIH2T3 fibroblasts at 5 μg/mL. Furthermore, myrmekioside A has also been found to prevent NIH2T3 cells from entering the S-phase of the cell cycle. Compounds **5.20** and **5.21** are similar glycolipids, and were isolated from *Myrmekioderma* by Letourneux *et al..*[17]

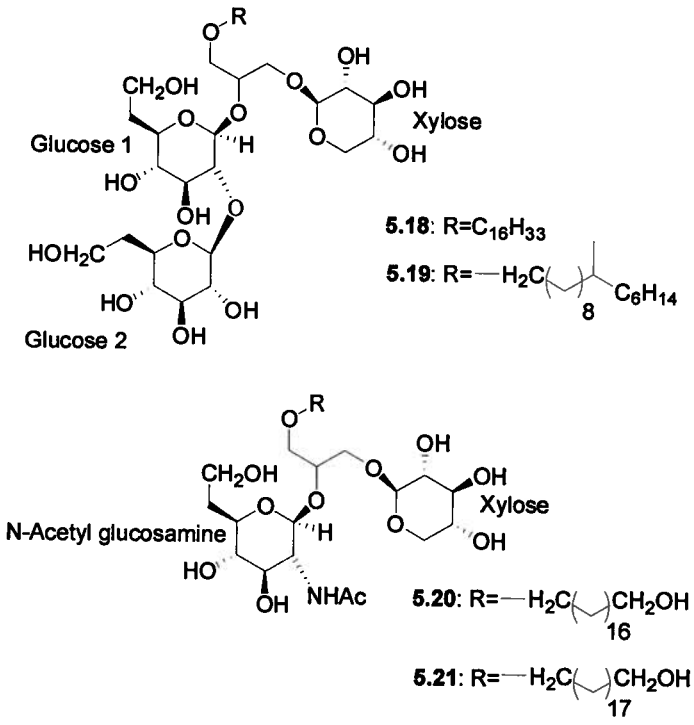

Figure 5.3.4. Glycolipids isolated from *Myrmekioderma* sp..

5.4. Isolation of bisabolane sesquiterpenes and myrmekioside C

A MeOH extract of the *Myrmekioderma granulatum* collected in Indonesia was subjected to flash reversed-phase column chromatography to yield two biologically active fractions. The more active fraction was subjected to reversed-phase HPLC to obtain **5.22**,[20] abolene (**5.23** mg) as a diastereotopic mixture,[20] (+)-curcudiol (**5.24**),[21] and abolenone (**5.25** mg). Biological studies revealed (+)-curcudiol (**5.24**) to be a ligand of SHBG. The less active fraction was purified using reversed-phase HPLC to yield (+)-curcuphenol (**5.26**),[21] and myrmekioside C (**5.27**). The structures of (+)-curcudiol (**5.24**),[21] abolene (**5.23**),[20] and (+)-curcuphenol (**5.26**)[21] were confirmed by comparing the optical rotation, NMR and the MS data to the literature values. The optical rotation of sesquiterpenoid **5.22**

is opposite in sign to the literature values, thus a new enantiomer was isolated.[20] For full experimental details, see Section 5.8.

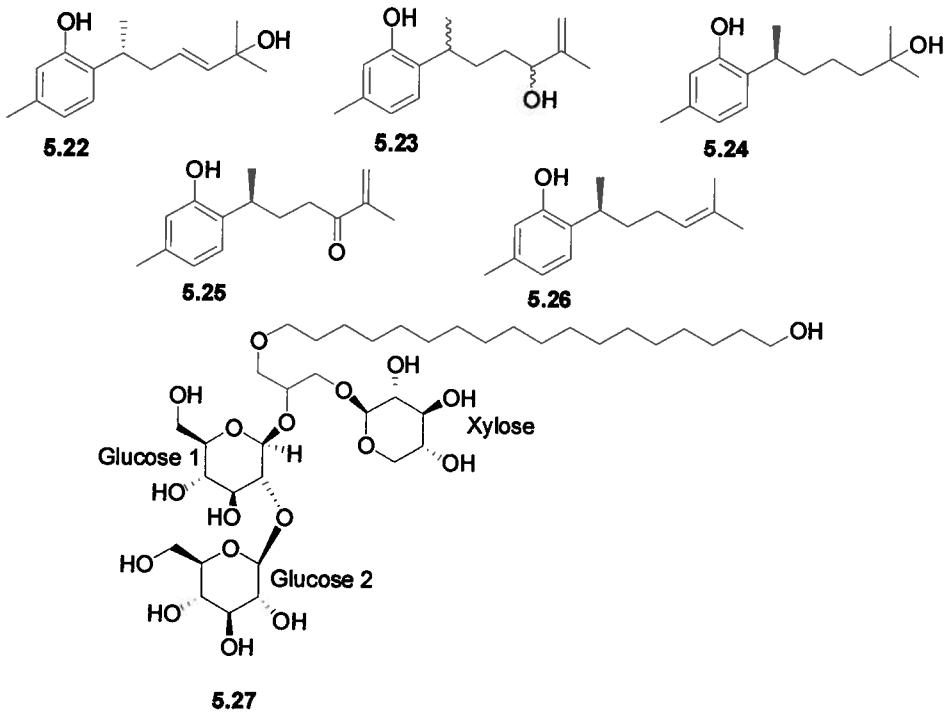

Figure 5.4.1. Compounds isolated from *Myrmekioderma styx*.

5.5. Structure Elucidation of Abolenone

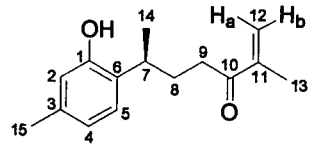

Figure 5.5.1: Abolenone.

Abolenone (**5.25**, figure 5.5.1) was isolated as an optically active yellow oil that gave a $[M+Na]^+$ ion at *m/z* 255.1360 in the HRESI-TOF, corresponding to a molecular formula of $C_{15}H_{20}O_2$ and requiring six degrees of unsaturation. 1D and 2D NMR experiments were run in both DMSO-d_6 and in C_6D_6. The best

dispersion in the ^{1}H NMR spectrum was found in C_6D_6 (Figure 5.5.3). The proton NMR revealed three aromatic proton resonances (δ_H 7.01, 6.72, δ_H 6.67), an exchangeable proton (δ_H 6.63), two olefinic protons (δ_H 5.36 and 5.16), and three methyl proton resonances (δ_H 2.14 and 1.68).

Analysis of the ^{13}C NMR spectrum (Figure 5.5.4), and the HMQC data (Figure 5.5.5) revealed four methines (δ_C 125.5, 120.6, 116.8 and 30.4), three methylenes (δ_C 124.5, 33.9 and 31.9), three methyls (δ_C 20.3, 18.7, 17.5), and four quaternary carbons (δ_C 202.4, 143.8, 136.4, 128.6). After using the HMQC data to assign proton resonances to their respective carbon atoms (Table 5.5.1), it was possible to deduce three substructures (I, II, II, Figure 5.5.2) from the HMBC (Figure 5.5.6) and COSY data (Figure 5.5.7).

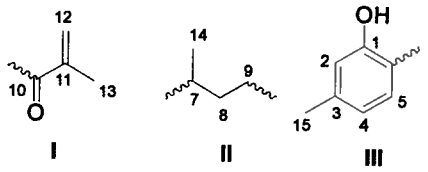

Figure 5.5.2. Substructures of abolenone as deduced from the HMBC and the COSY data.

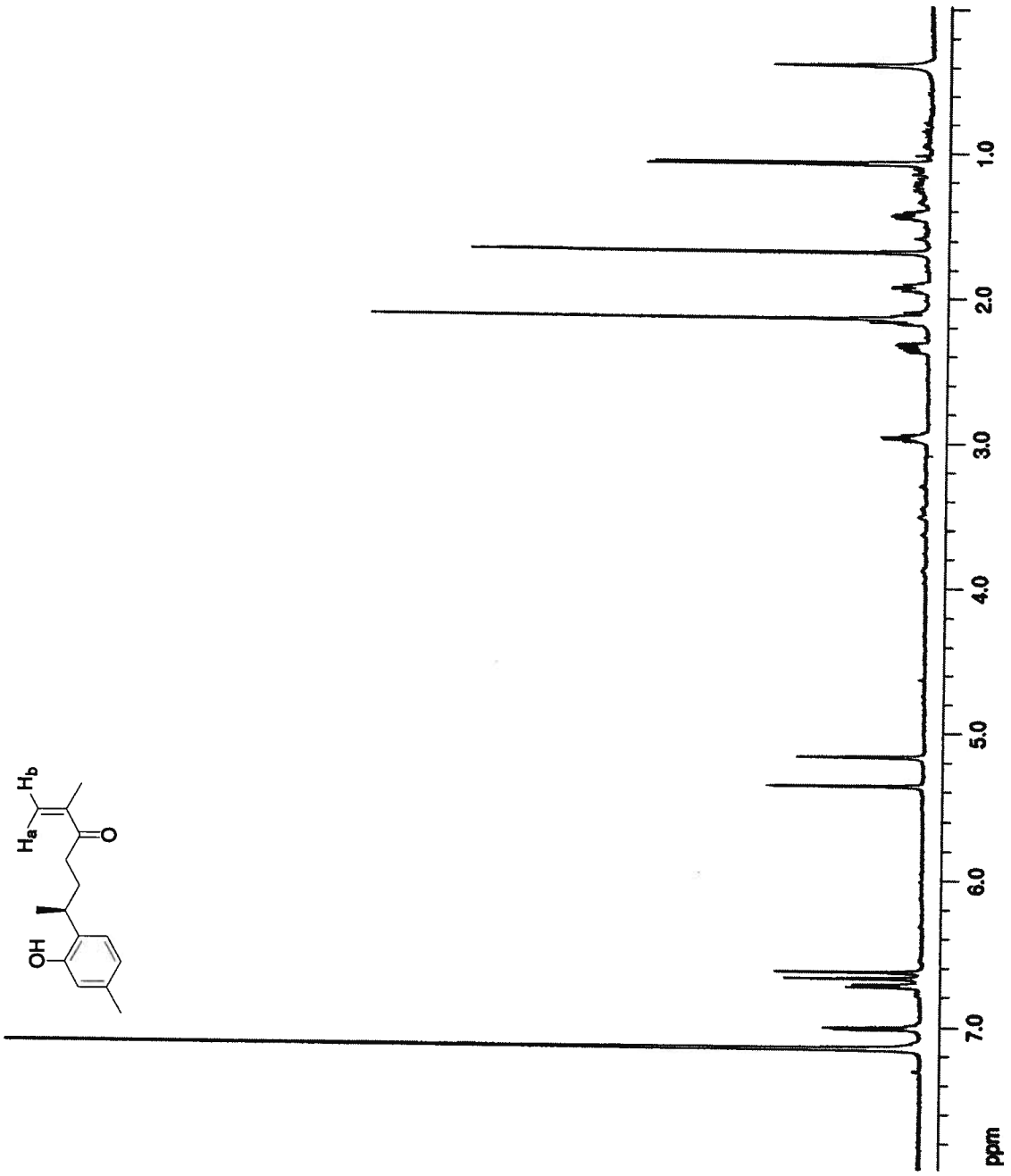

Figure 5.5.3. ^{1}H NMR spectrum of abolenone (**5.25**) at 600 MHz in C_6D_6.

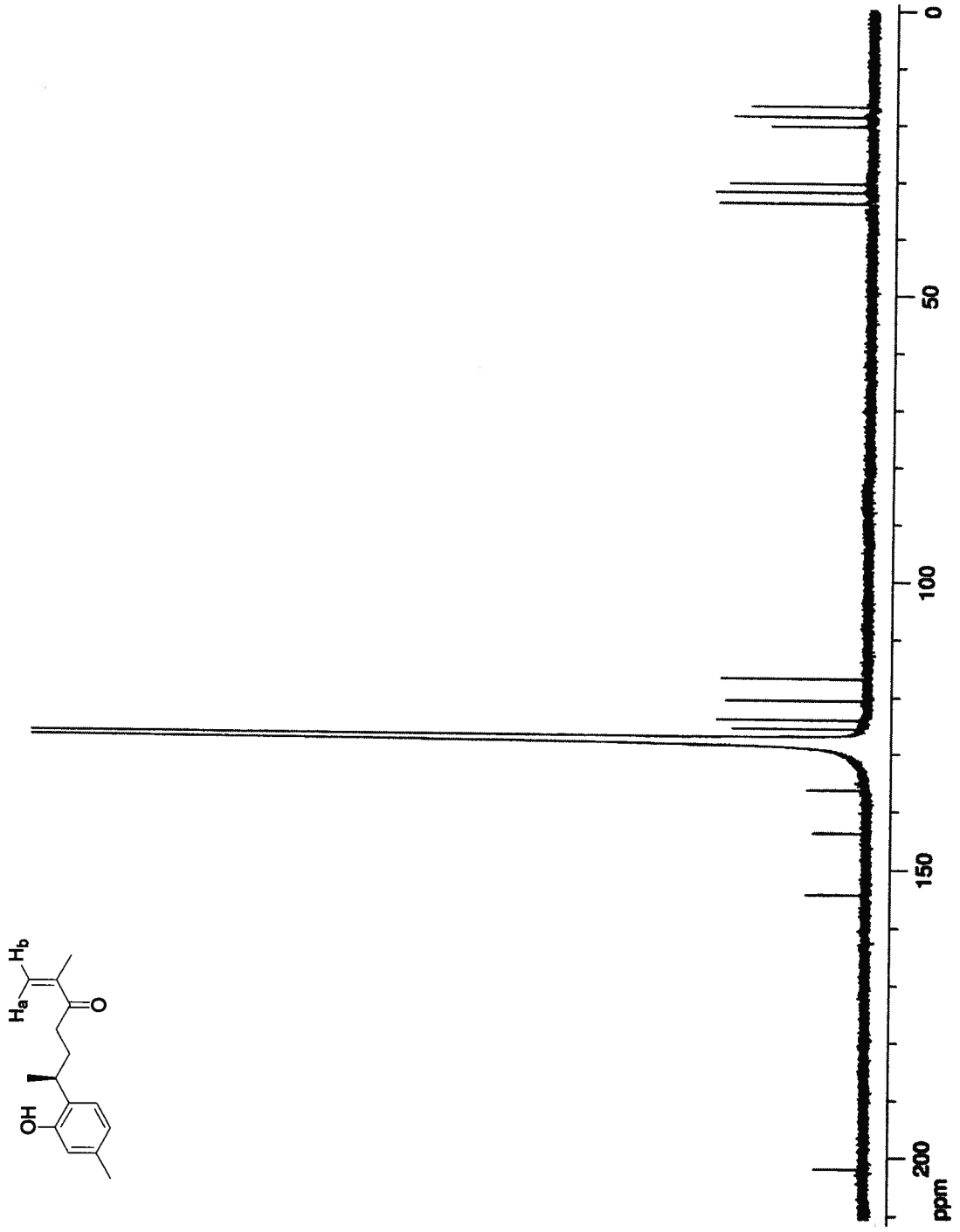

Figure 5.5.4. ^{13}C NMR spectrum of abolenone (**5.25**) at 150 MHz in C_6D_6.

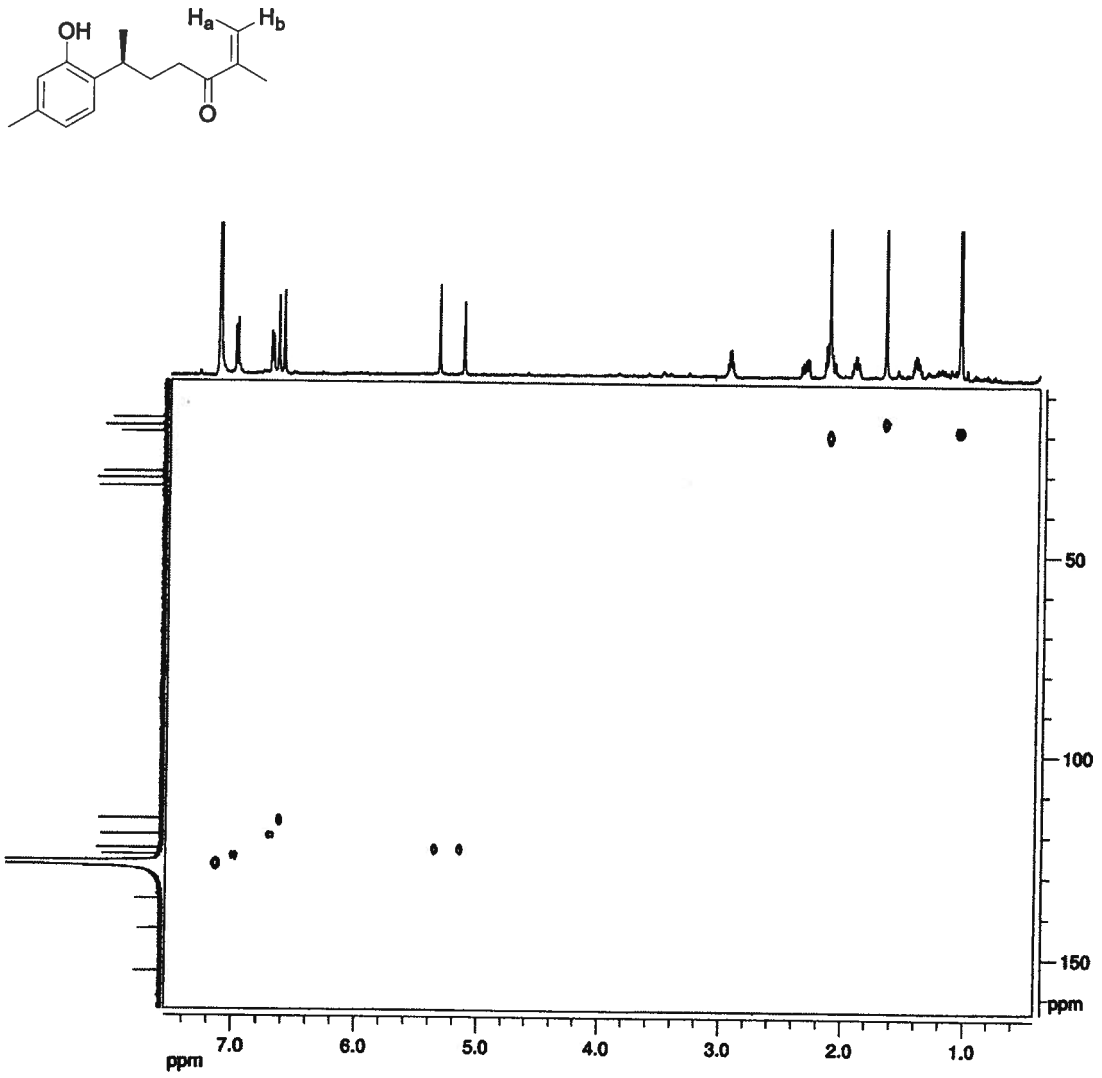

Figure 5.5.5. HMQC spectrum of abolenone (**5.25**) at 600 MHz in C_6D_6.

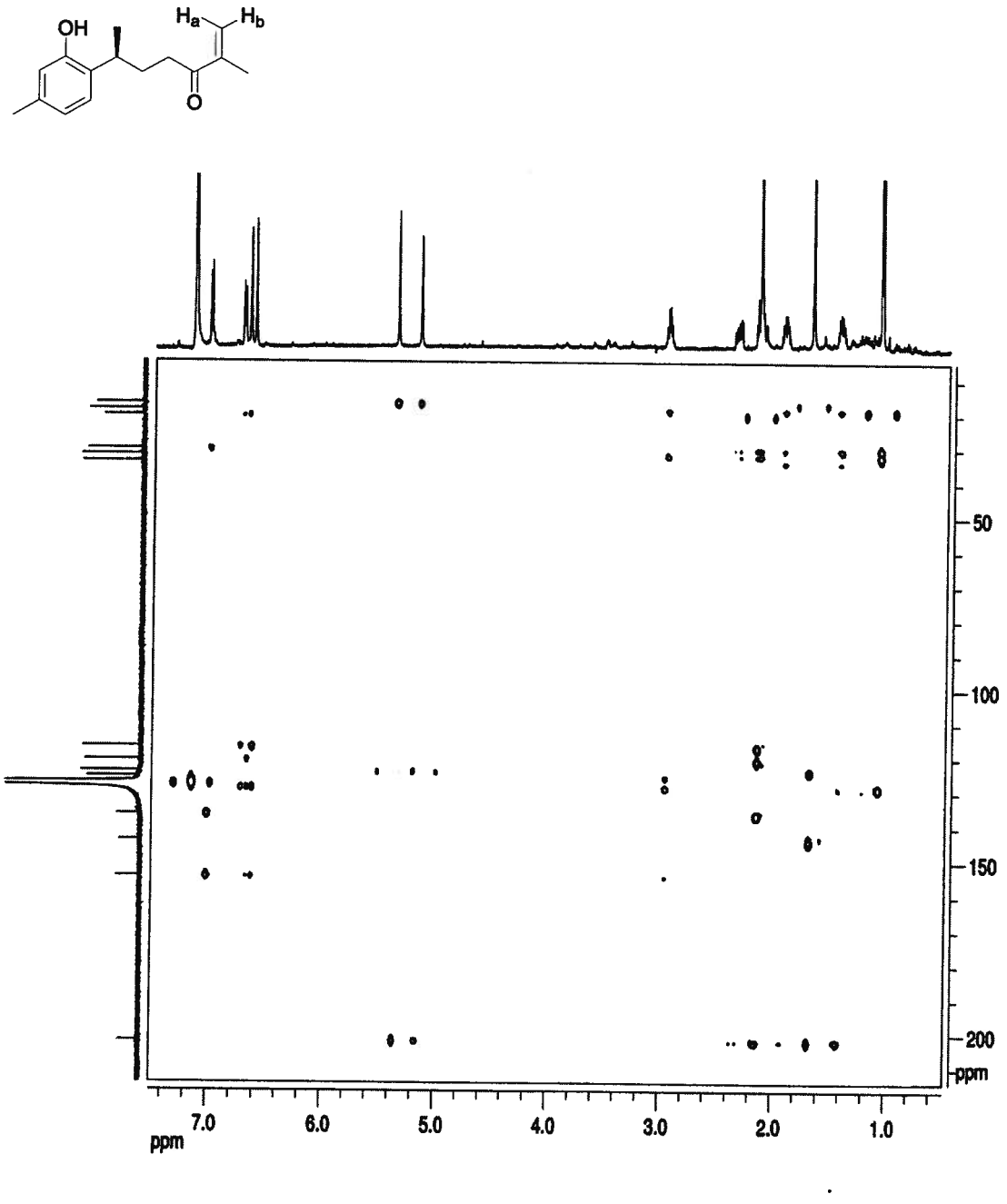

Figure 5.5.6. HMBC spectrum of abolenone (**5.25**) at 600 MHz in C_6D_6.

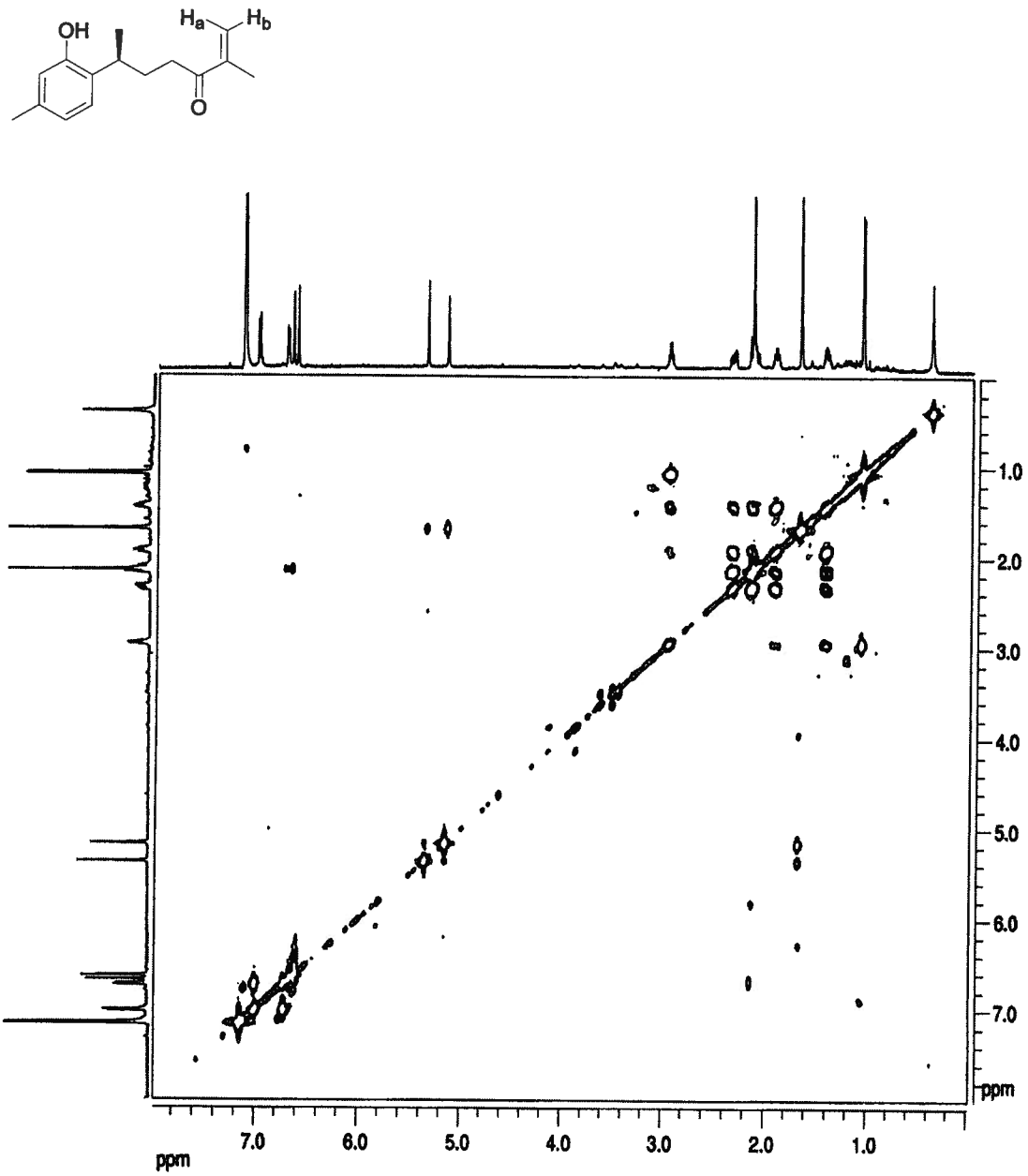

Figure 5.5.7. COSY spectrum of abolenone (**5.25**) at 600 MHz in C_6D_6.

Table 5.5.1. 1D and 2D NMR data of abolenone (**5.25**).[a]

Position	δ_C	δ_H (*J* in Hz)	HMBC	COSY
1	154.9			
2	116.8	6.67, s	C-1, C-6, C-4, C-15	H-15
3	136.4			
4	120.6	6.72, d, (8.0)	C-2, C-4, C-6, C-15	H-5
5	125.5	7.01, d, (8.0)	C-1, C-3, C-7	H-4
6	128.6			
7	30.4	2.95, m	C-1, C-5, C-6, C-8, C-9, C-14	H-8a, H-8b, H-14
8a[b]	31.9	1.92, m	C-6, C-7, C-9, C-10, C-14	H-7, H-8b, H-9a, H-9b
8b[b]		1.43, m	C-6, C-7, C-9, C-10, C-14	H-7, H-8a, H-9a, H-9b
9a[c]	33.9	2.34, m	C-7, C-8, C-10	H8a, H8b, H9b
9b[c]		2.14, m	C-7, C-8, C-10	H8a, H8b, H9a
10	202.4			
11	143.8			
12a[d]	124.6	5.36, s	C-10, C-13	H-12b, H-13
12b[d]		5.16, s	C-10, C-13	H-12a, H-13
13	17.5	1.68, s	C-10, C-11, C-12	H-12a, H-12b
14	18.7	1.07, d, (6.8)	C-6, C-7, C-8	H-7
15	20.4	2.14, s	C-2, C-3, C-4	H-2
1-OH		6.63, s	C-1, C-2, C-6	

[a]: ^1H and ^{13}C chemical shifts (ppm) are referenced to the C_6D_6 (δ_H 7.15 ppm and δ_C 128 ppm)
[b]: H-8a and H-8b are interchangeable signals
[c]: H-9a and H-9b are interchangeable signals
[d]: H-12a and H-12b are interchangeable signals

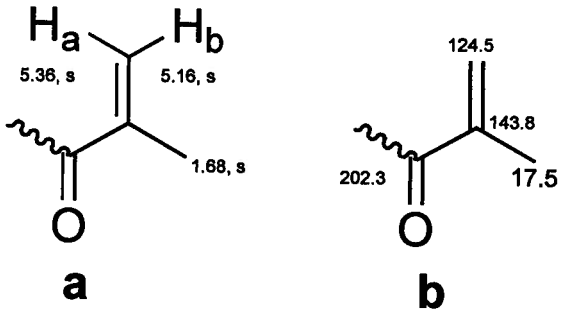

Figure 5.5.8. (**a**)^{1}H and (**b**)^{13}C chemical shifts of substructure **I** of abolenone (**5.24**).

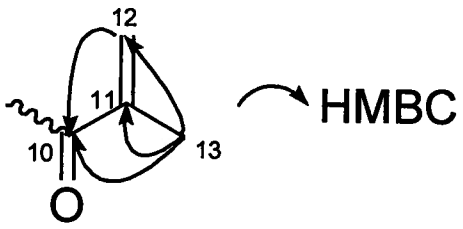

Figure 5.5.9. Key HMBC correlations of substructure **I** of abolenone (**5.25**).

Both proton resonances at δ_H 5.36 (H-12a) and δ_H 5.16 (H-12b) showed identical HMQC correlations to the carbon resonance at δ_C 124.5 (C-12), thus establishing the presence of an olefenic methylene. The methyl singlet proton resonance at δ_H 1.68 (H-13: HMQC to δ_C 17.5) showed HMBC correlations to the carbon resonance at δ_C 143.8 (C-11), which established that Me-13 was connected to C-11 (Figures 5.5.9 and 5.5.10). Further HMBC cross-peaks were observed between the proton resonance at δ_H 1.68 (H-13) and the carbon resonance at δ_C 124.5 (C-12) (Figures 5.5.9 and 5.5.10). The methylene proton resonances at δ_H 5.36 (H-12a) and δ_H 5.16 (H-12b) showed HMBC correlations to the methyl carbon resonance at δ_C 17.5 (C-13), which established that a methyl group was adjacent to an olefenic methylene. Finally, the proton resonances at δ_H 5.36 (H-12a), δ_H 5.16 (H-12b) and δ_H 1.68 (H-13) all showed HMBC

correlations to the carbonyl resonance at δ_C 202.4 (C-10). This established the presence of an α, β-unsaturated ketone shown as substructure **I** (Figures 5.5.8 and 5.5.9).

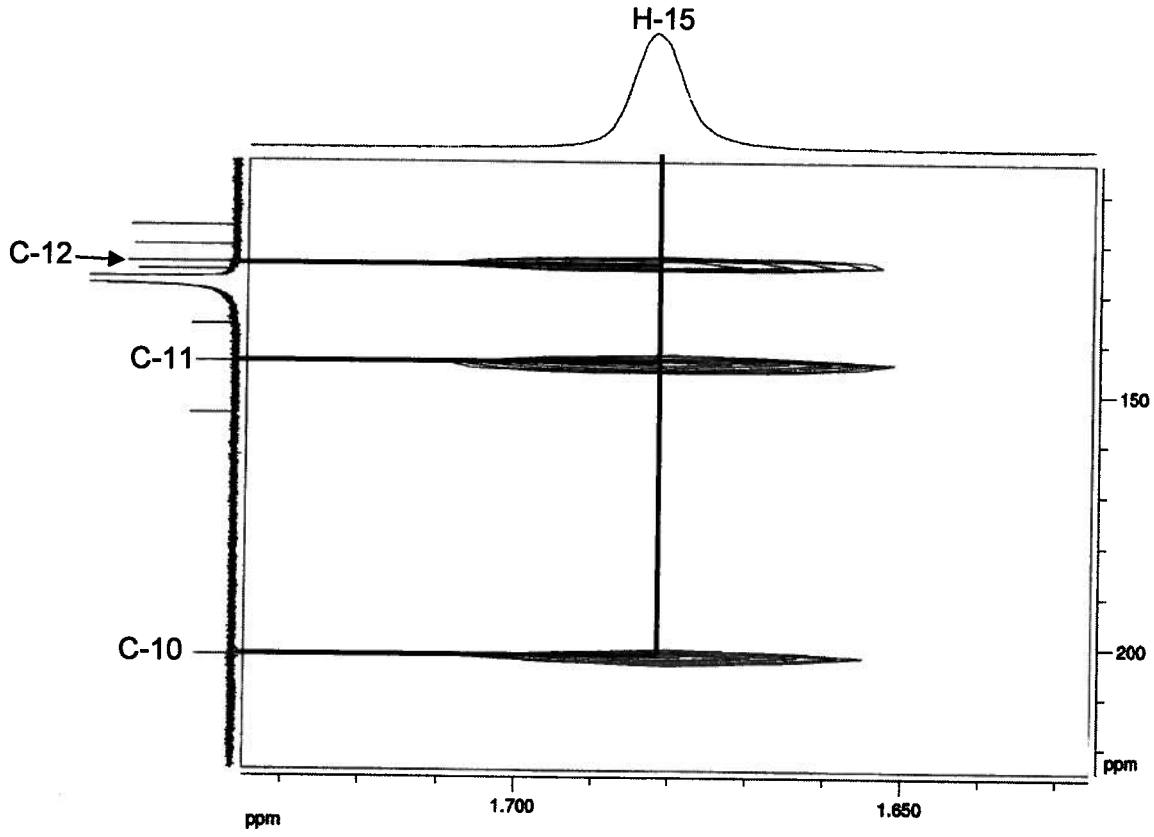

Figure 5.5.10. HMBC correlations for H-15 of substructure **I** of abolenone (**5.25**).

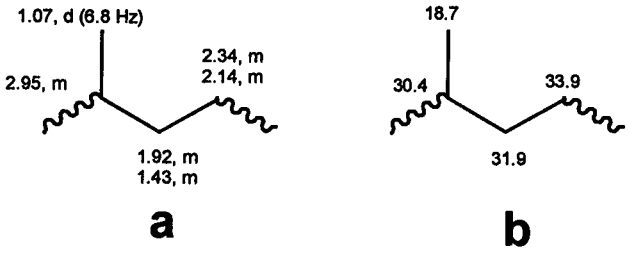

Figure 5.5.11. (**a**)^{1}H and (**b**)^{13}C chemical shifts of substructure **II** of abolenone (**5.25**).

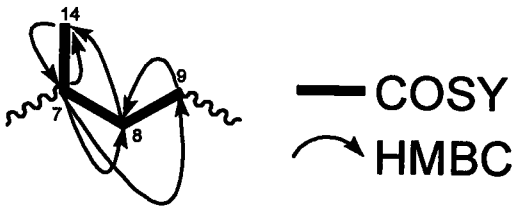

Figure 5.5.12. Key HMBC correlations of substructure **II** of abolenone (**5.25**).

The methyl proton resonance at δ_H 1.07 (H-14: HMQC to δ_C 18.7) showed a COSY correlation to the methine proton resonance at δ_H 2.95 (H-7: HMQC to δ_C 30.3) which linked C-14 (δ_C 18.7) to C-7 (δ_C 30.3). Additional COSY correlations were present between the proton resonance at δ_H 2.95 (H-7) and the two methylene proton resonances at δ_H 1.92 (H-8a: HMQC to δ_C 31.9) and δ_H 1.43 (H-8b: HMQC to δ_C 31.9), which indicated the connectivity between C-7 (δ_C 30.3) and C-8 (δ_C 31.9). Finally, the methylene C-8 (δ_C 31.9) was linked to methylene C-9 (δ_C 33.9) due to COSY correlations between H-8a/H-8b (δ_H 1.92 and 1.43, respectively) and H-9a/H-9b (δ_H 2.34 and 2.14, respectively) (Figure 5.5.13). These connections were supported by the HMBC data (Figure 5.5.12), and the above data is consistent with substructure **II** (Figure 5.5.11 and 5.5.12).

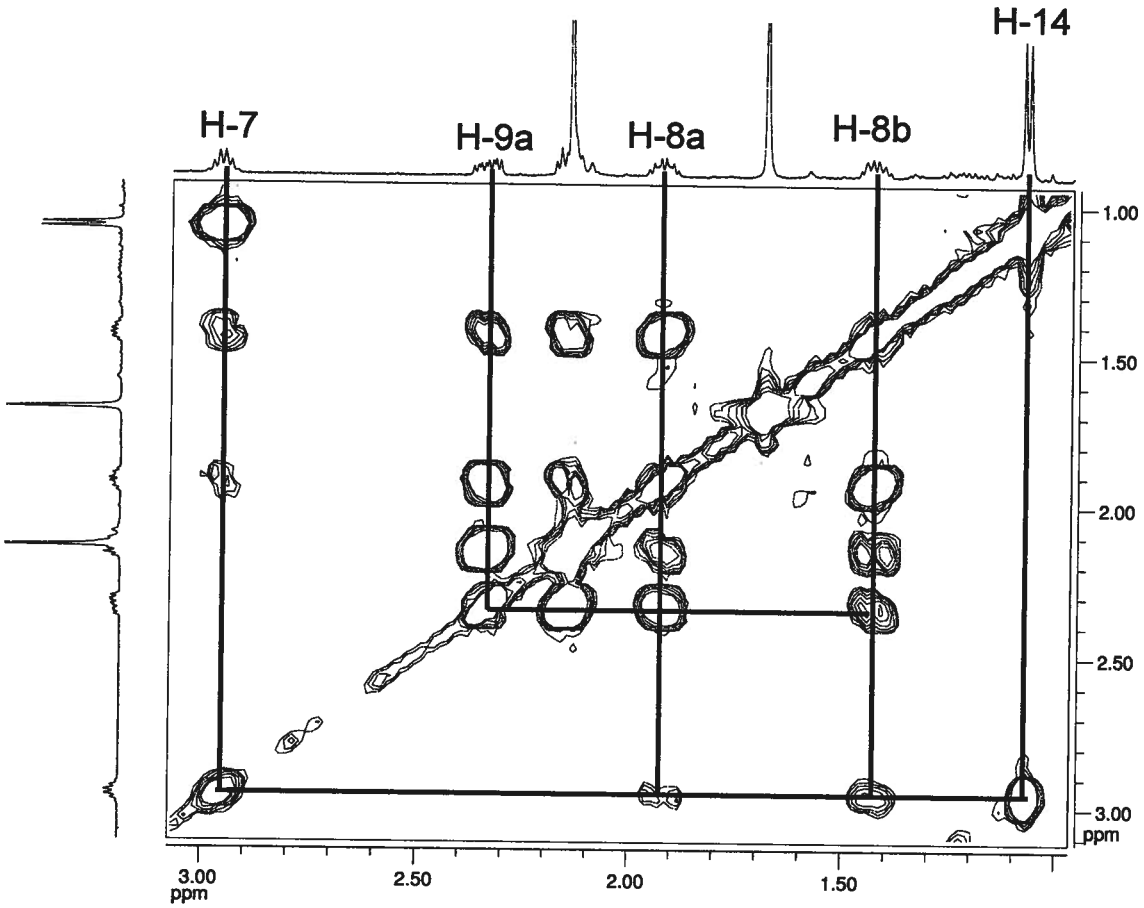

Figure 5.5.13. COSY expansion for substructure **II** of abolenone (**5.25**).

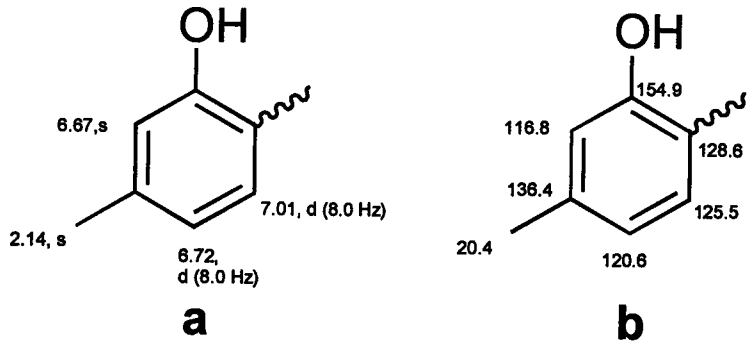

Figure 5.5.14. (**a**)^{1}H and (**b**)^{13}C chemical shifts of substructure **III** of abolenone (**5.25**).

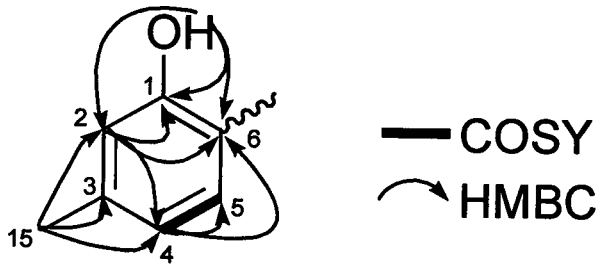

Figure 5.5.15. Key HMBC correlations of substructure **III** of abolenone (**5.25**).

The proton resonance at δ_H 6.63 (1-OH) did not show any HMQC correlations and was assigned as an exchangeable alcohol proton. HMBC correlations were present between the exchangeable proton resonance at δ_H 6.63 (1-OH) and the aromatic carbon resonance at δ_C 154.9 (C-1). This established that C-1 (δ_C 154.9) contained an alcohol moiety and its chemical shift was typical for an oxygenated aromatic carbon. Additional HMBC correlations were present between the proton resonance at δ_H 6.63 (1-OH) and the quaternary aromatic carbon resonance at δ_C 128.6 (C-6), which established the connectivity between C-1 (δ_C 154.9) and C-6 (δ_C 128.6) (Figure 5.5.17). HMBC cross-peaks were also observed between the proton resonance at δ_H 6.63 (1-OH) and the aromatic methine carbon at δ_C 116.9 (C-2). The HMBC correlations between the aromatic methine proton at δ_H 6.67 (H-2: HMQC to δ_C 116.9) and the oxygenated carbon resonance at δ_C 154.9 (C-1) determined the linkage between C-1 (δ_C 154.9) and C-2 (δ_C 116.9) (Figures 5.5.15 and 5.5.17). A methyl proton resonance at δ_H 2.14 (H-15: HMQC to δ_C 20.3) had an HMBC correlation to the aromatic carbon resonance at δ_C 116.9 (C-2). Cross-peaks in the HMBC between δ_H 6.67 (H-2) and δ_C 20.3 (C-15) established that Me-15 was ortho to an

aromatic methine proton (H-2). An aromatic methine proton at δ_H 6.72 (H-4: HMQC to δ_C 120.6) contained HMBC cross-peaks to the methyl carbon resonance at δ_C 20.3 (C-15). Additonal HMBC couplings between the proton resonance at δ_H 2.14 (H-15) and the carbon resonance at δ_C 120.6 (C-4) established that Me-15 was ortho to an additional aromatic methine proton (H-4) (Figure 5.5.17). The linkage between C-4 (δ_C 120.6) and C-5 (δ_C 125.5) was established from observation of a COSY correlation between the proton resonance at δ_H 6.72 (H-4), and the aromatic methine proton resonance at δ_H 7.01 (H-5: HMQC to δ_C 125.5) (Figure 5.5.16). Finally, a three bond HMBC correlation was observed between the proton resonance at δ_H 7.01 (H-5) and the carbon resonance at δ_C 154.9 (C-1), which showed that C-5 (δ_C 125.5) and C-6 (δ_C 128.6) were connected. The above data is consistent with a 1, 2, 4 trisubstituted aromatic ring shown as substructure **III** (Figures 5.5.14 and 5.5.15).

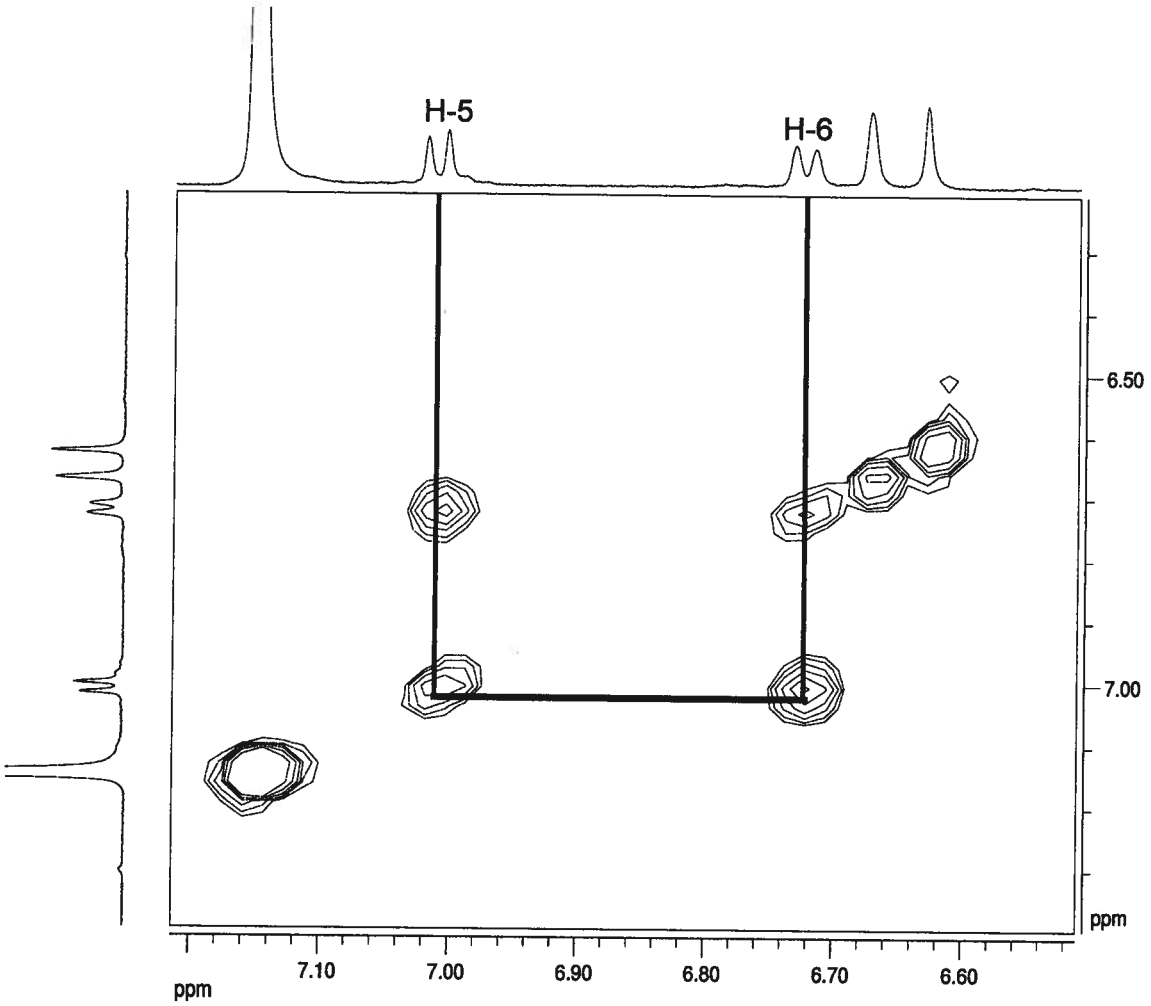

Figure 5.5.16. COSY expansion for substructure **III** of abolenone (**5.25**).

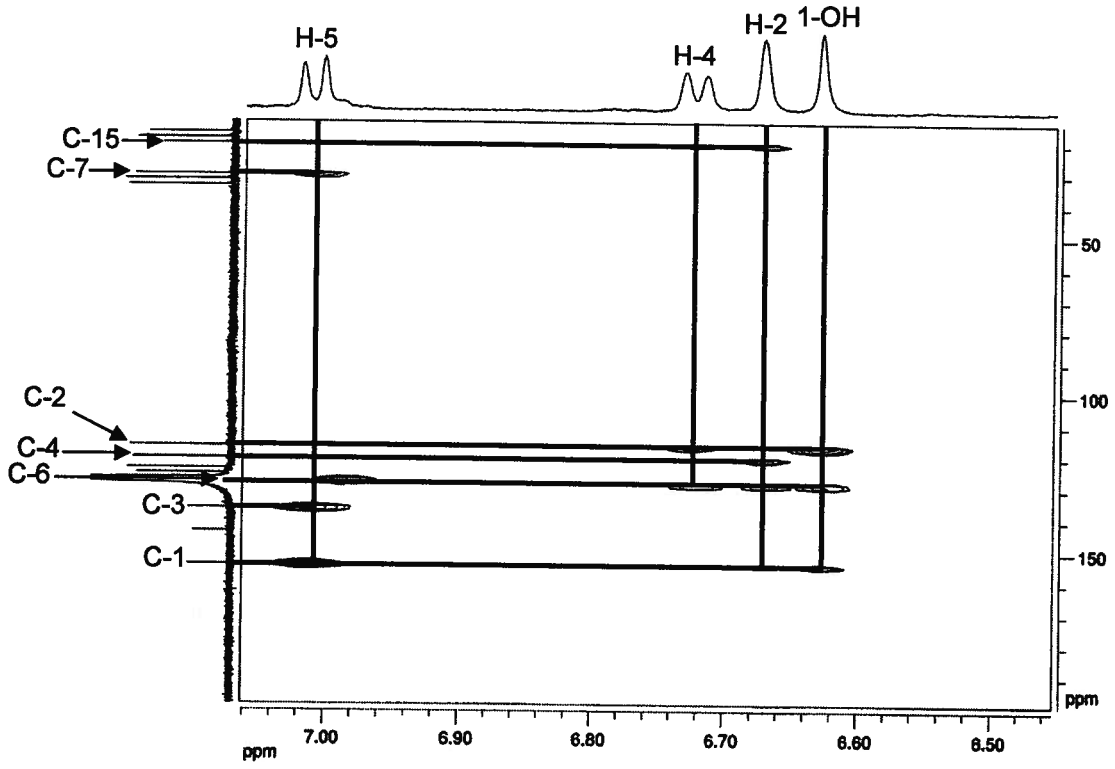

Figure 5.5.17. HMBC expansion for substructure **III** of abolenone (**5.25**).

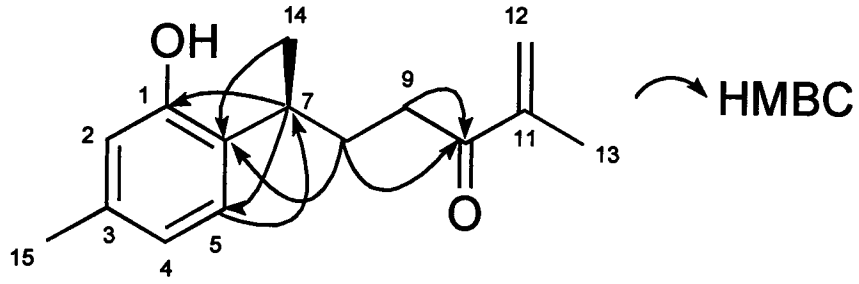

Figure 5.5.18. Key HMBC correlations of substructure of abolenone (**5.25**).

The methylene protons H-8a/H-8b and H-9a/H-9b all showed HMBC correlations to a carbonyl resonance at δ_C 202.4 (C-10), which established the connectivity between C-9 (δ_C 33.9) and C-10 (δ_C 202.4). Observation of the chemical shifts of H-9a (δ_H 2.32) and H-9b (δ_H 2.14) is consistent with this

assignment, therefore, C-9 (δ_C 33.9) is linked to substructure **I** (Figure 5.5.18). The aromatic methine proton H-5 (δ_H 7.01) had HMBC correlations to the methine carbon C-7 (δ_C 30.4). Additional HMBC correlations were observed between the methine proton resonance H-7 (δ_H 2.95, m) and the aromatic carbon resonances C-1 (δ_C 154.9), C-5 (δ_C 125.5) and C-6 (δ_C 128.6). This established the link between the trisubstituted benzene (substructure **III**) to the alkyl chain at C-7, which was further supported by key HMBC correlations (Figure 5.5.18). The CD spectra of both (+)-curcuphenol (**5.26**) and (+)-abolenone (**5.25**) were similar, which established that both molecules had identical 7S configurations (Figure 5.5.19).

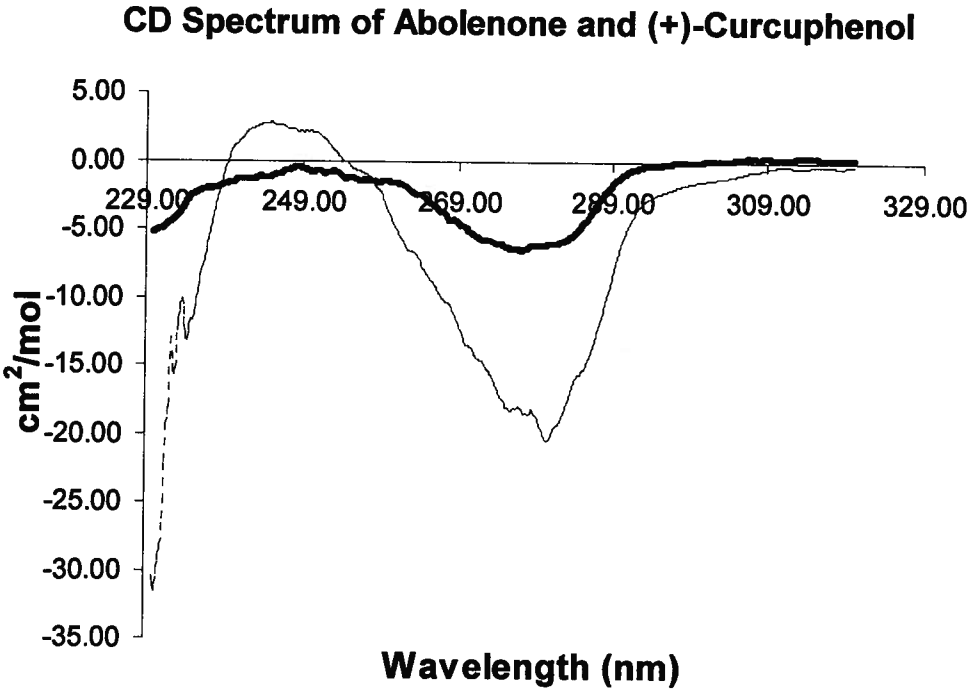

Figure 5.5.19. CD spectrum of curcuphenol (dashed line) and abolene (solid line).

5.6. Structure Elucidation of Myrmekioside C peracetate

Myrmekioside C (**5.27**, figure 5.4.1) was isolated as an optically active yellow oil that gave a $[M+H]^+$ ion at *m/z* 815.4640 in the HRESI-TOF mass spectrum, corresponding to a molecular formula of $C_{38}H_{72}O_{18}$ and requiring three degrees of unsaturation. The LRESIMS in MeOH gave a molecular ion peak at *m/z* 839.9, while the same experiment using MeOD afforded a molecular ion peak at *m/z* 850.8, thus establishing eleven exchangeable protons in the molecule. The ^1H NMR signals were poorly dispersed in DMSO-d_6 (Figure 5.6.2), so acetylation of myrmekioside C (for acetylation procedure see section 5.9) was performed to yield myrmekioside C peracetate (**5.28**, Figure 5.6.1). The ^1H NMR resonances of **5.28** were well dispersed in C_6D_6 and therefore all the NMR data was obtained with this solvent.

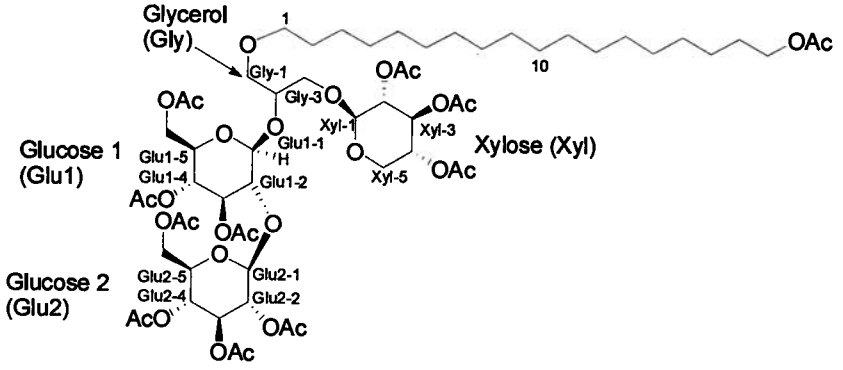

5.28

Figure 5.6.1: Myrmekioside C peracetate (**5.28**).

Myrmekioside C peracetate (**5.28**, figure 5.6.1) was obtained as an optically active yellow oil that gave a $[M+H]^+$ ion at *m/z* 1301.774 in the HRESI-TOF mass spectrum, corresponding to a molecular formula of $C_{60}H_{94}O_{29}$ and requiring 14 degrees of unsaturation. The increase in mass was suitable for the

addition of eleven acetate groups, consistent with the eleven exchangeable proton resonances noted for myremkioside C. The ^{1}H NMR spectrum (Figure 5.6.3) contained signals from δ_H 0.9 and 1.8 consistent with the presence of aliphatic methylenes. A series of acetate methyl proton resonances were found between δ_H 1.6 and 2.0. The ^{1}H NMR spectrum also revealed peaks from δ_H 3.3 to 5.5 which is suitable for protons attached to oxygenated sp^3 carbons. Observation of the ^{13}C (Figure 5.6.4), DEPT (Figure 5.6.5) and the HMQC (Figure 5.5.6) spectra confirmed the presence of 11 carbonyls (δ_C169-170), three anomeric carbons (δ_C 101.4, 101.5, 100.9), twenty carbons attached to oxygen atoms (δ_C 61.7-79.0) and a series of acetate methyls and aliphatic methylenes (δ_c 20.1-30.5). After the assignment of the proton resonances was done using the HMQC data (Table 5.6.1), five substructures of myrmekioside C (Figure 5.6.9) were deduced using the HMBC and COSY spectra (Figures 5.6.7 and 5.6.8).

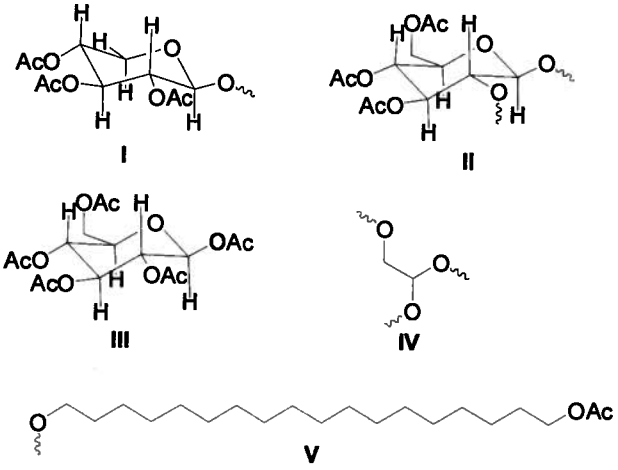

Figure 5.6.2. Five substructures of myrmekioside C peracetate (**5.28**).

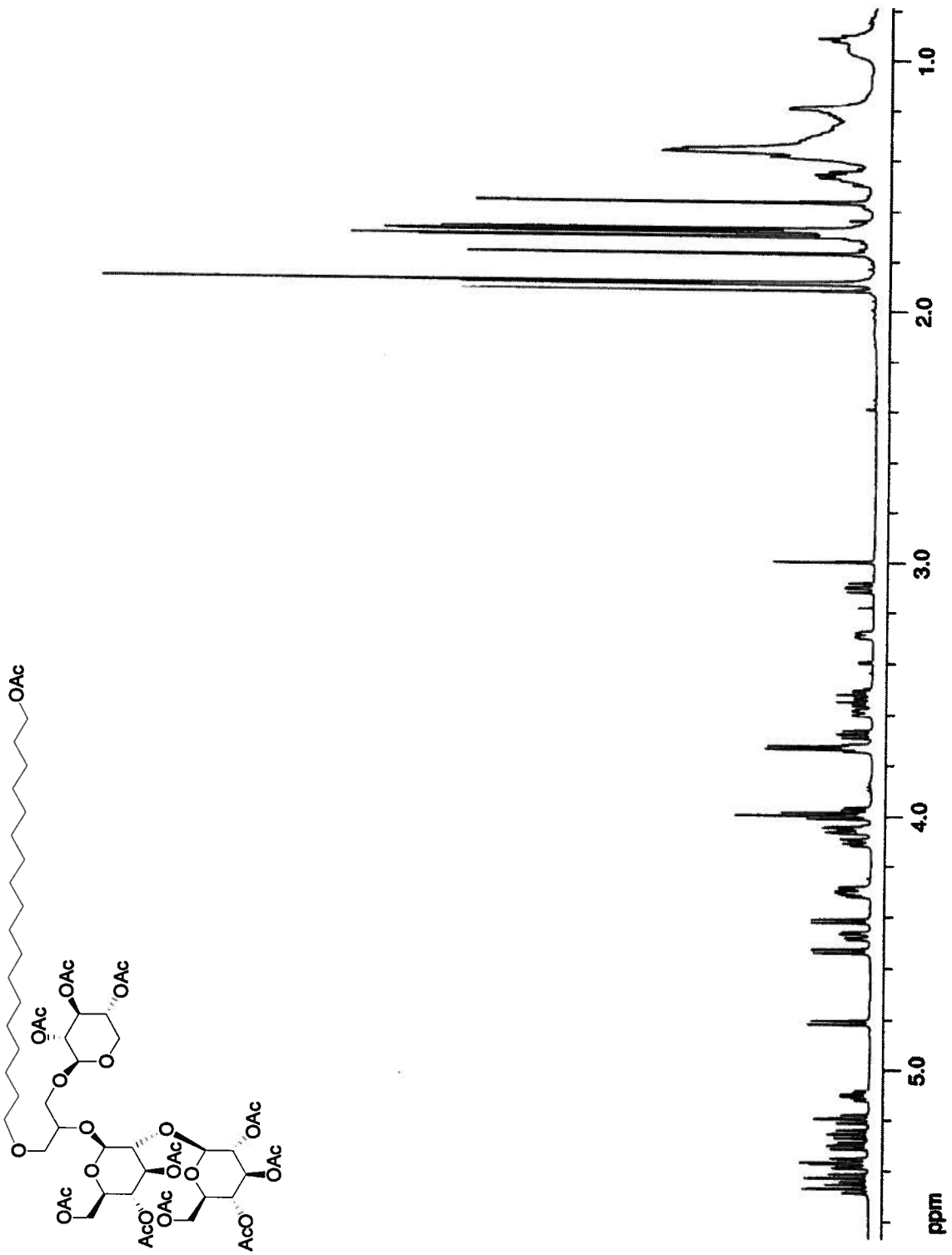

Figure 5.6.3. ^{1}H NMR spectrum of myrmekioside C peracetate (**5.28**) at 600 MHz in C_6D_6.

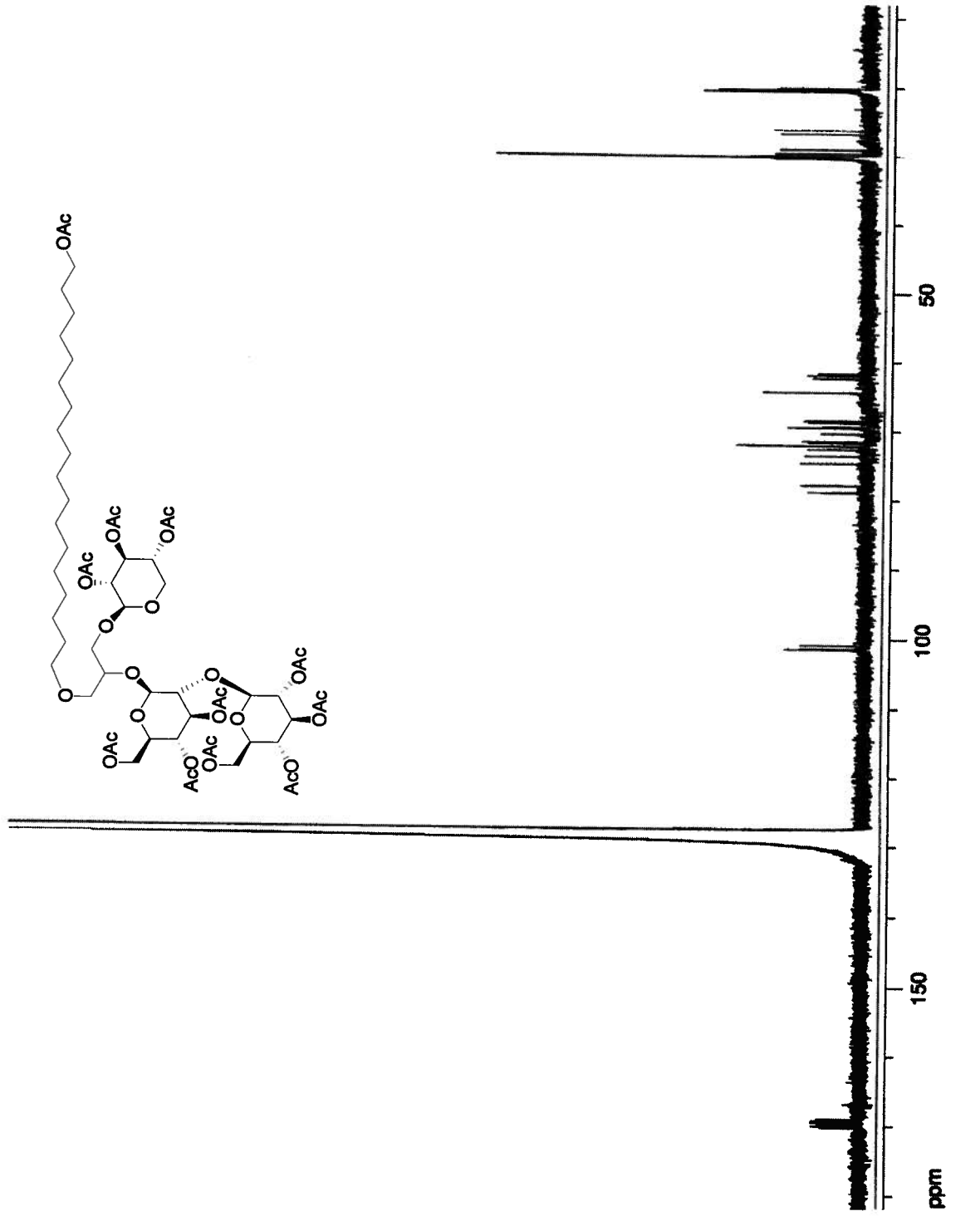

Figure 5.6.4. ^{13}C NMR spectrum of myrmekioside C peracetate (**5.28**) at 150 MHz in C_6D_6.

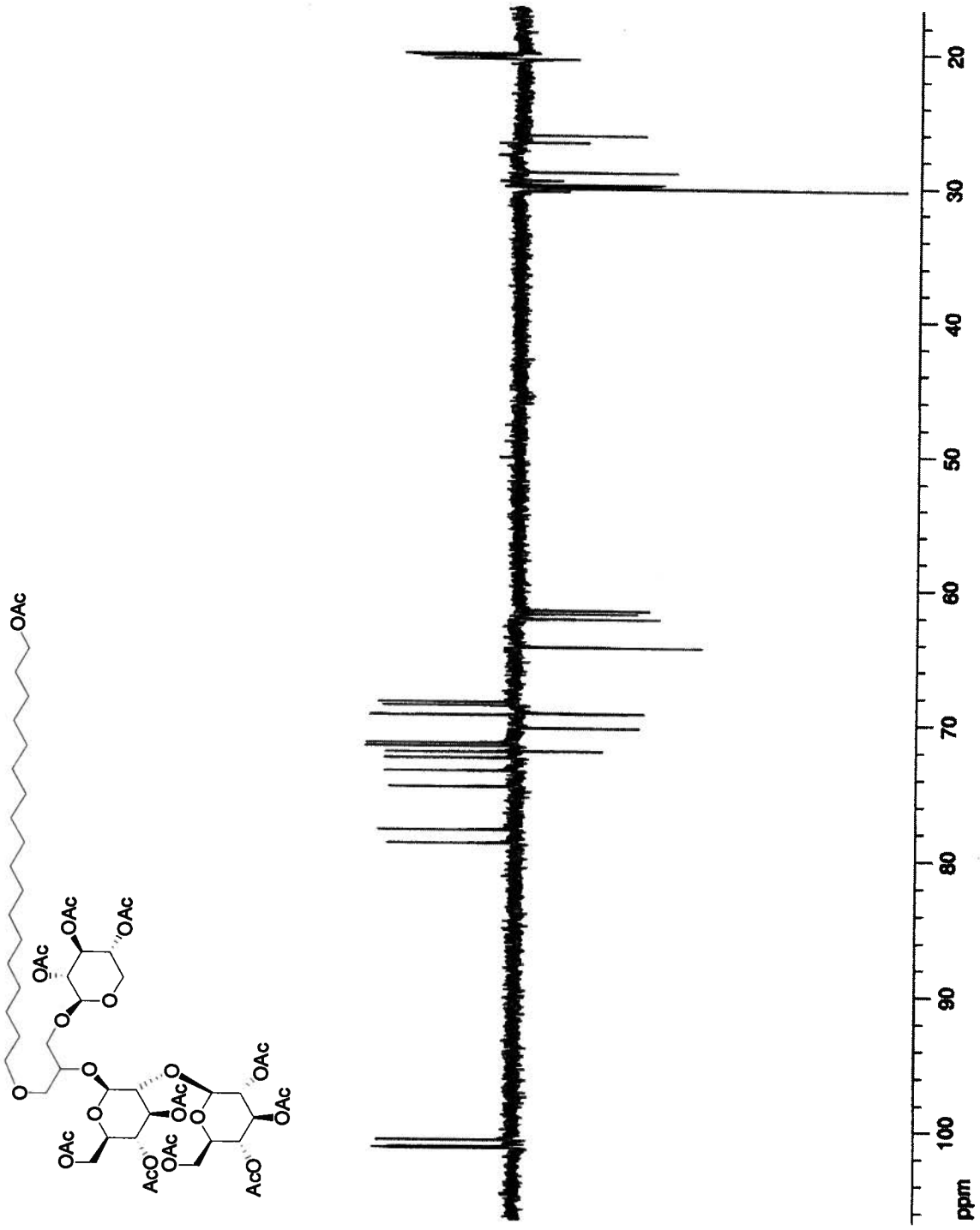

Figure 5.6.5. DEPT NMR spectrum of myrmekioside C peracetate (**5.28**) at 150 MHz in C_6D_6.

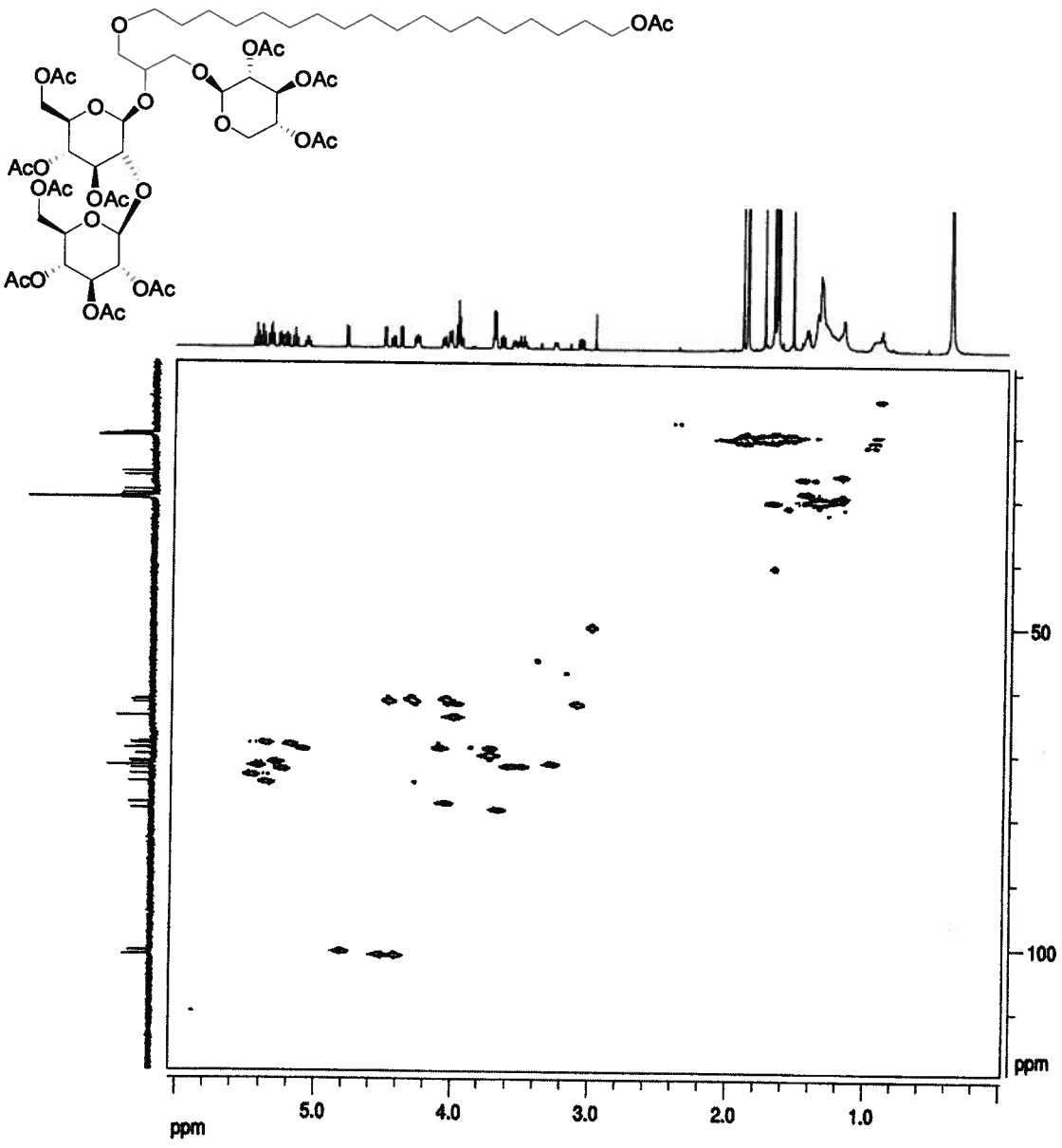

Figure 5.6.6. HMQC spectrum of myrmekioside C peracetate (**5.28**) at 600 MHz in C_6D_6.

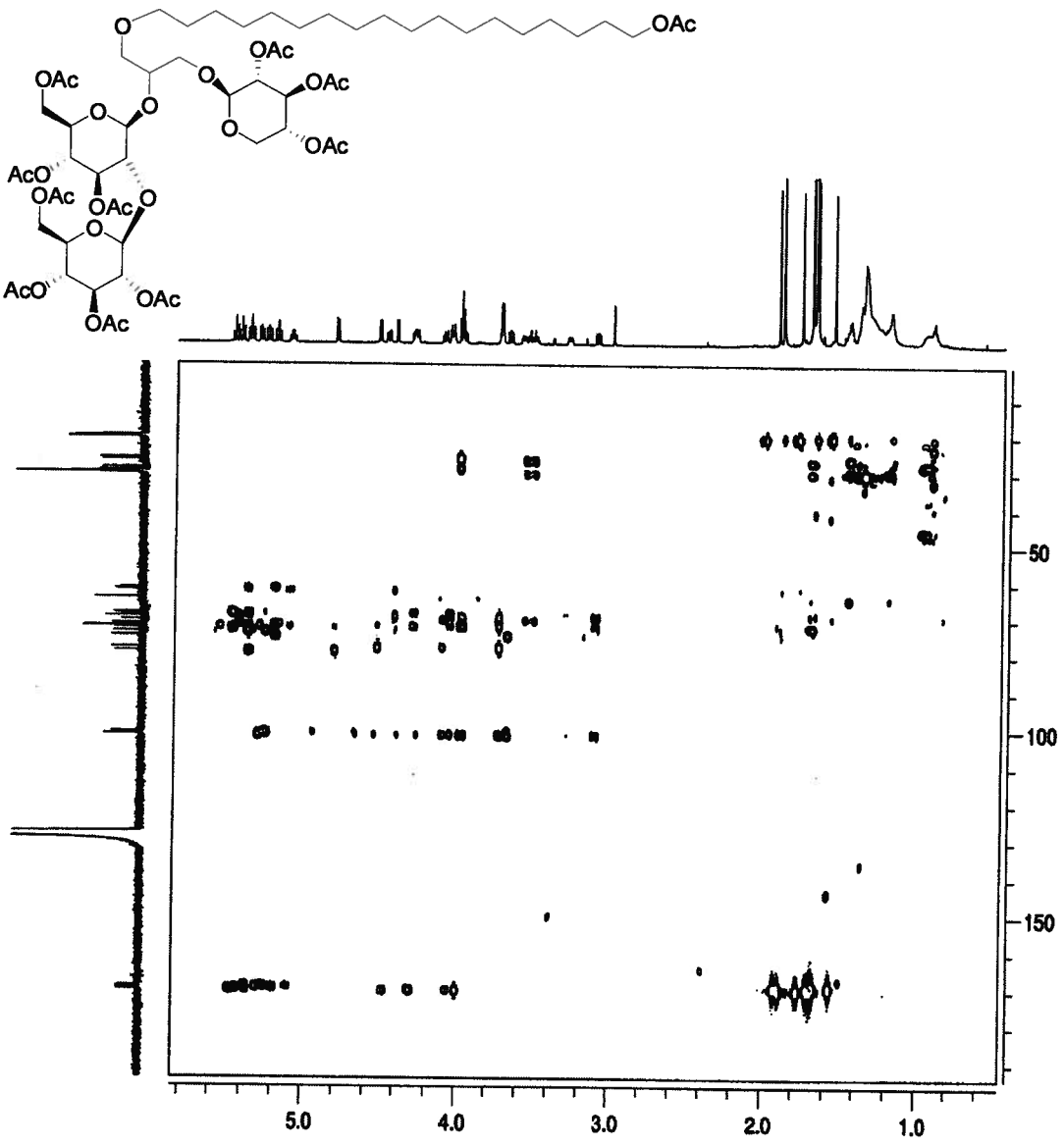

Figure 5.6.7. HMBC spectrum of myrmekioside C peracetate (**5.28**) at 600 MHz in C_6D_6.

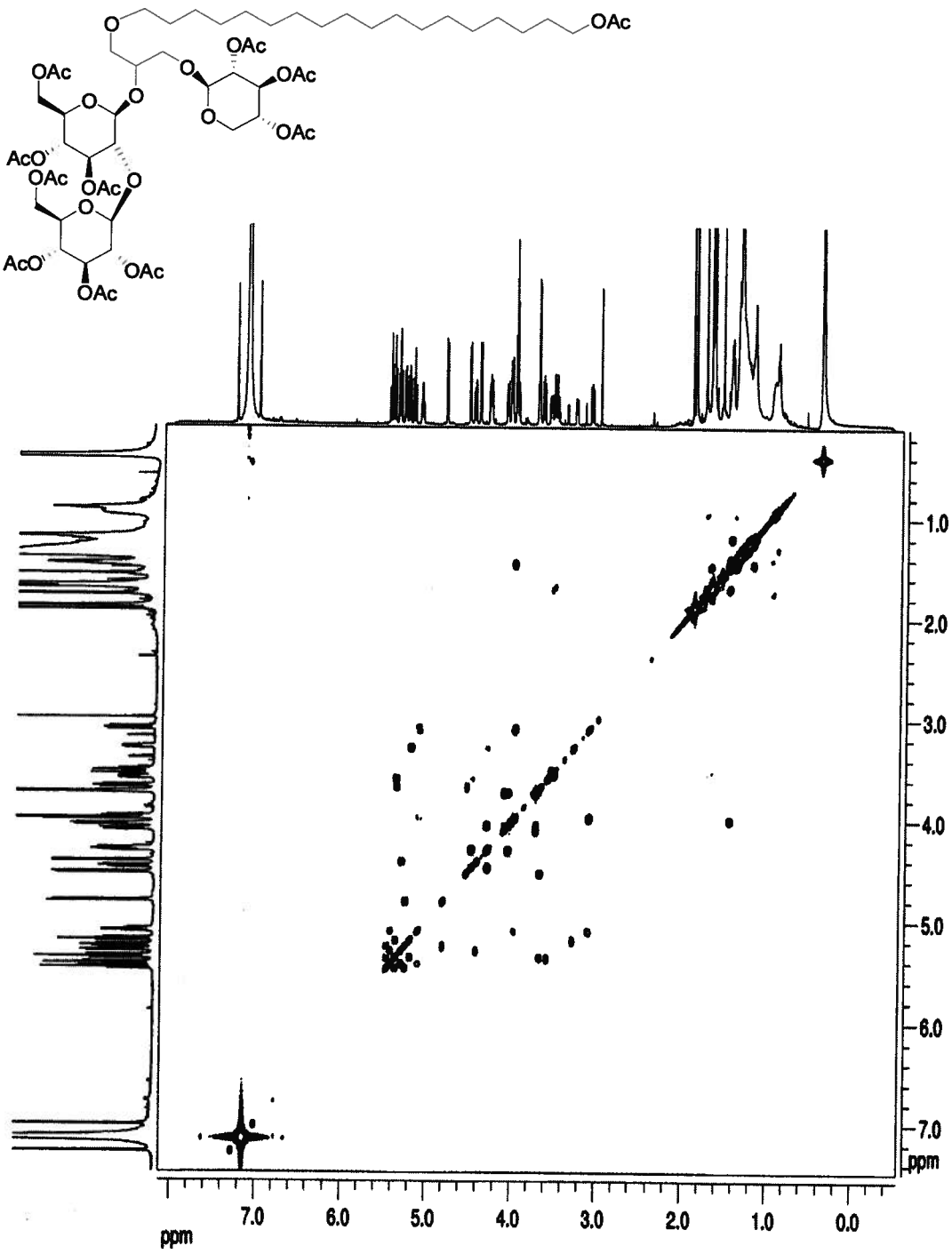

Figure 5.6.8. COSY spectrum of myrmekioside C peracetate (**5.28**) at 600 MHz in C_6D_6.

Table 5.6.1. 1D and 2D NMR data of myrmekioside C peracetate.[a]

Position	δ_C	δ_H (*J* in Hz)	HMBC	COSY
O'Alkyl Chain				
1	72.1	3.53, m	Gly-C-1, C-2, C-3	H-2
2	30.5	1.70, m	C-1, C-3, C-4	H-1, H-3
3	26.8	1.49, m		H-2
4-15	20.0-30.5, 12 C total	0.80-1.80 (24 H total)		
16	26.3	1.19, m	C-14, C-15	
17	29.0	1.46, m	C-15, C-16, C-18	H-16, H-18
18[b]	64.4	4.00, t, (6.7)	C-16, C-17	H-17
Glycerol (Gly)				
Gly-1[c]	70.4	3.70, d, (5.4)	Gly-C-2, Gly-C-3, C-1	Gly-H-2
Gly-2[d]	78.0	4.06, m	Glu-C -1, Gly-C -1	Gly-H-2, Gly-H-3b
Gly-3a	69.4	4.10, dd, (10.17, 4.2)	Xyl-C -1, Gly-C -1	Gly-H-2, Gly-H-3b
Gly-3b[c]		3.73, m	Xyl-C -1	Gly-H-2, Gly-H -3a
Xylose (Xyl)				
Xyl-1	101.5	4.42, d, (7.3)	Gly-C-3, Xyl-C -5	Xyl-H-2
Xyl-2	71.5	5.30, t, (8.3)	Xyl-C -1, Xyl-C -2	Xyl-H-1, Xyl-H -3
Xyl-3	72.2	5.43, t, (8.9)	Xyl-C -2, Xy-C l-4, Xy-C -5	Xyl-2, Xyl-4
Xyl-4	69.5	5.10, m	Xyl-C-3, Xyl-C -5	Xyl-H -3, Xyl-H -5a, Xyl-H -5b
Xyl-5a[b, e]	62.4	3.10, t, (10.1)	Xyl-C -1, Xy-C -3, Xyl-C -4	Xyl-H -4, Xyl-H -5b
Xyl-5b[e]		3.97, m	Xyl-C -1, Xyl-C -3, Xyl-C -4	Xy-H l-4, Xyl-H -5a
Glucose1 (Glu1)				
Glu1-1	101.4	4.53, d, (8.0)	Gly-C -2, Glu1-C -3, Glu1-C -5	Glu1-H -2
Glu1-2	78.9	3.68, t, (8.9)	Glu1-C -1, Glu1-C -3	Glu1-H -1, Glu1-H -3
Glu1-3[f]	74.7	5.37, t, (9.5)	Glu1-C -2, Glu1-C -4	Glu1-H -2, Glu1-H -4
Glu1-4	68.8	5.20, t, (9.9)	Glu1-C -3, Glu1-C -5, Glu1-C -6	Glu1-H -3, Glu1-H -5
Glu1-5	71.8	3.29, d, (10.2)	Glu1-C -1, Glu1-C -3, Glu1-C -4	Glu1-H -4, Glu1-H -6a, Glu1-H -6b
Glu1-6a[d, g]	61.7	4.05, m	Glu1-C -4	Glu1-H -5, Glu1-H -6b
Glu1-6b[g, h]		4.30, m	Glu1-C -4	Glu1-H -5, Glu1-H -6a

Position	δ_C	δ_H (*J* in Hz)	HMBC	COSY
Glucose 2 (Glu2)				
Glu2-1	100.9	4.80, d, (8.0)	Glu1-C -2, Glu2-C -2	Glu2-H -2
Glu2-2	72.6	5.25, t, (9.1)	Glu2-C -1, Glu2-C -3, Glu2-C -4	Glu2-H -1, Glu2-H -3
Glu2-3	73.6	5.47, t, (9.2)	Glu2-C -2, Glu2-C -4	Glu2-H -2, Glu2-H -4
Glu2-4[f]	68.6	5.37, t, (10.2)	Glu2-C -3, Glu2-C -6	Glu2-3, Glu2-5
Glu2-5	72.2	3.59, d, (10.1)	Glu2-C-1, Glu2-C -4	Glu2-H -4, Glu2-H -6a, Glu2-H -6b
Glu2-6a[h, i]	62.0	4.29, m	Glu2-C -4, Glu2-C -5	Glu2-H -5, Glu2-H -6b
Glu2-6b[i]		4.47, dd, (5.1, 12.4)	Glu2-C -4, Glu2-C -5	Glu2-H-5, Glu2-H-6a

[a]: ^1H and ^{13}C chemical shifts (ppm) are referenced to the C_6D_6 (δ_H 7.15 ppm and δ_C 128 ppm).
[b]: H-18 and Xyl-5a are overlapping signals
[c]: Gly-1 and Gly-3b are overlapping signals
[d]: Gly2 and Glu1-6a are overlapping signals
[e]: Xyl-5a and Xyl-5b are interchangeable signals
[f]: Glu1-3 and Glu2-4 are overlapping signals
[g]: Glu1-6a and Glu1-6b are interchangeable signals
[h]: Glu1-6b and Glu2-6a are overlapping signals
[i]: Glu2-6a and Glu2-6b are interchangeable signals

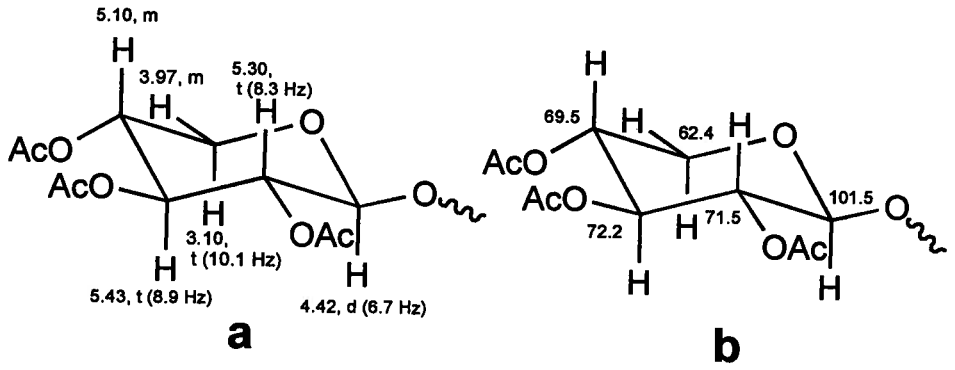

Figure 5.6.9. (**a**)^{1}H chemical shifts and coupling constants and (**b**) ^{13}C chemical shifts of substructure I of myrmekioside C peracetate (**5.28**).

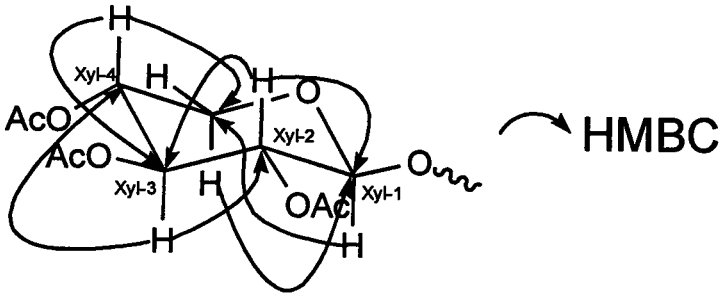

Figure 5.6.10. Key HMBC correlations of substructure I of myrmekioside C peracetate (**5.28**).

The chemical shift of Xyl-C-1 (δ_C 101.5) is typical of an sp^3 hybridized carbon attached to two oxygen atoms. The proton resonance at δ_H 4.42 (Xyl-H-1: HMQC to δ_C 101.5) showed COSY correlations to the methine proton at δ_H 5.30 (Xyl-H-2: HMQC to δ_C 71.5), which in turn had COSY correlations to the proton resonance at δ_H 5.43 (Xyl-H-3: HMQC to δ_C 72.2) (Figure 5.6.11). The COSY spectrum revealed that the proton resonance at δ_H 5.10 (Xyl-H-4: HMQC to δ_C 69.5) had correlations to the proton resonances at δ_H 5.43 (Xyl-H-3), δ_H 3.10 (Xyl-H-5a: HMQC to δ_C 62.4) and δ_H 3.97 (Xyl-H-5b: HMQC to δ_C 62.4). All of the above is consistent for fragment of five consecutive oxygenated carbons and this was supported by numerous HMBC correlations (Figure 5.6.10). Both

the methylene protons at δ_H 3.10 (Xyl-H-5a) and δ_H 3.97 (Xyl-H-5b) displayed HMBC correlations to the oxygenated methine carbon resonance at δ_C 101.5 (Xyl-C-1), which allowed the establishment of a pentose in its pyranose form. The vicinal coupling constants of the pentose from Xyl-H-1 to Xyl-H-4 showed a range from 7.3-10.1 Hz (Figure 5.6.9). This is consistent with all the protons having axial/axial coupling, therefore, the sugar was found to be a xylose residue in its β-anomeric form (substructure I, Figures 5.6.9 and 5.6.10).

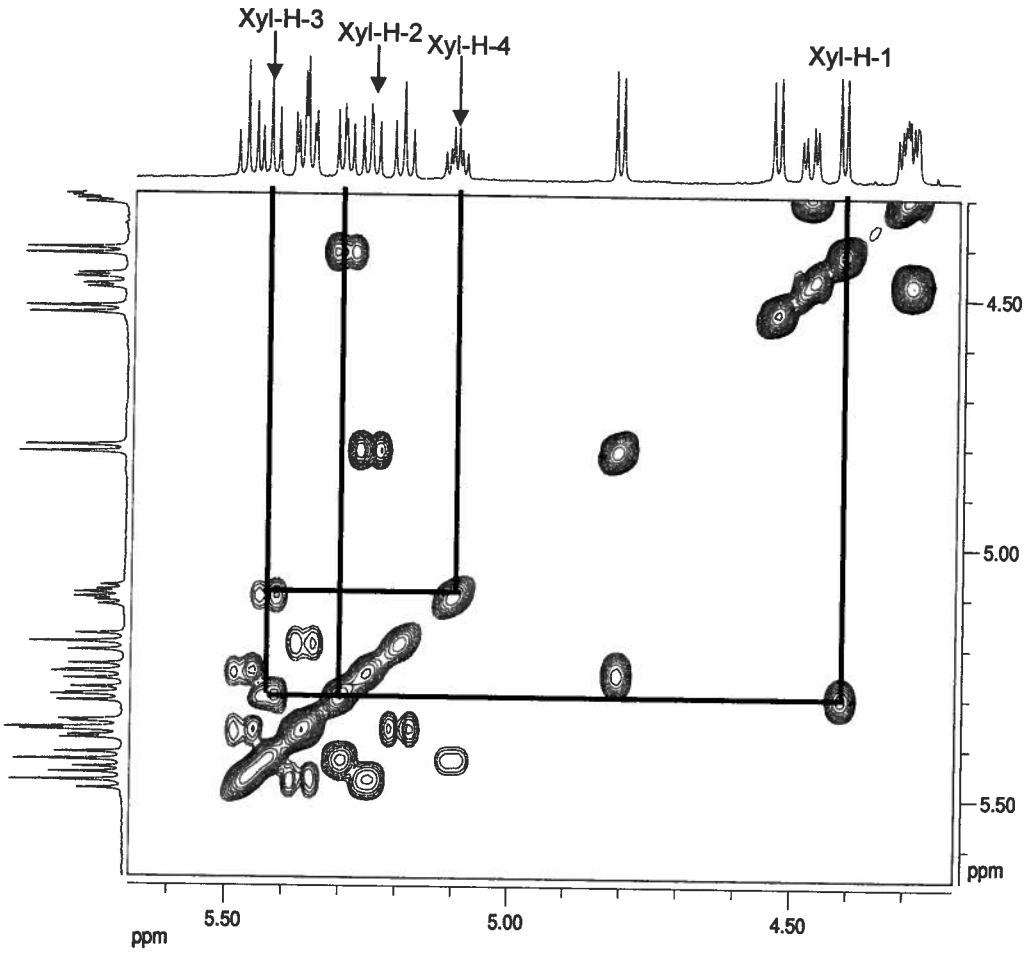

Figure 5.6.11. COSY expansion for substructure **I** of myrmekioside C peracetate (**5.28**).

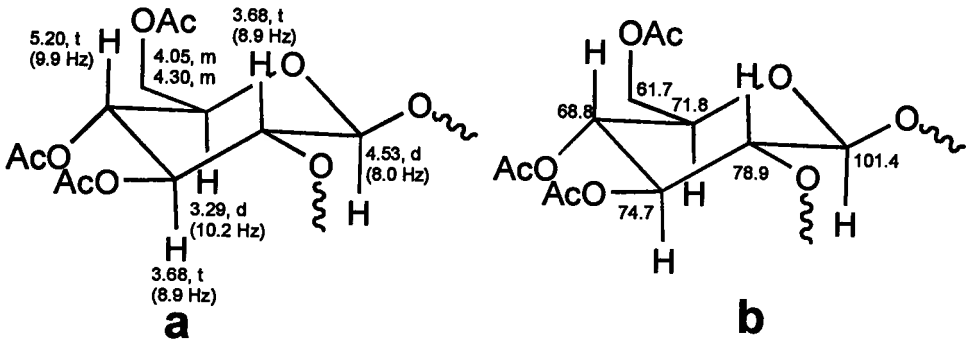

Figure 5.6.12. (**a**)^{1}H chemical shifts and coupling constants and (**b**) ^{13}C chemical shifts of substructure **II** of myrmekioside C peracetate (**5.28**).

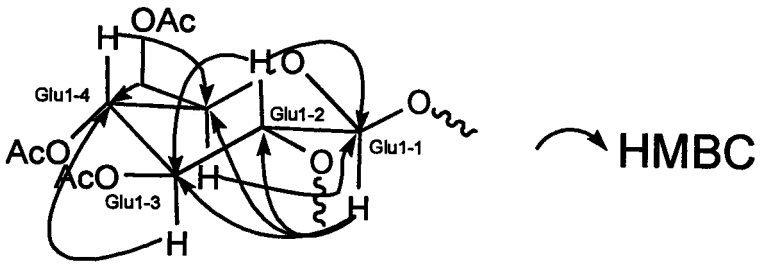

Figure 5.6.13. Key HMBC correlations of substructure **II** of myrmekioside C peracetate (**5.28**).

The downfield shift of the carbon at δ_C 101.4 (Glu1-C-1) indicated a dioxy methine. COSY cross-peaks were present between the proton resonance at δ_H 4.53 (Glu1-H-1: HMQC to δ_C 101.4) and the methine proton at δ_H 3.68 (Glu1-H-2: HMQC to δ_C 78.9). The proton resonance at δ_H 3.68 (Glu1-H-2) had COSY correlations to the methine proton at δ_H 5.37 (Glu1-H-3: HMQC to δ_C 74.7), which contained an additional COSY correlation to the proton resonance at δ_H 5.20 (Glu1-H-4: HMQC to δ_C 68.8). Further COSY correlations were present between the proton resonance at δ_H 5.20 (Glu1-H-4) and the oxygenated methine proton resonance at δ_H 3.29 (Glu1-H-5: HMQC to δ_C 71.8). Finally, COSY cross-peaks between the proton resonance at δ_H 3.29 (Glu1-H-5) and both proton resonances at δ_H 4.05 (Glu1-H-6a: HMQC to δ_C 61.7) and δ_H 4.30 (Glu1-H-6b: HMQC to δ_C 61.7) revealed a fragment of six adjacent oxygenated carbons. This fragment was confirmed by several key HMBC correlations (Figure 5.6.13). HMBC cross-peaks were present between the methine proton resonance at δ_H 4.53 (Glu1-H-5) and the dioxy methine carbon at δ_C 101.4 (Glu1-C-1). This established a hexose moiety in its pyranose form. Examination of the vicinal coupling constants from

Glu1-H-1 to Glu1-H-5 revealed a coupling constant range from 7.9-10.1 Hz, which is consistent with all the protons having axial/axial coupling (Figure 5.6.13). It can be deduced that a glucose moiety is present in its β-anomeric form (substructure **II**, Figures 5.6.12 and 5.6.13).

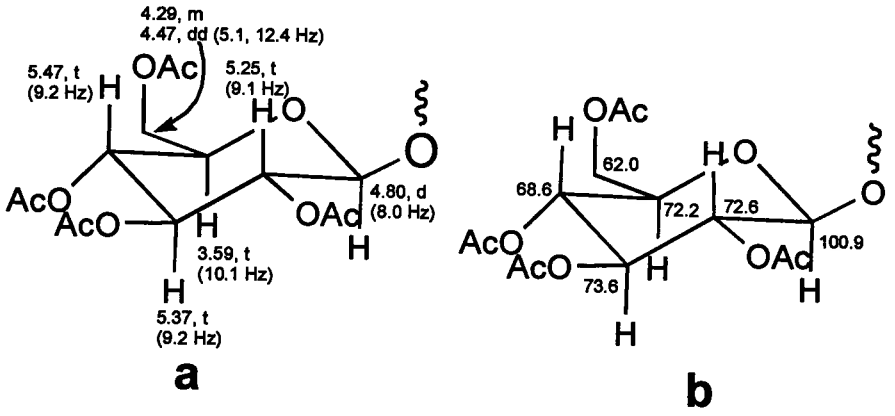

Figure 5.6.14. (**a**) ^{1}H chemical shifts and coupling constants and (**b**) ^{13}C chemical shifts of substructure **III** of myrmekioside C peracetate (**5.28**).

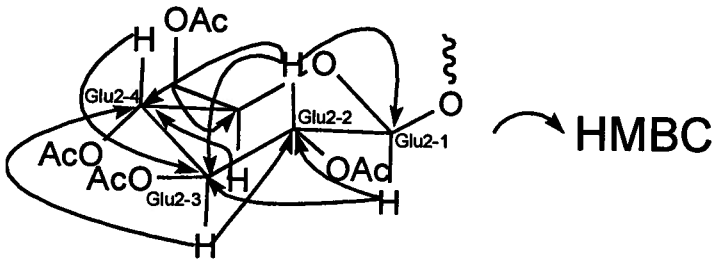

Figure 5.6.15. Key HMBC correlations of substructure **III** of myrmekioside C peracetate (**5.28**).

The methine carbon resonance Glu2-C-1 (δ_C 100.9) displayed a chemical shift suitable for a carbon attached to two oxygens. The COSY spectrum showed that the proton resonance at δ_H 4.80 (Glu2-H-2: HMQC to δ_C 100.9) had a correlation to the proton resonance at δ_H 5.25 (Glu2-H-2: HMQC to δ_C 72.6), which in turn had a correlation to methine proton at δ_H 5.47 (Glu2-H-3: HMQC to

δ_C 73.6). The proton resonance at δ_H 5.37 (Glu2-H-4: HMQC to δ_C 68.6) showed COSY correlations to both proton resonances at δ_H 5.47 (Glu2-H-3) and δ_H 5.47 (Glu2-H-5: HMQC to δ_C 72.2). Finally, COSY correlations were present between the proton resonance at δ_H 3.59 (Glu2-H-5) and the proton resonances at δ_H 4.29 (Glu2-H-6a: HMQC to δ_C 62.0) and δ_H 4.47 (Glu2-H-6b: HMQC to δ_C 62.0). All of the above data is consistent for a fragment of six consecutive oxygenated carbons which was confirmed by observation of the HMBC data (Figure 5.6.15). A key HMBC correlation between the proton resonance at δ_H 3.29 (Glu2-H-5) and the dioxy carbon resonance at 100.9 (Glu2-C-1) established the presence of a hexose in its pyranose form. The vicinal coupling constant range for Glu1-H-1 to Glu1-H-5 was found to be 8.0-10.2 Hz which corresponds to all the protons having axial/axial coupling. This is consistent for a glucose moiety in its β-anomeric form and substructure **III** (Figures 5.6.14 and 5.6.15).

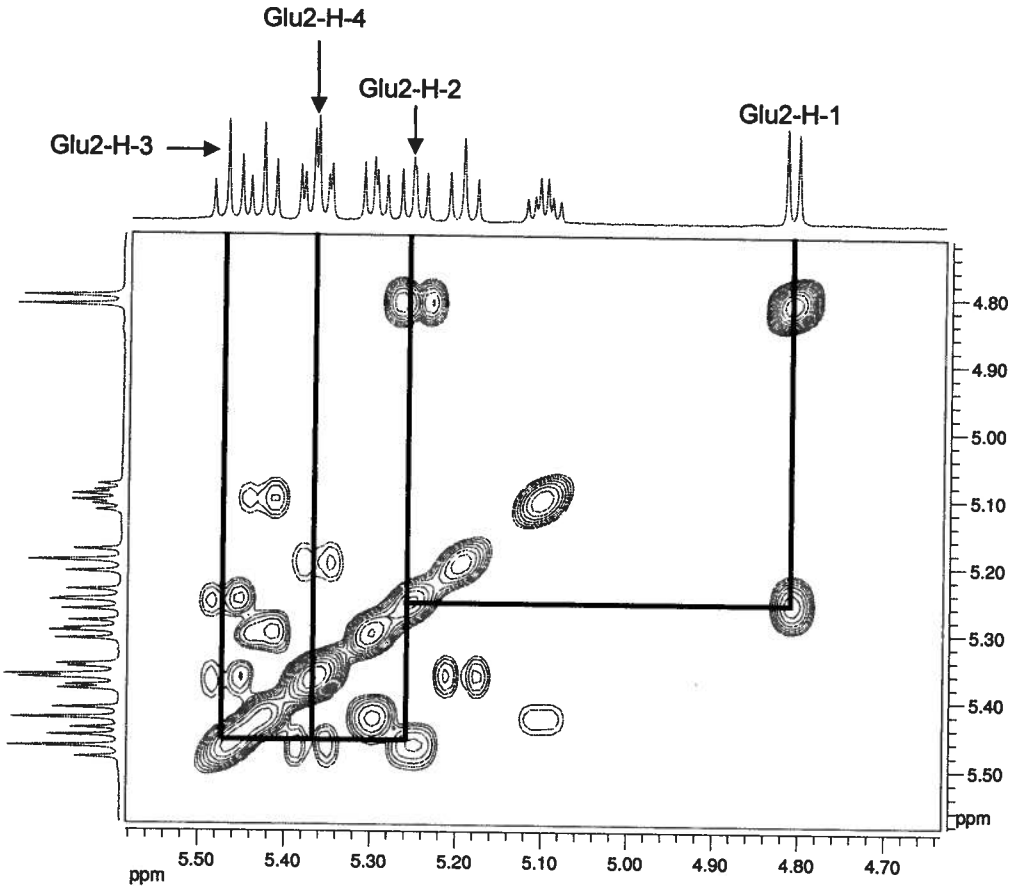

Figure 5.6.16. COSY expansion for substructure **III** of myrmekioside C peracetate (**5.28**).

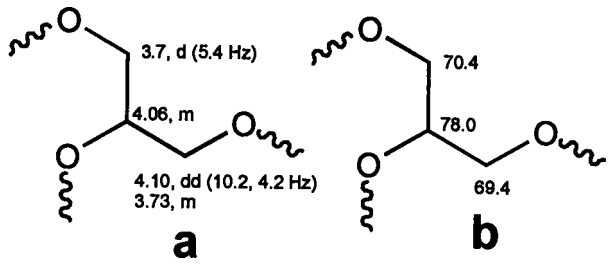

Figure 5.6.17. (**a**) ^{1}H chemical shifts and coupling constants and (**b**) ^{13}C chemical shifts of substructure **IV** of myrmekioside C peracetate (**5.28**).

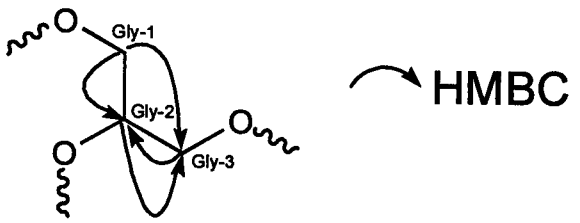

Figure 5.6.18. Key HMBC correlations of substructure **IV** of myrmekioside C peracetate (**5.28**).

The oxygenated methylene protons at δ_H 3.70 (Gly-H-1: HMQC to δ_C 70.4) displayed COSY correlations to the methine proton at δ_H 4.06 (Gly-H-2: HMQC to δ_C 78.0), which established the linkage between Gly-C-1 (δ_C 70.4) and Gly-C-2 (δ_C 78.0). Both methylene proton resonances at δ_H 4.10 (Gly-H-3a: HMQC to δ_C 69.4) and δ_H 3.73 (Gly-H-3b: HMQC to δ_C 69.4) showed COSY correlations to the proton resonance at δ_H 4.06 (Gly-H-2), which allowed the connectivity between Gly-C-2 (δ_C 78.0) and Gly-C-3 (δ_C 69.4). All of this is consistent with a linear chain of three oxygenated carbons and a glycerol moiety (substructure **IV**, Figure 5.6.17). This was supported by numerous correlations in the HMBC spectrum (Figure 5.6.18).

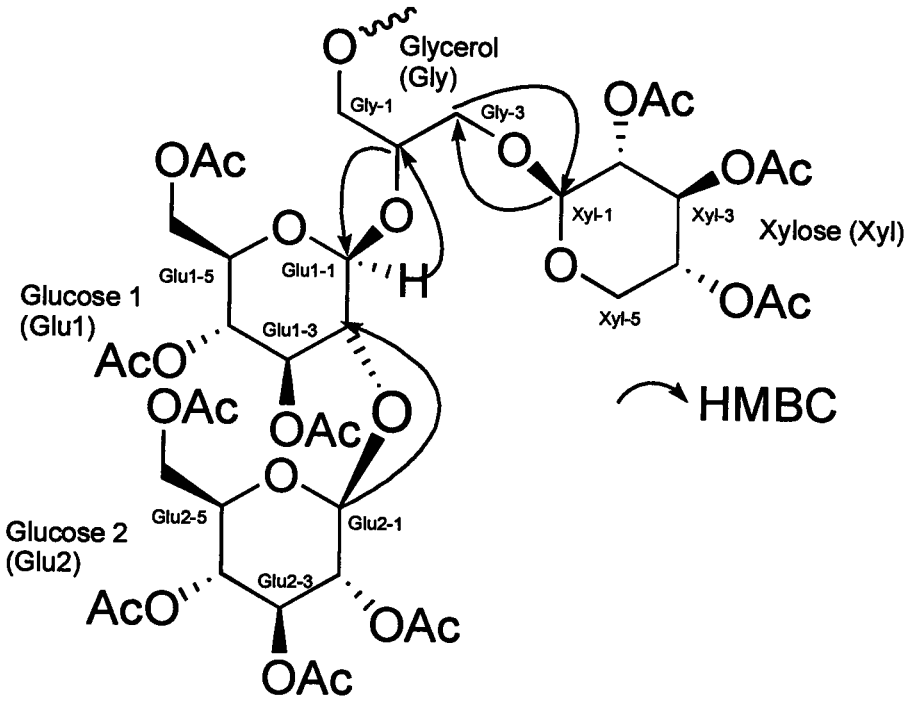

Figure 5.6.19. Key HMBC correlations of myrmekioside C peracetate (**5.28**).

HMBC cross-peaks were present between the anomeric proton resonance at δ_H 4.80 (Glu2-H-1) and the oxygenated carbon methine at δ_C 78.9 (Glu1-C-2). This established the linkage between Glu1 and Glu2 and supported a disaccharide moiety (Figure 5.6.20). The anomeric proton methine at δ_H 4.53 (Glu1-H-1) had HMBC correlations to the oxygenated carbon resonance at δ_C 70.0 (Gly-C-2). Additional three bond HMBC couplings were present between the methine proton resonance at δ_H 4.06 (Gly-H-2) and the oxygenated carbon resonance at δ_C 101.4 (Glu1-C-1). This confirmed the link between the glycerol and the disaccharide moieties at Glu1-C-1 (Figure 5.6.20). Both proton resonances at δ_H 4.10 (Gly-H-3a) and δ_H 3.73 (Gly-H-3b) showed HMBC correlations to the anomeric carbon resonance at δ_C 101.5 (Xyl-C-1). Additional HMBC cross-peaks were observed between the anomeric proton resonance at

δ_H 4.42 (Xyl-H-1) and δ_C 69.4 (Gly-C-3), which established the link between the xylose and glycerol moieties at Gly-C-3 (Figure 5.6.20).

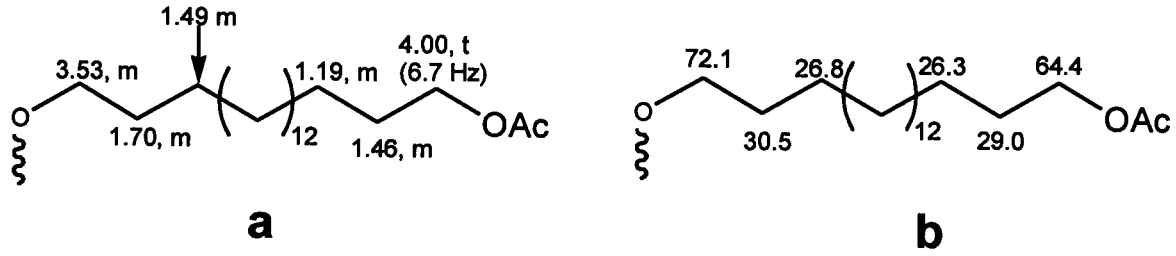

Figure 5.6.20. (**a**) ^{1}H chemical shifts and coupling constants and (**b**) ^{13}C chemical shifts of substructure **V** of myrmekioside C peracetate (**5.28**).

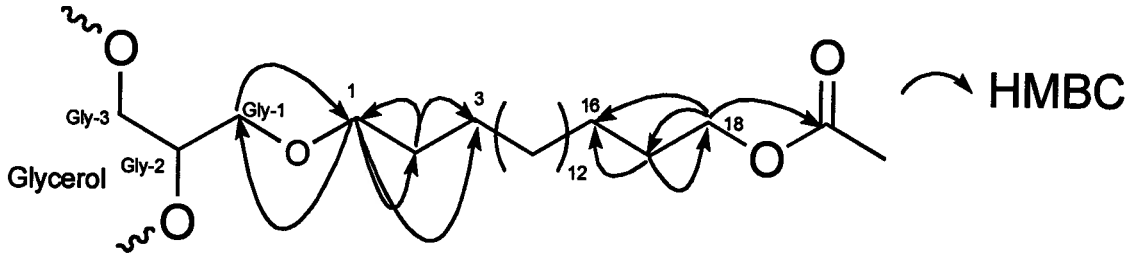

Figure 5.6.21. Key HMBC correlations of substructure **V** of myrmekioside C peracetate (**5.28**).

Analysis of the NMR data to this point had revealed a glycerol and three sugar subunits which is consistent with a molecular formula of $C_{41}H_{63}O_{27}$, leaving $C_{19}H_{41}O_2$ unaccounted for. Analysis of the ^{1}H, ^{13}C, and DEPT NMR spectra revealed no methyl doublets or triplets, 16 aliphatic methylenes, and two oxymethylenes. The proton resonance at δ_H 1.19 (H-16: HMQC to δ_C 26.3) contained COSY correlations to the proton resonance at δ_H 1.46 (H-17: HMQC to δ_C 29.0), which linked methylenes C-16 (δ_C 26.3) and C-17 (δ_C 29.0). Additional COSY cross-peaks between δ_H 1.46 (H-17) and δ_H 4.00 (H-18: HMQC to δ_C 64.4)

linked methylenes C-17 (δ_C 29.0) to C-18 (δ_C 64.4). These connections were supported by correlations in the HMBC (Figure 5.6.22). The downfield chemical shift of C-18 (δ_C 64.4) is typical of a carbon attached to oxygen. A methylene proton resonance at δ_H 4.00 (H-18) showed an HMBC correlation to an acetate carbonyl (δ_C 170.2) (Figure 5.6.21). This reveals that an aliphatic chain is terminated by an oxymethylene. The methylene proton at δ_H 1.49 (H-3: HMQC to δ_C 26.8) showed a COSY correlation with the proton resonance at δ_H 1.19 (H-2: HMQC to δ_C 30.5), which confirmed the connection between C-2 (δ_C 30.5) and C-3 (δ_C 26.8). The methylene C-1 (δ_C 72.1) was bonded to methylene C-2 (δ_C 30.5) from observation of a COSY correlation between δ_H 1.19 (H-2) and δ_H 3.53 (H-1: HMQC to δ_C 72.1). These linkages were supported by numerous HMBC correlations (Figure 5.6.21). The chemical shift of the methylene C-1 (δ_C 72.1) is consistent with a carbon attached to oxygen. From the above data, one can deduce a linear eighteen carbon aliphatic chain flanked by two terminal oxymethylenes (substructure **V**, Figures 5.6.20 and 5.6.21). HMBC cross-peaks were observed between the methylene proton reasonance at δ_H 3.53 (H-1) and the oxygenated methine carbon resonance at δ_C 70.4 (Gly-C-1). Finally, HMBC correlations between the proton resonance at δ_H 3.70 (Gly-H-1) and the carbon resonance at δ_C 72.1 established that one terminal of the aliphatic chain (C-1) is attached to the glycerol moiety at Gly-C-1, thus completing the structure of myrmekioside C peracetate (**5.28**). Even though the carbon skeleton of myrmekioside C is known, it contains a rare saturated lipid moiety that is

oxygenated on both ends of the linear chain. Only two other naturally occurring compounds, **5.20** and **5.21**, contain this rare lipid moiety. [17]

5.7. Biology of Secondary Metabolites isolated from *Myrmekioderma styx*

To screen for active ligands against SHBG, assays were run by the Hammond laboratory in the Child and Family research institute at the University of British Columbia. In this assay,[22] SHBG is saturated with tritium labeled dihydrotestoterone ([^{3}H]-DHT) and any excess steroid is removed. The desired ligand is then added to the SHBG/[^{3}H]-DHT mixture and incubated overnight. After removal of the displaced [^{3}H]-DHT, the quantity of [^{3}H]-DHT bound to SHBG in the presence of the ligand is compared to the amount of [^{3}H]-DHT bound to SHBG when no ligand was added. The determination of the IC_{50} concentration was achieved when the ligand released more than 50% of [^{3}H]-DHT from SHBG.[22] All of the pure natural compounds isolated were tested in the SHBG ligand binding assay. Only (+)-curcudiol (**5.24**; IC_{50} 100 μM) was identified as a ligand able to displace [^{3}H]-DHT from SHBG (Figure 5.7.1).

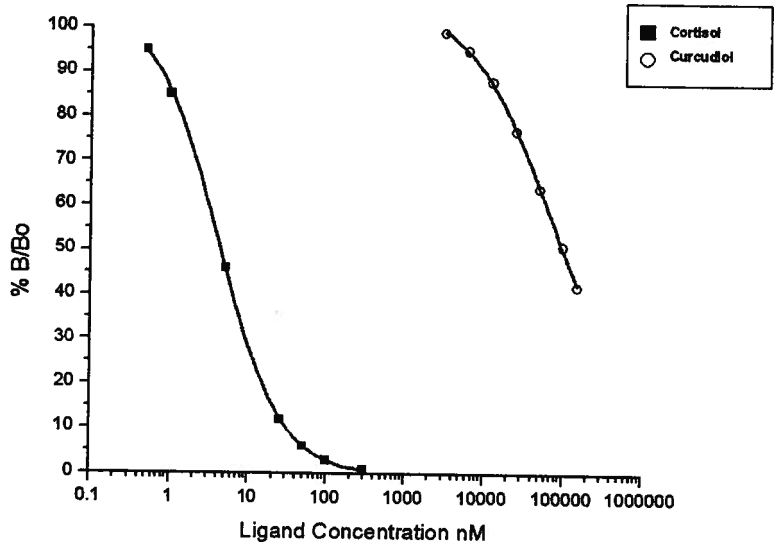

Figure 5.7.1. Dose response curve of (+)-curcudiol (**5.24**) in the SHBG assay. The graph was generated by Magid Fallahi of the Hammond laboratory.

5.8. Acetylation of myrmekioside C

Acetylation of **5.27** (1.1 mg, 0.001 mmol) was accomplished by stirring pyridine (1 mL; 12 mmol) and acetic anhydride (1 mL; 10 mmol) for 24 hours. The reaction mixture was dried *in vacuo* and purification was accomplished using a normal phase silica gel Sep Pak™ (eluent: 4:1 Hexanes: EtOAc) to obtain **5.28** (1.0 mg, 0.0007 mmol) in a 78% yield.

5.9. General Experimental Methods

All solvents used (except for NMR solvents) were HPLC grade (Fisher) and no further purification was performed. Solvents for HPLC were filtered through a 0.45 μm filter (Osmonics, Inc) before use. Acetic anhydride and pyridine were acquired from Aldrich and were used without further purification.

Reversed-phase C_{18} silica gel Sep Paks™ (10 g) and normal-phase silica gel Sep Paks™ (2 g) were purchased from Waters, Inc.. Separations on the HPLC was accomplished using either a Waters 2487 dual channel detector/system controller (Waters Series 515 pump; chart recorder, 0.25 cm/min), or a Waters 600 controller and Waters 486 Tunable Absorbance Detector (chart recorder, 0.25 cm/min). The HPLC column used was a 5 μm Inertsil column from Chromatography Sciences (Montreal, PQ). The conditions of the HPLC separation were as follows: 2.0 mL/min, monitoring at 220 nm. Thin-layer chromatography (TLC) plates were Whatman MKC18F (reversed-phase) and Kieselgel $60F_{254}$ (normal phase). TLC was visualized using either a dip solution of *p*-anisaldehyde (1% *p*-anisaldehyde, 2% H_2SO_4, 20% acetic acid and 77% EtOH) or under ultraviolet light (254 nm).

The ^{13}C spectra were recorded with either a Bruker AV600, AMX500, AM400, or AV400 spectrometer. ^1H spectra and 2D data sets were taken with either a Bruker AV600, AV500, or AV 400 spectrometer. NMR solvents were purchased from Cambridge Isotope laboratories and were referenced to solvent peaks C_6D_6 (δ_H 7.15 ppm and δ_C 128.0 ppm), DMSO-d_6 (δ_H 2.49 ppm and δ_C 39.5 ppm), and $CDCl_3$ (δ_H 7.24 ppm and δ_C 77.23 ppm). Low resolution ESI mass spectra were recorded on a Bruker Esquire LC mass spectrometer. High resolution ESI mass spectra was obtained using a Micromass LCT mass spectrometer. Optical rotations were recorded with a JASCO J-1010 polarimeter equipped with a halogen lamp (589 nm) and a 10 mm micro cell. The CD

spectra were recorded using a JASCO J-710 spectropolarimeter with a 1 mm micro cell.

5.10. Isolation of bisabolane sesquiterpenes and myrmekioside C

Myrmekioderma granulatum (75 g wet wt.) was collected by hand using SCUBA from Latondo Island of Besar, Takabonerati, Indonesia. The sponge was identified by Dr. R. van Soest (University of Amsterdam) and a voucher sample has been kept at the Zoologisch Museum, Amsterdam (ref. No. ZMA POR 18337). The material was frozen and stored until workup. The frozen sponge sample was extracted four times with MeOH (4 X 1 L). The combined MeOH extracts were reduced *in vacuo* to give a brown solid (2.6 g). The solid was subjected to a gradient reversed-phase Sep Pak™ to yield two biologically active fractions. The most active fraction was subjected to repeated reversed-phase HPLC (Inertsil C_{18}, 9.4 X 250 mm, 4:6 H_2O: MeOH, UV detection at 220 nm) to obtain the biologically active compound (+)-curcudiol (**5.24**, 16.7 mg),[21] abolene (**5.23**, 15.7 mg),[20] abolenone (**5.25**, 5.2 mg) and the bisabolane sesquiterpenoid **5.22** (32.8 mg).[20] The less active fraction was subjected to repeated reversed phase HPLC (Inertsil C_{18}, 9.4 X 250 mm, 3:7 H_2O: MeOH, UV detection at 220 nm) to yield (+)-curcuphenol (**5.26**, 16.7 mg),[21] and myrmekioside C (**5.27,** 4.3 mg).

5.11. Physical data of secondary metabolites from Myrmekioderma styx

(+)-Curcudiol (5.24): yellow oil. $[\alpha]_D^{22}$: +3.9 (c 0.3, MeOH); UV (MeOH) λ_{max} (log ε) 219 nm (3.17), 270 (3.10); ^{1}H NMR (500 MHz, DMSO-*d*$_6$):δ_H 8.96 (1H, bs, 1-OH) 6.91 (1H, d, *J* = 7.63 Hz, H-5), 6.55 (1H, s, H-2), 6.53 (1H, d, *J* = 7.63 Hz, H-4), 3.98 (1H, bs, 11-OH), 3.00 (1H, m, H-7), 2.15 (3H, s, H-15), 1.49 (1H, m, H-8a), 1.39 (1H, m, H-8b), 1.29 (2H, m, H-10), 1.23 (2H, m, H-9), 1.08 (3H, d, *J* = 7.05 Hz, H-14), 1.00 (3H, s, H-12), 0.99 (3H, s, H-13); ^{13}C NMR (100 MHz, DMSO-*d*$_6$): δ_C 154.4 (C, C-1), 135.0 (C, C-3), 130.3 (C, C-6), 126.3 (CH, C-5), 119.6 (CH, C-4), 115.6 (CH, C-2), 68.6 (C, C-11), 43.7 (CH_2, C-10), 37.8 (CH_2, C-8), 31.1 (CH, C-7), 29.3 (CH_3, C-12 or C-13), 29.1 (CH_3, C-12 or C-13), 21.9 (CH_3, C-15), 21.1 (CH_3, C-14), 20.6 (CH_2, C-9); LRESIMS *m/z* 259; HRESIMS *m/z* 259.1672 (calc'd for $C_{15}H_{24}O_2Na$ 259.1674).

Abolene (diastereotopic mixture) (5.23): yellow oil; UV (MeOH) λ_{max} (log ε) 276 (3.51); ^{1}H NMR (500 MHz, DMSO-*d*$_6$): δ_H 9.01 (1H, b, 9-OH), 6.90 (1H, d, *J* = 7.6 Hz, H-5), 6.56 (1H, s, H-2), 6.53 (1H, d, *J* = 7.6 Hz, H-4), 4.86 (1-H, s, H-12a or H-12b), 4.80 (1H, s, H-12b or H-12a), 4.59 (1H, s, 9-OH), 3.81 (1H, bm, H-10), 2.99 (1H, m, H-7), 2.16 (3H, s, H-15), 1.55 (3H, s, H-13), 1.3-1.5 (2H, m, H-8a, H-8b), 1.24 (2H, m, H-9), 1.08 (3H, bd, *J* = 6.8 Hz, H-14); ^{13}C NMR (100 MHz, DMSO-*d*$_6$):δ 154.8 (C, C-1), 148.6 (C, C-11), 148.6 (C, C-11), 135.5 (C, C-3), 130.4 (C, C-6), 126.8 (CH, C-5), 120.0 (CH, C-4), 116.0 (CH, C-2), 110.3 (CH_2, C-12), 110.0 (CH_2, C-12), 74.6 (C, C-10), 74.2 (C, C-10), 32.9 (CH_2, C-9), 32.5 (CH_2, C-8), 32.5 (CH_2, C-8), 31.1 (CH, C-7), 30.8 (CH, C-7), 21.1 (CH, C-

14), 21.0 (CH_3, C-14), 20.6 (CH_3, C-15), 17.4 (CH_3, C-13), 17.2 (CH_3, C-13); LRESIMS *m/z* 257; HRESIMS *m/z* 257.1512 (calc'd for $C_{15}H_{22}O_2Na$ 257.1517).

Phenol, 2-(5-hydroxy-1,5-dimethyl-3-hexenyl)-5-methyl-, [R-(E)] (5.22): yellow oil. $[\alpha]_D^{22}$: -6.9 (c 1.8, MeOH); UV (MeOH) λ_{max} (log ε) 277 (3.10), 227 (3.09), 241 (3.02); ^1H NMR (500 MHz, C_6D_6): δ_H 7.05 (1H, d, *J* = 7.6, H-3), 6.71 (1H, d, *J* = 7.6 Hz, H-4), 6.40 (1H, bs, H-2), 5.57 (1H, m, H-9), 5.52 (1H, bd, *J* = 15.3 Hz, H-10), 3.33 (1H, m, H-7), 2.42 (1H, m, H-8a or H-8b), 2.28 (1H, m, H-8b, or H8a), 2.14 (1H, s, H-15), 1.28 (3H, d, *J* = 7.0 Hz, H-14), 1.15 (3H, s, H-12 or H-13), 1.14 (3H, s, H-13 or H-12); ^1H NMR (500 MHz, DMSO-*d*$_6$): δ_H 9.09 (1H, b, 9-OH), 6.91 (1H, d, *J* = 7.63 Hz, H-5), 6.58 (1H, s, H-2), 6.53 (1H, d, *J* = 7.63 Hz, H-4), 5.53-5.39 (2H, m, H-9 and H-10), 4.35 (1H, b, 11-OH), 3.03 (1H, m, H-7), 2.28-2.05 (2H, m, H-8a, H-8b), 2.16 (3H, s, H-15), 1.16 (6H, bs, H-12, H-13), 1.09 (3H, bd, H-14); ^{13}C NMR (100 MHz, DMSO-*d*$_6$): δ_C 154.1 (C, C-1), 140.3 (CH, C-10), 135.2 (C, C-3), 129.7 (C, C-6), 126.3 (CH, C-5), 123.8 (CH, C-9), 119.4 (CH, C-4), 115.1 (CH, C-2), 68.7 (C, C-11), 38.8 (CH_2, C-8), 31.4 (CH, C-7), 29.7 (CH_3, C-12, C-13), 20.6 (CH_3, C-15), 19.7 (CH_3, C-14); LRESIMS *m/z* 257; HRESIMS *m/z* 257.1515 (calc'd for $C_{15}H_{20}O_2Na$ 257.1517).

Abolenone (5.25): yellow oil. $[\alpha]_D^{22}$: +8.8 (c 2.6, MeOH); UV (MeOH) λ_{max} (log ε) 277 (2.89); CD λ_{max} ($\Delta\varepsilon$ (MeOH) 280 nm (-187.87); ^1H NMR and ^{13}C NMR see Table 5.5.1; LRESIMS *m/z* 255; HRESIMS *m/z* 255.1360 (calc'd for $C_{15}H_{20}O_2Na$ 255.1361).

(+)-Curcuphenol (5.26): yellow oil. $[\alpha]_D^{21}$: +25.2 (c 0.84, $CHCl_3$); UV (MeOH) λ_{max} (log ε) 277 (3.03), 240 (2.65); CD λ_{max} (Δε (MeOH) 280 nm (-141.18); ^1H NMR (500 MHz, $CDCl_3$): δ_H 7.04 (1H, d, *J* = 7.8 Hz, H-5), 6.73 (1H, d, *J* = 7.8 Hz, H-4), 6.59 (1H, s, H-2), 5.13 (1H, m, H-10), 4.63 (1H, s, OH), 2.97 (1H, m, H-7), 2.27 (3H, s, H-15), 1.94 (2H, m, H-9), 1.69 (3H, s, H-12 or H-13), 1.69-1.56 (2H, m, H-8a, H-8b), 1.54 (3H, s, H-13 or H-12), 1.23 (3H, d, *J* = 7.0 Hz, H-14); ^{13}C NMR (125 MHz, $CDCl_3$): δ_C 153.0 (C, C-1), 136.5 (C, C-6), 131.9 (C, C-11), 130.0 (C, C-3), 126.8 (CH, C-5), 124.6 (CH, C-10), 121.6 (CH, C-4), 116.2 (CH, C-2), 37.3 (CH_2, C-8), 31.4 (CH, C-7), 26.1 (CH_2, C-9), 25.7 (CH_3, C-12 or C-13), 21.1 (CH_3, C-15), 20.9 (CH_3, C-14), 17.7 (CH_3, C-13 or C-12); LRESIMS *m/z* 217; HRESIMS *m/z* 217.1590 [M^+] (calc'd for $C_{15}H_{21}O$ 217.1592).

Myrmekioside C peracetate (5.28): yellow oil. $[\alpha]_D^{21}$: -18.2 (c 0.45, EtOAc); For ^1H NMR and ^{13}C NMR see Table 5.6.1.; LRESIMS *m/z* 1301; HRESIMS *m/z* 1301.5774 (calc'd for $C_{60}H_{94}O_{29}Na$ 1301.5778).

5.12. References

(1) Hammond G.L. *Trends in Endocrinology and Metabolism* **1995**, *6*, 398-304.

(2) Hammond G.L.; Avvakumov G.V.; Muller Y.A. *Journal of Steroid Biochemistry and Molecular Biology* **2003**, *85*, 195-200.

(3) Schottner M.; Spiteller G. *Journal of Natural Products* **1998**, *61*, 119-121.

(4) Selby C. *Annals of Clinical Biochemistry* **1990**, *27*, 532-541.

(5) Joseph D.R. *Vitamins and Hormones* **1994**, *49*, 197-280.

(6) Handelsman D.J.; Swerdloff R.S. *Clinics in endocrinology and metabolism* **1985**, *14*, 89-124.

(7) Estour B.; Pugaeat M.; Lang F.; Dechaud H.; Pellet J.; Rousset H. *Clinical Endocrinology* **1986**, *24*, 571-576.

(8) Rapuri P.B.; Gallagher J.C.; Haynatzki G. *The Journal of Clinical Endocrinology and Metabolism* **2004**, *89*, 4954-4962.

(9) Cherkasov A.; Shi Z.; Fallahi M.; Hammond G.L. *Journal of Medicinal Chemistry* **2005**, *48*, 3203-3213.

(10) Charkasov A.; Ban F.; Li Y.; Fallahi M.; Hammond G.L. *Journal of Medicinal Chemistry* **2006**, *49*, 7466-7478.

(11) Hooper J.N.A.; Soest R.W.M Van *System Porifera A Guide to Classification of Sponges*; Kluwer Academic/Plenum Publishers: New York, 2002.

(12) Albrizio S.; Faitorusso E.; Magno S.; Mangoni A. *Journal of Natural Products* **1992**, *55*, 1287-1293.

(13) Sennet S.H.; Pomponi S.A.; Wright A.E. *Journal of Natural Products* **1992**, *55*, 1421-1429.

(14) Peng J. Walsh K., Weedman V., Bergthold J.D., Lynch J., Lieu K.L., Braude I.A., Kelly M., Hamann M.T. *Tetrahedron* **2002**, *58*, 7809-7819.

(15) Peng J. Avery M.A., Hamann M.T. *Organic Letters* **2003**, *5*, 4575-4578.

(16) Tsukamato S.; Haryko K.; Hirota H.; Fusetani N. *Biofouling* **1997**, *11*, 283-291.

(17) Letourneux Y.; Brunel J.M.; Fernandez R.; Dherbomez M.; Debitus C. *Heterocyclic Communications* **2005**, *11*, 291-298.

(18) Peng J.; Franzblau S.G.; Zhang F.; Hamann M.T. *Tetrahedron Letters* **2002**, *43*, 9699-9702.

(19) Aoki S.; Higuchi K.; Kato A.; Murakami N.; Kobayashi M. *Tetrahedron* **1999**, *55*, 14865-14870.

(20) Butler M.S.; Capon R.J.; Nadeson R.; Beveridge A.A. *Journal of Natural Productrs* **1991**, *54*, 619-623.

(21) Wright A.E.; Pomponi S.A.; McConnell O.J.; Kohmoto S.; McCarthy P.J. *Journal of Natural Productrs* **1987**, *50*, 976-978.

(22) Hammond G.L.; Lahteenmaki P.L. *Clinica Chimica Acta* **1983**, *132*, 101-110.

Chapter 6: Conclusions

6.1. Conclusions

The overarching goal in the Andersen lab is to isolate bioactive small molecules that can be potential drug leads. The research presented in the second chapter of the dissertation describes a successful example of this goal. The MeOH extract of the sponge *Neopetrosia exigua* displayed potent inhibitory activity against IDO. Bioassay guided fractionation of *N. exigua* led to the isolation and identification of two novel alkaloids, exiguamines A (**2.58**) and B (**2.59**).[1] The proposed pharmacophore of the exiguamines is the tryptamine-quinone moiety. Currently, synthetic analogs of the tryptamine-quinone moiety are being prepared and evaluated as novel inhibitors of IDO. Very recently, one of the synthetic tryptamine-quinones was found to be an inhibitor of IDO in the yeast based assay.[2,3] Clearly, based on this result, derivatives of the tryptamine-quinone moiety represent a new drug lead to develop inhibitors of IDO as potential treatments for cancer.

Biological studies found that exiguamine A had a K_i of 210 nM, making it among the most potent IDO inhibitors found to date. Unfortunately, exiguamine A was unable to inhibit IDO in a yeast based assay.[2] The presence of the quaternary ammonium cation in exiguamine A most likely prohibited exiguamine A from crossing the cell membrane. Even though exiguamine B was found to be an inhibitor of IDO, a K_i value was not obtained for this alkaloid. Finding the K_i value may establish the effect on the biological activity of having a hydroxyl group on C-17. More biological studies on the exiguamines are needed to

determine if this family of alkaloids are competitive or non-competitive inhibitors. Finally, work is currently being done to crystallize exiguamine A with IDO. This may establish which parts of the compound form the pharmacophore.

Future investigations are required to determine the stability of the two enantiomers of exiguamine A. If the two enantiomers of exiguamine A can be separated, then one can evaluate to see if the configuration at C-19 plays a role in the inhibition of IDO. Finally, further purifications need to be performed to separate the diastereomers of exiguamine B. Biological studies may reveal the importance of the stereochemistry at both C-17 and C-19.

Another goal of the Andersen lab is to assist in the development of biological screens. Chapter three of this dissertation provides an example of this goal. Cyclo(S-Val-S-Phe) (**3.9**) and cyclo(R-Val-R-Phe) (**3.22**) were found to be neurite outgrowth activators using a novel bioassay. The study validates that this screen may be used to discover new axonal outgrowth activators from natural sources.

The discovery of cyclo(S-Val-S-Phe) (**3.9**) and cyclo(R-Val-R-Phe) (**3.22**) as both *in vivo* and *in vitro* activators of neuronal outgrowth may have an impact in the search for pharmaceuticals to promote spinal cord repair. Currently, the biological mechanism of these two compounds is unknown. Elucidation of how these two diketopiperazines overcome the inhibition of spinal cord repair may yield new protein targets and potentially a new class of drugs. Furthermore, because of the simple structures of both compounds, a combinatorial library of cis-diketopiperazines may yield a more potent neurite outgrowth activator.

Chapter four described the purification and structure elucidation of compounds inhibiting the G_2 checkpoint pathway. The MeOH extract of *Duguetia odorata* showed G_2 checkpoint inhibitory activity. Fractionation of a crude extract of *D. odorata* led to the isolation of the known alkaloids oliveroline (**4.32**), dehydrodiscretine (**4.34**), pseudopalmatine (**4.35**), and the new alkaloid, *N*-methylguatterine (**4.33**).[4] Oliveroline was active in the G_2 checkpoint assay at concentrations above 10 μM. This alkaloid is structurally distinct from other G_2 checkpoint inhibitors and does not inhibit Chk1. Finding oliveroline's mechanism of inhibition may yield new information about the G_2 checkpoint pathway, and may potentially lead to the discovery of a new target against cancer.

Chapter five describes the isolation and identification of potential ligands for SHBG. The MeOH extract of the marine sponge *Myrmekioderma granulatum* displayed activity in the SHBG ligand binding assay. Chromatographic separation of a crude extract of *M. granulatum* led to the isolation and identification of **5.22**, abolene (**5.23**), (+)-curcudiol (**5.24**), abolenone (**5.25**), (+)-curcuphenol (**5.26**), and myrmekioside C (**5.27**). Myrmekioside C (**5.27**) contained a rare saturated lipid moiety that is oxygenated on both ends of the linear chain. Biological studies have revealed (+)-curcudiol to be a weak ligand of SHBG. This terpenoid may be used as a lead structure to develop stronger binding SHBG ligands. The discovery of (+)-curcudiol represents the first SHBG ligand that was discovered from a marine source. This research provides proof of principle that marine organisms can provide new ligands for SHBG.

6.2. References

(1) Brastianos H.C.; Vottero E.; Patrick B.O.; Soest R. van; Matainaho T.; Mauk A.G.; Andersen R.J. *Journal of the American Chemical Society* **2006**, *128*, 16046-16047.

(2) Vottero E.; Balgi A.; Woods K.; Tugendreich S.; Melese T.; Andersen R.J.; Mauk A.G.; Roberge M. *Biotechnology Journal* **2006**, *1*, 282-288.

(3) Andersen R.J. Personal Communication, **June 2007**.

(4) Brastianos H.C.; Sturgeon C.M.; Roberge M.; Andersen R.J. *Journal of Natural Products* **2007**, *70*, 287-288.

Appendix: Experimental Details for X-ray Diffraction Analysis of Exiguamine A

A.1. Data Collection

An irregular red crystal of $C_{25}H_{27}N_5O_6.Cl.½VS_4H_2.2H_2O$ having approximate dimensions of 0.05 x 0.25 x 0.30 mm was mounted on a glass fiber. All measurements were made on a Bruker X8 APEX diffractometer with graphite monochromated Mo-Kα radiation.

The data were collected at a temperature of -100.0 ± 0.1°C to a maximum 2θ value of 45.2°. Data were collected in a series of φ and ω scans in 0.50° oscillations with 45.0 second exposures. The crystal-to-detector distance was 38.85 mm.

A.2. Data Reduction

The material crystallizes as a two-component twin with the two components related by a 180° rotation about the (1 0 0) reciprocal axis. Data were integrated for both twin components, including both overlapped and non-overlapped reflections. In total 41468 reflections were integrated (18959 from component one only, 18804 from component two only, 3667 overlapped). Data were collected and integrated using the Bruker SAINT[1] software packages. The linear absorption coefficient, μ, for Mo-Kα radiation is 4.65 cm^{-1}. Data were corrected for absorption effects using the multi-scan technique (TWINABS),[2] with minimum and maximum transmission coefficients of 0.682 and 0.977, respectively. The data were corrected for Lorentz and polarization effects.

A.3 Structure Solution and Refinement

The structure was solved by direct methods using non-overlapped data from the major twin component.[3] Subsequent refinements were carried out using an HKLF 5 format data set containing complete data from both twin components. It was immediately evident that the two anions in this material (Cl^- and $V(SH)_2S_2^{2-}$) are very different. The chloride anion was easily identified, however the vanadium anion was less evident. Residual electron density clearly showed a disordered tetrahedron residing on a two-fold axis. The bond distances to the central atom (2.2 –2.35 A) were too long to be any common organic anion (i.e. phosphate, chlorate, etc). Additionally, the electron density surrounding the central atom was greater than what one would expect for oxygen atoms. The residual electron density of the central atom is consistent with an early first-row transition metal. Ultimately, vanadium was chosen as the central atom, and refinement of its site-occupation factor (sof) gave a value of 1.08 (1). The disordered atoms surrounding the central V are consistent with sulfur atoms (i.e. refinement of their populations as sulfur gives a value nearly equal to 1, and V-S and V=S distances are consistent with those found in literature).[4,5] Additionally, two disordered water molecules are found in the lattice. All non-hydrogen atoms except C(11) were refined anisotropically. All hydrogen atoms were included in calculated positions but not refined. The batch scale refinement showed a roughly 96:4 ratio between the major and minor twin components. The final cycle of full-matrix least-squares refinement[6] on F^2 was based on 21334 reflections from both twin components and 395 variable parameters and converged (largest

parameter shift was 0.00 times its esd) with unweighted and weighted agreement factors of:

$$R1 = \Sigma \, ||Fo| - |Fc|| \, / \, \Sigma \, |Fo| = 0.247$$

$$wR2 = [\Sigma (w (Fo^2 - Fc^2)^2) / \Sigma \, w(Fo^2)^2]^{1/2} = 0.515$$

The standard deviation of an observation of unit weight was 1.02.[7] The weighting scheme was based on counting statistics. The maximum and minimum peaks on the final difference Fourier map corresponded to 1.04 and -1.07 $e^-/Å^3$, respectively.

Neutral atom scattering factors were taken from Cromer and Waber.[8] Anomalous dispersion effects were included in Fcalc,[9] the values for $\Delta f'$ and $\Delta f''$ were those of Creagh and McAuley.[10] The values for the mass attenuation coefficients are those of Creagh and Hubbell.[11] All refinements were performed using the SHELXTL crystallographic software package of Bruker-AXS.[12]

A.4.1. Experiemental Details, Crystal Data

Empirical Formula	$C_{25}H_{32}N_5O_8S_2ClV_{0.5}$
Formula Weight	655.60
Crystal Color, Habit	red, irregular
Crystal Dimensions	0.05 X 0.25 X 0.30 mm
Crystal System	monoclinic
Lattice Type	C-centered
Lattice Parameters	a = 32.833(7) Å b = 8.462(2) Å c = 23.947(5) Å $\alpha = 90^o$ $\beta = 114.891(9)^o$ $\gamma = 90^o$ V = 6035(2) $Å^3$
Space Group	*C* 2/*c* (#15)
Z value	8
D_{calc}	1.443 g/cm^3
F_{000}	2732.00
μ(MoKα)	4.65 cm^{-1}

A.4.2. Experimental Details, Intensity Measurements

Diffractometer	Bruker X8 APEX
Radiation	MoKα (λ = 0.71073 Å) graphite monochromated
Data Images	1105 exposures @ 45.0 seconds
Detector Position	38.85 mm
$2\theta_{max}$	45.2°
No. of Reflections Measured	Total: 21334
Corrections	Unique: 41468 (R_{int} = 0.108) Absorption (T_{min} = 0.682, T_{max}= 0.977) Lorentz-polarization

A.4.3. Experimental Details, Structure Solution and Refinement

Structure Solution	Direct Methods (SIR97)
Refinement	Full-matrix least-squares on F^2
Function Minimized	$\Sigma w (Fo^2 - Fc^2)^2$
Least Squares Weights	$w=1/(\sigma^2(Fo^2)+(0.1479P)^2+812.3206P)$
Anomalous Dispersion	All non-hydrogen atoms
No. Observations (I>0.00□(I))	21334
No. Variables	390
Reflection/Parameter Ratio	54.70
Residuals (refined on F^2, all data): R1; wR2	0.247; 0.515
Goodness of Fit Indicator	1.02
No. Observations (I>2.00σ(I))	12745
Residuals (refined on F): R1; wR2	0.188; 0.481
Max Shift/Error in Final Cycle	0.00
Maximum peak in Final Diff. Map	1.04 $e^-/Å^3$
Minimum peak in Final Diff. Map	-1.06$e^-/Å^3$

Table A.4.1. Atomic coordinates (x 10^4) and equivalent isotropic displacement parameters (A^2 x 10^3) for exigumaine A.
U(eq) is defined as one third of the trace of the orthogonalized Uij tensor.

	x	y	z	U(eq)
C(2)	3365(4)	4485(12)	5790(5)	60(3)
C(3)	3303(4)	3273(12)	6108(5)	58(3)
C(4)	2821(3)	3141(11)	5948(5)	43(3)
C(5)	2569(3)	2065(11)	6141(5)	44(3)
C(6)	2068(3)	2260(10)	5794(4)	38(3)
C(7)	1857(4)	3481(10)	5347(5)	44(3)
C(8)	2152(4)	4401(10)	5142(5)	47(3)
C(9)	2626(3)	4292(12)	5506(4)	46(3)
C(10)	1395(3)	3585(9)	5073(4)	37(3)
C(11)	1144(3)	2258(10)	5137(4)	35(2)
C(12)	672(4)	2140(10)	4889(5)	54(3)
C(13)	416(4)	3472(11)	4565(6)	62(3)
C(14)	646(4)	4803(11)	4515(5)	50(3)
C(16)	817(4)	7503(12)	4527(5)	64(3)
C(17)	1221(4)	6550(11)	4656(6)	64(3)
C(18)	1128(4)	4942(10)	4782(4)	48(3)
C(19)	1806(3)	1137(10)	5957(5)	39(3)
C(21)	1853(4)	256(11)	6893(5)	45(3)
C(23)	1999(4)	-597(15)	6099(6)	64(4)
C(24)	3690(5)	2315(14)	6575(5)	74(4)
C(25)	3728(4)	2450(15)	7224(4)	67(4)
C(27)	92(4)	6684(11)	4430(5)	57(3)
C(28)	277(6)	6163(18)	3534(6)	131(7)
C(29)	2125(4)	-2602(10)	6905(5)	58(3)
C(30)	1602(4)	2959(13)	6650(6)	81(4)
N(1)	2941(3)	5060(9)	5376(5)	63(3)
N(15)	445(3)	6295(9)	4259(4)	51(2)
N(20)	1759(3)	1501(8)	6523(4)	50(2)
N(22)	1988(3)	-1005(9)	6625(4)	46(2)
N(26)	4072(4)	1234(13)	7616(5)	104(4)
O(1)	1360(2)	931(7)	5447(3)	55(2)
O(2A)	3196(6)	-2396(18)	6616(7)	61(6)
O(2B)	3850(6)	-1629(17)	7091(7)	86(6)
O(4A)	4207(5)	4842(13)	8858(5)	61(5)
O(5)	2704(2)	1123(8)	6551(3)	56(2)
O(8)	1995(2)	5183(8)	4647(3)	60(2)
O(12)	466(3)	880(8)	4971(5)	85(3)
O(21)	1851(3)	198(8)	7395(4)	70(2)
O(23)	2071(2)	-1406(7)	5714(4)	51(2)
Cl(1)	882(1)	6298(3)	6078(1)	64(1)
V(1)	5000	-5491(2)	7500	31(1)
S(1)	4847(4)	-5644(9)	6461(3)	105(3)
S(2)	5049(3)	-8072(7)	7749(3)	80(2)
S(3A)	4468(3)	-4341(8)	7709(4)	87(2)
S(3B)	4369(3)	-4036(15)	7086(7)	182(7)
O(4B)	4682(12)	4750(30)	9096(14)	125(13)

Table A.4.2. Bond lengths [Å] and angles [deg] for exiguamine A.

Bonds	Bond Lenghts [Å] (angle (deg))
C(2)-C(3)	1.343(14)
C(2)-N(1)	1.412(14)
C(2)-H(2)	0.9500
C(3)-C(4)	1.467(15)
C(3)-C(24)	1.527(15)
C(4)-C(9)	1.381(13)
C(4)-C(5)	1.430(14)
C(5)-O(5)	1.196(11)
C(5)-C(6)	1.508(14)
C(6)-C(7)	1.439(12)
C(6)-C(19)	1.441(13)
C(7)-C(10)	1.379(14)
C(7)-C(8)	1.476(14)
C(8)-O(8)	1.263(11)
C(8)-C(9)	1.431(14)
C(9)-N(1)	1.367(13)
C(10)-C(18)	1.435(12)
C(10)-C(11)	1.439(12)
C(11)-O(1)	1.368(10)
C(11)-C(12)	1.411(14)
C(12)-O(12)	1.320(11)
C(12)-C(13)	1.424(13)
C(13)-C(14)	1.390(14)
C(13)-H(13)	0.9500
C(14)-N(15)	1.437(11)
C(14)-C(18)	1.440(15)
C(16)-C(17)	1.471(15)
C(16)-N(15)	1.513(13)
C(16)-H(16A)	0.9900
C(16)-H(16B)	0.9900
C(17)-C(18)	1.454(13)
C(17)-H(17A)	0.9900
C(17)-H(17B)	0.9900
C(19)-N(20)	1.461(13)
C(19)-O(1)	1.472(11)
C(19)-C(23)	1.577(14)
C(21)-O(21)	1.206(12)
C(21)-N(20)	1.326(12)
C(21)-N(22)	1.410(12)
C(23)-O(23)	1.249(14)
C(23)-N(22)	1.320(14)
C(24)-C(25)	1.510(15)
C(24)-H(24A)	0.9900
C(24)-H(24B)	0.9900
C(25)-N(26)	1.525(13)
C(25)-H(25A)	0.9900
C(25)-H(25B)	0.9900
C(27)-N(15)	1.420(13)
C(27)-H(27A)	0.9800
C(27)-H(27B)	0.9800
C(27)-H(27C)	0.9800
C(28)-N(15)	1.589(15)
C(28)-H(28A)	0.9800

C(28)-H(28B)	0.9800
C(28)-H(28C)	0.9800
C(29)-N(22)	1.492(11)
C(29)-H(29A)	0.9800
C(29)-H(29B)	0.9800
C(29)-H(29C)	0.9800
C(30)-N(20)	1.418(12)
C(30)-H(30A)	0.9800
C(30)-H(30B)	0.9800
C(30)-H(30C)	0.9800
N(1)-H(1)	0.8800
N(26)-H(26A)	0.9100
N(26)-H(26B)	0.9100
N(26)-H(26C)	0.9100
O(4A)-O(4B)	1.42(3)
O(12)-H(12)	0.8400
V(1)-S(3A)#1	2.233(7)
V(1)-S(3A)	2.233(7)
V(1)-S(3B)#1	2.249(10)
V(1)-S(3B)	2.249(10)
V(1)-S(2)#1	2.252(6)
V(1)-S(2)	2.252(6)
V(1)-S(1)	2.324(7)
V(1)-S(1)#1	2.324(7)
S(1)-S(3A)#1	2.543(13)
S(2)-S(2)#1	1.099(13)
S(3A)-S(3B)	1.412(14)
S(3A)-S(1)#1	2.543(13)
C(3)-C(2)-N(1)	108.8(10)
C(3)-C(2)-H(2)	125.6
N(1)-C(2)-H(2)	125.6
C(2)-C(3)-C(4)	108.4(9)
C(2)-C(3)-C(24)	122.8(12)
C(4)-C(3)-C(24)	128.7(10)
C(9)-C(4)-C(5)	123.5(10)
C(9)-C(4)-C(3)	104.3(9)
C(5)-C(4)-C(3)	132.1(9)
O(5)-C(5)-C(4)	128.7(10)
O(5)-C(5)-C(6)	117.8(9)
C(4)-C(5)-C(6)	113.4(8)
C(7)-C(6)-C(19)	121.4(9)
C(7)-C(6)-C(5)	124.0(8)
C(19)-C(6)-C(5)	114.6(8)
C(10)-C(7)-C(6)	119.2(9)
C(10)-C(7)-C(8)	123.5(8)
C(6)-C(7)-C(8)	116.7(9)
O(8)-C(8)-C(9)	121.0(10)
O(8)-C(8)-C(7)	121.5(10)
C(9)-C(8)-C(7)	117.4(8)
N(1)-C(9)-C(4)	111.1(9)
N(1)-C(9)-C(8)	124.4(9)
C(4)-C(9)-C(8)	123.1(9)
C(7)-C(10)-C(18)	127.4(9)
C(7)-C(10)-C(11)	117.7(8)
C(18)-C(10)-C(11)	114.5(9)
O(1)-C(11)-C(12)	113.3(8)

O(1)-C(11)-C(10)	120.6(8)
C(12)-C(11)-C(10)	126.0(8)
O(12)-C(12)-C(11)	122.4(8)
O(12)-C(12)-C(13)	119.9(10)
C(11)-C(12)-C(13)	117.7(9)
C(14)-C(13)-C(12)	118.1(10)
C(14)-C(13)-H(13)	121.0
C(12)-C(13)-H(13)	121.0
C(13)-C(14)-N(15)	125.4(11)
C(13)-C(14)-C(18)	124.3(9)
N(15)-C(14)-C(18)	109.9(8)
C(17)-C(16)-N(15)	102.4(8)
C(17)-C(16)-H(16A)	111.3
N(15)-C(16)-H(16A)	111.3
C(17)-C(16)-H(16B)	111.3
N(15)-C(16)-H(16B)	111.3
H(16A)-C(16)-H(16B)	109.2
C(18)-C(17)-C(16)	107.8(10)
C(18)-C(17)-H(17A)	110.1
C(16)-C(17)-H(17A)	110.1
C(18)-C(17)-H(17B)	110.1
C(16)-C(17)-H(17B)	110.1
H(17A)-C(17)-H(17B)	108.5
C(10)-C(18)-C(14)	118.9(8)
C(10)-C(18)-C(17)	135.3(11)
C(14)-C(18)-C(17)	105.8(9)
C(6)-C(19)-N(20)	114.8(8)
C(6)-C(19)-O(1)	110.6(8)
N(20)-C(19)-O(1)	109.8(8)
C(6)-C(19)-C(23)	116.2(9)
N(20)-C(19)-C(23)	100.7(8)
O(1)-C(19)-C(23)	103.8(8)
O(21)-C(21)-N(20)	126.8(10)
O(21)-C(21)-N(22)	124.0(9)
N(20)-C(21)-N(22)	109.1(9)
O(23)-C(23)-N(22)	130.6(11)
O(23)-C(23)-C(19)	122.3(10)
N(22)-C(23)-C(19)	106.2(11)
C(25)-C(24)-C(3)	113.2(10)
C(25)-C(24)-H(24A)	108.9
C(3)-C(24)-H(24A)	108.9
C(25)-C(24)-H(24B)	108.9
C(3)-C(24)-H(24B)	108.9
H(24A)-C(24)-H(24B)	107.7
C(24)-C(25)-N(26)	107.5(10)
C(24)-C(25)-H(25A)	110.2
N(26)-C(25)-H(25A)	110.2
C(24)-C(25)-H(25B)	110.2
N(26)-C(25)-H(25B)	110.2
H(25A)-C(25)-H(25B)	108.5
N(15)-C(27)-H(27A)	109.5
N(15)-C(27)-H(27B)	109.5
H(27A)-C(27)-H(27B)	109.5
N(15)-C(27)-H(27C)	109.5
H(27A)-C(27)-H(27C)	109.5
H(27B)-C(27)-H(27C)	109.5

N(15)-C(28)-H(28A)	109.5
N(15)-C(28)-H(28B)	109.5
H(28A)-C(28)-H(28B)	109.5
N(15)-C(28)-H(28C)	109.5
H(28A)-C(28)-H(28C)	109.5
H(28B)-C(28)-H(28C)	109.5
N(22)-C(29)-H(29A)	109.5
N(22)-C(29)-H(29B)	109.5
H(29A)-C(29)-H(29B)	109.5
N(22)-C(29)-H(29C)	109.5
H(29A)-C(29)-H(29C)	109.5
H(29B)-C(29)-H(29C)	109.5
N(20)-C(30)-H(30A)	109.5
N(20)-C(30)-H(30B)	109.5
H(30A)-C(30)-H(30B)	109.5
N(20)-C(30)-H(30C)	109.5
H(30A)-C(30)-H(30C)	109.5
H(30B)-C(30)-H(30C)	109.5
C(9)-N(1)-C(2)	107.0(9)
C(9)-N(1)-H(1)	126.5
C(2)-N(1)-H(1)	126.5
C(27)-N(15)-C(14)	111.4(8)
C(27)-N(15)-C(16)	109.4(8)
C(14)-N(15)-C(16)	105.5(8)
C(27)-N(15)-C(28)	112.5(10)
C(14)-N(15)-C(28)	106.9(8)
C(16)-N(15)-C(28)	110.9(11)
C(21)-N(20)-C(30)	123.5(10)
C(21)-N(20)-C(19)	111.4(8)
C(30)-N(20)-C(19)	124.9(9)
C(23)-N(22)-C(21)	112.1(9)
C(23)-N(22)-C(29)	122.8(10)
C(21)-N(22)-C(29)	125.0(9)
C(25)-N(26)-H(26A)	109.5
C(25)-N(26)-H(26B)	109.5
H(26A)-N(26)-H(26B)	109.5
C(25)-N(26)-H(26C)	109.5
H(26A)-N(26)-H(26C)	109.5
H(26B)-N(26)-H(26C)	109.5
C(11)-O(1)-C(19)	117.4(7)
C(12)-O(12)-H(12)	109.5
S(3A)#1-V(1)-S(3A)	128.3(4)
S(3A)#1-V(1)-S(3B)#1	36.7(4)
S(3A)-V(1)-S(3B)#1	108.9(3)
S(3A)#1-V(1)-S(3B)	108.9(3)
S(3A)-V(1)-S(3B)	36.7(4)
S(3B)#1-V(1)-S(3B)	113.6(6)
S(3A)#1-V(1)-S(2)#1	109.8(3)
S(3A)-V(1)-S(2)#1	120.5(3)
S(3B)#1-V(1)-S(2)#1	126.7(3)
S(3B)-V(1)-S(2)#1	117.7(4)
S(3A)#1-V(1)-S(2)	120.5(3)
S(3A)-V(1)-S(2)	109.8(3)
S(3B)#1-V(1)-S(2)	117.7(4)
S(3B)-V(1)-S(2)	126.7(3)
S(2)#1-V(1)-S(2)	28.2(3)

S(3A)#1-V(1)-S(1)	67.8(4)
S(3A)-V(1)-S(1)	115.2(4)
S(3B)#1-V(1)-S(1)	104.3(5)
S(3B)-V(1)-S(1)	79.3(5)
S(2)#1-V(1)-S(1)	72.7(3)
S(2)-V(1)-S(1)	100.9(3)
S(3A)#1-V(1)-S(1)#1	115.2(4)
S(3A)-V(1)-S(1)#1	67.8(4)
S(3B)#1-V(1)-S(1)#1	79.3(5)
S(3B)-V(1)-S(1)#1	104.3(5)
S(2)#1-V(1)-S(1)#1	100.9(3)
S(2)-V(1)-S(1)#1	72.7(3)
S(1)-V(1)-S(1)#1	173.6(4)
V(1)-S(1)-S(3A)#1	54.4(3)
S(2)#1-S(2)-V(1)	75.88(17)
S(3B)-S(3A)-V(1)	72.3(6)
S(3B)-S(3A)-S(1)#1	129.7(7)
V(1)-S(3A)-S(1)#1	57.8(3)
S(3A)-S(3B)-V(1)	71.0(5)

Symmetry transformations used to generate equivalent atoms:
#1 -x+1,y,-z+3/2

Table A.4.3. Anisotropic displacement parameters (A^2 x 10^3) for exiguamine A. The anisotropic displacement factor exponent takes the form: -2 pi^2 [h^2 a*^2 U11 + ... + 2 h k a* b* U12]

	U11	U22	U33	U23	U13	U12
C(2)	43(8)	56(7)	66(8)	8(6)	7(6)	-17(6)
C(3)	56(9)	66(7)	44(7)	22(6)	15(6)	11(6)
C(4)	31(7)	48(6)	47(6)	-4(5)	13(5)	-10(5)
C(5)	39(7)	45(6)	56(7)	15(5)	27(6)	13(5)
C(6)	30(6)	33(5)	47(6)	4(4)	13(5)	-9(4)
C(7)	47(8)	26(5)	47(6)	13(4)	10(6)	1(5)
C(8)	64(8)	25(5)	48(7)	21(5)	19(6)	6(5)
C(9)	28(7)	63(7)	36(6)	17(5)	3(5)	-3(5)
C(10)	34(7)	26(5)	41(6)	2(4)	5(5)	1(4)
C(12)	42(7)	24(5)	65(7)	6(5)	-9(6)	-6(5)
C(13)	45(8)	46(7)	91(9)	-29(6)	24(7)	-25(6)
C(14)	64(9)	36(6)	49(7)	6(5)	24(6)	-5(5)
C(16)	68(9)	51(7)	63(8)	17(6)	16(7)	15(7)
C(17)	73(9)	41(6)	77(9)	6(6)	31(7)	7(6)
C(18)	65(8)	24(5)	30(6)	5(4)	-4(6)	-6(5)
C(19)	21(6)	32(5)	62(7)	5(5)	15(5)	-1(4)
C(23)	27(7)	76(9)	92(10)	49(8)	29(7)	20(6)
C(24)	81(10)	74(8)	70(9)	18(7)	34(8)	21(7)
C(25)	55(8)	108(10)	30(6)	5(6)	12(6)	-11(7)
C(27)	75(9)	38(6)	67(8)	-5(5)	40(7)	14(6)
C(28)	173(19)	155(15)	70(10)	41(10)	55(12)	95(13)
C(29)	71(9)	31(5)	58(7)	11(5)	14(7)	-5(5)
C(30)	58(9)	72(8)	98(11)	-16(7)	18(8)	16(7)
N(1)	58(7)	42(5)	100(8)	8(5)	44(7)	-9(5)
N(15)	60(7)	36(5)	40(5)	13(4)	5(5)	16(5)
N(20)	57(6)	30(5)	59(6)	3(4)	20(5)	5(4)
N(22)	34(6)	53(5)	49(5)	20(4)	15(5)	4(4)
N(26)	66(8)	170(11)	84(8)	91(8)	39(7)	72(8)
O(1)	32(4)	50(4)	77(5)	28(4)	17(4)	8(3)
O(5)	38(5)	59(4)	63(5)	30(4)	14(4)	-2(4)
O(8)	50(5)	55(4)	65(5)	3(4)	16(4)	-16(4)
O(12)	40(5)	32(4)	167(9)	33(5)	27(6)	-2(3)
O(21)	89(7)	57(5)	83(6)	21(4)	53(5)	11(4)
O(23)	51(5)	25(4)	80(5)	16(4)	32(5)	8(3)
Cl(1)	74(2)	58(2)	65(2)	6(1)	33(2)	17(2)
V(1)	37(2)	23(1)	26(1)	0	6(1)	0
S(1)	167(9)	79(5)	62(5)	15(4)	43(5)	7(5)
S(2)	77(5)	67(4)	86(6)	23(3)	25(6)	19(4)
S(3A)	76(6)	69(4)	135(7)	-30(5)	62(5)	-19(4)
S(3B)	42(5)	236(13)	232(14)	166(11)	23(7)	3(6)

Table A.4.4. Hydrogen coordinates (x 10^4) and isotropic displacement parameters (A^2 x 10^3) for exiguamine A.

	x	y	z	U(eq)
H(2)	3647	4888	5836	73
H(13)	97	3451	4389	75
H(16A)	785	8354	4228	77
H(16B)	823	7976	4908	77
H(17A)	1297	6567	4297	77
H(17B)	1479	6985	5016	77
H(24A)	3649	1189	6451	89
H(24B)	3975	2679	6568	89
H(25A)	3433	2241	7230	80
H(25B)	3826	3528	7386	80
H(27A)	113	6016	4775	85
H(27B)	-198	6506	4079	85
H(27C)	117	7797	4553	85
H(28A)	98	5200	3386	197
H(28B)	538	6122	3434	197
H(28C)	93	7086	3335	197
H(29A)	2261	-3195	6675	87
H(29B)	1861	-3172	6889	87
H(29C)	2344	-2490	7334	87
H(30A)	1622	2942	7070	121
H(30B)	1289	3118	6357	121
H(30C)	1786	3824	6610	121
H(1)	2890	5778	5088	76
H(26A)	4020	297	7411	156
H(26B)	4049	1101	7978	156
H(26C)	4353	1580	7693	156
H(12)	314	454	4629	128

Table A.4.5. Torsion angles [deg] for exiguamine A.

N(1)-C(2)-C(3)-C(4)	-6.2(13)
N(1)-C(2)-C(3)-C(24)	176.8(10)
C(2)-C(3)-C(4)-C(9)	2.8(12)
C(24)-C(3)-C(4)-C(9)	179.6(11)
C(2)-C(3)-C(4)-C(5)	179.0(11)
C(24)-C(3)-C(4)-C(5)	-4(2)
C(9)-C(4)-C(5)-O(5)	-173.1(10)
C(3)-C(4)-C(5)-O(5)	11(2)
C(9)-C(4)-C(5)-C(6)	2.6(15)
C(3)-C(4)-C(5)-C(6)	-173.0(11)
O(5)-C(5)-C(6)-C(7)	171.6(9)
C(4)-C(5)-C(6)-C(7)	-4.6(14)
O(5)-C(5)-C(6)-C(19)	-6.8(14)
C(4)-C(5)-C(6)-C(19)	176.9(9)
C(19)-C(6)-C(7)-C(10)	0.7(15)
C(5)-C(6)-C(7)-C(10)	-177.6(9)
C(19)-C(6)-C(7)-C(8)	-170.5(9)
C(5)-C(6)-C(7)-C(8)	11.1(14)
C(10)-C(7)-C(8)-O(8)	-10.1(15)
C(6)-C(7)-C(8)-O(8)	160.7(9)
C(10)-C(7)-C(8)-C(9)	174.0(10)
C(6)-C(7)-C(8)-C(9)	-15.2(13)
C(5)-C(4)-C(9)-N(1)	-174.9(10)
C(3)-C(4)-C(9)-N(1)	1.7(12)
C(5)-C(4)-C(9)-C(8)	-8.0(17)
C(3)-C(4)-C(9)-C(8)	168.7(10)
O(8)-C(8)-C(9)-N(1)	3.5(16)
C(7)-C(8)-C(9)-N(1)	179.5(10)
O(8)-C(8)-C(9)-C(4)	-161.7(10)
C(7)-C(8)-C(9)-C(4)	14.3(15)
C(6)-C(7)-C(10)-C(18)	158.2(9)
C(8)-C(7)-C(10)-C(18)	-31.2(16)
C(6)-C(7)-C(10)-C(11)	-14.5(14)
C(8)-C(7)-C(10)-C(11)	156.1(9)
C(7)-C(10)-C(11)-O(1)	-1.5(14)
C(18)-C(10)-C(11)-O(1)	-175.1(8)
C(7)-C(10)-C(11)-C(12)	-179.7(10)
C(18)-C(10)-C(11)-C(12)	6.7(15)
O(1)-C(11)-C(12)-O(12)	2.0(16)
C(10)-C(11)-C(12)-O(12)	-179.7(10)
O(1)-C(11)-C(12)-C(13)	179.1(9)
C(10)-C(11)-C(12)-C(13)	-2.6(17)
O(12)-C(12)-C(13)-C(14)	176.9(11)
C(11)-C(12)-C(13)-C(14)	-0.2(16)
C(12)-C(13)-C(14)-N(15)	-173.6(10)
C(12)-C(13)-C(14)-C(18)	-1.5(17)
N(15)-C(16)-C(17)-C(18)	-29.0(12)
C(7)-C(10)-C(18)-C(14)	179.3(10)
C(11)-C(10)-C(18)-C(14)	-7.8(13)
C(7)-C(10)-C(18)-C(17)	2(2)
C(11)-C(10)-C(18)-C(17)	174.7(11)
C(13)-C(14)-C(18)-C(10)	5.9(16)
N(15)-C(14)-C(18)-C(10)	179.0(9)
C(13)-C(14)-C(18)-C(17)	-175.9(11)

N(15)-C(14)-C(18)-C(17)	-2.8(12)
C(16)-C(17)-C(18)-C(10)	-161.8(11)
C(16)-C(17)-C(18)-C(14)	20.5(12)
C(7)-C(6)-C(19)-N(20)	-98.6(11)
C(5)-C(6)-C(19)-N(20)	79.9(11)
C(7)-C(6)-C(19)-O(1)	26.3(13)
C(5)-C(6)-C(19)-O(1)	-155.2(8)
C(7)-C(6)-C(19)-C(23)	144.2(10)
C(5)-C(6)-C(19)-C(23)	-37.2(13)
C(6)-C(19)-C(23)-O(23)	-58.7(15)
N(20)-C(19)-C(23)-O(23)	176.6(11)
O(1)-C(19)-C(23)-O(23)	63.0(13)
C(6)-C(19)-C(23)-N(22)	131.0(10)
N(20)-C(19)-C(23)-N(22)	6.3(11)
O(1)-C(19)-C(23)-N(22)	-107.3(10)
C(2)-C(3)-C(24)-C(25)	116.6(14)
C(4)-C(3)-C(24)-C(25)	-59.7(16)
C(3)-C(24)-C(25)-N(26)	170.6(10)
C(4)-C(9)-N(1)-C(2)	-5.4(12)
C(8)-C(9)-N(1)-C(2)	-172.2(10)
C(3)-C(2)-N(1)-C(9)	7.2(13)
C(13)-C(14)-N(15)-C(27)	39.2(14)
C(18)-C(14)-N(15)-C(27)	-133.8(9)
C(13)-C(14)-N(15)-C(16)	157.8(11)
C(18)-C(14)-N(15)-C(16)	-15.2(11)
C(13)-C(14)-N(15)-C(28)	-84.0(14)
C(18)-C(14)-N(15)-C(28)	103.0(12)
C(17)-C(16)-N(15)-C(27)	146.6(9)
C(17)-C(16)-N(15)-C(14)	26.6(12)
C(17)-C(16)-N(15)-C(28)	-88.8(10)
O(21)-C(21)-N(20)-C(30)	-5.3(19)
N(22)-C(21)-N(20)-C(30)	178.4(10)
O(21)-C(21)-N(20)-C(19)	178.8(11)
N(22)-C(21)-N(20)-C(19)	2.5(12)
C(6)-C(19)-N(20)-C(21)	-130.9(9)
O(1)-C(19)-N(20)-C(21)	103.8(9)
C(23)-C(19)-N(20)-C(21)	-5.2(11)
C(6)-C(19)-N(20)-C(30)	53.3(14)
O(1)-C(19)-N(20)-C(30)	-72.1(12)
C(23)-C(19)-N(20)-C(30)	179.0(10)
O(23)-C(23)-N(22)-C(21)	-174.6(12)
C(19)-C(23)-N(22)-C(21)	-5.4(12)
O(23)-C(23)-N(22)-C(29)	8(2)
C(19)-C(23)-N(22)-C(29)	177.3(8)
O(21)-C(21)-N(22)-C(23)	-174.3(11)
N(20)-C(21)-N(22)-C(23)	2.2(13)
O(21)-C(21)-N(22)-C(29)	3.0(17)
N(20)-C(21)-N(22)-C(29)	179.5(9)
C(12)-C(11)-O(1)-C(19)	-150.5(9)
C(10)-C(11)-O(1)-C(19)	31.1(12)
C(6)-C(19)-O(1)-C(11)	-41.8(12)
N(20)-C(19)-O(1)-C(11)	86.0(9)
C(23)-C(19)-O(1)-C(11)	-167.1(8)
S(3A)-V(1)-S(1)-S(3A)#1	123.2(4)
S(3B)#1-V(1)-S(1)-S(3A)#1	3.8(4)
S(3B)-V(1)-S(1)-S(3A)#1	115.7(3)

S(2)#1-V(1)-S(1)-S(3A)#1	-120.7(3)
S(2)-V(1)-S(1)-S(3A)#1	-118.6(3)
S(1)#1-V(1)-S(1)-S(3A)#1	-119.6(2)
S(3A)#1-V(1)-S(2)-S(2)#1	-74.7(10)
S(3A)-V(1)-S(2)-S(2)#1	117.9(9)
S(3B)#1-V(1)-S(2)-S(2)#1	-116.8(9)
S(3B)-V(1)-S(2)-S(2)#1	80.5(11)
S(1)-V(1)-S(2)-S(2)#1	-4.1(10)
S(1)#1-V(1)-S(2)-S(2)#1	175.8(10)
S(3A)#1-V(1)-S(3A)-S(3B)	68.4(6)
S(3B)#1-V(1)-S(3A)-S(3B)	104.4(10)
S(2)#1-V(1)-S(3A)-S(3B)	-96.4(6)
S(2)-V(1)-S(3A)-S(3B)	-125.4(6)
S(1)-V(1)-S(3A)-S(3B)	-12.4(7)
S(1)#1-V(1)-S(3A)-S(3B)	173.8(7)
S(3A)#1-V(1)-S(3A)-S(1)#1	-105.3(3)
S(3B)#1-V(1)-S(3A)-S(1)#1	-69.4(5)
S(3B)-V(1)-S(3A)-S(1)#1	-173.8(7)
S(2)#1-V(1)-S(3A)-S(1)#1	89.8(3)
S(2)-V(1)-S(3A)-S(1)#1	60.8(3)
S(1)-V(1)-S(3A)-S(1)#1	173.9(4)
S(1)#1-S(3A)-S(3B)-V(1)	6.9(7)
S(3A)#1-V(1)-S(3B)-S(3A)	-129.5(5)
S(3B)#1-V(1)-S(3B)-S(3A)	-90.3(7)
S(2)#1-V(1)-S(3B)-S(3A)	104.8(6)
S(2)-V(1)-S(3B)-S(3A)	73.0(8)
S(1)-V(1)-S(3B)-S(3A)	168.6(6)
S(1)#1-V(1)-S(3B)-S(3A)	-6.0(6)

Symmetry transformations used to generate equivalent atoms: #1 -x+1,y,-z+3/2

Table A.4.6. Hydrogen Bonds

Donor	H	Acceptor	[ARU]	D-H	H...A	D...A	D-H...A
N(1)	H(1)	O(23)	[7556.01]	0.88	2.05	2.8333(13)	148
O(12)	H(12)	*S(1)	[7546.02]	0.84	2.44	3.145(13)	142
N(26)	H(26A)	>O(2B)	[ ]	0.91	1.79	2.685(18)	168
N(26)	H(26B)	C1(1)	[6546.04]	0.91	2.18	3.067(12)	165
N(26)	H(26C)	*S(2)	[1565.02]	0.91	2.25	3.143(17)	166
N(26)	H26(C)	*S(2)	[2666.02]	0.91	2.61	3.400(14)	146

Translation of ARU-code to Equivalent Position Code
[7556.]= 1/2-x, 1/2-y, 1-z
[7546.]= 1/2-x, -1/2-y, 1-z
[1565.]= x, 1+y,z
[2666.]= 1-x, 1+y, 3/2-z
[6546.]= 1/2-x, -1/2+y, 3/2-z

A.5. References

(1) SAINT; Version 7.03A; Bruker AXS Inc.: Madison, Wisconsin, USA, 1997-2003.

(2) TWINABS. Bruker Nonius scaling and absorption for twinned crystals; V1.05; Bruker AXS Inc.: Madison, Wisconsin, USA, 2003.

(3) Altomare A.; Burla M.C.; Camalli M.; Cascarano G.L.; Giacovazzo G.L.; Guagliardi A.; Moliterni A.G.G.; Polidori G.; Spagna R. *Journal of Applied Crystallography* **1999**, *32*, 115-119.

(4) Lee S.C.; Li J.; Mitchell J.C.; Holm R.H. *Inorganic Chemistry* **1992**, *31*, 4333-4338.

(5) Heinrich D.D.; Folting K.; Hoffman J.C.; J.G. Reynolds; Christou G. *Inorganic Chemistry* **1991**, *30*, 300-305.

(6) Least squares function minimized:

$$\Sigma w(F_o^2-F_c^2)^2$$

(7) Standard deviation of an observation of unit weight:

$$[\Sigma w(F_o^2-F_c^2)^2/(N_o-N_v)]^{1/2}$$

(8) Cromer D.T.; Waber J.T. *International Tables for X-ray Crystallography,* Vol IV; The Kynoch Press: Birmingham, England, 1974, Table 2.2A.

(9) Ibers J.A.; Hamiltion W.C. *Acta Crystallographica* **1964**, *17*, 781-782.

(10) Creagh D.C.; McAuley W.J. In *International Tables for Crystallography,* Vol. C; Wilson, A. J. C., Ed.; Kluwer Academic Publishers: Boston, 1992; 219-222.

(11) Creagh D.C.; Hubbell J.H. In *International Tables for Crystallography,* Vol C; Wilson, A. J. C., Ed.; Kluwer Academic Publishers: Boston, 1992, 200-206.

(12) SHELXTL; Version 5.1; Bruker AXS Inc.: Madison, Wisconsin, USA, 1997.